UNIVERSITÉ DE STRASBOURG

ÉCOLE DOCTORALE SCIENCES DE LA VIE ET DE LA SANTÉ

UPR 3212

THÈSE

présentée par :

Álvaro SANZ DÍEZ

soutenue le : **20 Juillet 2017**

pour obtenir le grade de : **Docteur de l'université de Strasbourg**

Discipline/ Spécialité : Neurosciences

Functional study of mouse olfactory bulb inhibitory circuits

THÈSE dirigée par :
M DE SAINT JAN Didier — Dr., Institut des Neurosciences Cellulaires et Integratives, Strasbourg

RAPPORTEURS :
Mme BUONVISO Nathalie — Dr., Centre des Recherches en Neurosciences de Lyon
Mme DIDIER Anne — Pr., Centre des Recherches en Neurosciences de Lyon

AUTRES MEMBRES DU JURY :
M SCHLICHTER Rémy — Pr., Institut des Neurosciences Cellulaires et Integratives, Strasbourg

UNIVERSITÉ DE STRASBOURG

École Doctorale des Sciences de la Vie et de la Santé STRASBOURG

UNIVERSITE DE STRASBOURG

ÉCOLE DOCTORALE SCIENCES DE LA VIE ET DE LA SANTÉ

UPR 3212

THÈSE

présentée par :

Álvaro SANZ DÍEZ

soutenue le : **20 Juillet 2017**

pour obtenir le grade de : **Docteur de l'université de Strasbourg**

Discipline/ Spécialité : Neurosciences

Functional study of mouse olfactory bulb inhibitory circuits

THÈSE dirigée par :

M DE SAINT JAN Didier	Dr., Institut des Neurosciences Cellulaires et Integratives, Strasbourg

RAPPORTEURS :

Mme BUONVISO Nathalie	Dr., Centre des Recherches en Neurosciences de Lyon
Mme DIDIER Anne	Pr., Centre des Recherches en Neurosciences de Lyon

---

AUTRES MEMBRES DU JURY :

M SCHLICHTER Rémy	Pr., Institut des Neurosciences Cellulaires et Integratives, Strasbourg

A mi padre,

Gracias por todo

Objective statement

Neurons, the principal cell type in the nervous system, form a vast and complex network of interconnected cells in constant exchange of information. The diversity of neurons present in one single organism is great but they can be classified into two major categories, excitatory and inhibitory neurons. Excitatory neurons release neurotransmitters that depolarize targeted cells and facilitate, in return, the release of other messengers by the targeted cells. Inhibitory neurons have the exact opposite role. They release neurotransmitters that hyperpolarize their targets and temporally inhibit their activity.

Excitatory neurons carry the information coming both from the outside as well as the internal medium of each individual. This information is critical for all species to interact with their environment and cover all their vital needs. Although this information is crucial for survival it often needs to be tuned, shaped or sharpened so the information gets to be as accurate and precise as possible. Local inhibitory neurons play an active role in this process of information refinement modulating the activity of excitatory neurons within a particular circuit and constitute the majority of inhibitory neurons in the nervous system. However, they represent a great heterogeneous group of cells with different anatomical, physiological and molecular properties that suggest specific different functions that remain poorly understood. In recent years, many neuroscientists have joined minds, resources and strength in order to better understand the functional diversity of local interneuronal circuits.

In the mammalian olfactory bulb, inhibitory interneurons are especially abundant and as an exception to the rule, they outnumber excitatory neurons. Among bulbar interneurons granule cells and periglomerular cells are the most common inhibitory cell types. However, each group of cells is heterogeneous and can be subdivided in subgroups due to intrinsic differences. The abundance and diversity across and within classes, makes fundamental to understand the physiological relevance of this heterogeneity. Moreover, the OB also receives centrifugal inhibitory inputs from the basal forebrain (Zaborszky et al., 1999; García-Llanes et al., 2010; Nuñez-Parra et al., 2013). However, these poorly studied projections densely innervate the olfactory bulb and have the potential to coordinate the timing of activity in the bulb, playing a major role in network activity coordination.

In this thesis, I present in an introduction the state of the art of the anatomical, cellular

and synaptic organization of the olfactory bulb, paying special attention to the inhibitory interneurons, the circuits they form and their functional implications. Then, I present two chapters of results. In the first chapter, I highlight how my results, which have been incorporated in two papers (Najac et al., 2015; Benito et al., in preparation) provide a new classification of the diversity of periglomerular cell subtypes based on their synaptic inputs, membrane properties and molecular markers. In the second part of the results I intended to decipher the circuits that mediate the inhibition of these interneurons and their physiological relevance. This part is presented as a paper manuscript which will be submitted soon (*Sanz Díez et al., GABAergic projections from the basal forebrain control multiple inhibitory interneuron subtypes in the olfactory bulb*). To do so, I used several transgenic mouse lines and a combination of electrophysiological, optogenetic, immunohistochemical and neuronal tracing techniques that have allowed me to explore these questions. Each chapter of results is followed by a discussion that puts in perspective the achievements.

Table of contents

Acknowledgments

I would like to thank in the first place Dr. Didier Desaintjan for giving me the opportunity to do my doctoral thesis under his supervision and accept me to join him in Strasbourg. I thank him for his scientific advice and guidelines in the professional field and his friendship in the personal life. Thank you for all your time, energy and patience. I'm glad we did this together.

Thanks to Dr. Philippe Isope and Dr. Bernard Poulain for hosting me on their lab and for their scientific advice. Thanks to Nuria Benito for sharing her thoughts, ideas and joy with me. A special thank you to Jean Luc Dupont for all the things he had taught me. Thank you to Francesca Binda for sharing her skills on stereotaxic viral injections with me. Thank you to Fred Dousseau, Kevin Dorgans, Anaïs Gangeray, Fernando Giuliani, Flavia Heid, Aline Huber, Seher Kossar, Orkan Ozcan, Sebastien Roux and Ludovic Spaeth for sharing everyday life in the lab I have learned from all of you and I have loved working next to you.

Thank you to Aurea Blancas, Catherine Estay, Tando Maduna and Elise Savier, four women that have specially inspired me during the last three years for their strength, intelligence and resources.

Thank you to Benjamin Bellanger, Dhanasak Dhanasobhon, Inés González, Sherazat Kavraal, Mari Carmen Medrano, Jérôme Wahis and Ivan Weinsanto, great colleagues that have become great friends.

Thanks to all my INCI colleagues that have me advice and provided material for my research, specially Anne Marie Heberlé, Matilde Cordero and Ipek Yalcin and of course to the Noemi, Sophie, Dom, Stephane and Edouard from the animal facility that have always taken so good care of my animals.

I want to specially thank Romain Sabathier for his personal support during all this years. He has been next to me to celebrate on the good occasions and to listen and support me during the hardest moments.

Thanks a lot, to my brother and my parents, with a special thought to my father, for giving me an education, believe in me and encourage me to always keep learning. Without it, I would have never come until here.

To all those people other that have somehow contributed to achieve this thesis by making part of my life these last years: David, Sylvain, Marion, Ara, Céline, Vero. And all my frieds and family that are still there despite the distance Thanks to all of you.

List of abbreviations

-A-

ACh Acetylcholine
AIS Axon initial segment
AMPA α-amino-3-hydroxy-5-methyl-4-isoxazolepropionic acid
AON Anterior olfactory nucleus

-C-

CB Calbindin
Chrna cholinergic receptor nicotinic α subunit
ChR2 Channelrhodopsin 2
CR Calretinin

-D-

DA Dopamine
DAT Dopamine transporter
dSAC Deep short axon cell

-E-

EGFP Enhanced green fluorescent protein
EPL External plexiform layer
EPSC Excitatory postsynaptic current
ET External tufted cell
EYFP Enhanced yellow fluorescent protein

-G-

GABA *gamma*-Aminobutyric acid (γ-Aminobutyric acid)
GAD
GBZ Gabazine
GC Granule cell
GCL Granule cell layer
GFP Green fluorescent protein
GL Glomerular layer

-H-

HCN Hyperpolarization-activated cyclic nucleotide-sensitive cation
HDB Horizontal limb of the diagonal band of Broca

-I-

IN Interneuron
IPL Internal plexiform layer
IPSC Inhibitory postsynaptic current

-J-

JG Juxtaglomerular

-L-

LCA Loose cell attached
LLD Long lasting depolarization
LOT Lateral olfactory tract

-M-

M Mitral
MCL Mitral cell layer
mGluR1 metabotropic glutamate receptor 1

-N-

NA **Noradrenaline**
NMDA *N*-Methyl-D-aspartic acid
NOS Nitric oxide synthase

-O-

OB Olfactory Bulb
OC Olfactory cortex
ONL Olfactory nerve layer
OR Olfactory receptor
OSN Olfactory sensory neurons

-P-

PC Piriform cortex
PG Periglomerular
PV Parvalbumin

-R-

RMS Rostral migratory stream

-S-

SAC Superficial short axon cell
SOM Somatostatin
sSAC Superficial short axon cell
SVZ Subventricular zone

-T-

T Tufted
TH Tyrosin hydroxylase
TTX Tetrodotoxin

-V-

VGAT Vesicular GABA transporter
VIP Vasointestinal peptide

Resumé en Français

Contexte

Le bulbe olfactif est le premier relai de l'information sensorielle olfactive dans le cerveau. Les neurones sensoriels détectent les particules odorantes dans l'épithélium nasal grâce à des récepteurs olfactifs. L'activation de ces récepteurs provoque une dépolarisation membranaire du neurone sensoriel qui génère des potentiels d'action et transmet l'information directement au bulbe olfactif (Buck and Axel, 1991). Chaque neurone sensoriel exprime un seul type de récepteur olfactif et tous les neurones exprimant le même récepteur projettent au même endroit dans le bulbe olfactif, plus concrètement, dans des structures sphériques nommés glomérules situés dans la couche la plus superficielle du bulbe. Au niveau glomérulaire, l'information olfactive est transmise aux cellules mitrales et à panache, les cellules principales qui projetent leurs axones vers des régions corticales supérieures pour le traitement de l'information.

Le bulbe olfactif est une structure organisée en couches. L'extérieur du bulbe est recouvert par les axones des neurones sensorielles qui forment la couche du nerf. Immédiatement sous cette couche se trouve la couche glomérulaire qui contient les glomérules. Autour des glomérules se situent divers types de neurones glutamatergiques, gabaergiques et dopaminergiques. Les glomérules sont des structures sphériques contenant un grand nombre de synapses entre les neurones sensoriels, les cellules principales glutamaterigiques et les interneurones. Dans les glomérules les neurones sensoriels forment des synapses avec les dendrites apicales des cellules mitrales et à panache. Les somas des cellules mitrales se situent alignés plus en profondeur et forment la couche des cellules mitrales. Du soma des mitrales sort une dendrite apicale. Elle traverse la couche plexiforme externe jusqu'à la couche des glomérules et un axone myélinisé qui traverse la couche plexiforme interne et la couche granulaire vers intérieur du bulbe. Ici, les axones des cellules principales forment un faisceau d'axones et abandonnent le bulbe formant le tracte latéral olfactif.

Dans le bulbe olfactif il y a environ 50.000 cellules mitrales et 150.000 cellules à panache (Meisami and Safari, 1981 ; Richard et al., 2010). Ces deux types de cellules possèdent une dendrite apicale qui projette dans un seul glomérule et des dendrites latérales qui projettent dans la couche plexiforme externe où elles font des synapses avec les dendrites des interneurones ici présentes (Macrides and Schneider, 1982 ; Orona 1984). Les cellules à panache sont légèrement plus petites que les cellules mitrales et leur corps cellulaire se situe au niveau de la couche plexiforme externe (Macrides and Schneider, 1982). Un glomérule reçoit les dendrites d'environ 10-15 cellules mitrales et le double des cellules à panache (Richard et al., 2010). En revanche, ces neurones projettent dans des endroits différents dans le cortex olfactif, ce qui fait perdre la somatotopie du bulbe (Poo and Isaacson, 2009; Apicella et al., 2010).

Dans le bulbe olfactif, la grande majorité des neurones sont des interneurones inhibiteurs. Il existe quatre types principaux d'interneurones bulbaires qui modulent de façon directe ou indirecte la décharge des cellules principales du bulbe : les cellules periglomerulaires (PG), les interneurones de la couche plexiforme externe, les cellules granulaires et les "short axon cells" (SAC). Les cellules PG sont une population hétérogène de petits neurones, qui entourent chaque glomérule dans lesquels elles établissent des synapses dendro-dendritiques avec les cellules mitrales (Panzanelli et al., 2007) de la même façon que les cellules granulaires et les interneurones de la couche plexiforme externe le font dans des couches plus profondes (Isaacson and Strowbridge, 1998). Au contraire, les SAC situées dans la couche des glomérules (superficielles) ou dans la couche des granules (profondes) possèdent de très longues axons ramifiés qui interagissent avec différents types de neurones (Eyre et al., 2008 ; Kiyokage et al., 2010).

Comme je l'ai mentionné auparavant les cellules PG forment une population hétérogène qui se reflète au niveau de leur anatomie, des marqueurs moléculaires, des propriétés membranaires ou encore de leur connectivité synaptique.

Morphologiquement il n'est pas clair si les cellules PG ont ou non un axone et quelle est l'étendue de leur arbre dendritique. De mon expérience, je suis prêt à affirmer que les cellules PG n'ont pas d'axone et que leur arborization dendritique est limité à un seul glomérule ou deux occasionnellement (Kosaka and Kosaka, 2010).

Au niveau moléculaire il est clair que les cellules PG sont des neurones GABAergiques par leur expression de GAD, l'enzyme de synthèse du GABA. Cependant, il existe des sous-groupes de neurones qui expriment d'autres marqueurs tels que les protéines de liaison au calcium Calbindine (CB) ou Calretinine (CR) ou encore la Tyrosine hydroxylase, l'enzyme de synthèse du précurseur de la dopamine (Panzanelli et a., 2007 ; Parrish-Aungst et al., 2007). Ceux-ci sont les trois marqueurs les plus communs parmi les cellules PG. Ils sont toujours exprimés de façon indépendante et dans les mêmes proportions, les neurones CR (+) étant deux à trois fois plus nombreux que les autres. De plus, les neurones qui expriment tyrosine hydroxylase ont des projections vers plusieurs glomérules, une morphologie qui ressemble plus aux "short axon cells" superficielles qu'aux PG (Kiyokage et al., 2010). Pour cette raison je ne considère pas ces neurones comme des PG.

Plusieurs études ont montré une large diversité parmi les patrons de décharge des cellules PG. Cela révèle ce qui reflète des différences de proprietés membranaires.

Au niveau synaptique, les cellules PG ont été historiquement classées comme type 1 ou type 2 en fonction de leurs entrées synaptiques excitatrices. Les cellules de type 1 reçoivent des entrées directes des neurones sensoriels olfactifs (Kosaka et al., 1998 ; Shao et al., 2009). En revanche, les cellules PG de type 2 reçoivent ses entrées excitatrices des dendrites des cellules mitrales et à panache(Kosaka et al., 1998 ; Shao et al., 2009). De plus, les cellules PG de type 2 peuvent être subdivisées en fonction de l'expression des marqueurs moléculaires CR et CB (Panzanelli et al., 2007).

Il existe de nombreuses évidences qui suggèrent que les cellules PG jouent un rôle majeur dans la modulation de la décharge des cellules mitrales et touffues (Shao et al., 2006; Fukunaga et al., 2014; Geramita et al., 2017). L'objectif de ma thèse a été de caractériser la diversité des neurones PG du bulbe et de déterminer l'origine de leurs entrées inhibitrices. Je me suis principalement servi de la technique du patch-clamp et de l'optogénétique sur des tranches de bulbe olfactif pour resoudre ces questions.

Le grand nombre d'interneurones GABAergiques dans le bulbe et leur diversité suggèrent l'importance de l'inhibition dans cette structure. C'est pourquoi l'impact de l'inhibition sur les neurones principales du bulbe a été longtemps étudié. Les interneurones GABAergiques du bulbe sont aussi sous influence inhibitrice, mais les circuits de cette inhibition ont été peu étudiés. Une des sources majeures d'afférences

GABAergiques du bulbe olfactif est la branche horizontale de la bande diagonale de Broca (HDB) (Garcia-Llanes et al., 2010 ; Niedworok et al., 2012 ; Nuñez-Parra et al., 2013). Cette structure est située dans la partie ventrale du téléncéphale et est constituée par des neurones GABAergiques et cholinergiques qui projettent vers les couches granulaire et glomérulaire du bulbe. Récemment il a été démontré que les projections GABAergiques de la HDB exercent une inhibition fonctionnelle des cellules granulaires mais cela n'a jamais été démontré pour les cellules PG (Nuñez-Parra et al., 2013).

Résultats

I. Caracterisation de la diversité des cellules periglomerulaires.

Pendant la première partie de ma thèse j'ai utilisé des lignées de souris transgéniques qui expriment une protéine fluorescente dans les populations des cellules PG CB(+) ou CR(+) afin d'étudier leurs propriétés intrinsèques et leur connectivité. J'ai pu contribuer à la caractérisation de ces deux sous-types de cellules en collaboration avec d'autres membres de l'équipe. On a pu démontrer que les cellules PG CB(+) sont représentatives d'un groupe plus large de PG de type 2 responsable d'une grande partie de l'inhibition intraglomerulaire. En revanche, les cellules PG CR(+), qui sont le type le plus abondant, conservent des propriétés de neurones immatures et ne semblent pas participer de façon très active à l'inhibition intraglomerulaire (Benito et al. in prep). J'ai aussi pu décrire un troisième sous type de cellules PG qui se différencie des PG CB (+) ou CR (+) par sa réponse à la stimulation du nerf olfactif. A la différence des groupes décrits précédemment cette stimulation provoque une bouffée de courants excitateurs postsynaptiques d'une durée beaucoup plus longue (>100ms). De plus, on a pu constater que ces cellules ont des propriétés membranaires intrinsèques à chaque groupe. Ces résultats démontrent que les neurones PG de type 2 sont plus complexes que ce que l'on croyait précédemment.

II. Etude des circuits d'inhibition des cellules periglomerulaires.

Sur des tranches de bulbe on peut constater que toutes les cellules PG reçoivent des entrées synaptiques inhibitrices (IPSCs). Afin d'élucider l'origine de ces entrées j'ai premièrement exploré la possibilité que les cellules PG s'inhibent entre elles. Nos observations nous ont mené à écarter cette hypothèse puisqu'une stimulation glomérulaire suffisante pour provoquer la décharge par des cellules PG ne produit pas d'IPSCs sur les neurones PG de type 2. Par contre, quand une stimulation est faite dans la couche glomérulaire à plusieurs centaines de micromètres d'écart, ou même dans la couche granulaire il est possible de provoquer un IPSC monosynaptique dans toutes les différentes classes de PG de type 2. Ces résultats suggèrent que l'inhibition des cellules

PG de type 2 provient d'axones remontant des couches profondes du bulbe et parcourant horizontalement la couche glomérulaire. Dans le cas des cellules PG de type 1 nos expériences ont montré que la stimulation glomérulaire peut activer des entrées inhibitrices. Ces résultats laissent penser que les cellules PG de type 1 peuvent être inhibées par d'autres cellules PG mais cette option n'a pas été confirmée.

J'ai ensuite cherché à élucider l'origine de l'inhibition des neurones PG de type 2. L'un des possibles candidats pour cette inhibition sont les "short axon cells" profondes. Certaines de ces cellules ont leurs somas dans la couche granulaire et projettent leurs axones à travers la couche des glomérules. De plus, il existe des évidences anatomiques qui suggèrent que ces cellules font des synapses sur des interneurones de la couche glomérulaire (Eyre et al., 2008 ; Burton et al., 2017). Pour étudier cette hypothèse, j'ai recouru à une approche opto-génétique en utilisant la lignée transgénique murine Thy1-ChR2-EYFP. Ces animaux expriment une protéine-canal actionnable par la lumière (ChR2) couplée à une protéine fluorescente (EYFP) sous le control du promoteur Thy1. Sur des tranches aiguës du bulbe olfactif de souris Thy1-EYFP-ChR2 j'ai constaté que les cellules PG de type 2 répondent à une stimulation lumineuse par des IPSCs monosynaptiques. Ce constat montre que les neurones responsables de cette inhibition expriment la ChR2 dans cette lignée. J'ai aussi constaté que la même stimulation lumineuse provoque des IPSCs similaires au niveau des cellules granulaires et des SAC profondes. Or, mes enregistrements démontrent que ni les SAC, ni aucun autre type d'interneurone bulbaire, n'expriment ici la ChR2. Par conséquent, si ces résultats n'excluent pas l'inhibition des cellules PG par des "short axon cells", ils suggèrent qu'il y a aussi une voie GABAergique extrabulbaire qui pourrait exercer son influence sur les principaux types d'interneurones du bulbe olfactif.

L'objectif suivant a été de déterminer l'origine de ces afférences. On a établi alors l´hypothèse que les neurones PG du bulbe sont inhibés par des neurones GABAergiques provenant de la HDB. Conformément à cette hypothèse j'ai montré une forte expression de ChR2 dans la HDB des souris Thy1-ChR2-YFP. Pour la confirmer, j'ai effectué une ablation unilatérale de la HDB par injection locale de NMDA à forte concentration. J'ai ensuite enregistré l'inhibition des interneurones bulbaires et comparé les deux hémisphères. Mes résultats indiquent que la probabilité d'induire

avec la lumière des réponses inhibitrices dans les interneurones du bulbe olfactif est plus faible cöté lésé que du côté contrôle.

Afin de raffiner mon approche et vérifier l'implication de la HDB dans l'inhibition des interneurones du bulbe, j'ai induit une expression locale et sélective de ChR2 dans les neurones GABAergiques de la HDB. J'ai utilisé lors de ces expériences des souris qui expriment Cre spécifiquement dans les neurones GABAergiques. Pour cela, j'ai injecté dans la HDB des souris transgéniques Dlx 5/6-Cre une construction virale floxée codant pour la ChR2. Ces expériences ont révélé une forte expression de ChR2 des afférences GABAergiques de la HDB ainsi que dans leurs axones dans toutes les couches du bulbe olfactif. Mes expériences d'électrophysiologie sur tranche ont montré que dans les animaux ayant subi ces injections, un flash de lumière est suffisant pour évoquer des IPSCs monosynaptiques dans les cellules PGs de type 2 appartenant aux trois groupes décrits précédemment. Cependant, les IPSCs reçus par les différents types de cellules PG de type 2 semblent avoir des cinétiques différentes. De plus, on a observé que les afférences GABAergiques de la HDB inhibent aussi les cellules granulaires ainsi que les SAC profondes. Ces résultats confirment que les projections GABAergiques provenant de la HDB sont envoyées dans toutes les couches du bulbe olfactif et qu'elles contactent les trois types majeurs d'interneurones dans le bulbe olfactif.

Finalement, on s'est intéressés à l'impact fonctionnel des afférences de la HDB sur la décharge des cellules PG. On a examiné les effets de l'IPSC évoqué par la lumière dans des tranches de bulbe olfactif des souris Dlx 5/6-ChR2-EYFP. Dans des enregistrements en cellule attachée des cellules PG on a pu constater que l'activation des fibres en provenance de la HDB peut altérer le patron de décharge de trois façons différentes. Dans un premier groupe de cellules l'IPSC produit une excitation de la cellule qui produit un seul potentiel d'action. Dans le deuxième groupe, l'activation des fibres de la HDB par la lumière inhibe la décharge pendant ~100ms. Enfin, dans un troisième groupe de cellules, l'activation de ces fibres a un effet inhibiteur suivi d'une excitation soutenue pendant plusieurs secondes. Des résultats préliminaires suggèrent que le premier groupe correspond aux PG CR(+) et le troisième aux PG dont la stimulation évoque une bouffée des courants excitateurs plus longue.

Les résultats obtenus pendant cette thèse approfondissent la diversité des interneurones periglomerulaires du bulbe olfactif et permettent une classification plus

approfondie. Ils démontrent aussi que la plupart des interneurones du bulbe olfactif sont sous le contrôle de la HDB, une région du cerveau qui pourrait par conséquent synchroniser l'inhibition dans le bulbe olfactif.

Introduction

Chapter I. Anatomical and cellular organization of the olfactory system

Chemosensation is the ability of metazoans to perceive the external chemicals present in their surrounding environment. Chemosensory systems (smell and taste) are crucial for many species to successfully achieve vital functions such as food seeking, predator or pray detection and mate recognition. In terrestrial animals, the olfactory system is specialized in the detection of volatile chemicals present in the air. In mammals, odorant particles present in the air enter the nasal cavity at each respiration. There, they bind to specialized receptors expressed by olfactory sensory neurons (OSNs) in the nasal epithelium. The odorant information is then transmitted to the olfactory bulb (OB) where it is transformed in a spatial and temporal code. Olfactory bulb principal neurons finally transfer the sensory information to the olfactory cortex for further processing of the olfactory perception. In this chapter I will describe the anatomical and cellular organization of the mammalian olfactory system, from the olfactory epithelium to the highest regions of the brain. I will pay special attention to the organization of the olfactory bulb, a spherical structure organized in layers, bilaterally located in the rostral extremity of each hemisphere of the brain.

1.1Odorant detection by Olfactory Sensory Neurons

1.1.1 The olfactory epithelium

The olfactory epithelium is located in the caudal region of the nasal cavity. It is composed of basal and supporting cells and contains the soma of millions of OSNs. OSNs are bipolar neurons with apical ciliate dendrites that bath in the olfactory mucosa, a diffusing medium for volatile odorant molecules secreted by the olfactory epithelium (Figure 1A). From the basal pole of the OSN somas arise long non-ramified axons that leave the olfactory epithelium and gather in bundles forming the olfactory nerve. The axonal terminals of OSNs project directly in the most superficial layer of the OB, making synapses with bulbar principal neurons inside concrete spherical structures called glomeruli. OSNs have an average lifespan of 30-40 days, and are continuously renewed from basal cell division (Costanzo, 1991; Caggiano et al., 1994).

1.1.2 Odor coding from the OSNs, from chemical to electrical

OSN cilia express seven transmembrane domain G-protein-coupled receptors called olfactory receptors (OR) (Buck and Axel, 1991). When an odorant binds an OR, the receptor interacts with the G-protein and the GTP-coupled α-subunit (Gαolf) stimulates adenylyl cyclase type III. The resulting cAMP increase induces the opening of nucleotide-gated cation channels and the entrance of cations (Na^+ and Ca^{2+} ions) into the cell. As a result, OSN membrane depolarizes and generates action potentials that directly transmit the odor information to the OB (Figure 1B)(Buck and Axel, 1991; Firestein, 2001)

ORs are encoded by a family of ~1000 genes for mouse and rat, ~600 genes for humans and ~100 genes in zebra fish with five conserved amino acid motifs that differentiate them from other seven transmembrane domain G-protein-coupled receptors (Buck and Axel, 1991; Parmentier et al., 1992; Mombaerts, 1999). OR expression is monoallelic, ensuring that each OSN only expresses one type of OR (Buck and Axel, 1991; Ressler et al., 1993; Vassar et al., 1993). The olfactory epithelium is divided in four zones or stripes. OSNs

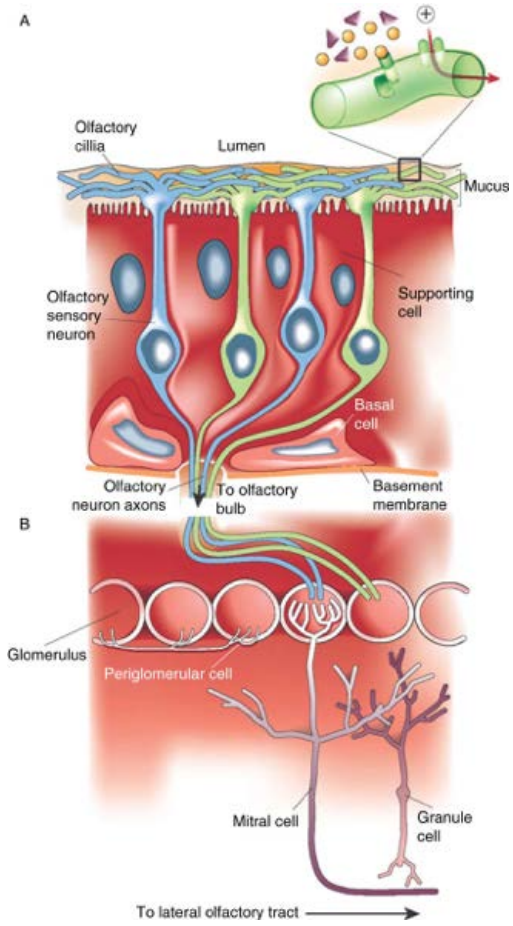

Figure 1. Anatomical representation of the olfactory epithelium and OSN projections. *(A) Odorant molecules bind to OR on the surface of OSN cilia provoking changes in the membrane conductance of the cells. The newly generated odor code is directly sent to the OB. (B) OSN axons make synapses onto mitral cells apical dendrites. The information is transmitted to higher regions though the principal cells axons to be integrated and processed (Adapted from Fierstein, 2001)*

expressing the same OR are located in the same zone, but their distribution in that zone is stochastic (Ressler et al., 1993; Vassar et al., 1993; Mombaerts et al., 1996). OSNs expressing the same OR converge in two glomeruli per bulb, distant and symmetrically positioned in each OB, and each glomerulus exclusively receives inputs from OSNs expressing the same OR (Ressler et al., 1993; Vassar et al., 1993; Mombaerts et al., 1996). The glomerular map is precise and conserved among individuals of the same species, as well as among different species like mouse and rat (Potter et al., 2001; Mombaerts, 2006; Imai and Sakano, 2007; Soucy et al., 2009).

1.1.3 OSN activation creates spatial maps in the Olfactory Bulb

ORs have a low selectivity for odorants. Thus, different odorants with similar chemical properties can bind to the same OR and one odorant can also bind to several ORs. Such effect increases with odor concentration (Friedrich and Korsching, 1997; Rubin and Katz, 1999; Wachowiak and Cohen, 2001; Bozza et al., 2004; Brunert et al., 2016). As a result, each odorant molecule, depending on its concentration, will activate a specific group of glomeruli forming a spatial map at the surface of the bulb. These maps are present in many different animal species such as insects, fish or mammals. Several techniques allow the visualization of odor-activated spatial maps *in vivo.* Some researchers have used intrinsic signaling to capture small activity changes from the glomerular pattern (Luo and Katz, 2001; Soucy et al., 2009; Banerjee et al., 2015). It has been recently reported that intrinsic imaging detection relies in water changes along OSN axons reflecting water movement following action potential propagation (Vincis et al., 2015). The activity of presynaptic OSNs can also be monitored with voltage sensitive dyes (Friedrich and Korsching, 1997), calcium imaging (Lecoq et al., 2009; Soucy et al., 2009) or pH sensitive proteins detecting synaptic vesicle fusion (Bozza et al., 2004; Fleischmann et al., 2008). Others have monitored the activity of postsynaptic neurons using calcium or voltage-sensitive probes (Spors and Grinvald, 2002; Davison and Katz, 2007; Tan et al., 2010) demonstrating that spatial activation maps detected at the postsynaptic level match well with those revealed at the OSN presynaptic level.

Different odorants from similar chemical classes activate clusters of glomeruli in specific regions of the bulb (Johnson and Leon, 2007). Yet, this organization is not precise and nearby glomeruli do not present more similarities in their odor sensitivity than distant

glomeruli (Soucy et al., 2009). Moreover, the activation of the spatial map follows temporal dynamics. In mammals, the input frequency from the OSNs to the OB is primarily determined by the respiration frequency but OSNs coding for different odorants have distinct temporal dynamics and activate odor-specific sequences of glomeruli (Spors et al., 2006).

1.2 The olfactory bulb

1.2.1 The olfactory bulb is organized in concentric layers

The anatomy of the OB is structured as a set of concentric layers recovered by the olfactory nerve forming the Olfactory Nerve Layer (ONL). Aligned glomeruli form the Glomerular layer (GL) just below the ONL. Diverse GABAergic, glutamatergic and dopaminergic neurons, collectively called juxtaglomerular (JG) cells, surround each glomerulus. Glomeruli are spherical neuropils containing a high density of synapses. They are highly compartmentalized with OSN projection zones and non-OSN zones (Chao et al., 1997; Kasowski et al., 1999). In the OSN-zones, OSNs make synapses with the apical dendrites of mitral and tufted (M/T) cells, the principal glutamatergic cells of the bulb. The non-OSN glomerular zones contain dendro-dendritic synapses between M/T cells and interneurons and between interneurons. M cell somas are aligned in a single plane forming the Mitral cell layer (MCL). From the M/T cell somas arises their apical dendrite, crossing the External Plexiform layer (EPL) up to the GL, and a myelinated axon that crosses the Internal Plexiform layer (IPL) and the Granule cell layer (GCL) towards the core of the bulb, gathering into axonal bundles to form the Lateral Olfactory Tract (LOT) which constitutes the main bulbar output to higher brain regions. The most inner part of the OB layers is formed by the Rostral Migratory Stream (RMS), the access pathway for newborn cells (Figure 2).

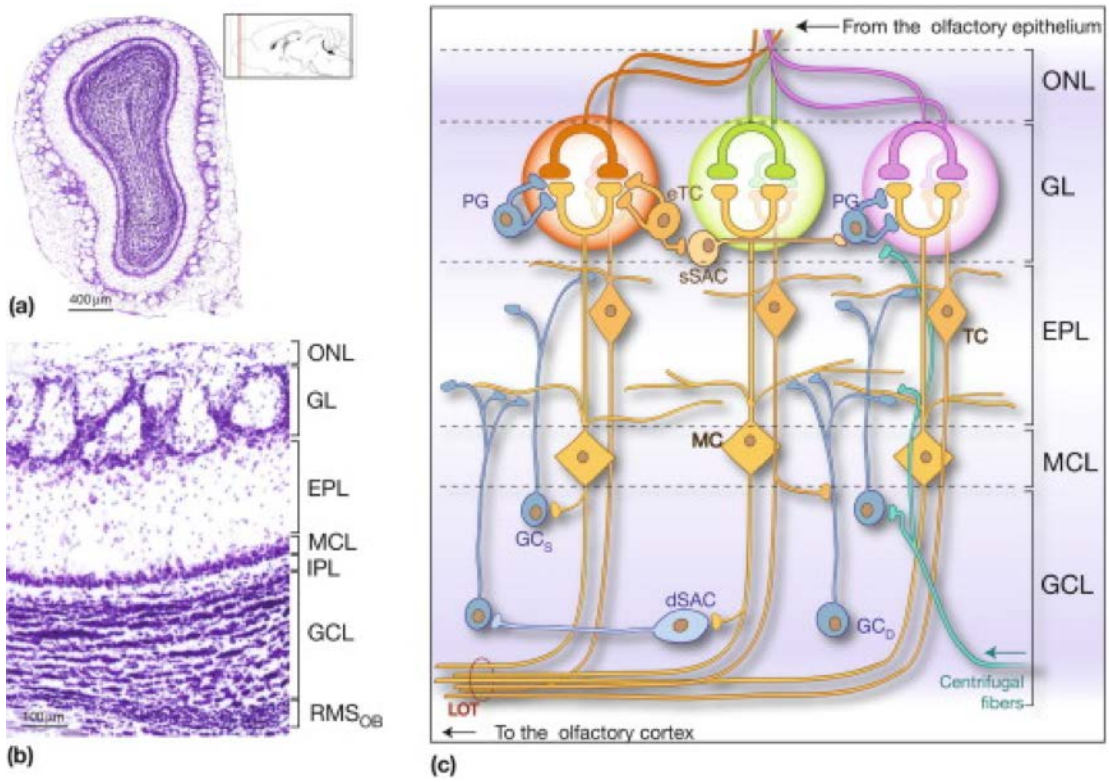

Figure 2. Laminar organization of the OB. *(a) Nissl staining of a coronal section of OB. (b) Inset of A to highlight all the layers. Outside-in: Olfactory Nerve Layer (ONL), Glomerular Layer (GL), External Plexiform Layer (EPL), Mitral Cell Layer (MCL), Internal Plexiform Layer (IPL), Granule Cell Layer (GCL), RMS (Rostral Migratory Stream). (c) Scheme of the OB layers and principal cell types. Glutamatergic cells are represented in yellow (M/T cells), GABAergic cells appear in blue (PG cells, GC and dSAC) and GABA/dopaminergic cells in pale orange (sSAC). From Lepousez and Lledo, 2013.*

1.2.2 Cellular organization

i. Excitatory cells of the OB

In each OB there are around 33.000-70.000 M cells and 100.000-160.000 T cells (Meisami and Safari, 1981; Richard et al., 2010). Although much less abundant than inhibitory neurons, bulbar excitatory neurons have the important role of receiving olfactory information from the outside and transferring it as a spatiotemporal sensory code directly to higher processing areas of the brain, without any thalamic relay in contrast with other sensory systems.

a. Mitral Cells

M and T cells are the principal glutamatergic neurons of the bulb. M cells present piriform somas of 20-30 µm diameters, the largest in the OB. Several dendrites arise from

the M soma. A thick primary apical dendrite crosses the EPL and projects inside a single glomerulus were it densely ramifies forming an apical tuft (Macrides and Schneider, 1982; Orona et al., 1984). According to recent studies, only 10-15 M cells project into the same glomerulus (Richard et al., 2010; Ke et al., 2013; Kikuta et al., 2013). These so called "sister" M cells are dispersed within a 4-7 fold larger radius than the average radius of a glomerulus and intermingled with other M cells projecting into different glomeruli (Buonviso et al., 1991; Ke et al., 2013; Kikuta et al., 2013). M cells also emit several lateral dendrites that project into the inner part of the EPL, spreading parallel to the MCL (Figure 3A). These dendrites ramify and extend over up to one millimeter making synaptic dendro-dendritic contacts with GABAergic interneurons (Mori et al., 1983; Kishi et al., 1984; Orona et al., 1984).

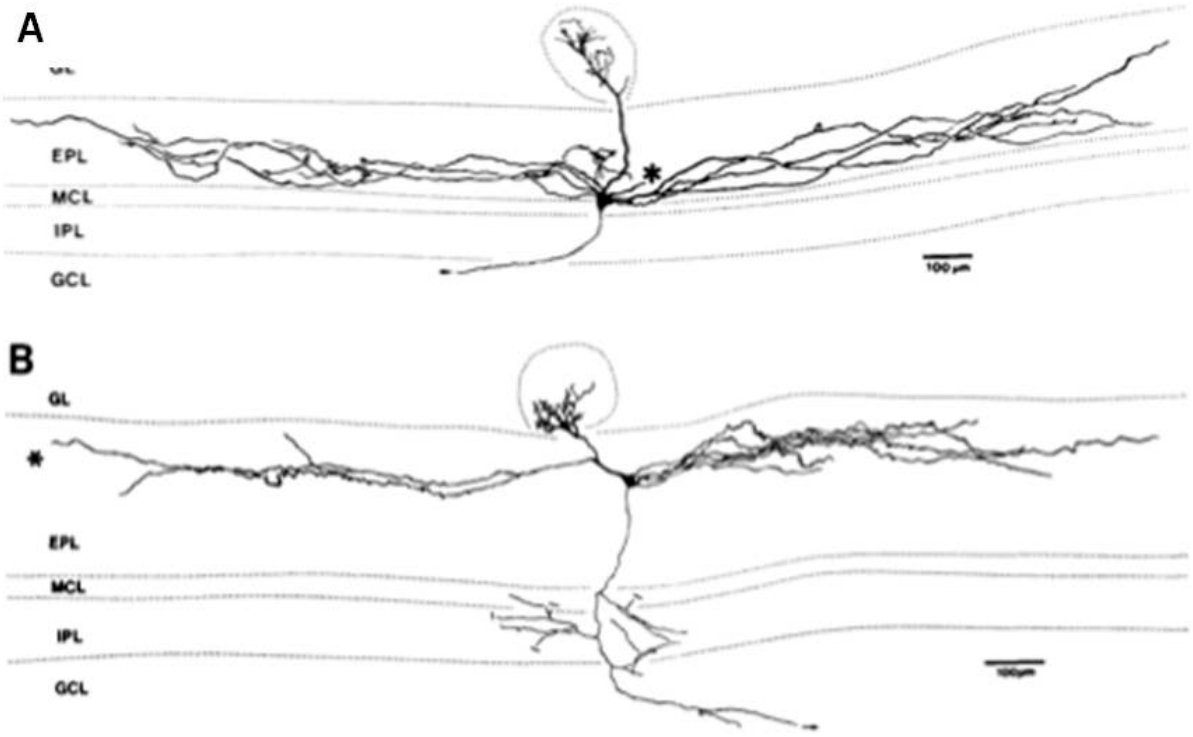

Figure 3. Morphology of mitral (A) and tufted cells (B). *M/T cells apical dendrite projects into one glomerulus where it densely ramifies and forms a tuft. Lateral dendrites arising close to the soma project in the EPL parallel to the bulbar layers. Cells filled by iontophoresis after Horse Radish Peroxidase injection (asterisk shows injection site) (modified from Orona et al., 1984).*

b. Tufted cells

T cells anatomy is very similar to M cells. However, their somas are smaller (15-20µm) and distributed across the EPL. Since Cajal, T cells have been classified as deep (or internal), intermediate (or medial) and superficial (or external) depending on the position of their

soma in the EPL. Like M cells, they have one single apical dendrite that projects into one glomerulus and emit long lateral dendrites expanding horizontally across the intermediate and superficial portion of the EPL (Macrides and Schneider, 1982) (Figure 3B). However, the number of T cells projecting into one same glomerulus is around 2-3 fold larger than M cells (Meisami and Safari, 1981; Kikuta et al., 2013). T cells have lateral dendrites that occupy the upper half of the EPL whereas M cell lateral dendrites occupy the deepest half. As I will describe later, the functional properties of T cells also resemble those of mitral cells (See chapter 2.1.1), albeit with some small differences.

c. Axonal projections of M and T cells in the olfactory cortex

A major difference between M and T cells resides in their axonal projection. Several anatomical studies show that M and T cells axons target different regions of the olfactory cortex (OC) (Scott, 1981; Ghosh et al., 2011; Miyamichi et al., 2011; Sosulski et al., 2011; Igarashi et al., 2012). The OC is located in the ventral and ventrolateral portion of the forebrain and composed of several cortical and striatal subregions that differ in their output and local circuits. Thus, the anterior olfactory nucleus (AON), tenia tecta, dorsal peduncular cortex, piriform cortex (PC), olfactory tubercule, cortical amygdala, granular insulata and the entorhinal cortex are all part of the OC, the PC being the principal structure of this complex ensemble. The axons of T cells are shorter and project to discrete zones in anterior areas of the OC (AON, anterior PC, and olfactory tubercle). In contrast, M cells have much longer and complex axon anatomy with a high number of collateral ramifications that disperse and project to all OC areas (AON, the olfactory tubercle, the PC, the cortical nucleus of the amygdala and the entorhinal area)(Igarashi et al., 2012).

The OB spatial organization in well-defined odor-evoked spatial maps of activated glomeruli is lost in the OC. Thus, a single M cell which is activated by OSNs expressing the same OR sends collaterals to several pyramidal cells and a single pyramidal cell receives inputs from M cells associated with distinct glomerular units (Poo and Isaacson, 2009; Stettler and Axel, 2009; Apicella et al., 2010). As a result, a single odorant activates an ensemble of pyramidal cells scattered across the cortex.

d. External Tufted Cells

External T cells have recently received a lot of attention. They are a particular subtype with unique properties that distinguish them from other T cells located in or close to the GL. This subtype, that has often been called ET cell, has a 10-15 µm soma located in the ventral part of the GL, a single apical dendrite that projects inside a glomerulus, and in contrast to M and T cells, no lateral dendrites suggesting that it does not interact with granule cells (GC) (Hayar et al., 2004b; Antal et al., 2006). The absence of lateral dendrites, which is somehow controversial perhaps because they can be confounded with basal dendrites, is however, not the only feature that differentiates ET cells from other T cells. ET cells spontaneously fire bursts of action potentials at theta frequencies, an activity that persists when synaptic transmission is blocked (Hayar et al., 2004a). This pacemaker activity is mediated by a unique repertoire of several voltage-dependent ion channels (Ih, INaP, ICaL, ICaT,…)(Hayar et al., 2004a; Liu and Shipley, 2008) that make ET cells hyperexcitable. We will see in chapter 2.1.1 that ET cells, thanks to their explosive membrane properties and strong OSN connections, have a critical role in driving the activity of the glomerular network and in shaping the synaptic activation of M and T cells. ET cells have an axon that projects into the EPL but the final targeting site remains unknown. It is therefore not demonstrated that they are, like M and T cells, real principal output neurons. However, the confusion persists in the literature and it is not rare that this subtype is considered as a principal neuron (see for instance Vaaga and Westbrook, 2016).

ii. Inhibitory cells of the OB

Inhibitory cells represent approximately 80-90% of the total cell population in the OB (Parrish-Aungst et al., 2007). OB interneurons have diverse morphologies, molecular markers expression, intrinsic membrane properties, synaptic connections and functions. Most of them, if not all, are constantly generated and integrated into the OB network throughout lifetime, including adulthood, from neural stem cells located in the walls of the subventricular zone (SVZ). The proportion and abundance of inhibitory cells along with their permanent renewal, suggest that inhibition in the OB is of great relevance for olfactory processing. In the following part I will describe the different subtypes of inhibitory interneurons present in the OB.

a. Periglomerular cells

Classically, periglomerular (PG) cells have been defined as small round (occasionally ovoid) JG cells with one or more thin dendrites that arborize within the depths or near the periphery of the glomeruli (Pinching and Powell, 1971; (Kosaka and Kosaka, 2010). Occasionally they give rise to a very thin axon coursing more or less tangentially between glomeruli and then ends by ramifying within one of them (Pinching and Powell, 1971). Precise quantification of PG cells is hard to assess. Yet, Parrish-Aungst et al. (2007) estimated that each glomerulus is surrounded by 400-450 PG cells, representing 60-70% of all juxtaglomerular neurons. PG cells are considered to be GABAergic interneurons. They express glutamate descarboxilase (GAD), the enzyme responsible for gamma-aminobutyric acid (GABA) synthesis and the vesicular transporter for GABA (VGAT), at presumed synaptic contacts facing clusters of $GABA_A$ receptors (Kosaka et al., 1998; Panzanelli et al., 2007; Parrish-Aungst et al., 2007). However, this cell population is highly heterogeneous and GABAergic markers are often associated with other non-overlapping markers. Such diversity is further supported by anatomical and physiological evidence. Characterizing PG cell diversity has been one of my objectives during my thesis and I will therefore dedicate a specific chapter (1.3) to the description of this complex heterogeneity.

b. Superficial Short Axon cells

Unlike what their name suggests, these bulbar inhibitory interneurons have a long ramifying axon that forms broad intrabulbar and interglomerular connections. Short axon cells (SACs) can be classified in two subgroups regarding the location of their soma: *superficial* and *deep* SACs.

Superficial SACs (sSACs) are intermediate size (8-12 µm soma) juxtaglomerular cells that extend their projections throughout the GL. They are GABAergic/DAergic cells immunoreactive to the GAD67 isoform (Toida et al., 2000; Parrish-Aungst et al., 2007; Kosaka and Kosaka, 2008, 2009; Kiyokage et al., 2010) and to Tyrosine-hydroxylase (TH) and Dopamine transporter (DAT) (Kosaka and Kosaka, 2008, 2009; Kiyokage et al., 2010; Kosaka and Kosaka, 2010; Banerjee et al., 2015). However, two distinct populations of TH-expressing SACs with different morphologies and temporal origins have been described (Kosaka and Kosaka, 2008, 2009; Kiyokage et al., 2010). The first population projects its axons only into adjacent glomeruli (Figure 4A) (i.e. *oligoglomerular* projection). This sSAC subtype is mainly

generated postnatally, including during adulthood (Kosaka and Kosaka, 2009, 2010). The second group presents larger somata and an axon that expands throughout several hundreds of µm within the GL, making contacts within up to 50 glomeruli (Figure 4B). These large poliglomerular sSACs are mainly generated prenatally but not in juvenile or adult animals (Aungst et al., 2003; Kosaka and Kosaka, 2009; Kiyokage et al., 2010; Kosaka and Kosaka, 2010).

TH(+) sSACs have also been classified in two groups based on their excitatory input. Electrophysiological evidence suggests that only 30% of the population of dSACs receives a direct excitatory input from OSNs. The other 70% receives excitatory inputs from principal glutamatergic neurons (Figure 4C) (Kiyokage et al., 2010). These functional data seem contradictory with previous ultrastructural studies claiming that 70% of TH(+) JG neurons project their dendrites into the OSN-zone of the glomeruli where they make asymmetrical synapses with OSN terminals (Kosaka et al., 1997; Kosaka and Kosaka, 2005). However, recent physiological and confocal evidence suggest that all SACs receive both inputs, the majority coming from OSN axon terminals on distal parts of the dendrites (Kiyokage et al., 2017). Those distal OSN inputs may therefore be smaller and more difficult to detect than proximal excitatory inputs provided by principal glutamatergic cells (Hayar et al., 2004b; Kiyokage et al., 2010; Kiyokage et al., 2017).

***Figure 4. Superficial Short Axon Cells**. (A,B) Morphology of poliglomerular (A) and oligoglomerular (B) GAD67(+)/TH(+)sSACs. Scale bar 100 µm. (C) Representative traces of sSAC monosynaptic excitatory OSN-evoked response (green trace) and polysynaptic excitatory OSN evoked response (red trace).*

c. Deep Short Axon cells

As their name suggests, deep SACs (dSACs) are located in the deepest bulbar layers (IPL and GCL). Their somas are ovoid and can measure from 10 to 20 µm. dSACs can be classified into three groups based on the bulbar layer into which their axon projects: GL, EPL or GCL (Eyre et al., 2008). GL-dSACs have their elongated soma in the MCL and the IPL, and axons projecting up to the GL where they ramify and horizontally expand over several hundreds of µm. In addition, long dendrites arising from the soma project into the MCL and the IPL. In early studies, these cells were identified as Horizontal cells or Golgi cells (Schneider and Macrides, 1978). EPL-dSACs soma are located in the GCL and their axon cross the MCL and ramify in the EPL while dendritic ramifications are restricted to inframitral layers. These cells where previously known as Blanes cells or Cajal cells (Schneider and Macrides, 1978). Finally, GCL-dSACs soma and axonal projections are restricted to the IPL and GCL. Interestingly, (Eyre et al., 2008) and (Kosaka and Kosaka, 2007) suggest that some GCL-dSACs project axon collaterals outside the OB, towards higher olfactory brain structures like the PC or the AON, establishing the idea of inhibitory bulbar projections. All these cellular types are illustrated in Figure 5.

Diverse dSACs express a wide range of molecular markers. Classical interneuronal markers such as Calbindin (CB), Nitric oxide synthase (NOS) or vasoactive intestinal peptide (VIP) label small subpopulations, whereas, voltage-gated potassium channel subunits Kv2.1, Kv3.1b, Kv4.3 and the $GABA_A$ receptor α1 subunit are present in 70-95% of dSACs, without any subtype-selective expression. It is thus complicated to selectively identify dSACs subpopulations (Eyre et al., 2009). Two studies, however, have found markers of GL-dSACs. 20% of dSACs, preferentially GL-dSACs, are immunoreactive to the metabotropic glutamatergic receptor 1α (mGluR1α) (Eyre et al., 2009). However, mGluR1α is not selectively expressed by SACs but also strongly by M cells (Vandenpol, 1995). In a recent study, (Burton et al., 2017) identified the nicotinic cholinergic receptor α2 subunit (chrna2) as a selective marker of GL-dSACs, using it to explore the synaptic and membrane properties of this specific cell subtype (Burton et al., 2017). Unfortunately, this marker is also expressed by other neuronal types that project into the OB, making it complicated to use chrna2-cre mice to selectively manipulate GL-dSACs.

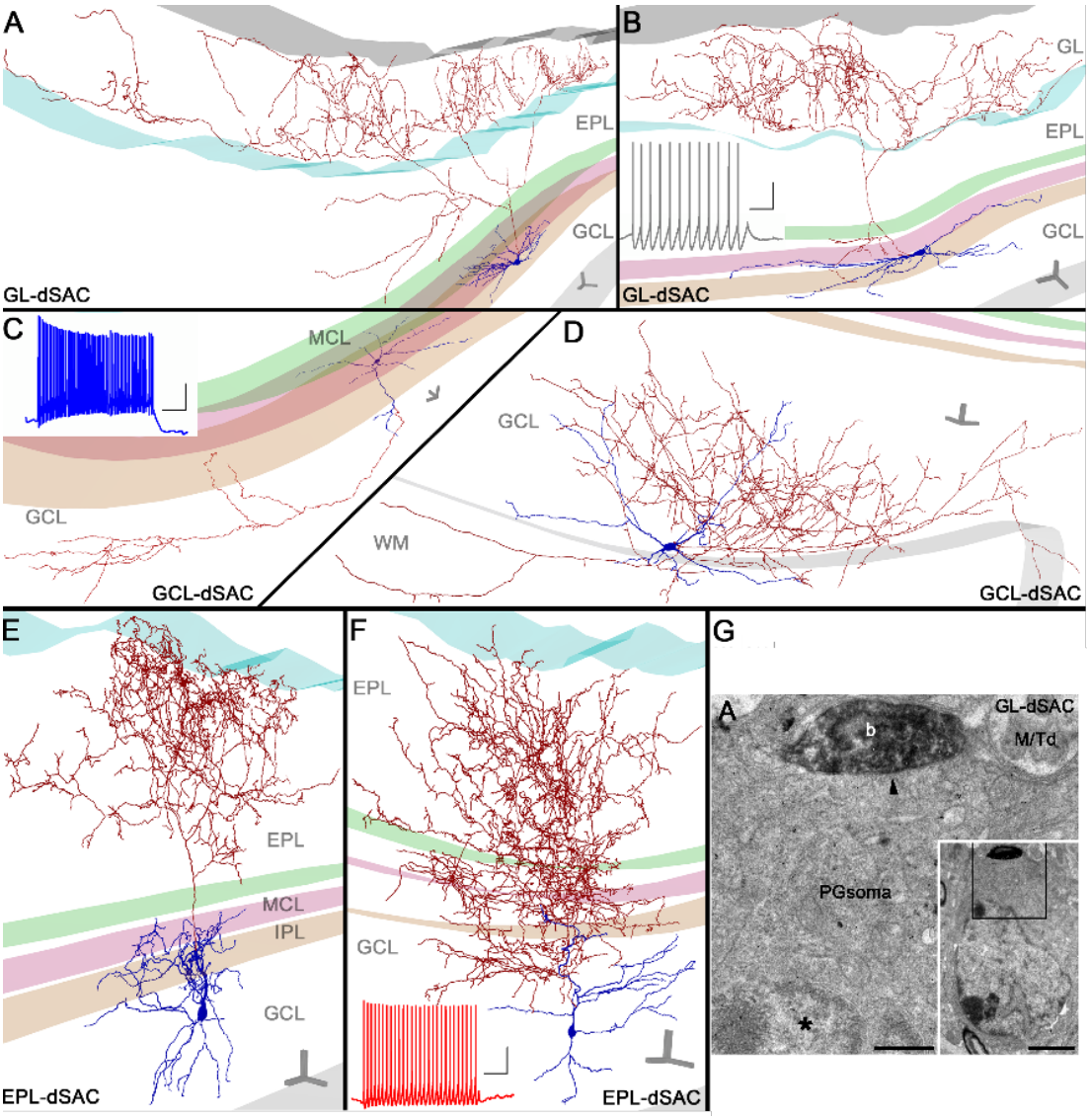

Figure 5. Deep Short Axon Cells. (A-F), *Examples of Post-hoc reconstruction of biocytin filled dSACs. (A and B) GL-dSACs have their soma and dendrites located in the IPL, the axon and its collaterals project and ramify in the GL. (C and D) GCL-dSACs: all the parts of the cell are located in the GCL. (E and F) EPL-dSACs: their somas are located in the GCL and their axons densely ramify within the EPL. Gray scale bars A-F 50 µm. Insets in B, C and F show cell response in current clamp to 100pA/1s depolarizing step. Scale 10mV/200ms. The color bands represent the edges of bulbar layers. G, Electron microscopy photograph of a synaptic contact (arrow) between a biocytin filled GL-dSAC (b) and the soma of a PG cell. Bottom-right, image enlarged. Scale bars 500nm, 2µm. (Modified from Eyre et al., 2008).*

dSACs membrane properties are divergent among the three subpopulations. EPL-dSACs and GCL-dSACs have, for example, lower spontaneous firing rates than GL-dSAC but all of them present a regular firing profile in response to a depolarizing current (Figure 5B and 5F). However, some GL-dSAC can also fire bursts of action potentials (Eyre et al., 2008; Burton et al., 2017). There are also marked differences in their membrane resistance values which reflect differences in membrane channel expression. Thus, EPL-dSACs have lower membrane resistance values (~160 MΩ) than GC-dSACs (~400 MΩ) or GL-dSACs (~300 MΩ).

Functional and anatomical evidence suggest that dSACs only target GABAergic interneurons. Electron microscopy images show symmetric synapses from dSACs onto GC and PG cells (Figure 5G) (Eyre et al., 2008). Paired recordings between dSACs and GCs have further demonstrated functional connections (Pressler and Strowbridge, 2006; Eyre et al., 2008), while optogenetic experiments supported functional connections between dSACs and PG cells (Burton et al., 2017). The heterogeneous morphologies and membrane properties of dSACs together with the diversity of their cellular targets suggest that different types of dSACs could execute different inhibitory functions.

d. Granule cells

GC are the most abundant cells in the OB, some estimations oscillate between $6x10^6$ to 10^7 GCs (Parrish-Aungst et al., 2007; Richard et al., 2010). GCs are small GABAergic neurons (6-8 µm) disposed in the inner part of the bulb, forming the GCL. GCs are axonless but use a ramifying apical dendrite to interact with M and T cells lateral dendrites in the EPL. GC dendrites are covered with synaptic spines that host reciprocal contacts with the lateral dendrites of principal cells (Figure 6) (Mori et al., 1983; Orona et al., 1983; Geramita et al., 2016). GCs have been divided into three different types regarding their anatomy (Figure 6). Type I GC somas have a widespread distribution in the GCL and their dendrites are present all the way from the MCL to the upper part of the EPL, suggesting that they establish synapses with the lateral dendrites of M and T neurons. Type II GC somas are located deeply in the GCL and their dendrites project to the deepest portion of the EPL, right above MCL, establishing contacts more likely with M cells lateral dendrites. Finally, type III GCs have their somas in the most superficial fraction of the GCL and their apical dendrite projects to the outer portion of the EPL, suggesting preferred interactions with T cells lateral dendrites (Mori et al., 1983; Orona et al., 1983). GC also have relatively short basal dendrites in the GCL, covered in synaptic spines as well but that most likely receive axonal inputs from M/T cell axon collaterals (Halabisky and Strowbridge, 2003) and from centrifugal projections (Boyd et al., 2012; Markopoulos et al., 2012; Nunez-Parra et al., 2013). More recently, Merkle and colleagues described type IV and type V GCs (Merkle et al., 2014). Type IV GC soma and dendrites are located in the GCL and rarely overpass the MCL, while type V GC have their soma in the MCL and do not have basal dendrites. Only few molecular markers have been associated to GCs. Some superficial GCs are responsive to calretinin (CR) staining

(Batista-Brito et al., 2008) and 5T4, a leucine-rich-repeat transmembrane protein (Imamura et al., 2006; Yoshihara et al., 2012).

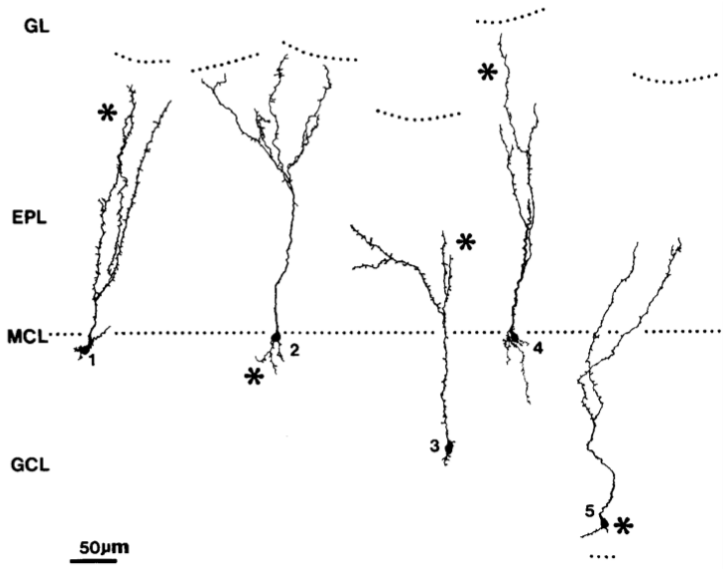

Figure 6. Granule cells. *Examples of different morphologies of GC obtained with Camera lucida following HRP staining processed with Hanker-Yanes method. Asterisk indicated HRP injection site. Dotted lines represent the limits of GL and MCL (Orona et al., 1983*

e. Interneurons from the EPL

GABAergic interneurons with heterogeneous morphology are also found in the EPL. These cells are immunoreactive to several molecular markers like somatostatin (SOM), parvalbumin (PV), VIP or CR (Schneider and Macrides, 1978; Lopezmascaraque et al., 1989; Kosaka et al., 1994; Toida et al., 1994; Crespo et al., 2002; Shepherd et al. 2004). Most of these cells are axonless and make reciprocal interactions with MCs lateral dendrites. PV(+) are the most common interneuron cell type in the EPL and around 90% of them co-express corticotropin-releasing hormone (Huang et al., 2013). PV(+) cells are fast spiking neurons that make reciprocal dendritic and non-reciprocal perisomatic synapses with ~60% of the surrounding M cells, in contrast to GCs that make synapses with a much lower number of surrounding M cells (~5%). In addition, PV(+) EPL-interneurons make perisomatic synapses onto M cells, a more effective inhibitory input than dendro-dendritic synapses to drive M cell inhibition. Thus, PV(+) neurons represent a powerful and broad source of M cell inhibition (Kato et al., 2013; Miyamichi et al., 2013).

SOM(+) neurons are located in the basal portion of the EPL, outlining the region where M cell lateral dendrites interact with GC. 50% of SOM(+) EPL-interneurons co-express PV (Lepousez et al., 2010b). SOM(+) cells were previously known as Van Gehuchten SACs. These cells were described as a subpopulation of axonless EPL interneurons with a medium-

sized fusiform soma, from which emerge one or two thick and highly varicosed dendrites that arborize next to the cell body forming a dense ovoid dendritic field (Schneider and Macrides, 1978; Lopezmascaraque et al., 1990; Brinon et al., 1992; Kosaka et al., 1994). The functional implication of M cell-SOM(+) interneuron interactions is not clear although it has been proposed they have an active role in rhythm generation in the bulb (Lepousez et al., 2010a).

f. Adult Newborn interneurons

It has long been considered as a dogma that neurogenesis only occurred during pre- and perinatal stages. However, in the 1990 decade the combination of new techniques combining graft experiments, BrdU staining, confocal microscopy and transgenic mice generation proved that adult neurogenesis occurs in two niches of the brain: The Subgranular zone of the Hippocampus and the SVZ. For instance, (Lois and Alvarezbuylla, 1994) grafted labeled neuroblasts from a donor transgenic mouse into a non-transgenic adult host and after several days they observed that grafted and endogenous cells coming from the SVZ migrate to the OB through the RMS and differentiate into GCs and PGs as ilustrated in Figure 7 (Luskin, 1993; Alvarez-Buylla and Garcia-Verdugo, 2002).

Many studies have explored the maturation process of adult newborn cells. Much of this work has been conducted in adult newborn cells of the hippocampus, showing how these cells go under a complex and gradual process of maturation before becoming functional interneurons integrated in the circuits. The maturation degree of adult-newborn hippocampal cells can be defined by the expression of several molecular markers that gradually appear and follow up each other in time, such as Nestin, CR and Doublecortin. The membrane of these cells follows a functional maturation as well, highlighted by a number of factors. In early stages, immature neurons have very high membrane resistance, indicating lack of ion channels. They express small Na+ currents and are not able to fire full size action potentials. In early stages these cells do not establish synaptic contacts with other cells. The first synaptic inputs they receive are GABAergic but their high Cl^- internal concentration makes GABA depolarizing. Later on, excitatory synaptic inputs appear and GABA becomes hyperpolarizing. Finally, neurite length that progressively increases while the new cell creates new synapses, is another marker of maturation (For review see Overstreet-Wadiche and Westbrook, 2006).

The maturation process is essentially similar for newborn neurons in the OB but far less studied. Newly generated GCs form the majority (~90%) of adult born interneurons in the bulb (Hack et al., 2005). During migration, adult-born GCs have a very simple morphology. When they arrive to their final destination, indistinctly in all regions of the GCL, their apical dendrite starts to develop and ramify reaching mature morphology when dendritic spines appear. Once mature, adult-generated GCs are able to fire action potentials and establish functional synapses with output neurons as well as with local interneurons (Carleton et al., 2003; Whitman and Greer, 2007; Kelsch et al., 2008; Bardy et al., 2010). This migration and maturation process can last from two weeks up to a month (Petreanu and Alvarez-Buylla, 2002). Although 50% of adult GC cells die within the first month following their birth (Lemasson et al., 2005; Magavi et al., 2005), new-born GCs generated during adulthood become functional and integrate the preexisting OB network.

PG cells are also constantly generated throughout adult life in the SVZ from where they migrate to OB and integrate the network (Alvarez-Buylla and Garcia-Verdugo, 2002; De Marchis et al., 2007; Whitman and Greer, 2007). However, only ~10% of adult newborn cells migrates and maturates in the GL. The maturation process of these cells follows a similar time-course as GCs and within 6 weeks these cells have mature-like spiny dendritic morphology, although not all the generated cells reach complete maturation (Whitman and Greer, 2009). As in GCs, the functional maturation of newborn PG cells is reflected by a gradual expression of voltage dependent ion channels, an increasing number of synaptic inputs as well as a growing expression of glutamate and GABA receptors (Belluzzi et al., 2003). *In vivo*, newborn PG cells are activated by odorants as early as 2 weeks after their birth. 2 weeks later, newborn PG cells are highly responsive and non-selective to odor stimuli (Livneh et al., 2014). Odor enrichment during newborn PG cells maturation narrows their odor response selectivity, suggesting that the physiological fate of newly generated PG cells is experience dependent (Livneh et al., 2014).

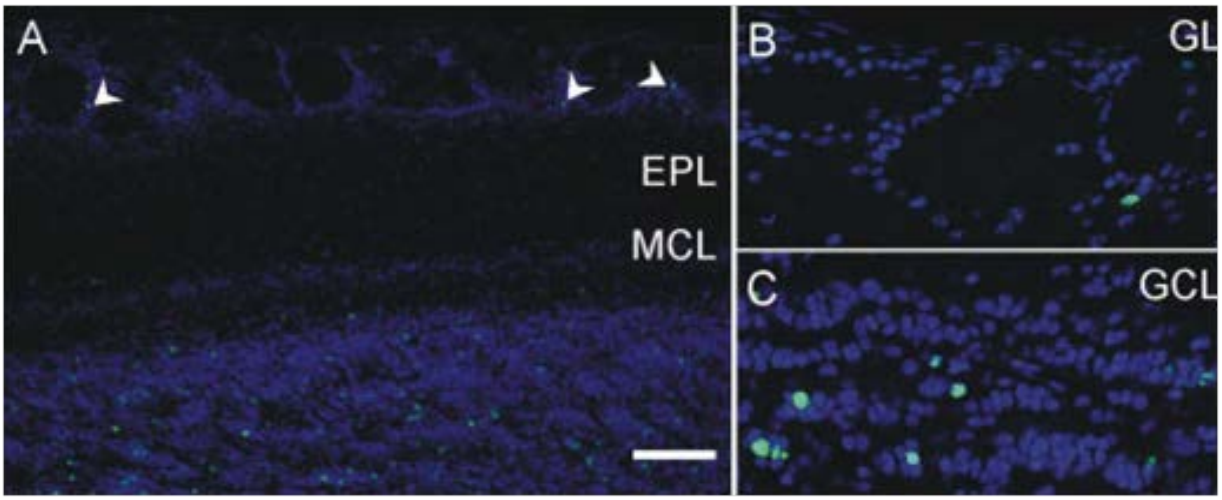

Figure 7. Adult generated interneurons in the Olfactory Bulb. *(A) Low magnification image showing BrdU labeled cells (green) 30 days after BrdU injection, in the glomerular (arrowheads) and granule cell layers. The number of new PG cells is small compared with the number of new granule cells. (B) High magnification view of the GL showing an individual BrdU labeled cell. (C) High magnification view of the GCL showing several BrdU labeled cells. Scale bar 100 µm in A and 38µm in B and C. (Whitman and Greer; 2007)*

1.3 The diversity of Periglomerular cells

As I mentioned previously, PG cells form a heterogeneous population of interneurons. This heterogeneity is reflected by anatomical differences (Pinching and Powell, 1971; Hayar et al., 2004b; Kosaka and Kosaka, 2010; Kiyokage et al., 2010), expression of different molecular markers (Panzanelli et al., 2007; Parrish-Aungst et al., 2007; Whitman and Greer, 2007; Batista-Brito et al., 2008), different membrane properties (McQuiston and Katz, 2001; Hayar et al., 2004b; Murphy et al., 2005; Shao et al., 2009) and differences in synaptic connectivity (Toida et al., 1998; Hayar et al., 2004; Shao et al., 2009; Kiyokage et al., 2010). In the following chapter I will describe these differences in detail and explore the extension of the heterogeneity within the population.

1.3.1 Morphological diversity

The morphological diversity of PG cells lies in their axonal and dendritic projections. Historical controversy resides in the presence or absence of axon from these cells. Some authors consider that PG cells have axons based on Golgi staining showing a short and thin axon-like structure, different than dendritic processes, that projects within a distance of 3 or 4 glomeruli (Pinching and Powell, 1971; Lopezmascaraque et al., 1990). However, the Golgi staining technique only allowed axon detection in rare occasions, and instead of excluding

the axonal presence from other PG cells, it was argued that a staining problem prevented axon visualization in other PG cells. The presence of axon bearing PG cells has also been observed with confocal imaging of newborn interneurons (Tucker et al., 2006). Electron microscopy imaging of the axon initial segment (AIS) of axon-bearing PG cells revealed marked differences with common neuron AIS (Pinching and Powell, 1971). Classical AIS shows typical cellular machinery as neurotubules, free ribosomes, high vesicular concentration, Golgi apparatus and synaptic contacts among others. In contrast, if PG cells presumed AIS contains a limited amount of granular endoplasmic reticulum and many ribosomes, it lacks the presence of most elements cited above. More recently, Kosaka and Kosaka, (2011) did not detect the AIS classical molecular markers, i.e. sodium channel clusters, AnkyrinG, ßIV-spectrin and Phospho-IkBa in thin axon like projections from PG cells. In addition, studies in which PG cells where filled with biocytin then morphologically reconstructed *ad-hoc* suggest that at least a fraction of PG cells do not have axons (Hayar et al., 2004b; Kiyokage et al., 2010; Najac et al., 2015). In conclusion, it is possible that some PG cells do not have axons and others do, reflecting two distinct morphological groups. However, based on my own experience, most of (if not all) the PG cells that I have visualized during patch-clamp recording were axonless suggesting that axon bearing PG neurons described in some studies may in fact be sSACs.

PG cells also have diverse dendritic projections (Figure 8). Most PG cells have a small dendritic tuft that projects inside a single glomerulus (Pinching and Powell, 1971; Hayar et al., 2004b; Kosaka and Kosaka, 2005, 2007, 2008; Kiyokage et al., 2017). However, some PG cells send dendritic projections into two neighboring glomeruli or within the interglomerular neuropil. These PG cells have been called transglomerular cells. They express Secretagogin, a calcium binding protein, and perhaps may be classified as a new cell type (Kiyokage et al., 2010; Kosaka and Kosaka, 2013).

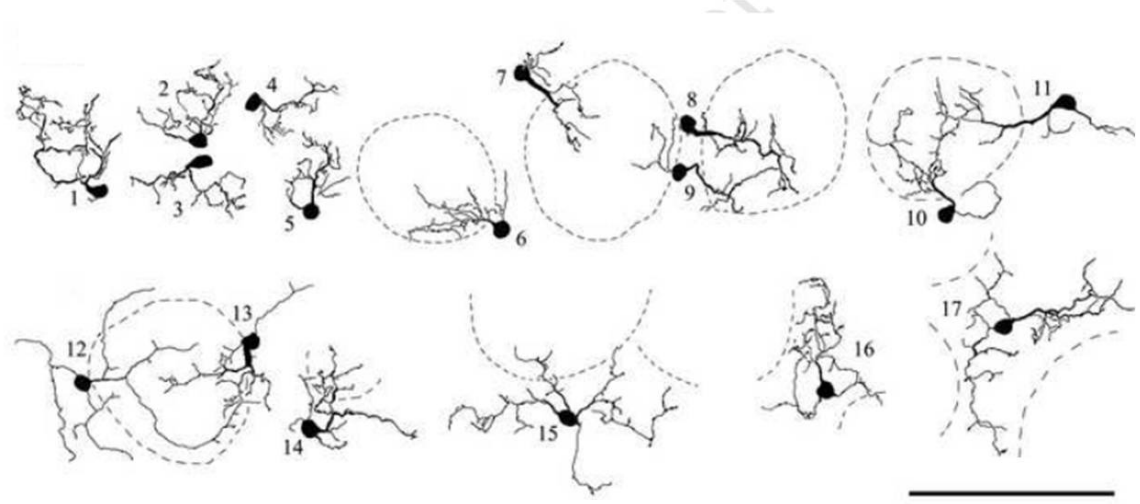

Figure 8. Periglomerular cells morphological diversity. *Camera lucida drawins of calbindin immunostained PG cells. Cells 1-5 and 8 extend their processes into a glomerulus, cell 9into two glomeruli and cells 6, 7, 10-13 extend their major processes into a glomerulus and other processes in the periglomerular region.Dotted lines represent the glomerular edges. Scale bar: 100 µm (Kosaka and Kosaka, 2010)*

1.3.2 PG cell subtypes express diverse molecular marker

Considering the morphological differences among PG cells, it is hard to give a precise definition of what exactly a PG cell is. To narrow these criteria, immunohistochemical labeling is a common tool for identification of interneuron populations. Some of the classical molecular markers of interneurons are calcium binding proteins such as CR, CB or PV and neuroptides such as VIP or SOM (Demeulemeester et al., 1991; Kawaguchi and Kondo, 2002; Rudy et al., 2011). Immunohistochemical characterization of the OB in different mammal species has revealed that most PG cells are immunoreactive to at least one of four molecular markers. Among these markers there are two neurotransmitters and two calcium-binding proteins. The neurotransmitters are: GABA or its synthesis enzyme GAD and dopamine (DA) or the enzyme involved in its synthesis TH. The calcium binding proteins most commonly expressed by PG cells are CB and CR (Figure 9) (Kosaka et al., 1997; Toida et al., 1998; Panzanelli et al., 2007; Parrish-Aungst et al., 2007).

Immunohistochemistry combined with transgenic mouse lines expressing green fluorescent protein (GFP) under the promotor of one of the two GAD isoforms were used to roughly quantify each subpopulation. In the GAD65-GFP mouse, ~37% of the GL cell population are labeled with GFP while immunolabeled GAD67(+) cells represent ~30% indicating that GABAergic neurons constitute the majority of al JG cells (Parrish-Aungst et al., 2007). An interesting feature is that, most GABAergic cells co-localize either with TH(+),

CB(+) or CR(+) neurons, revealing the existence of at least three non-overlapping GABAergic subpopulations. The three markers can be coexpressed with either GAD isoforms, although preferentially with GAD67. This observation suggests that GAD isoforms expression is not a good means to differentiate PG cell populations (Panzanelli et al., 2007; Parrish-Aungst et al., 2007). Among all the immunohistochemical studies comparing the proportions of these three populations, CR(+) immunoreactive cells are always 2-3 times more abundant than CB or TH-expressing cells (Kosaka and Kosaka, 2007; Panzanelli et al., 2007; Parrish-Aungst et al., 2007). Moreover, CB(+) and TH(+) cells represent each ~15% of the glomerular GABAergic cell population. In other words, together these analysis suggest that CR(+) cells may constitute up to 45% of the total population of PG cells (Kosaka and Kosaka, 2007; Panzanelli et al., 2007; Parrish-Aungst et al., 2007).

The classification of TH(+) juxtaglomerular cells as PG cells is a matter of debate and complicates the analysis of PG cell diversity. As already mentioned, TH(+) JG cells englobe two morphologically distinct populations (Pignatelli et al., 2005; Kosaka and Kosaka, 2008; Chand et al., 2015). 70% of the TH(+) neurons in the GL coexpress the GAD67 isoform (Parrish-Aungst et al., 2007). Anatomical *post-hoc* reconstruction of TH(+) / GAD67(+) cells clearly show two groups innervating multiple glomeruli. One group is formed by cells with large ovoid somas (~11µm) and pluriglomerular extending projections whereas the second group includes round small soma-sized (~7µm) neurons projecting into nearby glomeruli (Davis and Macrides, 1983; Kosaka and Kosaka, 2007; Kosaka and Kosaka, 2008; Kiyokage et al., 2010). If we consider that PG cells are monoglomerular and lack axons this criteria would exclude all GAD67(+)/TH(+) neurons from the PG cell classification. However, approximately 7% of the TH(+) JG cells are GAD65(+) and essentially monoglomerular (Kiyokage et al., 2010) suggesting that this small fraction of TH(+) cells may be the only one to be considered as PG cells whereas the majority should be considered as SACs.

The calcium binding protein neurocalcin is another marker that labels a specific group of JG cells. However, these neurocalcin (+) neurons have large somas (10 µm) compared to CB(+) or CR(+) PG cell, resembling more to ET cells. Other molecular markers have been used, but less frequently, to identify additional PG cell subtypes. A group of PG cells that does not overlap with CB, CR and TH(+) cells, express the alpha5 $GABA_A$ receptor subunit. This group coexpressed the GAD67 isoform and represents 15% of the GAD67(+) population in the GL (Panzanelli et al., 2007). PV(+) neurons are also present in the GL, but their

presence is almost anecdotic with an average of 2 cells/glomerulus (Parrish-Aungst et al., 2007; Whitman and Greer., 2007). NOS, the enzyme involved in nitric oxide catalysis that may act as a neurotransmitter (Yamamoto et al., 2015) labels a heterogenous population among which 60% are small PG-like cells, that colocalize with GAD/GABA and CR staining (Crespo et al., 2003; Kosaka and Kosaka, 2007).

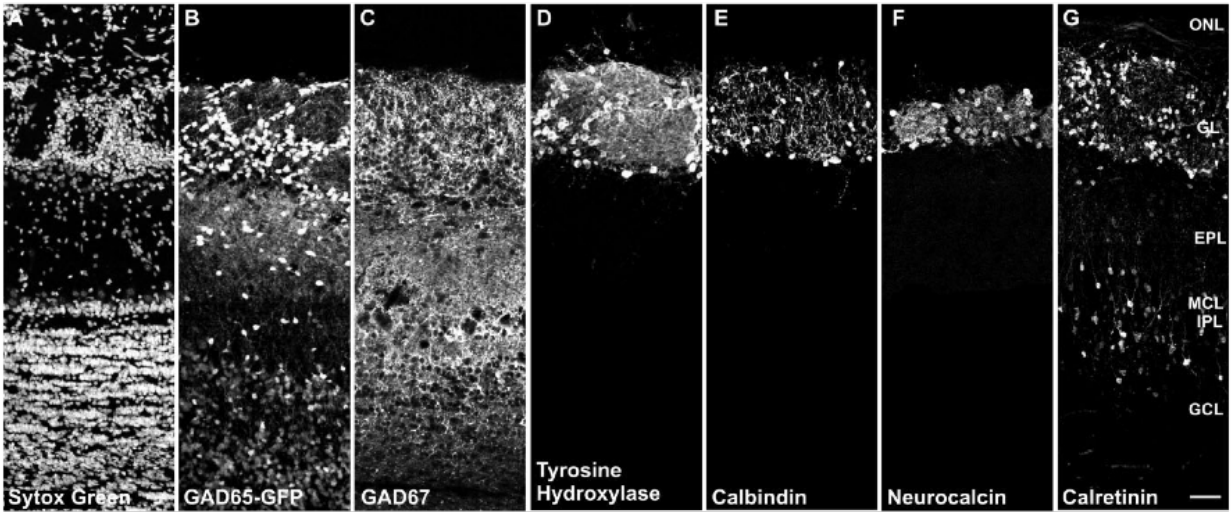

Figure 9. Expression of different molecular markers in the Olfactory Bulb. (A) Sytox Green nuclear staining. *(B) GFP is expressed in all the layers of the OB of theGAD65-GFP transgenic mouse except the ONL.(C) GAD67(+) immunostainig labels cells in all the layers except de ONL. (D-F) TH, CB and Neurocalcin staining is restriced to the GL. (G) CR expression is detected in all the layers of the bulb and highly concentrated in the GCL and GL. Scale bar 50µm. (Parrish-Aungst et al., 2007).*

1.3.3 PG cells have diverse membrane properties

Several studies have shown diverse action potential firing patterns among PG cells (Figure 10) (Wellis and Scott, 1990; Puopolo and Belluzzi, 1998b, a; McQuiston and Katz, 2001; Murphy et al., 2005; Shao et al., 2009; Najac et al., 2015; Fogli Iseppe et al., 2016). Thus, some PG cells respond to a suprathreshold depolarizing step with accommodating or non-accommodating trains of action potentials, some with a single sodium spike and some with sodium action potentials riding on the top of a calcium channel-mediated action potential. PG neurons also show diverse responses to a brief hyperpolarizing current, a protocol that reveals the expression of hyperpolarization-activated cyclic nucleotide-sensitive cation (HCN) channels. Hyperpolarization-activated cationic currents (Ih) are seen in only a subset of PG cells (Figure 10) (McQuiston and Katz, 2001; Wahl-Schott and Biel, 2009; Najac et al., 2015) Consistent with this, Holderith et al., (2003) found that only 10% of JG cells strongly express HCN1, one of the subunit forming the HCN channels. Finally, PG

cells are also diverse regarding K^+ conductances (Puopolo and Belluzzi, 1998b). One group expresses a delayed rectifier potassium current and a fast transient A-type current of similar amplitude, while a second group of PG cells only express the fast transient A-type current. Recently, Fogli Iseppe and colleagues identified identified the latter group as CR(+) PG cells. (Fogli Iseppe et al., 2016) CR(+) PG cells also express Ih currents and fire a single action potential. This work and the work recently done in our lab, are among the few studies matching an immunohistochemically-defined subclass of cells with physiological properties.

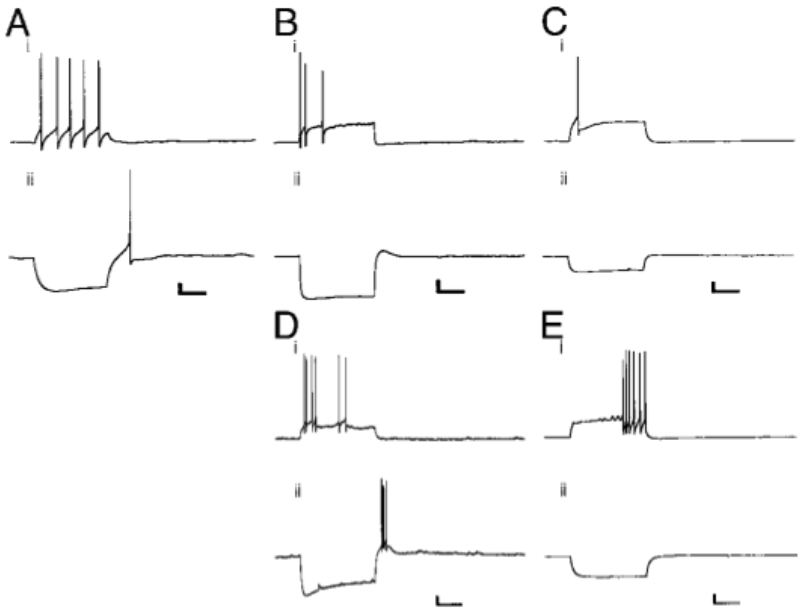

Figure 10. Periglomerular cells responses to current injection reveals membrane properties diversity*. Ai, Bi, Ci, Di, Ei: Membrane potential (Vm) response of a PG cell to a depolarizing current injection (600 ms). Ai produced non accommodating action potentials; Bi produced accommodating action potentials; Ci produced only an individual action potential response; Di displayed irregular firing; Ei produced a delayed firing in response to depolarizing current injection. Aii, Bii, Cii, Dii, Eii: The Vm response of the same cells to hyperpolarizing current injection (600 ms). Aii overshoots rest and produced an action potential; Bii and Cii, show a small depolarizing sag during hyperpolarizing current injection. Dii produced a depolarizing sag during hyperpolarizing current injection. Eii, did not show any depolarizing sag during hyperpolarizing current injection. All scale bars: vertical, 10 mV; horizontal, 200 ms. (McQuiston and Katz, 2001)*

1.3.4 Synaptic diversity: Type1 vs Type2 PG cells

In terms of synaptic connectivity PG cells have been classified into two classes, commonly referred as type 1 and type 2 PG cell. This classification was established during the 1990s by Kosaka and colleagues based on morphological features revealed using electron microscopy and immohistochemistry techniques in different mammal species (Kosaka et al 1997, 1998, 2005). Type 1 PG cells have dendrites projecting into the OSN and non-OSN zones of the glomeruli. In contrast, type 2 PG cells only project their dendrites into

the non-OSN zones. Quantification analysis based on this morphological feature revealed that type 2 cells are more numerous than type 1 PG cells in a 3:1 ratio, although this ratio has to be taken with caution due to errors on PG cell identification (Kosaka et al 1997). Consistent with this classification, only a minority of PG cells receive monosynaptic OSN inputs in patch-clamp recording and can be functionally classified as type 1 PG cells (Shao et al., 2009). Combination of immunostained cells and transgenic mice expressing GFP under the control of GAD promoters revealed that CR(+) and CB(+) PG cells are type 2 PG cells and make dendro-dendritic reciprocal synapses onto M/T cells within the non OSN-zone of the glomeruli (Kosaka et al. 1997; Toida et al., 1998; Kosaka and Kosaka, 2005; Panzanelli et al., 2007; Parrish-Aungst et al., 2007).

1.3.5 Heterogeneity of postnatally-generated periglomerular cells

Several studies have shown the presence of CR(+), CB(+), PV(+) and TH(+) populations among adult-generated PG cells (Figure 11) (Winner et al., 2002; Mandairon et al., 2006; Whitman and Greer, 2007). This knowledge is of great importance to selectively study the origin and fate of the different subpopulations of newly generated interneurons. Using diverse techniques such as viral infection, genetic fate-mapping or targeted electroporation it has been shown that the different walls of the SVZ give rise to specific populations of GCs and PG cells (Kohwi et al., 2007; Merkle et al., 2007; Figueres-Onate and Lopez-Mascaraque, 2016). There is multiple evidence about anatomical and temporal differences in the generation of the different types of PG cells. CR(+) cells are generated by the medial and dorsal walls of the SVZ, whereas CB(+) and TH(+) cells are generated by the dorsal and lateral wall, respectively (Kohwi et al., 2007; Merkle et al., 2007; Fernandez et al., 2011). Timewise, there is a decrease in PG cell generation from neonatal to adult stages in mice, as well as a shift in the molecular identity of the newly generated PG cells. At neonatal stages newborn generated PG cells are ~50% CB(+) and ~25% CR(+). However, during adulthood, CB(+) PG cell production dramatically drops to ~10%, while CR(+) adult born PG cell generation increases up to 50% (De Marchis et al., 2007). The reason of this change remains unknown but it suggest that CR(+) PG neurons could have some active implication in odor processing during adulthood.

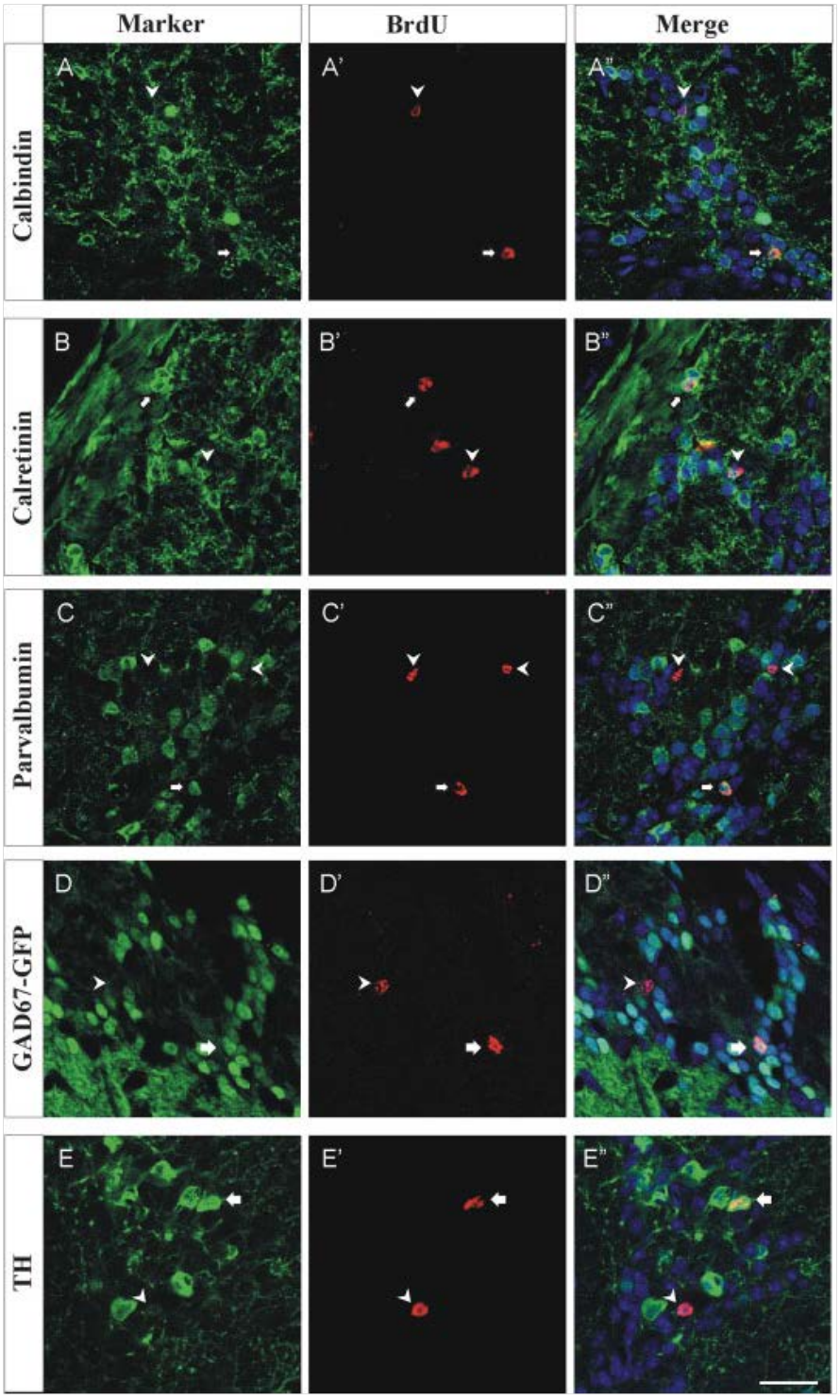

Figure 11. Adult newborn Periglomerular cell heterogeneity. *Thirty days after BrdU injection, BrdU labeled cells (red, middle column) can be found expressing calbindin (A,A"), calretinin (B,B"), parvalbumin (C,C"), GAD67 (D,D"), and TH (E,E"). Double labeled cells are marked with arrows. Examples of BrdU labeled cells not expressing each marker are labeled with arrowheads. (Whitman and Greer, 2007)*

Chapter II. SYNAPTIC CIRCUITS AND PHYSIOLOGY OF THE OLFACTORY BULB

In the OB, synaptic connections mainly occur at two levels, the GL and the EPL. In the GL, glomeruli are the basic functional unit for early odor processing. These compartmentalized neuropils of high synaptic density receive odor information from specific OR-expressing OSNs and transform it into a spatial and temporal code. The activity of each unit is not only controlled by specific OSN inputs but also by intraglomerular and interglomerular synaptic interactions. Dendro-dendritic interactions between M/T cell lateral dendrites and GABAergic interneurons in the EPL mediate reciprocal and lateral inhibition of principal neurons. Toghether, these synaptic interactions cause and shape odor-evoked gamma, beta and theta oscillations that are thought to contribute to odor coding. I will here review the principal OB synaptic circuits and highlight their function for odor processing.

2.1 Intraglomerular synaptic circuits

2.1.1 Glomerular activation of M/T and ET cells

Early electron microscopy studies show the existence of asymmetric excitatory synapses between the terminals of the OSNs and the apical dendrites of principal bulbar neurons within the OSN glomerular compartments (Pinching and Powell, 1971). For a long time this was the only evidence of such interactions but the postsynaptic cell subtype (M, T or ET) could not be precisely identified. However, in OB slices, an electrical stimulation of the OSN evokes different excitatory responses in M, T and ET cells (Figure 12A). In ET cells, OSN stimulation produces a large and fast monosynaptic α-amino-3-hydroxy-5-methyl-4-isoxazolepropionic acid (AMPA) receptor-mediated depolarization that drives a burst of action potentials (Hayar et al., 2004b; De Saint Jan et al., 2009). In contrast, M cells respond to the same stimulus with a complex biphasic and long-lasting glutamatergic response. These evoked synaptic responses have a similar time course as spontaneously occurring long lasting depolarization (LLD) that are synchronized in M/T cells projecting in the same glomerulus (Carlson et al., 2000; Schoppa and Westbrook, 2001; De Saint Jan and Westbrook, 2007; De Saint Jan et al., 2009; Najac et al., 2011).

The first phase of the M cell response is fast, mediated by AMPA receptors, and occurs within a short latency after the stimulation consistent with a monosynaptic response mediated by glutamate release from the OSNs. The slow component is mediated by AMPA, N-methyl-D-aspartic acid (NMDA) and mGluR1 receptors (De Saint Jan and Westbrook, 2007; De Saint Jan et al., 2009; Najac et al., 2011) and results from dendro-dendritic recurrent glutamatergic interactions between all principal cells projecting into the same glomerulus (Figure 12B) (De Saint Jan et al., 2009; Najac et al., 2011; Vaaga and Westbrook, 2016). Excitatory synapses between principal cells projecting into the same glomerulus have been described first between M cells (Schoppa and Westbrook, 2002; Urban and Sakmann, 2002) and later between M, T and ET cells (Figure 12C) (De Saint Jan et al., 2009; Najac et al., 2011). This second phase is driven by the highly excitable ET cells that fire earlier and in response to weaker OSN inputs than M/T cells. Activated ET cells release glutamate onto M and T cells leading to their activation, and subsequent recurrent excitation between them. This cascade of events leads to an intraglomerular build-up of glutamate that produces LLDs (De Saint Jan et al., 2009; Najac et al., 2011). T cells responses are essentially similar as those of M cells (Najac et al., 2011; Gire et al., 2012; Burton and Urban, 2014; Vaaga and Westbrook, 2016) although they receive a stronger OSN inputs than M cells (Gire et al., 2012; Burton and Urban, 2014).

Under some conditions, OSN stimulation only evokes a slow excitatory response lacking the fast component in M cells as you can see in Figure 12 D (Carlson et al., 2000; Gire and Schoppa, 2009; Najac et al., 2011; Gire et al., 2012; Vaaga and Westbrook, 2016). This observation led some researchers to question the direct excitation of M/T cells by OSNs and to claim that the M cell response is a purely plurisynaptic feedforward excitation driven by ET cells. These authors argue that the initial fast component of the M/T response is an artefact caused by the direct electrical stimulation of the dendrites (Gire and Schoppa, 2009; Gire et al., 2012). ET cell OSN-evoked excitatory post synaptic currents (EPSCs) are certainly larger than the first component of the M cell response, suggesting more OSN synaptic contacts, but their delay and time course are identical (Najac et al., 2011; Gire and Schoppa, 2012; Vaaga and Westbrook, 2016). Moreover, Vaaga and Westbrook (2016) demonstrated that OSNs release glutamate with the same release probability and quantal amplitude on both M and ET cells. Finally, recent ultrastructural evidence unambiguously confirmed the

existence of OSNs to M cells synapses ruling out Gire and Schoppa's hypothesis (Najac et al., 2011; Vaaga and Westbrook, 2016; Bourne and Schoppa, 2017).

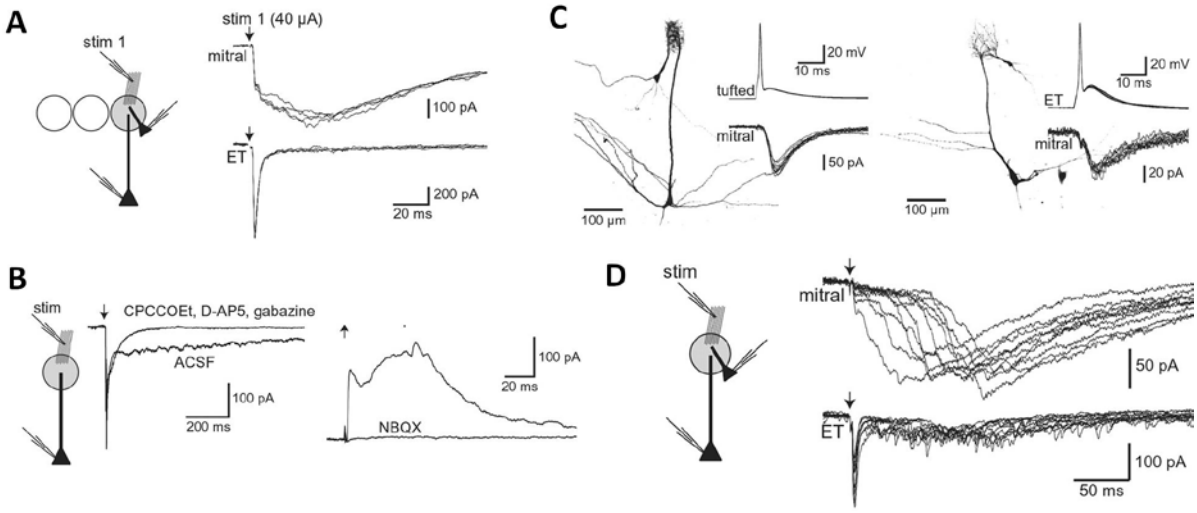

Figure 12. Activation of External Tufted and Mitral cells. *A, OSN-evoked responses recorded simultaneously in a mitral cell and an ET cell projecting into the same glomerulus. OSN stimulation evoked a biphasic slow AMPA receptor-mediated EPSC in the mitral cell and a fast monosynaptic EPSC in the ET cell. B, The slow component of the mitral cell response is shortened in the presence of NMDA receptor, mGluR and $GABA_AR$ antagonists (left, in voltage-clamp). Yet, the AMPA receptor-mediated component is still biphasic (right, in current clamp). C, Paired recording between T and M cells (left) and between ET and M cells (right) demonstrate excitatory synaptic interactions between these neurons. D, Paired recording of a mitral and ET cell response to weak stimulations of the OSNs. The monosynaptic input is lacking or difficult to detect in some of the mitral cell responses, whereas it is clearly visible in the ET cell.(from Najac et al., 2011)*

2.1.2 Odor-evoked M/T cells activation *in vivo*

Odor evoked responses in M/T cells are diverse and concentration dependent. Thus, M/T cells can be excited, inhibited or both in response to a given odorant (Wellis and Scott, 1990; Cang and Isaacson, 2003; Fletcher et al., 2009; Davison and Katz, 2007; Fukunaga et al., 2012; Kato et al., 2012; Economo et al., 2016). M/T cells fine tuning at low odor concentration broadens with concentration increase (Tan et al., 2010). One odorant evokes diverse responses among a group of cells but the response of one given cell is always specific to one specific odor. Thus, a given odorant is represented by the modulation of the firing within a given population.

In vivo, in absence of olfactory inputs, M/T cells exhibit slow respiration-locked membrane depolarizations at low theta frequency (Margrie and Schaefer, 2003; Fukunaga et

al., 2012). It has been suggested that this activity may possibly be driven by ET cells spontaneous firing and reflect the LLDs observed in slices (Hayar et al., 2004a). However, these theta oscillations are also very closely related to the respiration cycle and sniffing (Carey and Wachowiak, 2011; Rojas-Libano et al., 2014). At resting state the respiration rhythm is ~2 Hz in rats and ~5 Hz in mice, but it changes with sniffing, reaching ~10 Hz frequency. The increase of the respiration rhythm is correlated with an increase of M/T cell rhythmicity and firing frequency, that can reach 100 Hz per respiration cycle (Carey and Wachowiak, 2011). Thus, M/T cell firing is rhythmic and narrowly coupled with respiration rhythm. This tight coupling between respiration frequency and postsynaptic theta rhythms suggests that OSN inputs also contribute in driving M/T cell theta activity.

In vivo experiments suggest that T cells respond to lower concentrations of odors and within a shorter latency than M cells (Igarashi et al., 2012; Kikuta et al., 2013). *In vitro* and *in vivo* experiments recently confirmed that T cells fire earlier than M cells in response to weak OSN stimulation (Fukunaga et al., 2012; Geramita and Urban, 2017). Geramita and Urban proposed that this difference between M and T cells is caused by stronger OSN excitatory inputs and weaker intraglomerular inhibition on T cells than on M cells. Consistent with this idea, T cells periodic subthreshold depolarizations and firing phase occur earlier than M cells within the respiration cycle. T cells fire during the exhalation phase of the respiration cycle while M cells preferentially fire during the inhalation phase. This temporal shift is abolished when intraglomerular inhibition is impaired (Fukunaga et al., 2012, 2014).

Most experiments *in vivo* are done in anesthetized mice. However, Kato et al., (2012) recently demonstrated that anesthesia has a major impact on odor-evoked cell activation. They compared the effect of an odor in the same groups of cells in awake and anesthetized mice using electrophysiological recordings and calcium imaging. Their results show that wakefulness sparsens M cell odor responses and enhances GC activity, revealing that the activation maps in anesthetized animals are not completely precise, and more importantly, that the generated temporal activity is certainly altered.

2.1.3 Glomerular activation of PG cells

As I previously mentioned, so called type 1 PG cells partially project into OSN-zones of the glomeruli. In these PG cells, OSN stimulation evokes short latencies, synchronous monosynaptic EPSCs mediated by glutamate AMPA receptors consistent with direct

glutamatergic synaptic inputs from the OSNs (Figure 13 A,C) (Toida et al., 1998; Hayar et al., 2004b; De Saint Jan and Westbrook, 2007; Shao et al., 2009; Kiyokage et al., 2010), followed, in some cases, by a burst of EPSCs consistent with a disynaptic or polysynaptic input (Hayar et al., 2004b). In contrast, type 2 PG cell dendrites do not enter the OSN zones and exclusively establish dendro-dendritic synapses with principal neurons within the non-OSN zone. Type 2 PG cells respond to OSN stimulation with a barrage of polysynaptic EPSCs mediated by AMPA and NMDA receptors (Figure 13 C, D). This response has a longer onset latency and larger jitter than the monosynaptic response of type 1 PG cells. Yet, latencies and jitters of type 2 PG cell responses decrease with increasing stimulation intensities which reflects an increasing fidelity of a disynaptic circuit at higher stimulus intensity (Figure 13E, F) (Hayar et al., 2004a; Shao et al., 2009).

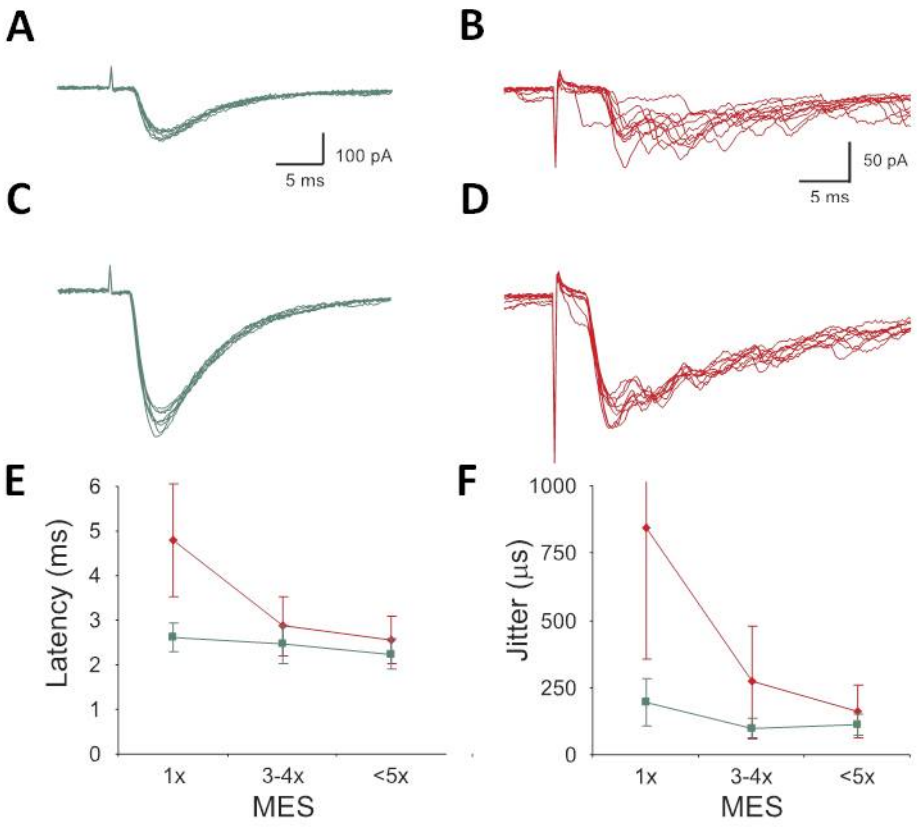

Figure 13. Activation of Type1 vs Type2 PG cells. *A and C, Type 1 PG cells respond to OSN stimulation with a fast monosynaptic EPSC whose latency and jitter vary little with the strength of the stimulation. B and D, In contrast, type 2 PG cells respond with a burst of polysynaptic EPSCs whose latency and jitter decrease with the stimulation intensity. E and F, Graphs showing the latency of the OSN evoked response (E) and the jitter (J) in type 1 PG cells (green) and type 2 PG cells (red) at increasing intensities of stimulation. MES (Minimal effective stimulation) (Shao et al., 2009).*

The Shipley group has claimed that ET cells provide the main excitatory input to type 2 PG cells because ~65% of GAD65(+) PG cells spontaneously received burst of EPSCs, consistent with postsynaptic responses to the bursts of action potentials fired by ET cells (Hayar et al., 2004a; Shao et al., 2009). This assumption also relies on paired PG-ET cell recordings occasionally showing correlated spontaneous activities. However, these observations do not exclude the implication of M/T cells on type 2 PG cells excitation. Indeed, we have recently demonstrated using paired recordings that CB(+) type 2 PG cells are not only connected to ET cells but also receive glutamatergic inputs from M and T cells (Najac et al., 2015).

2.1.4 Type 1 PG cells mediate presynaptic inhibition of OSN glutamate release

Whole cell recordings of type 1 PG cells have shown that the amplitude of their OSN-evoked EPSC is decreased when the stimulation is preceded by a depolarizing step on the recorded cell. This effect disappears in the presence of a $GABA_B$ receptor antagonist (Figure 14) (Murphy et al., 2005; Shao et al. 2009). This simple experiment demonstrates that GABA release from type 1 PG cells activates presynaptic $GABA_B$ receptors that inhibit glutamate release from OSN terminals. Thus, type1 PG cells mediate a form of $GABA_B$ receptor-dependent feedback inhibition of OSN axon terminals (McGann et al., 2005; Murphy et al., 2005; Shao et al., 2009). *In vitro*, OSN presynaptic inhibition is restricted to the activated glomerulus and does not affect OSNs projecting into neighboring glomeruli. Consistent with this, this pathway does not modify odor-evoked glomerular activation cartography *in vivo* (McGann et al., 2005; Pirez and Wachowiak, 2008).

$GABA_B$ receptor activation is not the only mechanism involved in the modulation of OSN release probability (Ennis et al., 2001). DA and GABA released from sSACs act together to modulate presynaptic glutamate release (Maher and Westbrook, 2008). Selective activation of sSACs in mice expressing light gated protein Channelrhodopsin 2 (ChR2) on TH(+) neurons reduces OSN release probability via DA D2 receptors thereby reducing postsynaptic spiking of both M and ET cells (Pirez and Wachowiak, 2008; Vaaga et al., 2017).

Feedback inhibition from type1 PG cells and sSACs on OSN axon terminals might therefore have a major role in spatiotemporal odor representation. By controlling glutamate release and synaptic transmission between OSNs and M/T cells these pathways modulate both the OB sensory input and output. Moreover, as PG cells have a high input resistance (~1

GΩ), they can be activated by weak OSN inputs and play the role of gatekeepers shunting weak OSN inputs (Gire and Schoppa, 2009).

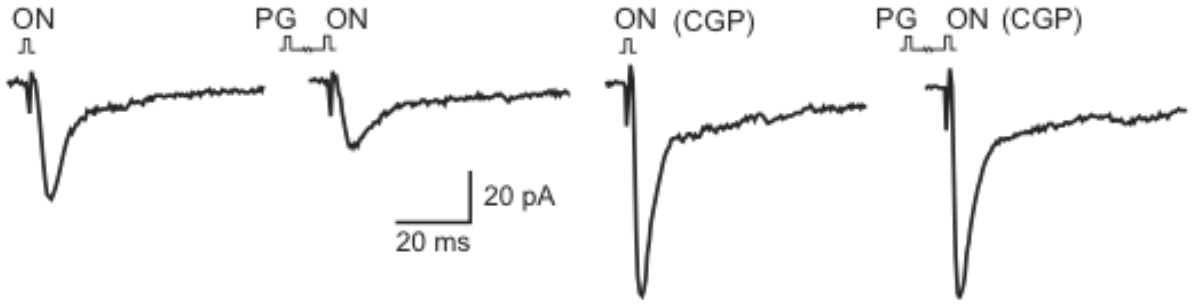

Figure 14. $GABA_B$ dependent OSN-evoked presynaptic inhibition. *Top left traces, The amplitude of the OSN-evoked Type 1 PG cell EPSC is reduced when the stimulation is preceded by a depolarization step of the recorded cell. This effect is blocked in the presence of the $GABA_B$ receptor antagonist CGP55845 (right traces). Note the larger amplitudes of the EPSC in the presence of CGP suggesting tonic inhibition of OSN glutamate release by $GABA_B$ receptors (Shao et al., 2009)*

2.1.5 Type 2 PG cells mediate intraglomerular inhibition of principal neurons

Pinching and Powel (1971) anatomical observations indicate that PG cells make synapses onto principal neurons, some of them being reciprocal. Consistent with this, Murphy et al. (2005) suggested that the reciprocal inhibition produced by a single ET cell depolarization comes from PG cells, although direct evidence is lacking. According to Dong et al. (2007) PG cells could provide as much as 50% of M/T cells inhibitory inputs (Dong et al., 2007). More recently, M/T and ET cell recordings show that OSN stimulation produces a barrage of $GABA_A$ receptor mediated inhibitory post synaptic currents (IPSCs) competing with the excitatory response (Figure 15B) (Najac et al., 2011; Shao et al., 2012; 2013). Local intraglomerular perfusion of a $GABA_A$ receptor antagonist abolishes this inhibition, thus demonstrating its intraglomerular origin, and increases M cell and ET firing (Figure 15 B,C) (Shao et al., 2012; 2013). We have recently confirmed using paired-cell recordings reciprocal signaling between CB(+) type 2 PG cells and M/T or ET cells. We further showed how this PG cell mediated inhibition modulates spike timing of M/T cells (Najac et al., 2015). Thus, by reducing ET cell excitatory influence and directly inhibiting M cells, type 2 PG cells may have a critical role in shaping the OB output.

Although these recent findings demonstrate that PG cells mediate a robust inhibition of principal neurons, the physiological implications of this intraglomerular inhibition are still poorly understood. The lack of specific genetic tools to manipulate PG cells and the difficulty to directly record from these small cells *in vivo* also makes it difficult to investigate their

roles in odor processing. However, recent evidence suggests that intraglomerular inhibitory circuits differently modulate M/T cells theta rythms, attributing PG cells a major role causing the temporal segregation of M/T cell activity within a respiration cycle (Fukunaga et al. 2012; 2014). Future research will hopefully clarify how the diverse PG cell subtypes mediate different intraglomerular inhibitory pathways and perform different roles

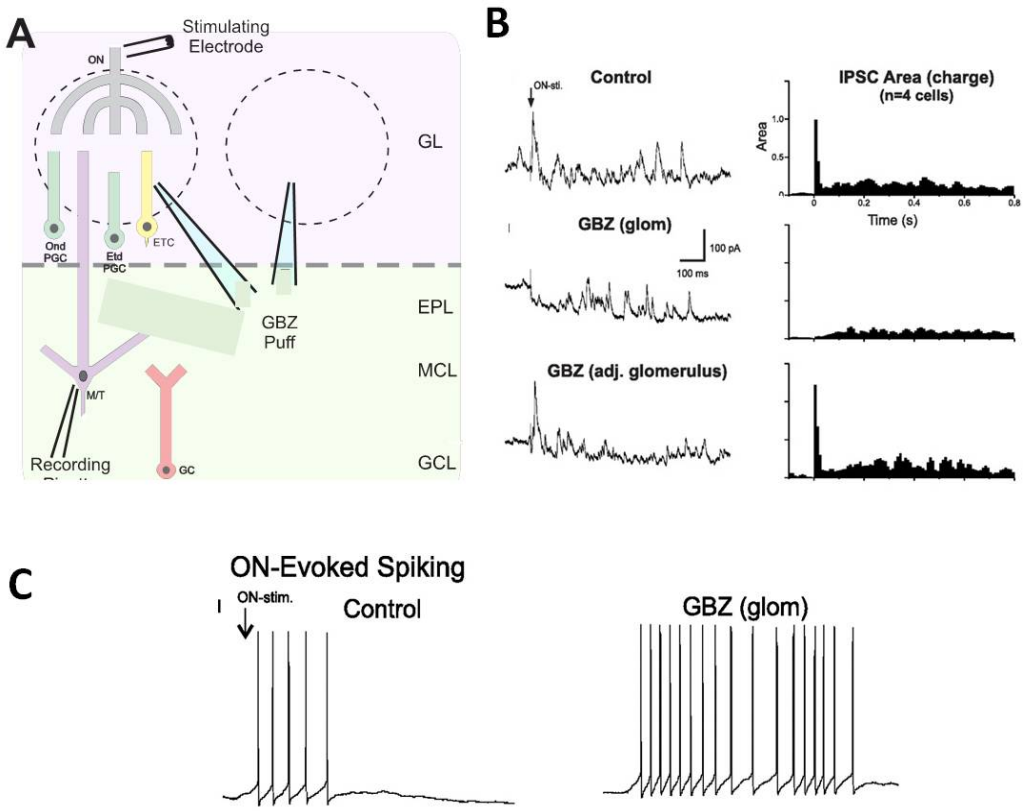

Figure 15. OSN-evoked intraglomerular inhibition of Mitral cells. *A, Diagram of the glomerular circuit and experimental paradigm. B, Top, OSN stimulation evokes an IPSC on the recorded M/T cell. Middle, local perfusion of gabazine (GBZ) within the glomerulus where the recorded M/T cell projects abolishes the early IPSC induced by the stimulation of the OSNs Bottom, GBZ puff in the adjacent glomerulus does not abolish the OSN evoked IPSC. C, OSN-evoked mitral cell spiking is enhanced when glomerular inhibition is blocked (Modified from Shao et al., 2012).*

2.2 Interglomerular lateral interactions

In 2013, two teams simultaneously published *in vitro* studies in which M or ET cells were recorded in horizontal OB slices while a stimulation electrode was placed distant in the GL (Liu et al., 2013; Whitesell et al., 2013). The slices were cut below the GL in between the recording and the stimulation electrode, isolating the ONL and the GL from infraglomerular layers. In both sets of experiments, the electrical stimulation provoked a $GABA_A$ receptor-mediated monosynaptic IPSC in the principal cells. This response was abolished when the

section was done at the glomerular level between both electrodes. These experiments elegantly demonstrated the presence of GABAergic fibers in the GL that mediate interglomerular inhibition (Liu et al., 2013; Whitesell et al., 2013). The two studies identified sSAC as the cell type responsible for this lateral inhibition and ET cells appear as the principal postsynaptic targets of sSAC.

GABA release from sSAC induces a postsynaptic hyperpolarization of ET cells that is followed by a DA-dependent spiking rebound (Liu et al., 2013). Moreover, Liu et al., (2016) recently demonstrated that TH(+) SACs also inhibit M and T cells. This inhibition is strong and suppresses OSN evoked activation of M/T cells. The function of this circuit remains unclear as it could serve to synchronize activity across interconnected glomeruli (Liu et al., 2013) or suppress M/T cell activity in nearby glomeruli (Whitesell et al., 2013; Liu et al., 2016). Interglomerular inhibition might also have a significant temporal component. Indeed, when TH(+)-SACs are activated at sniffing frequencies, M/T cells activity is blocked suggesting that activation of one glomerulus could inhibit less active glomeruli during the respiration cycle (Liu et al., 2016).

In vivo, TH(+)-sSACs respond to odor stimulus in an odor-specific and concentration-dependent manner (Banerjee et al., 2015). In this study, the authors demonstrate that optogenetic manipulation of TH(+)-sSACs suppress odor-evoked responses of M cells. According to the authors, the observed effect is indirect, and primarilly target ET cells coupled to sSACs through chemical and electrical synapses. This observation suggests that the SAC-ET cell circuit may play the role of gatekeeper of the glomerular output.

2.3 Dendro-dendritic interactions in the EPL

The EPL hosts the synapses between GCs, EPL-interneurons and M/T cells lateral dendrites. Most of these synapses are reciprocal and connect M/T cells projecting into different glomeruli. They are poised to mediate lateral inhibition between glomeruli coding for different odorants. In addition, they are instrumental in binding the firing of principal neurons and inducing fast odor-evoked gamma oscillations.

2.3.1 Local dendro-dendritic inhibition at reciprocal synapses

Reciprocal synapses are a particular feature of the OB classically defined as "two synaptic complexes immediately adjacent to each other, which are polarized in opposite directions" (Figure 16) (Rall et al., 1966; Price, 1968). Thus, a release site for glutamate in the principal neurons faces a release site for GABA in the interneuron dendrite. Dendritic action potential propagation along M/T dendrites (Bischofberger and Jonas, 1997; Chen et al., 1997; Chen et al., 2002; Debarbieux et al., 2003) triggers dendritic release of glutamate that activates AMPA and NMDA receptors located on postsynaptic GC spines. The resulting local postsynaptic depolarization of the spine induces GABA release and hence, recurrent or reciprocal inhibition of the M/T dendrite. GABA release is strongly impaired when NMDA receptors are blocked suggesting that NMDA receptors-mediated Ca^{2+} entry and slow spine depolarization are essential in this local signaling (Isaacson and Strowbridge, 1998; Schoppa et al., 1998; Chen et al., 2000; Halabisky et al., 2000; Isaacson, 2001; Halabisky and Strowbridge, 2003; Dietz and Murthy, 2005; Schoppa, 2006; Balu et al., 2007). In contrast, recurrent inhibition persists in presence of the sodium channel blocker tetrodotoxin (TTX) indicating that dendro-dendritic interaction can be local and does not require GC firing (Isaacson and Strowbridge, 1998; Schoppa 1998; Chen et al., 2000). In OB slices, M/T cells OSN-evoked excitation evokes long lasting depolarization of GCs reflecting sustained glutamate release from M cells (Schoppa, 2006). The same stimulation not surprisingly induces a long barrage of $GABA_A$ mediated IPSCs that can last up to several seconds in M/T cells (Schoppa et al., 1998; Carlson et al., 2000). Direct M cell depolarization evokes similar long lasting inhibitory inputs on the recorded cell (Jahr and Nicoll, 1982; Isaacson and Strowbridge, 1998; Schoppa et al., 1998; Chen et al., 2000; Halabisky et al., 2000). This NMDA receptor dependent recurrent inhibition has long been attributed solely to GC, the most abundant and most studied interneurons in the bulb. However, as we have seen earlier, part of this inhibition is most probably mediated by intraglomerular circuits and EPL interneurons. Thus, although the precise function of these local networks remains elusive, recent advances in OB circuits indicate that M/T cells modulation by reciprocal dendro-dendritic inhibitory circuits is not only mediated by GCs.

In odor discrimination tasks, activated spatio-temporal maps can be very similar. Inhibitory circuits are thought to refine these neural representation of odors (Abraham et al., 2010) and sharpen the activity onset (Margrie and Schaefer, 2003). In rodents, single odors

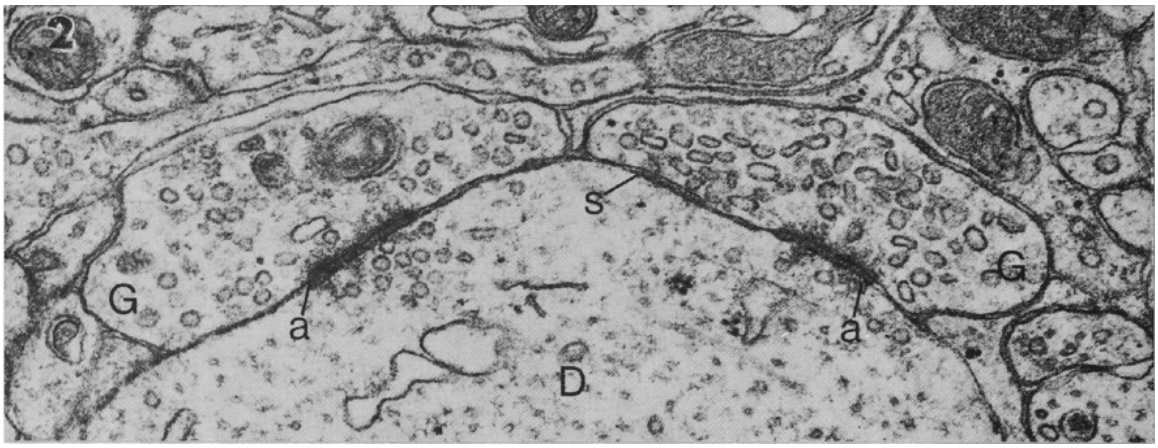

Figure 16. The reciprocal synapse. *Two GC gemmules (G) making synapses on a M/T cell dendrite (D). On the synapse on the right symmetrical (s) and asymmetrical (a) synapse are tagged. The gemmules contain flattened vesicles and the dendrite spherical vesicles. (modified from Price, 1968).*

or simple odor mixture discrimination can occur within less than 200 ms (Uchida and Mainen, 2003; Abraham et al., 2004). However, to discriminate highly similar odors a longer time is required (270-300 ms) (Abraham et al., 2004). When time allowed for discrimination drops below the 200 ms window, odor discrimination accuracy decreases (Uchida and Mainen, 2003; Abraham et al., 2004). Thus, it exists a commitment among accuracy and time response. Selectively manipulating AMPA and NMDA receptors on GCs, Abraham and colleagues demonstrated that synaptic interactions between GC and M/T cells are crucial for fast and accurate discrimination of similar odor mixtures (Abraham et al., 2010). Suppression of NMDA receptors on GCs slows similar odor discrimination, while hyper excitation of GCs has the opposite effect.

Spontaneous and odor-evoked activity provokes Beta (20-30 Hz) and Gamma (40-100 Hz) frequency oscillations across all the layers of the OB (Buonviso et al., 2003; Neville and Haberly, 2003; Lagier et al., 2004; Fukunaga et al., 2014). Buonviso et al., 2003 described that these two frequency bands occur at a different phase within the respiration cycle independently of odor administration. More interestingly, they also described that odor administration drives rhythms coupled to the activity of various cell types in OB layers. Multiple evidence indicate that gamma synchrony and spike timing of M/T cells are orchestrated by GCs through dendro-dendritic reciprocal synapses (Lagier et al., 2004; Schoppa, 2006; Lagier et al., 2007; Lepousez and Lledo, 2013; Fukunaga et al., 2014). For instance, pharmacological manipulations *in vivo* and *in vitro* demonstrate that □gamma activity in the OB is dependent on $GABA_A$ and NMDA receptors (Lagier et al., 2004; Lepousez and Lledo, 2013). Moreover, in mice lacking the $GABA_A$ alpha 1 subunit in M/T cell lateral

dendrites, gamma frequency is notably reduced suggesting the importance of this synapse in fast oscillation generation (Lagier et al., 2007). Finally, recent evidence indicates that fast oscillations mediated by M-GC interactions are necessary for the correct discrimination of similar odors (Lepousez and Lledo, 2013).

The mechanism generating beta oscillations is less clear. However, lesion experiments have shown that when cortical descending inputs are blocked, beta oscillations are reduced or abolished, suggesting that they require reciprocal interactions between the cortex and the OB to be generated (Gray and Skinner, 1988; Martin et al., 2006; Neville and Haberly, 2003)

2.3.2 Lateral inhibition of principal neurons

Lateral inhibition is well described in other sensory systems to filter and tune information. In OB slices, activation of a M cell induces inhibitory inputs in neighboring M cells most likely projecting in different glomeruli (Isaacson and Strowbridge, 1998; Urban and Sakman, 2002). *In vivo*, odorants excite an ensemble of M/T cells associated with a specific subset of glomeruli and suppress the activity of others projecting in different glomeruli (Economo et al., 2016). This form of lateral inhibition could act as a signal filter in which strongly activated OR-specific glomeruli suppress weakly activated glomeruli, thereby reinforcing contrast and increasing the signal to noise ratio between activated and non- or weakly activated glomeruli (Mori et al., 1999; Urban, 2002; Aungst et al., 2003; Shepherd et al., 2007; Arevian et al., 2008). Due to the anatomical organization of the EPL this feature could be mediated by GCs or EPL-interneurons. Using pharmacogenetics, Kato et al., (2013) demonstrate that inactivation of PV(+) EPL-interneurons multiplies the number of M/T cells activated by an odor. These observations suggest that lateral inhibitory circuits tuning the output gain control.

2.4 Inhibition of GABAergic interneurons

Most efforts in understanding the physiology of bulbar interneurons have focused on the activation mechanism of these cells and how their activity impacts the network activity. In contrast, the question of understanding how inhibition of bulbar interneurons influences

OB circuits has not been a major subject of study. Thus, very little is known about the inhibition of bulbar interneurons and only few studies investigated the circuits mediating inhibition of inhibition in the OB. However, given the abundance and functional implications of inhibition in the OB, it seems very likely that this question is of crucial importance.

Puopolo and Belluzzi, (1998a) described for the first time that PG cells in the rat receive spontaneous IPSCs. In this study, they also observed that electrically driven IPSCs could be evoked by directly stimulating in the GL. Understanding how inhibition of PG cells truly impact OB circuits requires to understand the source of this inhibition. Intrabulbar interactions between PG cells have been studied by Murphy et al. (2005). Using paired recordings, the authors show that while an action potential fired by the presynaptic PG cell fails to evoke any postsynaptic current in the postsynaptic PG cell, a longer presynaptic depolarization produces a delayed GABAergic inhibitory current (Figure 17). The time course of this event is slow compared to synaptic IPSCs and not consistent with a direct synaptic input. These experiments have nevertheless been interpreted as evidence for direct PG-PG cell interactions although they are more consistent with indirect signaling through GABA spillover. A fraction of the PG cells also release GABA onto themselves (Figure 17) (Smith and Jahr, 2002; Murphy et al., 2005) but the physiological relevance of this self inhibition is unclear.

Assuming that GABA is inhibitory in PG cells, inhibition of PG cells could lead to disinhibition of the principal neurons and thus modulate the OB output. However, recent evidence suggests that GABA is depolarizing in, at least, some PG cells (Smith and Jahr, 2002; Parsa et al., 2015). Most of these data have been obtained on OB slices from young animals (P12-P17) and the effect has not been clearly demonstrated in adults. Moreover, Smith and Jahr (2002) showed that even if external GABA administration depolarizes PG cells, it still produces a shunting inhibition that impairs the postsynaptic cell to spike. Depolarizing GABA may also induce GABA release thereby enhancing intraglomerular inhibition (Parsa et al., 2015). Besides its effect on OB circuits, the question of depolarizing GABA in developing brain is still a matter of debate. Recent recordings in intact postnatal brain indicate that GABA is inhibitory during development *in vivo* (Valeeva et al., 2016) while evidence suggest that the depolarizing effects of GABA most often observed in slices are attributable to inadequate energy supply in brain slices when glucose is the sole energy source (Rheims et al., 2009; Kirmse et al., 2010).

Even less is known about GC-GC interactions. To my knowledge the only evidence of GC-GC interactions has been provided by Bardy et al. (2010). However, in this study the authors concentrated on adult-generated new neurons and demonstrated using optogenetics that their activation produces IPSCs in PG cells, GCs and dSACs (Bardy et al., 2010). Although most newborn neurons are indeed GCs, diverse subtypes of interneurons may have been activated in this study. These results nonetheless suggest that all major types of interneurons in the OB receive inhibitory inputs from adult-born interneurons.

So far, dSACs are the only interneuronal type proven to mediate intrabulbar interactions with several types of bulbar interneurons (Pressler and Strowbridge, 2006; Eyre et al., 2008; Boyd et al., 2012). More recently, Burton et al. (2016) expressed ChR2 under the chrna2 promoter to activate dSACs with light. They show that a brief pulse of blue light evokes a monosynaptic $GABA_A$ mediated IPSC in PG cells, indicating functional connections between GL-dSACs and PG cells. However, this result has to be considered with caution because the selective expression of ChR2 in dSACs is not clearly demonstrated and expression in centrifugal GABAergic fibers cannot be excluded.

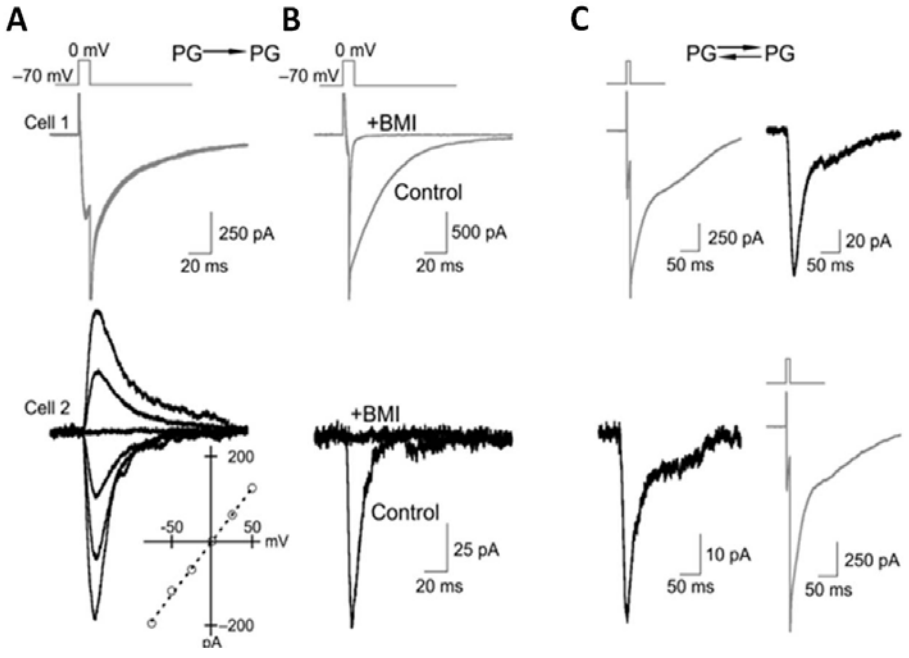

Figure 17. PG-PG cells local interactions. *In paired recordings between two PG cells, a 10 ms long activation of PG cell 1 generates self-inhibition in itself and postsynaptic currents in PG cell 2 held at a variety of membrane potentials. B, both self-inhibitory and postsynaptic currents are abolished by the $GABA_AR$ antagonist bicuculin (BMI). C, This GABAergic signaling is reciprocal (Murphy et al., 2005).*

2.4.1 Centrifugal inhibition

Long range projection inhibitory neurons in the mammalian nervous system are rare and their functional implication is poorly studied. However, such connections are present between cortical and subcortical areas (Alonso and Kohler, 1982; Jinno and Kosaka, 2004; Tomioka et al., 2005) or linking bilateral hippocampus through commissural connections (Ribak et al., 1986; Leranth and Frotscher, 1987). They are usually less considered or underestimated as a key element in most networks but these neurons have all the characteristics to coordinate the timing of activity across different brain areas and might play a major role in network activity (Buzsaki and Chrobak, 1995; Jinno et al., 2007).

The OB receives centrifugal GABAergic afferences from the horizontal limb of the diagonal band of Broca (HDB), a GABAergic/cholinergic structure located in the basal forebrain. However, only one recent paper has reported functional connections between HDB GABAergic centrifugal afferences and bulbar interneurons. Araneda and colleagues selectively transfected GABAergic neurons of the HDB with ChR2 expressing virus (Nuñez-Parra et al. 2013). After 3-4 weeks, in OB slices, optical stimulation provoked monosynaptic IPSCs on GCs, demonstrating functional inhibition of the GCs by the HDB centrifugal fibers (Nuñez-Parra et al. 2013). Local photo stimulation and GABA uncaging experiments were done to explore the precise location of GABAergic synapses in GC. The authors speculate that centrifugal HDB GABAergic afferences act at the somatic and proximal level in GC and thus may have a strong impact on GCs activity. Consistent with this, earlier *in vivo* studies have shown that electrical stimulation of the HDB induces hyperpolarization of GCs and facilitate M cell firing (Figure 18) (Kunze et al., 1991, 1992). Furthermore, electrical lesion in a restricted volume of the HDB/MCPO impairs habituation memory for odors and produces deficits in olfactory sensitivity and motivation (Paolini and McKenzie, 1993, 1996). Using a DREADD/CNO paradigm that allows a pharmacological block of the HDB inhibitory neurons, Nuñez-Parra et al. (2013) also reported that disruption of this pathway alters odor discrimination.

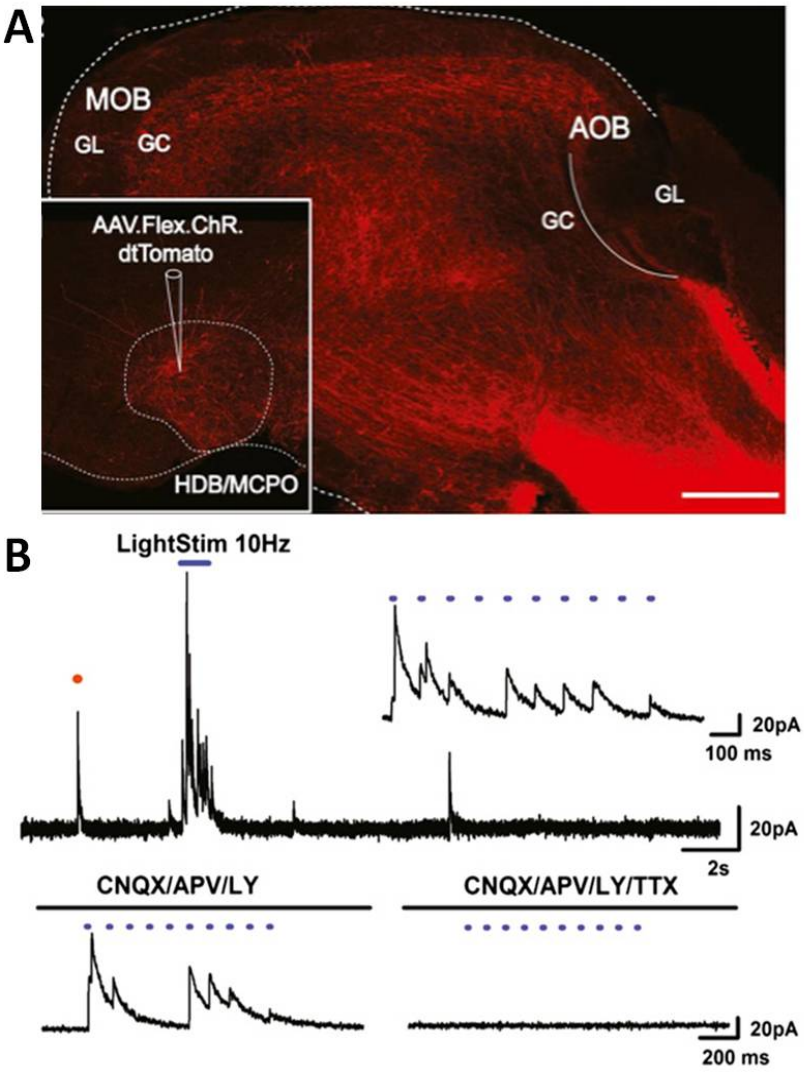

Figure 18. GABAergic centrifugal projections from the HDB inhibit GCs in the OB. *A, Confocal image of a sagittal OB section from a GAD65-Cre mouse injected in the HDB with a Flex.ChR2.dtTomato exoressing virus. This resulted in an extensive labeling of GABAergic fibers expressing ChR2 (red) throughout the inner layers of the OB after injection of ChR2 virus into the HDB/MCPO (inset). Scale bar: 500 µm. B. Top, Blue light stimulus (10 Hz) evokes robust IPSCs in a GC. Inset, expanded evoked response. Bottom, the evoked IPSCs are monosynaptic and persist in presence of AMPA receptor, NMDA receptor and mGluR1α antagonists (CNQX, 10µM; APV, 100 µM; LY367385 100 µM) but are completely abolished by the addition of TTX (0.5µM) (Nuñez-Parra et al., 2013.)*

2.5 Centrifugal afferences to the OB

The OB receives multiple centrifugal afferences arising from the olfactory cortex and other non-olfactory structures of the brain. We have already seen in the previous paragraph that some of the centrifugal afferences are GABAergic and originate from the basal forebrain. In addition, glutamatergic, cholinergic, serotoninergic and adrenergic fibers project within all the layers of the bulb and greatly influence the activity of the bulbar network.

2.5.1 Glutamatergic cortical feedback

The olfactory cortex pyramidal cells send dense glutamatergic feedback projections to the bulb. Anatomical tracing studies showed that these fibers mainly target the GCL and the GL (de Olmos et al., 1978; (Luskin and Price, 1983; Shipley and Adamek, 1984), where they contact GABAergic interneurons thus modulating in an indirect manner M/T cell activity (Balu et al., 2007; Boyd et al., 2012; Markopoulos et al., 2012). In OB slices, stimulation of glutamatergic cortical feedback evokes fast AMPA-mediated EPSCs on the proximal dendrites of the recorded GCs. This proximal glutamatergic input has a stronger effect than the input of M cell lateral dendrites, and increase GC firing rate and therefore presumably influence M cell inhibition (Balu et al., 2007).

Cortical feedback projections are not restricted to the GCL and its global influence on the OB circuit has recently been studied. Stereotaxic injection of viral constructs encoding the light-gated channel ChR2 in the AON of young rats revealed that AON pyramidal neurons activation evokes a monosynaptic excitation followed by a disynaptic inhibition in M cells. The disynaptic inhibition results from the activation of three types of GABAergic interneurons: GCs, sSACs, and PG cells (Markopoulos et al., 2012). Similar experiments targeting the PC provide evidence that this cortical region sends feedback innervation on the same interneuron populations and also mediates disynaptic inhibition of M and ET cells (Figure 19). Deep SACs receive the strongest depolarization from PC pyramidal cells (Boyd et al., 2012). Taken together, these data demonstrate that cortical feedback can modulate the inhibition of principal cells and shape intra- and interglomerular signaling. In awake animals Ca2+ imaging of cortical feedback axons revealed that olfactory cortical feedback is odor specific and sparse (Otazu et al., 2015). Inactivation of the piriform cortex strongly decreases M cell odors selectivity while T cells remained unaffected.

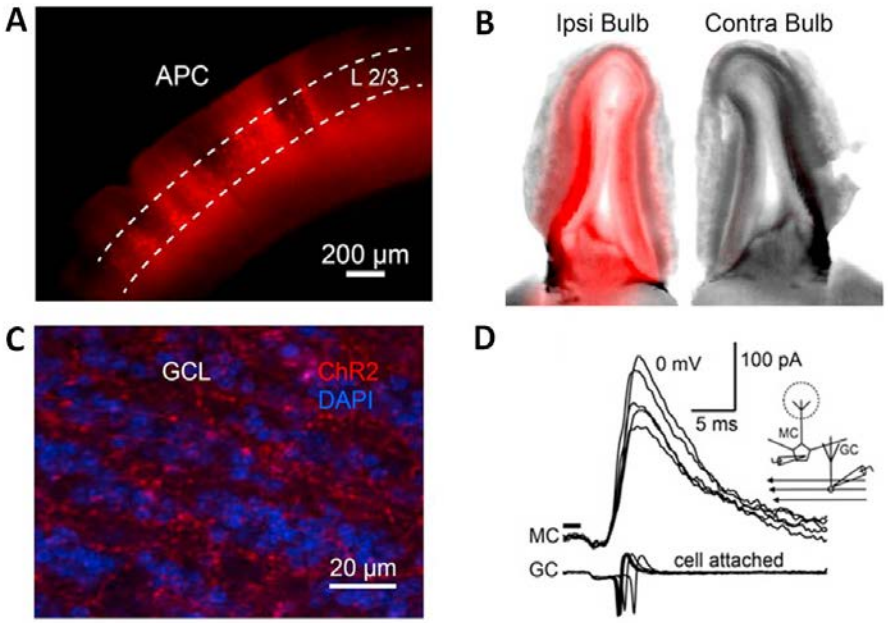

Figure 19. Glutamatergic cortical feedback to the OB. *A, Local viral injection allows the infection of pyramidal neurons with ChR2-mCherry in the Anterior Piriform Cortex . B, Overlay of fluorescence and bright field images of the two bulbs, demonstrating the projection of ChR2-mCherry labeled axons in the ipsilateral olfactory bulb. C, Close view of ChR2-mCherry expressing fibers in the GCL D, Simultaneous voltage clamp recording of a mitral cell and cell-attached recording of a GC show that light-evoked activation of cortical axons produces action potentials in the GC and IPSCs in the mitral cell (Boyd et al., 2012).*

2.5.2 Cholinergic modulation from the basal forebrain

The cholinergic system is a major neuromodulator of the OB. Cholinergic fibers that project to the OB also originate from the HDB, as previously said. Centrifugal cholinergic fibers mainly target the GL and, moderately, infraglomerular layers (Macrides et al., 1981; Zaborszky et al., 1986; Salcedo et al., 2011). Acetylcholine (ACh) released by centrifugal cholinergic terminals has a dual effect in the glomerular network. In OB slices, local glomerular ACh administration causes a rapid excitation of M/T and ET cells mediated by ionotropic nicotinic ACh receptors. ACh also activates metabotropic muscarinic ACh receptors expressed by sSACs and PG cells thereby increasing glomerular GABAergic inhibition (Liu et al., 2015). GCs express muscarinic ACh receptors as well. Araneda and colleagues applied the mAChR agonist Oxotremorine (Oxo) in OB slices and observed that GCs response is dual and complex. Oxo administration has a hyperpolarizating effect on GCs followed by a depolarization (Smith et al., 2015). These results suggest that centrifugal cholinergic innervation has a double effect in the OB network activity. ACh release may first have a rapid excitatory effect on M/T cells followed by an increase of glomerular and granule-mediated inhibition, thus, modulating the global network.

2.5.3 Serotoninergic afferences from the Raphe Nucleus

Serotoninergic afferences arising from the Raphe Nucleus target all layers of the OB (Deolmos et al., 1978; McLean and Shipley, 1987). *In vitro* and *in vivo* studies have shown direct 5-HT excitatory effect on M/T cells (Huang et al., 2016; Kapoor et al., 2016) and in some cases an indirect inhibitory effect (Petzold et al., 2009; Huang et al., 2016) via the activation of JG interneurons (Hardy et al., 2005; Petzold et al., 2009). A recent *in vivo* imaging study reported that direct optical stimulation of the Raphe nucleus enhances the activity of GAD65(+) PG cells and TH(+) sSACs thus modestly enhancing their response to odorant inhalation. The observed effect is mediated by increased glutamatergic drive onto these neurons suggesting that 5-HT may alter the degree to which OB output is shaped by inhibition during behavior (Brunert et al., 2016).

2.5.4 Noradrenergic afferences from the Locus

Another important neuromodulator present in the OB is noradrenaline (NA). NAergic fibers originate from the Locus Coeruleus and project into all but the most superficial layers of the bulb, mainly targeting the GCL (Shipley et al., 1985; McLean et al., 1989). The three types of NAergic receptors (α1, α2 and ß) are coexpressed on the same cells in multiple layers of the bulb. GCs express both α1 and α2 NA receptors. However, the activation of α1 and α2 receptors is concentration-dependent and they mediate opposite effects on M cell inhibition. Activation of the α2 receptor is possible at NA concentrations lower than 1µM, due to its extremely high ligand affinity. At low NA concentration, GC-α2 receptor activation hyperpolarizes GC thus reducing the rate of spontaneous postsynaptic inhibition on M cells (Nai et al., 2009; Nai et al., 2010). When α1 receptors are activated at intermediate and high NA concentrations, α1 receptor-mediated response has a dominant effect over α2 (Nai et al., 2009; Nai et al., 2010) increasing postsynaptic M cell inhibition and at the same time directly depolarizing M cell (Hayar et al., 2001; Nai et al., 2009; Zimnik et al., 2013). *In vivo*, NA infusion in adult rat brain proved to improve odor detection and discrimination at very low concentration. However, infusion of receptor agonist demonstrated that α1 receptor activation is required for NA modulatory effect (Escanilla et al., 2010).

Results

Results I: Characterization of PG cell diversity

Introduction

As we have seen in the introduction of this thesis manuscript, PG cells are highly diverse at the morphological, functional and neurochemical level. We believe that this diversity has a physiological relevance i.e. that different subtypes of PG cells with different intrinsic and synaptic properties may execute different functions during olfactory processing. Yet, this heterogeneity has so far most often been neglected, perhaps because the functional classification of the different PG cells in only two classes, type 1 and type 2, is still quite rudimentary. Identifying PG cell subtypes is a first important step towards understanding the functions of intraglomerular inhibition in odor processing.

During my thesis I have explored the synaptic and physiological properties of PG cells. Using genetic models allowing the identification of neurochemically-identified subclasses of PG cells, I have tried to define and compare the electrophysiological properties of labeled and non-labeled subclasses. My results are incorporated in three articles. In the first publication (*Najac, Sanz Diez et al., Intraglomerular Lateral Inhibition Promotes Spike Timing Variability in Principal Neurons of the Olfactory Bulb. JNeurosci., 2015*), we used the transgenic mouse line Kv3.1-EYFP (Metzger et al., 2002) that express the fluorescent protein EYFP in ~30% of the total PG cell population. In this mouse, labeled PG cells are all type 2 and include CB-expressing PG cells. This article is included at the end of this chapter of results. In a second paper currently in preparation (*Benito, Gaborieau, Sanz Diez et al., Origin and properties of calretinin-expressing periglomerular neurons in the olfactory bulb*), we used the CR-EGFP transgenic line that express EGFP under the control of the CR promoter (Caputi et al., 2009) in ~50% of the CR-expressing PG cells.

My investigations in these two transgenic lines demonstrate that the diversity of type 2 PG cells is greater than previously thought and that type 1 PG cells are less abundant than previously estimated. Based on these investigations, I propose in this first chapter of results a new classification of PG cells that identifies four functionally different subtypes taking into account their molecular identity, membrane properties and excitatory inputs. For clarity, I put together and illustrated my results slightly differently than in Najac et al. (principally in Figure 3 of this article). Details of these results are in the article. I also present here, in greater details since they are not yet published, results I have contributed to for the characterization of CR(+) PG cells.

This classification is further enriched and confirmed with a third article characterizing the inhibitory inputs received by these different classes of PG cells (*Sanz Diez et al., GABAergic projections from the basal forebrain control multiple inhibitory interneuron subtypes in the olfactory bulb*). This article constitutes the principal part of my thesis work and is presented in the second chapter of the results section.

Most of my data have been obtained using patch-clamp recordings and optogenetic experiments in olfactory bulb slices from juvenile and adult mice. Details of the materials and methods can be found in the Najac et al. paper (page 69) and in the Sanz Diez et al. paper (page 83).

Results

Kv3.1 EYFP(+) PG cells are type 2 PG cells with fast OSN-evoked excitatory responses

As described in detail in Najac et al., (2015), Kv3.1-EYFP(+) mice express EYFP in all the CB(+) PG neurons, which, according to several studies (Panzanelli et al., 2007; Parrish-Aungst et al., 2007), constitute ~15% of the total PG cell population. However, CB-expressing cells form only half of the EYFP(+) PG cells. Thus, if approximately 30% of the entire population of PG cells is labeled in the Kv3.1-EYFP mouse, EYFP(+) PG cells are neurochemically heterogeneous and, not surprisingly, have diverse membrane properties. Some cells responded to depolarizing currents with one or few spikes preceding a plateau potential, others responded with a regular firing of action potentials and others with a burst of action potentials riding on the top of a calcium spike (Figure 1B in Najac et al. 2015). However, as illustrated here in Figure 1A, the population of EYFP(+) PG cells also have common properties. EYFP(+) PG cells were all type 2 PG cells responding to a brief electrical stimulation of an OSN axon bundle converging into their glomerulus with a short barrage of fast summating EPSCs. To quantify the duration of these evoked responses, we constructed PSTHs of the evoked response and fitted the decay of the histogram with an exponential. Most of the recorded EYFP(+) cells (n=26/31) had a short response that quickly returned to baseline with a time constant below 100ms (average 64 $\pm$ 66 ms) (Figure 1A).

Type 2 PG cells are more abundant and more diverse than previously thought

To further explore PG cell diversity, I examined OSN-evoked whole-cell voltage-clamp excitatory responses of randomly chosen non-fluorescent PG cells in Kv3.1-EYFP mice (Figure 3 in Najac et al. 2015). Approximately 80% (n=33/40) of the recorded cells were type 2 PG cells responding to OSN stimulation with a plurisynaptic barrage of EPSCs of variable duration and amplitude. In contrast, type 1 PG cells (n=7/40) responded to OSN stimulation with a fast-onset monosynaptic EPSC whose latency and jitter were significantly smaller than those of EYFP (+) PG cells (Figure 1C). In my recordings, type 1 PG cell responded to supra-threshold depolarizing currents with a train of spikes with accommodating amplitudes and sometime riding on the top of a calcium spike (Figure 1Ci). If we consider that EYFP(-) PG cells represent 70% of the total population of PG cells, this implies that >85% of the PG cells

are type 2 and <15% are type 1, a ratio that differ from the 2/3rd – 1/3rd ratio previously admitted (Shao et al., 2009).

A peculiar subtype of type 2 PG cells respond to OSN stimulation with a long-lasting barrage of EPSC

Among the remaining EYFP(-) type 2 PG cells (n=33), three response profiles were observed. As expected, a large fraction (n=13/40) had properties consistent with those of CR (+) PG cells. This population of PG cells has been further examined in the CR-EGFP mouse (see next paragraph). Another group had short (<100 ms) OSN-evoked polysynaptic responses and diverse membrane properties and therefore cannot be functionally distinguished from EYFP(+) PG cells. In contrast, a third group of cells emerged with clear distinctive features. They responded to OSN-stimulation with a long-lasting barrage of EPSCs that could last several hundreds of milliseconds (n=9 cells with OSN evoked responses >100ms) (Figure 1B). Moreover, these PG cells consistently responded to depolarizing currents with regular firing of action potentials. These results thus reveals the existence of a novel subtype of PG cell, different from CR(+) and CB(+) PG cells, but that remains to be associated with a molecular marker.

CR(+) PG cells conserve functional properties of immature neurons.

In order to study the properties of CR(+) PG cells, we used patch-clamp recording in acute olfactory bulb horizontal slices from CR-EGFP transgenic mice expressing EGFP in about half of CR(+) cells (Caputi et al. 2009). Some of the results have been published in Figure 2 of Najac et al., (2015) and the full characterization will constitute a paper currently under preparation. I here present the results I contributed to.

In a first set of experiments, we used paired loose cell-attached recording to compare the spontaneous and OSN-evoked firing activity of CR/EGFP(+)PG cells with those of other subtypes of PG cells (Figure 2A). OSN stimulations that reliably elicited the discharge of a randomly chosen EGFP(-) PG cells were first determined. Then, we simultaneously recorded from a CR/EGFP(+) cell projecting into the same glomerulus. As illustrated in Figure 2, spontaneous and evoked action potential capacitive currents were large (133 ± 38 pA, range 36-532 pA) and biphasic in EGFP(-) PG cells. The number of spikes elicited within the 200 ms following the stimulation of OSN (from 2 to >16 spikes, average 6.3 ± 4.6) as well as the

duration of the burst varied across cells, consistent with the diversity of OSN-evoked activation profiles in PG cells (Najac et al., 2015c). In sharp contrast, very little spontaneous or evoked activity was detected in the simultaneously recorded CR/EGFP(+) PG cells. OSN stimulations produced no response at all (n=4) or small monophasic capacitive currents (16 ± 2 pA, n=9) in CR/EGFP(+) PG cells. Increasing the intensity of stimulation did not evoke larger responses suggesting that the weak responses of CR/EGFP(+) PG cells do not reflect a higher firing threshold. CR(+) PG cells are therefore remarkably silent compared with other PG cell subtypes.

We then compared the excitatory synaptic inputs of CR/EGFP(+) PG cells with those of other PG cell subtypes. As shown in the figure 2 of Najac et al. 2015, CR/EGFP(+) PG cells receive significantly less spontaneous EPSCs than EYFP(+) PG cells in the Kv3.1-EYFP mouse (Figure 3B). Consistent with these data, they also respond to a stimulation of the olfactory nerve with a smaller, plurisynaptic composite EPSC (Figure 2 in(Najac et al., 2015c). This is here illustrated with a paired recording between two PG cells, a CR/EGFP(+) cell and a randomly chosen EGFP(-) type 2 PG cell (Figure 3A). Taken together, these results indicate that the most abundant PG cells are weakly connected to mitral and tufted cells compared to other PG cells.

We also examined the intrinsic membrane properties of CR/EGFP(+) PG cells. EGFP(+) PG cells had a high membrane resistance of 2.3 ± 0.16 GOhm (n=37), a value that is most likely underestimated because of the current leak through the pipette seal, suggesting the expression of few ionic channels. In the current-clamp mode, depolarizing current injections from a holding potential maintained around -70 mV induced at most a single full action potential, occasionally followed by a spikelet (Figure 3C). However, only half of the cells (n=18/40) were able to fire an overshooting spike (with an amplitude > ~40 mV) (Figure 3D). The other half did not fire at all or fired a single rudimentary action potential (amplitude <40 mV, n=22), much like immature newborn neurons (Belluzzi et al., 2003; Carleton et al., 2003; Overstreet et al., 2004). Three typical examples of this diversity are illustrated in Figure 3C. PG cells firing a full-size action potential had more complex voltage responses, consistent with a maturation of the membrane properties. Thus, the action potential was sometime riding on the top of a long-lasting depolarization possibly mediated by a calcium spike, and hyperpolarizing steps evoked a sag in membrane potential suggesting the activation of an Ih

current. This cell to cell variability, that can be illustrated using the size of the spike as an indicator of cell maturation, was often seen within the same slice from animals at different developmental ages (P15-P38) (Figure 3E). Thus, consistent with their ongoing production from neural stem cells located in the SVZ, CR/EGFP(+) PG cells constitute a population of neurons with variable membrane properties that likely reflect different stages of maturation.

The diversity of membrane properties observed in our random sampling of CR/EGFP(+) PG cells (Figure 3) is consistent with a developmental maturation of the intrinsic membrane properties. How synaptic integration progress with time is less clear. To clarify this question, we examined the properties of age-matched CR/EGFP(+) PG cells co-labeled, using neonatal targeted electroporation of neural stem cells in the SVZ with tdTomato (Fernandez et al., 2011). Tom(+)/EGFP(+) PG cells were recorded at different intervals after electroporation (n=50, 15-65 days post electroporation (dpe)). As expected, these cells had similar properties as those described above, i.e. they fired at most a single spike and received little spontaneous synaptic inputs. However, most of the cells tested (n=22/25) and 100% of the cells tested after 30 dpe (n=8) fired an overshooting action potential (Figure 4B). This confirms that the size of the spike is an indicator of maturation and that cells that did not fire or fired a rudimentary action potential in our random sampling of CR/EGFP(+) PG cells were likely the most recently generated neurons. In contrast, the frequency of their spontaneous synaptic inputs was not correlated with the age of the cell (Figure 3C). Similar to randomly chosen CR/EGFP(+) PG cells, Tom(+)/EGFP(+) PG cells received between 0 and 10 EPSCs per second (mean 2.3 ± 2.7, n=47) and for the majority of them less than 3 IPSCs/s (mean 1.0 ± 1.7, n=41) whether they were young (15-23 dpe) or older (54-63 dpe). Thus, the mean frequency of sEPSC was not different in young cells (2.2 ± 0.5 EPSCs/sec, n=25) and in old cells (2.4 ± 0.8 EPSCs/sec, n=12, P=0.88). The mean sIPSC frequency was also not different in young cells (0.7 ± 0.2 IPSC/sec, n=21) and in old cells (1.2 ± 0.3 IPSCs/sec, n=11, P=0.17). Of note, cells without any detectable synaptic inputs were recorded at all ages indicating that synaptic integration does not improve over time. Taken together, these results indicate that CR(+)cells are unique PG cells that conserve immature properties over prolonged period of time.

Discussion

I have contributed to characterize genetically-identified PG cells populations using two different transgenic mouse lines. Along with this work, I have elaborated a new functional classification of PG cells mainly based on their activation pattern by OSN inputs and matching when possible their neurochemical identity. To date, PG cells functional classification only differentiated cells that received their excitatory inputs directly from OSN axons (type 1) or from the dendrites of principal cells (type 2) (Kosaka and Kosaka, 2007; Shao et al., 2009). My results show that the excitatory inputs of type 2 PG cells are more diverse than previously described, and I propose a classification that identifies four subtypes of functionally distinct PG cells.

First, CB(+) PG cells, which are labeled in the Kv3.1-EYFP(+) mouse and respond to a stimulation of OSNs with a short barrage of EPSCs that last only few tens of milliseconds. These cells are representative of an even larger group of type 2 PG cells with similar excitatory connections and play a dominant role in mediating OSN-evoked intraglomerular inhibition of principal neurons (Najac et al., 2015).

Second, a distinctive group of regularly firing type 2 cells receives a long-lasting burst of EPSC in response to OSN stimulation. The functional implication of this population has not been explored but its functional properties suggest that it can mediate a sustained inhibitory output. Their long-lasting excitation raises interesting questions about the modulation of intraglomerular microcircuits. It most likely reflects glutamate release from mitral cells that fire for several hundreds of ms after OSN stimulation. However, we have demonstrated that Kv3.1-EYFP(+) PG cells are also synaptically contacted by mitral cells and these cells respond to the same OSN input with a much shorter excitation. These different activation patterns thus suggest that local mechanisms modulate presynaptic glutamate release at specific dendro-dendritic synapses. One possibility is that a mechanism selectively limits dendritic glutamate release on Kv3.1-EYFP(+) PG cells but not on regularly firing PG cells with long-lasting OSN-evoked responses.

Third, CR(+) PG cells surprisingly conserve properties of immature neurons for weeks if not months. These immature properties are reflected by a low connectivity to the glomerular network and stereotyped intrinsic membrane properties. Similar intrinsic membrane properties were recently reported by (Foglie Iseppe et al., 2016) in another CR-

GFP mouse strain. One could think that EGFP expression is transient in these cells and disappears with maturation, explaining why only half of the CR-expressing PG cells are EGFP(+) in our transgenic line. To address this question, we used targeted electroporation to selectively transfect CR progenitors in the SVZ. Two months after their birth, CR(+) PG cells were still EGFP(+) and exhibited similar properties as 3 weeks-old CR(+) PG cells. Moreover, we also recorded from electroporated cells that were EGFP(-) but had similar properties than CR/EGFP(+) PG cells suggesting that EGFP(+) cells do not form a subpopulation of CR(+) PG cells with specific properties but are rather representative of the entire population. Our results indicate that CR(+) cells unlikely participate in intraglomerular inhibitory pathways but their function remains unknown. One possibility is that the functional phenotype of these cells may evolve towards a more mature state to address a specific task. If this scenario is true, then CR(+) PG cells constitute a previously unknown reservoir for plasticity.

Fourth, type 1 PG cells are the unique population of PG cells directly connected with OSN terminals. Current models of PG cell functions incorporate classical feedforward inhibitory circuits that principally rely on type 1 PG cells. Thus, it as been suggested that intraglomerular feedforward inhibition serves as gatekeepers that inhibit weakly activated principal neurons (Gire and Schoppa, 2009) and differently modulates the slow respiration-locked membrane potential oscillations of tufted and mitral cells thereby separating the firing phase of these two output channels along the respiration cycle (Fukunaga et al., 2012; Fukunaga et al., 2014). However, my results suggest that type 1 PG cells are less abundant than previously described and there is still no evidence that they inhibit mitral or tufted cells. In contrast, as we have seen earlier, robust evidence suggest that they modulate glutamate release from OSN terminals.

The classification proposed here is far from complete. A general problem that we are facing today is the lack of markers to identify subgroups of PG cells. For instance, CB(+) PG cells only constitute a subclass of PG cells with fast OSN-evoked excitation. New genetic models of neurochemically-identified PG cells would certainly allow a finer discrimination of subclasses within this large population of type 2 PG cells. However, our results underlie the diversity of PG cells and suggest that diverse PG cells execute different functions. These observations should be taken in consideration when exploring the functional role of PG cells in odor processing. Hopefully, new studies will shade some light into this matter and more precise description of the different groups of PG cells will be obtained.

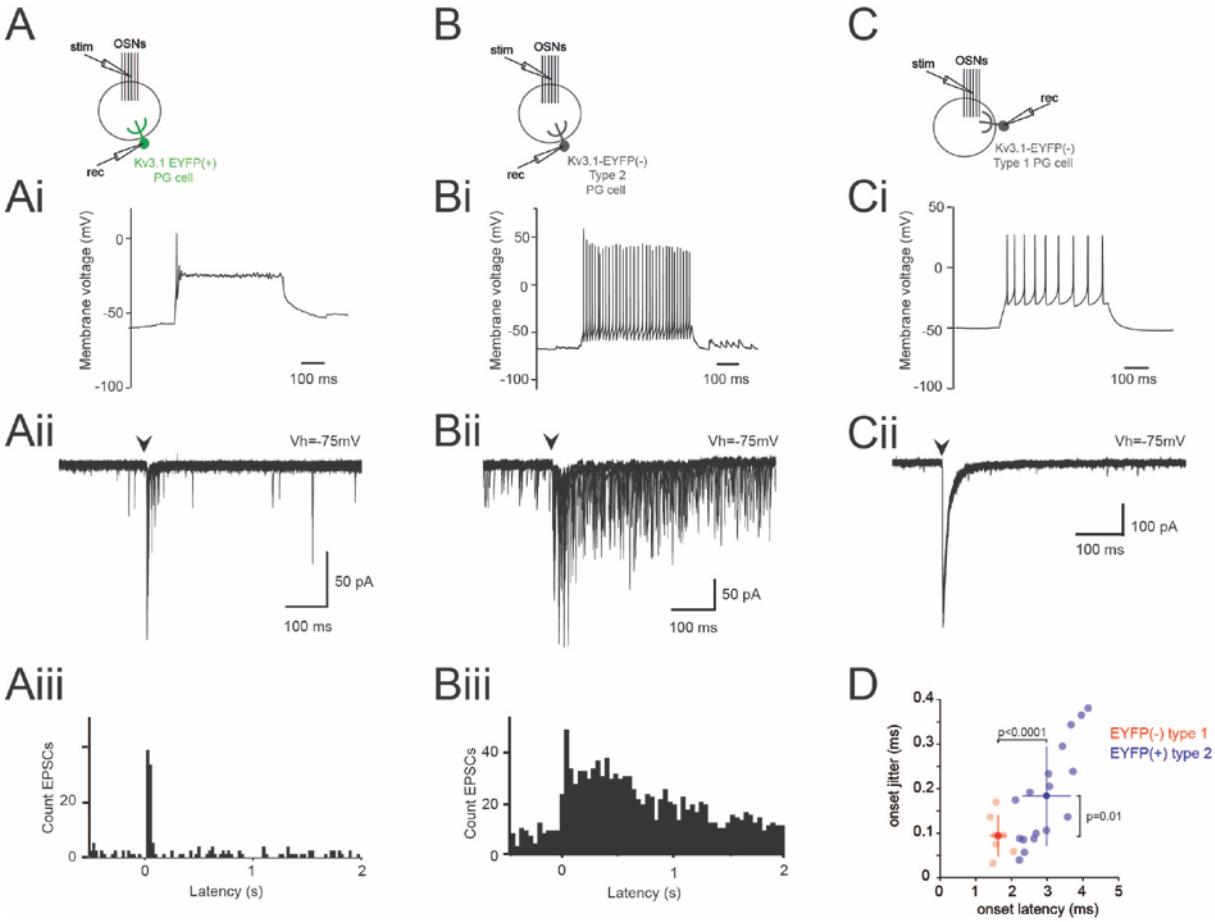

Figure 1. Kv3.1-EYFP(+) PG cells characterization.

A, Kv3.1-EYFP(+) PG cell recorded in whole-cell configuration. The electric stimulation electrode is placed on the OSN axon bundle that projects in the same glomerulus. Ai, PG cell recorded in current clamp configuration. A depolarizing step was injected (500ms) at a membrane potential around -60mV. Aii, Same cell as in Ai. Top, OSN stimulation evokes a short polisynaptic barrage of EPSCs. Bottom, PSTH for the same cell plotting the timing of individual EPSCs before and after OSN stimulation at t=0 (data for 10 sweeps, beams 20ms). Arrow heads represent OSN stimulation. B, type 2 EYFP(-) PG cell recorded in whole-cell configuration. Bi, PG cell recorded in current clamp configuration. A depolarizing steps was injected (500ms) at a membrane potential around -60mV. Bii, Top, Representative traces of a polysinaptic long-lasting response of Kv3.1-EYFP(-) PG cells recorded at Vh=-75mV. Bottom, PSTH for the same cell plotting the timing of individual EPSCs before and after OSN stimulation at t=0 (data for 10 sweeps, beams 20ms). C, Type1 Kv3.1-EYFP(-) PG cell recorded in whole-cell configuration. Ci, PG cell recorded in current clamp configuration. Depolarizing steps were injected (500ms) at a membrane potential around -60mV. Cii, Same cell as in Ci recorded in voltage clamp configuration. Representative traces of a monosynaptic response of Kv3.1-EYFP(-) PG cells recorded at Vh=-75mV. D, The onset latency versus onset jitter of individual ON-evoked responses is plotted for EYFP+ PG cells (blue circles) and EYFP− type 1 PG cells (red circles). Dark symbols and bars show the mean ± SD.

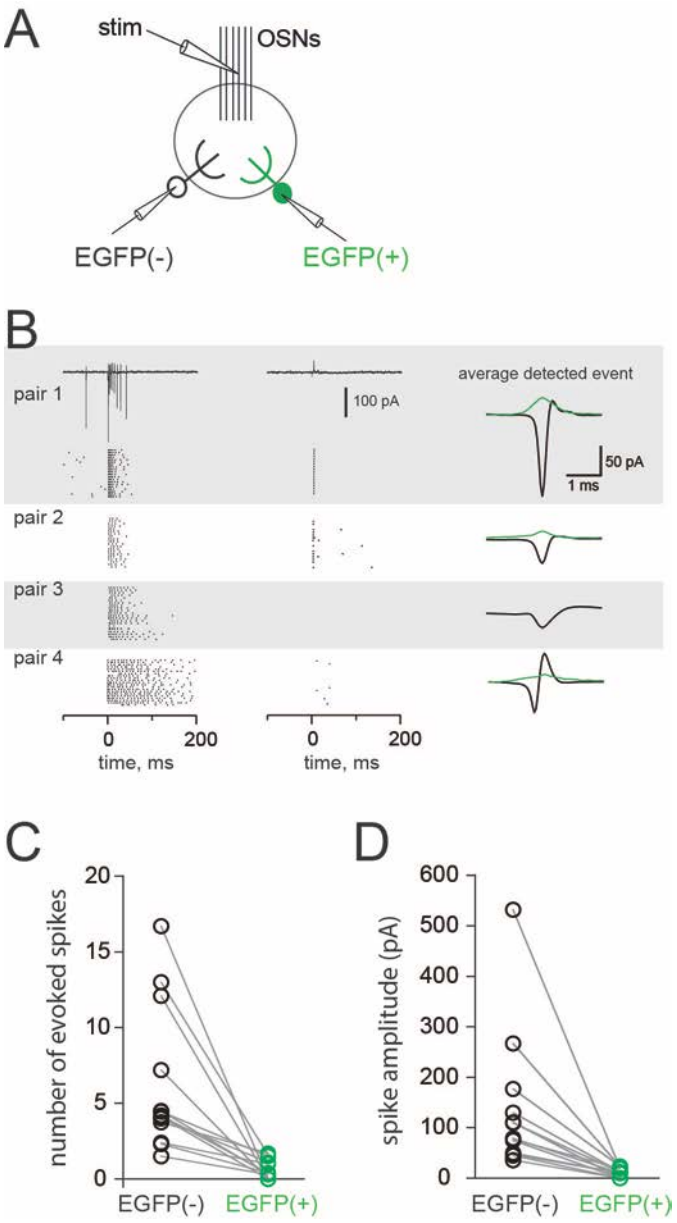

Figure 2. Comparison of OSN-evoked discharges in CR-expressing PG cells and in other PG cells. A, schematic of the experiment. Two PG cells projecting into the same glomerulus, one EGFP(+) and one EGFP(-), were recorded in the loose-cell attached configuration. Their firing was elicited by an electrical stimulation of the OSNs. B, Raster plots from 4 out of 13 pairs are shown with 20 consecutive sweeps for each pair. A typical response is shown for pair 1. OSNs were stimulated at t=0, at an intensity of 30-200 µA. The average evoked capacitive action current is shown on the right for each pair (green trace: EGFP(+) cell; black trace: EGFP(-) cell). C and D, summary plots of the results (n=13 pairs). C, Average number of spikes evoked within the 200 ms following the stimulation. D, Amplitude of the average capacitive current evoked by the stimulation. Dots from the same pair are connected.

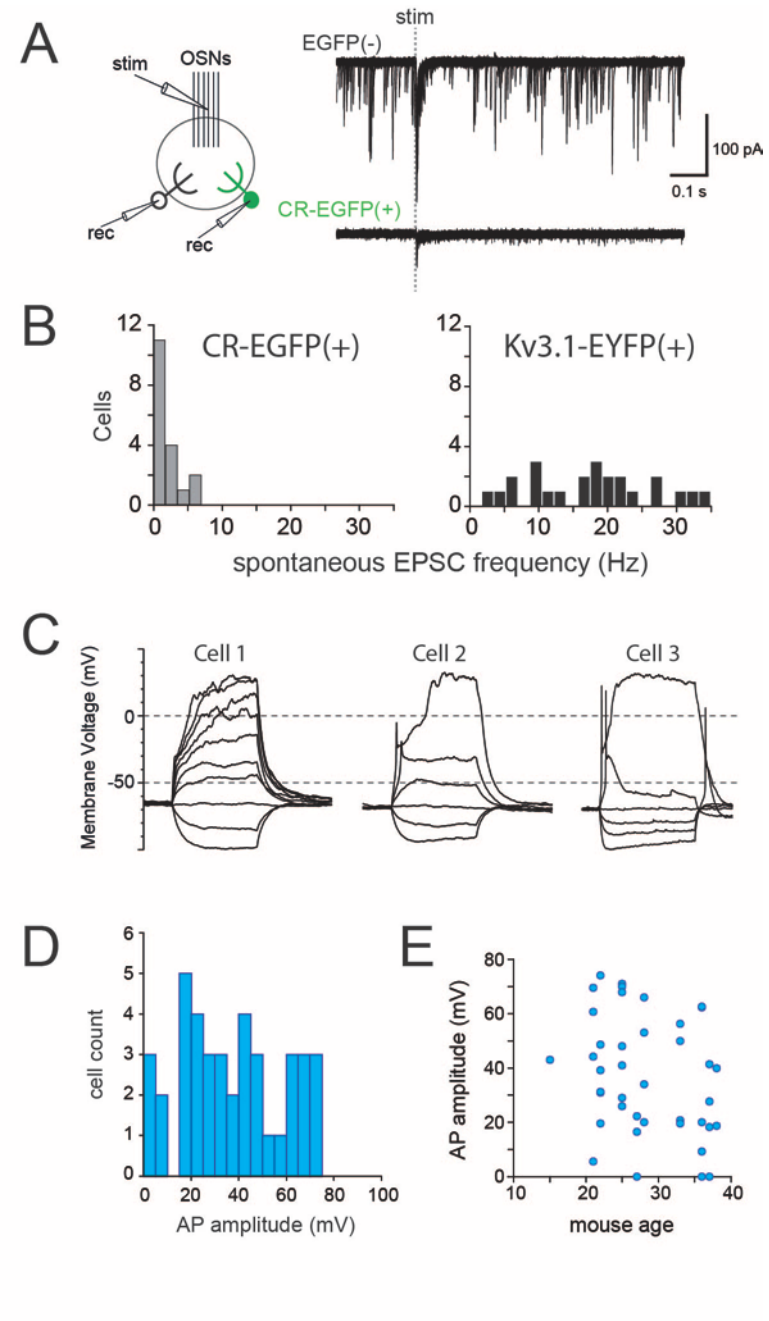

Figure 3. CR-EGFP(+) PG cells characterization.

A, Two PG cells projecting into the same glomerulus, one EGFP(+) and one EGFP(-), were recorded in the whole-cell configuration. The electric stimulation electrode is placed on the OSN axon bundle that projects in the same glomerulus. OSN evoked response is smaller in CR-EGFP(+) PG cells than in EGFP(-). B, Histograms representing the spontaneous EPSC frequency of CR-EGFP(+) cells (n=18) and Kv3.1-EYFP(+) cells (n=24). C-E, Diversity of intrinsic membrane properties across EGFP(+) PG cells. C, Some cells did not fire at all (as cell 1) or fired a single rudimentary action potential (cell 2). Cells firing an overshooting action potential (as cell 3) had more complex membrane properties but also fired at most a single spike. D, Distribution histogram of action potential amplitude in all the EGFP(+) PG cells tested. E, The ability to fire a full spike did not depend on the age of the mouse.

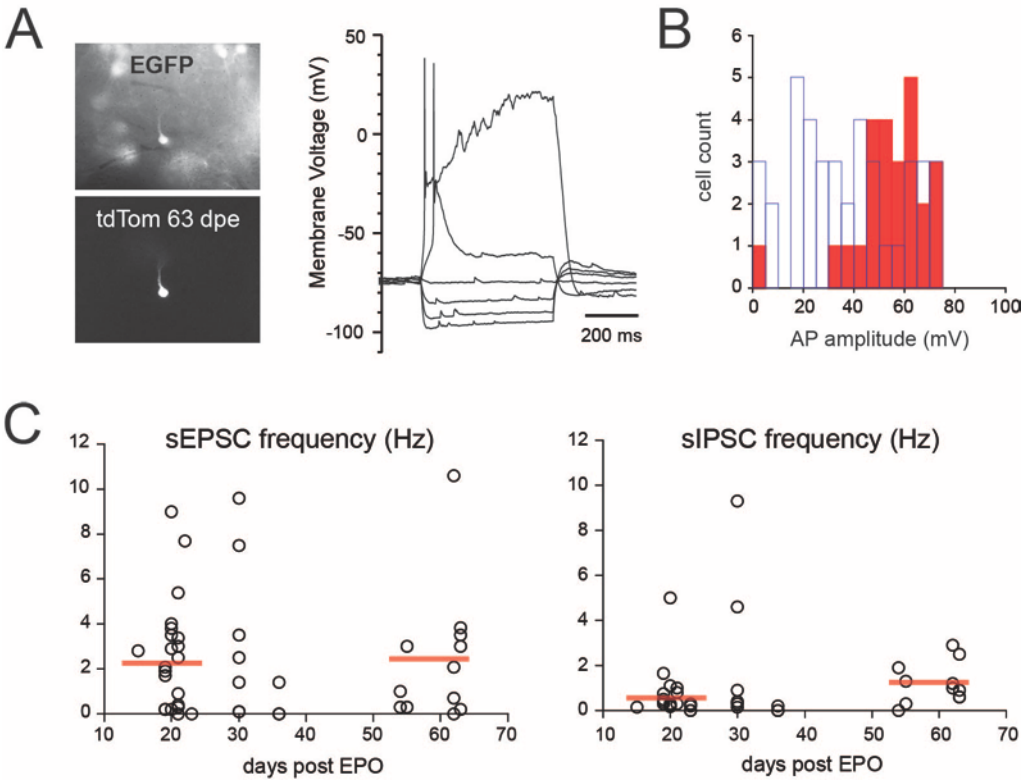

Figure 4. Synaptic and intrinsic properties of CR(+) PG cells do not mature over time.
A, Left, CR-EGFP(+) PG cell expressing tdTomato 63 days after perinatal electroporation in the lateral ventricule of the brain. Right, the same cell recorded in the whole-cell configuration only fire one action potential. B, Histogtam representing the amplitude of the spike of a group of CR-EGFP PG cells perinataly electroporated (red, recorded 15-65 dpe) compared with CR-EGFP(+) cells ploted in Figure 3C. C, Distribution histogram of the frequency of the spontaneous synaptic excitatory and inhibitory inputs of electroporated CR-EGFP PG cells throughout diferent ages. The average input frequency does not change overtime.

Article: Najac, M. et al., (2015) JNeurosci.

Intraglomerular Lateral Inhibition Promotes Spike Timing Variability in Principal Neurons of the Olfactory Bulb

Systems/Circuits

Intraglomerular Lateral Inhibition Promotes Spike Timing Variability in Principal Neurons of the Olfactory Bulb

Marion Najac,[1,2] Alvaro Sanz Diez,[3] Arvind Kumar,[4] Nuria Benito,[3] Serge Charpak,[1,2] and Didier De Saint Jan[1,2,3]

[1]Institut National de la Santé et de la Recherche Médicale Unité 1128, and [2]Université Paris Descartes, 75006 Paris, France, [3]Institut des Neurosciences Cellulaires et Intégratives, Centre National de la Recherche Scientifique, Unité Propre de Recherche 3212, Université de Strasbourg, 67084 Strasbourg, France, and [4]Computational Biology, School of Computer Science and Communication, Royal Institute of Technology, Stockholm, SE-110 40, Sweden

The activity of mitral and tufted cells, the principal neurons of the olfactory bulb, is modulated by several classes of interneurons. Among them, diverse periglomerular (PG) cell types interact with the apical dendrites of mitral and tufted cells inside glomeruli at the first stage of olfactory processing. We used paired recording in olfactory bulb slices and two-photon targeted patch-clamp recording *in vivo* to characterize the properties and connections of a genetically identified population of PG cells expressing enhanced yellow fluorescent protein (EYFP) under the control of the Kv3.1 potassium channel promoter. Kv3.1–EYFP$^+$ PG cells are axonless and monoglomerular neurons that constitute ~30% of all PG cells and include calbindin-expressing neurons. They respond to an olfactory nerve stimulation with a short barrage of excitatory inputs mediated by mitral, tufted, and external tufted cells, and, in turn, they indiscriminately release GABA onto principal neurons. They are activated by even the weakest olfactory nerve input or by the discharge of a single principal neuron in slices and at each respiration cycle in anesthetized mice. They participate in a fast-onset intraglomerular lateral inhibition between principal neurons from the same glomerulus, a circuit that reduces the firing rate and promotes spike timing variability in mitral cells. Recordings in other PG cell subtypes suggest that this pathway predominates in generating glomerular inhibition. Intraglomerular lateral inhibition may play a key role in olfactory processing by reducing the similarity of principal cells discharge in response to the same incoming input.

Key words: **glomerulus; inhibition; olfactory bulb; periglomerular cell**

Introduction

The olfactory bulb is the first station in the brain for odor processing (Shepherd, 2004). It receives sensory afferents from olfactory sensory neurons (OSNs) that bind odorants in the nasal epithelium. This information is transmitted to mitral and tufted cells, the principal output neurons of the bulb, within anatomical structures called glomeruli. Olfactory bulb networks modulate how mitral and tufted cells integrate and transform the spatiotemporal map of activated glomeruli into a temporal pattern of action potentials, i.e., the odor code that is ultimately decoded by downstream cortical neurons. However, the role of bulbar inhibitory circuits in shaping this temporal code is only partly understood.

Several types of interneurons interact with mitral and tufted cells. Granule and parvalbumin-positive (PV$^+$) cells make reciprocal synapses with the lateral dendrites of mitral and tufted cells. Mitral and tufted cells activate these interneurons that in turn release GABA onto mitral and tufted cells (Isaacson and Strowbridge, 1998; Schoppa et al., 1998; Christie et al., 2001; Kato et al., 2013; Miyamichi et al., 2013). PV$^+$ cells mediate a broad and nonselective interglomerular lateral inhibition of widely distributed mitral and tufted cells, whereas granule cells inhibit fewer narrowly confined principal neurons projecting into specific glomeruli (Kato et al., 2013; Miyamichi et al., 2013). Models of olfactory bulb processing stress the importance of interglomerular lateral inhibition for sharpening odor tuning of principal neurons, enhancing contrast between glomerular units and facilitating odor discrimination (Yokoi et al., 1995; Mori et al., 1999; Abraham et al., 2010).

In contrast, little is known about the role of periglomerular (PG) interneurons that surround glomeruli and make synapses onto mitral and tufted cell intraglomerular dendrites (Pinching and Powell, 1971a; Toida et al., 1998; Kosaka and Kosaka, 2007). However, PG cells may provide as much as 50% of their inhibitory inputs (Dong et al., 2007), and recent evidence suggest that a stimulation of OSNs evokes a potent intraglomerular inhibition

Received May 29, 2014; revised Dec. 12, 2014; accepted Feb. 2, 2015.

Author contributions: S.C. and D.d.S.J. designed research; M.N., A.S.D., N.B., and D.D.S.J. performed research; S.C. contributed unpublished reagents/analytic tools; M.N., A.S.D., A.K., and D.D.S.J. analyzed data; M.N. and D.D.S.J. wrote the paper.

This work was supported by the Leducq Foundation, Human Frontier Science Program Organisation Grant RGP0089/2009-C, National Agency for Research Grants ANR-12-JSV4-006-01 (D.D.S.J.) and ANR-R11036KK (S.C.), the Foundation for Medical Research, the National Institute of Health and Medical Research, the National Center of Scientific Research, and the Ministry of Higher Education and Research. We thank Thomas Knöpfel for the kind gift of the Kv3.1–EYFP transgenic mouse and Hannah Monyer for the kind gift of the CR–EGFP transgenic mouse. We also thank Gwenaëlle Bouchery and Andréa Virolle for technical assistance and members of the laboratory for constructive comments throughout the project.

Correspondence should be addressed to either of the following: Didier De Saint Jan, Institut des Neurosciences Cellulaires et Intégratives, Centre National de la Recherche Scientifique, Unité Propre de Recherche 3212, 5, rue Blaise Pascal, 67084 Strasbourg, France, E-mail: desaintjan@inci-cnrs.unistra.fr; or Serge Charpak, Laboratoire de Neurophysiologie et des Nouvelles Microscopies, Institut National de la Santé et de la Recherche Médicale, Unité 1128, 45, rue des Saints Pères, 75006 Paris, France. E-mail: serge.charpak@parisdescartes.fr.

DOI:10.1523/JNEUROSCI.2181-14.2015

 0270-6474/15/354319-13$15.00/0

in mitral cells (Najac et al., 2011; Shao et al., 2012). However, PG cells constitute a diverse population of interneurons with different membrane properties (McQuiston and Katz, 2001; Hayar et al., 2004; Murphy et al., 2005; Shao et al., 2009), morphologies (Pinching and Powell, 1971b; Hayar et al., 2004; Kiyokage et al., 2010; Kosaka and Kosaka, 2010), and immunohistochemical properties (Kosaka and Kosaka, 2007; Panzanelli et al., 2007; Parrish-Aungst et al., 2007; Whitman and Greer, 2007), suggesting that each subtype may form circuits playing different functions.

Thus, to get a better insight into the function of intraglomerular inhibition, we investigated the properties and the synaptic circuits made by a specific subset of PG cells expressing enhanced yellow fluorescent protein (EYFP) under the control of the Kv3.1 potassium channel promoter (Metzger et al., 2002). We determined *in vivo* and *in vitro*, using targeted patch-clamp recording, the circumstances under which labeled PG cells are activated. Our results demonstrate that they generate a prominent intraglomerular lateral inhibition that is activated at each respiration cycle and modulates the frequency and precision of mitral and tufted cell discharges.

Materials and Methods

Slice preparation. Experimental protocols were approved by the National Institute of Health and Medical Research and the National Center of Scientific Research guidelines. Horizontal olfactory bulb slices were prepared from 14- to 30-d-old transgenic mice of either sex expressing the EYFP under the control of the Kv3.1 K^+ channel promoter (Metzger et al., 2002) or the enhanced green fluorescent protein (EGFP) under the control of the calretinin (CR) promoter (Caputi et al., 2009). Note that, in these mice, the fluorescent protein expression may differ from the expression pattern of the Kv3.1 protein (Metzger et al., 2002) or the CR protein (Caputi et al., 2009). Mice were killed by decapitation, and the bulbs were dissected rapidly in ice-cold oxygenated (95% O_2/5% CO_2) solution containing the following (in mM): 83 NaCl, 26.2 $NaHCO_3$, 1 NaH_2PO_4, 2.5 KCl, 3.3 $MgSO_4$ 0.5 $CaCl_2$, 70 sucrose, and 22 D-glucose, pH 7.3 (osmolarity, 300 mOsm/L). Slices (300 μm) were cut using a Leica VT1000S or a Microm HM650V vibratome in the same solution, incubated for 30–40 min at 34°C, and stored at room temperature in a regular artificial CSF (ACSF) until use. ACSF contained the following (in mM): 125 NaCl, 25 $NaHCO_3$, 2.5 KCl, 1.25 NaH_2PO_4, 1 $MgCl_2$, 2 $CaCl_2$, and 25 D-glucose (continuously bubbled with 95% O_2/5% CO_2).

Electrophysiological recordings in slices. Experiments were conducted at 32–34°C on an upright microscope (Olympus BX51WI) with differential interference contrast optics. Whole-cell voltage-clamp recordings of mitral, tufted, and external tufted (ET) cells were made with patch pipettes (~2–4 MΩ) filled with an intracellular solution containing the following (in mM): 120 Cs-$MeSO_3$, 20 tetraethylammonium-Cl, 5 4-aminopyridine, 2 $MgCl_2$, 0.025 $CaCl_2$, 1 EGTA, 4 Na-ATP, 0.5 Na-GTP, and 10 HEPES, pH 7.3 (~280 Osm/L, ~10 mV junction potential). Whole-cell current-clamp recordings were made with an internal solution containing the following (in mM): 135 K-gluconate, 2 $MgCl_2$, 0.025 $CaCl_2$, 1 EGTA, 4 Na-ATP, 0.5 Na-GTP, and 10 HEPES, pH 7.3 (~280 Osm/L, ~15 mV junction potential). PG cell recordings were all made with pipettes (~4–6 MΩ) filled with the K-gluconate-based internal solution. We discriminated between tufted cells and ET cells as described previously (Najac et al., 2011). Alexa Fluor 594 (6 μM; Invitrogen) was always added to the internal solution to confirm the glomerular projection of the recorded cell. For paired recording of synaptic transmission, the K-gluconate-based internal solution in the presynaptic neuron was supplemented with 10 mM glutamate or 10 mM GABA to avoid transmitter depletion and the resulting rundown of the postsynaptic response. Loose cell-attached recordings (15–100 MΩ seal resistance) were made with pipettes filled with ACSF and used several times on different neurons. Bundles of OSN axons projecting inside a given glomerulus were stimulated using a theta pipette filled with ACSF as described previously (Najac et al., 2011). The electrical stimulus (100 μs) was delivered using an isolator-11 Stimulus Isolation Unit (Molecular Devices). Recordings were acquired with a multiclamp 700A amplifier (Molecular Devices), low-passed filtered at 2–4 kHz, and digitized at 10 kHz using Clampex 9 software (Molecular Devices). In current-clamp recordings, a constant hyperpolarizing current was injected to maintain the cell at a potential of −60/−70 mV. In voltage-clamp recordings, access resistance ($R_a < 10$ MΩ for mitral, $R_a < 20$ MΩ for tufted and ET cells, $R_a < 30$ MΩ for PG cells) were not compensated. Voltages indicated throughout were corrected for the junction potential estimated with the Clampex software.

Drugs. 6-Nitro-7-sulfamoylbenzo[*f*]quinoxaline-2,3-dione (NBQX), D-2-amino-5-phosphonopentanoic acid (D-AP-5), 2-(3-carboxypropyl)-3-amino-6-(4 methoxyphenyl)pyridazinium bromide (GBZ), 7-(hydroxyimino)cyclopropa[b]chromen-1a-carboxylate ethyl ester (CPCCOEt), and 4-ethylphenylamino-1,2-dimethyl-6-methylaminopyrimidinium chloride (ZD7288) were purchased from Tocris Bioscience or Ascent Scientific.

Intraglomerular application of GBZ. Local intraglomerular applications of GBZ were made with a patch pipette filled with ACSF supplemented with GBZ. Alexa Fluor 594 (10 μM) was also added to the pipette solution to monitor diffusion with fluorescence. Air pressure at the back of the pipette was applied either transiently (100–200 ms) using an electrical valve or continuously using a syringe.

PG cell morphology. To reconstruct the morphology of PG cells, biocytin (10 mM) was added to the intracellular solution, and the patch pipette was slowly withdrawn immediately after breaking the membrane to avoid damaging the cell bodies. Slices were then fixed in 4% paraformaldehyde overnight, washed three times, and incubated in a permeabilizing solution containing Cy5-conjugated streptavidin (1 μg/ml; Jackson ImmunoResearch) for 1 d. After three wash cycles with PBS, sections were mounted. Labeled cells were imaged with a confocal microscope (Zeiss LSM 510).

Two-photon targeted patch-clamp recordings in vivo. Six- to 12-week-old Kv3.1–EYFP transgenic mice were anesthetized with an intraperitoneal injection of xylazine (16 mg/kg) and ketamine (100 mg/kg) and placed in a custom stereotaxic apparatus. The posterior cisterna was drained, and a small craniotomy was done on the dorsal side of one olfactory bulb. The dura was removed before stabilizing the bulb with agarose (2% w/v). After surgery, the animal was placed under a custom-built two-photon laser scanning microscope (Charpak et al., 2001) equipped with a 40× water-immersion objective (numerical aperture, 0.8) and a Mira 900 mode-locked titanium:sapphire laser (Coherent). Anesthesia was switched to isoflurane (1–2%, 3 L/min in moisturized air/O_2), and its depth was monitored throughout by respiration rates along with lack of response to toe pinch. Body temperature was measured with a rectal probe (FHC) and maintained at 36–37°C with a heating pad (FHC). Respiration was monitored with a pressure pad (Biopac Systems) positioned under the chest. For recordings, we followed the two-photon targeted patching approach (Margrie et al., 2003) using regular patch pipettes (~4–8 MΩ) containing Alexa Fluor 594 (10–20 μM). The dye-filled patch pipette and $EYFP^+$ neurons were imaged simultaneously with two detection channels using an excitation wavelength of 900 nm. The pipettes were filled with (in mM) 130 K-gluconate, 4 $MgCl_2$, 4 Na-ATP, 0.5 Na-GTP, 10 HEPES, and 10 phosphocreatinine, pH 7.3 (~280 Osm/L) for the experiments shown in Figure 6*A* or with the Cs-$MeSO_3$-based internal solution used in slices for the experiments shown in Figure 6*B*. Data were acquired the same way as in slices using an Axopatch 200B amplifier (Molecular Devices). Access resistances (25–40 MΩ) were not compensated.

Analysis. Voltage-clamp data were digitally low-passed filtered offline at 1–2 kHz when necessary and analyzed using Axograph X (Axograph Scientific) and Igor Pro (WaveMetrics). We measured the onset of EPSC and IPSCs at 5% of the first peak of the response. The latency of olfactory nerve (ON)-evoked EPSCs and IPSCs were defined as the time interval between the beginning of the stimulation artifact and the onset of the EPSC/IPSC. The latency of lateral inhibition in Figure 5 was defined as the time interval between the peak of the first action potential and the onset of the average IPSC. Trains of action potentials in the presynaptic cell were first aligned on the first spike of the train before computing the average IPSC. The jitter of EPSCs was defined as the SD of their latencies.

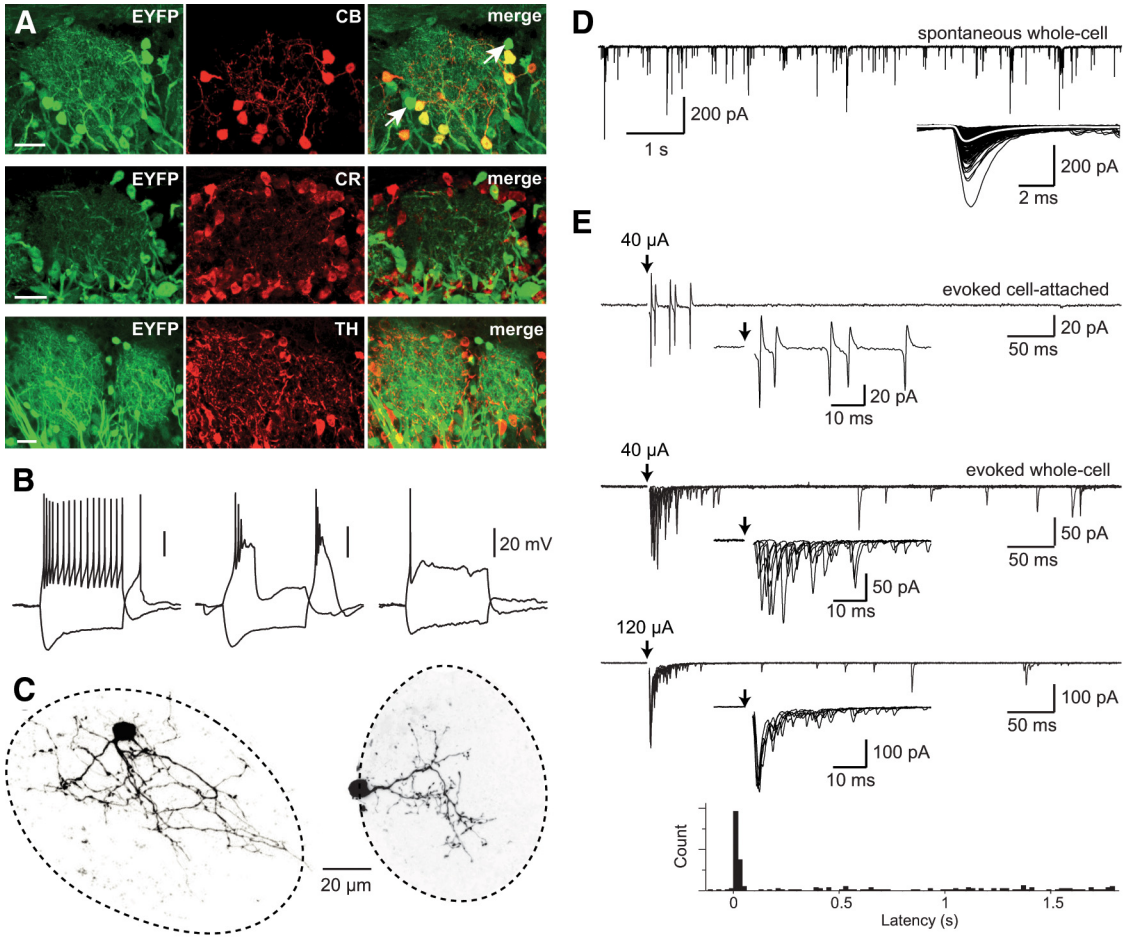

Figure 1. Characterization of EYFP $^+$ PG cells in Kv3.1–EYFP transgenic mice. ***A***, Immunofluorescence staining for CB (top), CR (middle), and TH (bottom) in the glomerular layer of Kv3.1–EYFP transgenic mice. Note that all CB $^+$ PG cells express EYFP, but some EYFP $^+$ PG cells do not express CB (arrows). Scale bars, 20 μm. ***B***, Intrinsic membrane properties were diverse in EYFP $^+$ PG cells. Depolarizing and hyperpolarizing steps (500 ms) were injected in EYFP $^+$ PG cells recorded in current-clamp at a membrane potential of approximately -60 mV. The three examples show individual traces from three cells responding differently to a step depolarization. ***C***, Two biocytin-filled EYFP $^+$ PG cells. Dashed lines delimit the glomerulus into which each PG cell projected its dendrites. ***D***, Spontaneous EPSCs in an EYFP $^+$ PG cell recorded at $V_h = -75$ mV. Onset, Individual spontaneous EPSCs (black traces) and their average (white trace) are superimposed. ***E***, Responses evoked by stimulation of OSNs (arrow) recorded in an EYFP $^+$ PG cell in the cell-attached (top) or whole-cell voltage-clamp mode at two intensities of stimulation indicated on the left (bottom; $V_h = -75$ mV). Individual traces are superimposed. Insets are zooms on the initial part of the response. Note that the latency and jitter of the responses decreased with the intensity of stimulation. The histogram plots the timing of individual EPSCs in responses evoked by the highest intensity of stimulation (bin width, 20 ms; stimulation at $t = 0$).

Peristimulus time histograms (PSTHs) represent the average number of EPSCs (Fig. 1) or spikes (see Fig. 8) per bin during a sweep or during a respiration cycle (see Fig. 6). Spike timings were detected automatically with NeuroMatic (http://www.neuromatic.thinkrandom.com/) by a *y*-threshold level detector for values on a positive slope deflection. Reliability of mitral cell spiking responses (see Fig. 8) was analyzed using MATLAB (MathWorks). For the ensemble analysis of mitral cell responses to the stimulation of OSNs (see Fig. 8*G*), we constructed a nine-neuron ensemble by pooling the nine recorded mitral cells, each of them having at least 14 trials for each condition, with and without GBZ. By random non-redundant combination of nine trials of 9×14, we created 14 artificial trials of the activity of an ensemble of nine mitral cells.

Unless indicated otherwise, we used the unpaired *t* test to compare two sets of data acquired from different populations. Results are expressed as mean ± SD.

Immunohistochemistry. Adult mice (1–3 months old) were deeply anesthetized with an intraperitoneal injection of xylazine (16 mg/kg) and ketamine (100 mg/kg) and perfused with 4% paraformaldehyde in which the brains were kept overnight. Slices were cut with either a vibratome (50 μm) or a cryostat (20 μm). Before slicing with the cryostat, brains were cryoprotected and frozen. Blocking steps were performed by PBS solution containing 2% BSA and 0.1% Triton X-100. Sections were incubated 48 h at 4°C with primary antibodies: mouse monoclonal anti-calbindin D-28k (CB; 1:1000; Swant), rabbit anti-CR 7699/4 (1:1000; Swant), or rabbit polyclonal anti-tyrosine hydroxylase (TH; 1:500; Millipore). After washing, they were incubated 2 h at room temperature with secondary antibodies: Alexa Fluor 594-conjugated anti-mouse or anti-rabbit (1:300–1:500; Invitrogen). After washing, sections were mounted in Vectashield (Vector Laboratories). Confocal images were taken using a Zeiss LSM 510 confocal microscope, and cells were counted manually.

Results

Morphology, immunohistochemical identity, and membrane properties of a genetically identified PG cell subtype

In Kv3.1–EYFP transgenic mice, mitral and tufted cells, as well as a population of juxtaglomerular cells, express EYFP (Metzger et al., 2002). Using slices from juvenile olfactory bulb (15–30 postnatal days), we identified the EYFP $^+$ juxtaglomerular cells as PG cells (hereafter called EYFP $^+$ PG cells) on the basis of the small size of their round soma, their localization around glomeruli (Fig. 1*A*), and their large input resistance (950 ± 375 MΩ, $n = 20$). EYFP $^+$ PG cells filled with biocytin apparently had no axon ($n = 11$), and 10 of 11 projected their dendrites in a single glomerulus (Fig. 1*C*). PG cells have been classified anatomically into

two broad classes (Kosaka and Kosaka, 2007): so-called type 1 PG cells are synaptically contacted by OSN axon terminals, whereas type 2 PG cells are not and receive excitatory inputs from the dendrites of mitral, tufted, or ET cells. Prototypical type 2 PG cells express the calcium binding proteins CB or CR (Kosaka and Kosaka, 2007). In Kv3.1–EYFP transgenic mice, virtually all PG cells immunoreactive for CB were EYFP$^+$ (388 of 392 cells, $n = 5$ mice), but only half of EYFP$^+$ PG cells expressed CB (388 of 695 cells; Fig. 1*A*). EYFP$^+$ PG cells did not overlap with cells that express CR ($n = 4$ mice; Fig. 1*A*) nor with dopaminergic–GABAergic cells expressing TH ($n = 4$ mice; Fig. 1*A*). Thus, the population of EYFP$^+$ PG cells encompasses cells with different immunohistochemical properties. Because CB$^+$ neurons constitute 14% of all PG cells (Panzanelli et al., 2007), we estimate that ~30% of all PG cells are EYFP$^+$ in Kv3.1–EYFP mice. Intrinsic membrane properties and firing patterns of EYFP$^+$ PG cells were also diverse (Fig. 1*B*). The majority of the cells responded to depolarizing current steps with large calcium spikes ($n = 16$) and the others with sustained firing of sodium action potentials ($n = 8$) or with few sodium spikes preceding a plateau potential ($n = 4$). In most ($n = 27$ of 28) EYFP$^+$ PG cells, hyperpolarizing current steps caused a voltage sag. This rebound was blocked by ZD7288 (50 μM), an antagonist of I_h-mediating hyperpolarization-activated cyclic nucleotide gated channels ($n = 7$ cells; data not shown).

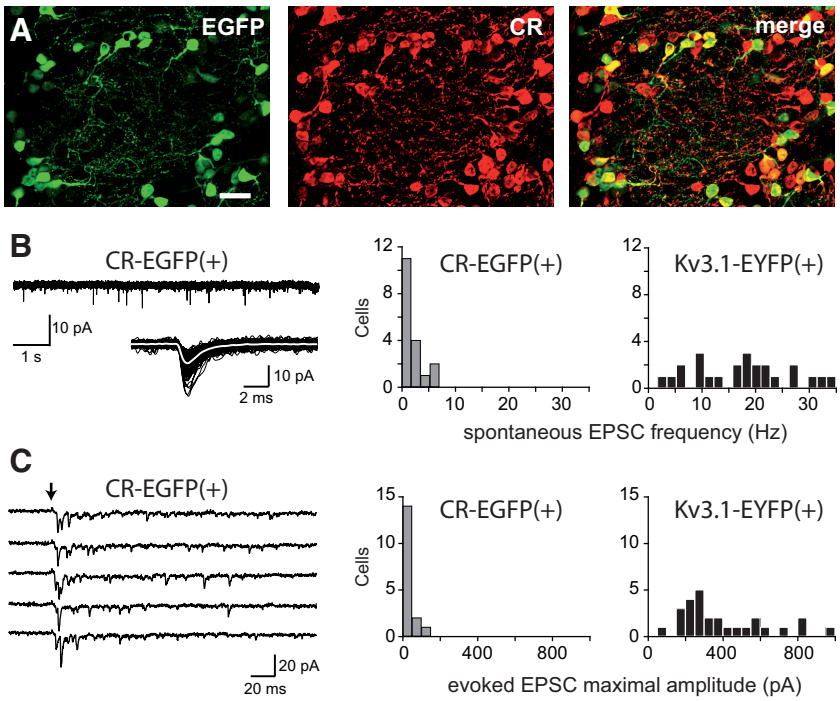

Figure 2. A large fraction of CR$^+$ PG cells is weakly connected to the glomerular network. ***A***, Immunofluorescence staining for CR (red, middle) revealed that only a fraction of CR$^+$ PG cells express EGFP (green, left) in CR–EGFP transgenic mice. Scale bar, 20 μm. ***B***, Spontaneous EPSCs recorded in the whole-cell voltage-clamp mode ($V_h = -75$ mV) in a CR–EGFP$^+$ PG cell. Onset, Individual events (black) superimposed with the average EPSC (white). Distribution histograms compare the frequency of spontaneous EPSCs in CR–EGFP$^+$ PG cells (left) and Kv3.1–EYFP$^+$ PG cells (right). ***C***, Five consecutive ON-evoked whole-cell responses ($V_h = -75$ mV) in a CR–EGFP$^+$ PG cell. This stimulus (200 μA, arrow) produced the largest responses. Distribution histograms compare the maximal amplitudes of ON-evoked responses in CR–EGFP$^+$ PG cells (left) and Kv3.1–EYFP$^+$ PG cells (right).

Synaptic properties of EYFP$^+$ PG cells

To characterize the synaptic properties of EYFP$^+$ PG cells, we first examined their spontaneous excitatory synaptic inputs and their responses to a brief (100 μs) electrical stimulation of an OSN axon bundle converging into their glomerulus. Whole-cell voltage-clamp recordings of EYFP$^+$ PG cells ($V_h = -75$ mV) revealed spontaneous EPSCs at a rate of 17.5 ± 8.9 per second ($n = 24$; Fig. 1*D*). The average EPSC had an amplitude of 50 ± 23 pA and a fast time course (20–80% rise time, 0.28 ± 0.05 ms; decay time constant, 1.48 ± 0.2 ms). In the cell-attached configuration preceding whole-cell recordings, ON stimulation evoked a burst of few action potentials usually restricted to the first 50 ms after the stimulus (3.7 ± 1.4 spikes, 94 ± 6% within this temporal window, $n = 14$; Fig. 1*E*). The first spike of the burst occurred with an average latency of 6.8 ± 3.1 ms (range of 3–13.7 ms, $n = 14$) that decreased with increasing stimulation intensity (data not shown). In the whole-cell configuration, ON stimulation evoked a brief barrage of fast summating EPSCs that summed up to 424 ± 302 pA ($n = 31$) at strong intensities of stimulation (153 ± 107 μA; Fig. 1*E*). To quantify the duration of these responses, we constructed PSTHs of EPSCs and fitted the decay of the histogram with an exponential. As in the example shown in Figure 1*E*, the majority of the cells ($n = 26$ of 31) had a response that quickly returned to baseline with a time constant <100 ms (mean of 64 ± 66 ms; see Fig. 3*A*). At $V_h = -75$ mV, the AMPA receptor antagonist NBQX (10 μM) abolished evoked EPSCs ($n = 3$; data not shown), whereas at $V_h = 30$ mV, addition of the NMDA receptor antagonist d-AP-5 (50 μM) was required to block the EPSC ($n = 4$; data not shown). As reported previously (Shao et al., 2009), the latency of the first EPSC and the jitter of the latency depended on the intensity of stimulation (Fig. 1*E*). A strong stimulus (110 ± 101 μA) evoked an EPSC with an average latency of 3 ± 0.7 ms and a jitter of 0.18 ± 0.11 ms ($n = 17$). With a weak stimulus (36 ± 14 μA), the average latency was 4.4 ± 1.1 ms and the jitter was 0.6 ± 0.5 ms ($n = 17$). However, the latencies and jitters of responses evoked by stronger intensities were significantly larger than those of monosynaptically connected ET cells (latency, 2.0 ± 0.4 ms, $p < 0.0001$; jitter, 0.07 ± 0.06 ms, $p = 0.0007$; $n = 12$ ET cells; data not shown) and those of PG cells type 1 (see Fig. 3*B*) and were consistent with a polysynaptic activation.

PG cell functional diversity

To evaluate the functional relevance of EYFP$^+$ PG cells, we compared their ON-evoked activation patterns with those of other PG cell subtypes. PG cells expressing CR are three times more numerous than CB-expressing PG cells and constitute the most abundant immunohistochemical subtype (Panzanelli et al., 2007; Parrish-Aungst et al., 2007; Whitman and Greer, 2007). We used transgenic mice expressing EGFP under the control of the CR promoter to identify these PG cells (Caputi et al., 2009). In CR–EGFP mice, only 56% of the cells immunoreactive for CR were also EGFP$^+$ (1173 of 2098 cells), but almost all EGFP$^+$ PG cells were immunoreactive for CR (1173 of 1185 cells, $n = 6$ mice; Fig. 2*A*). In the whole-cell configuration, CR–EGFP$^+$ PG cells had a high input resistance (2 ± 1.3 GΩ, $n = 30$) and received significantly less spontaneous EPSCs (1.8 ± 1.9 per second, $n = 18$)

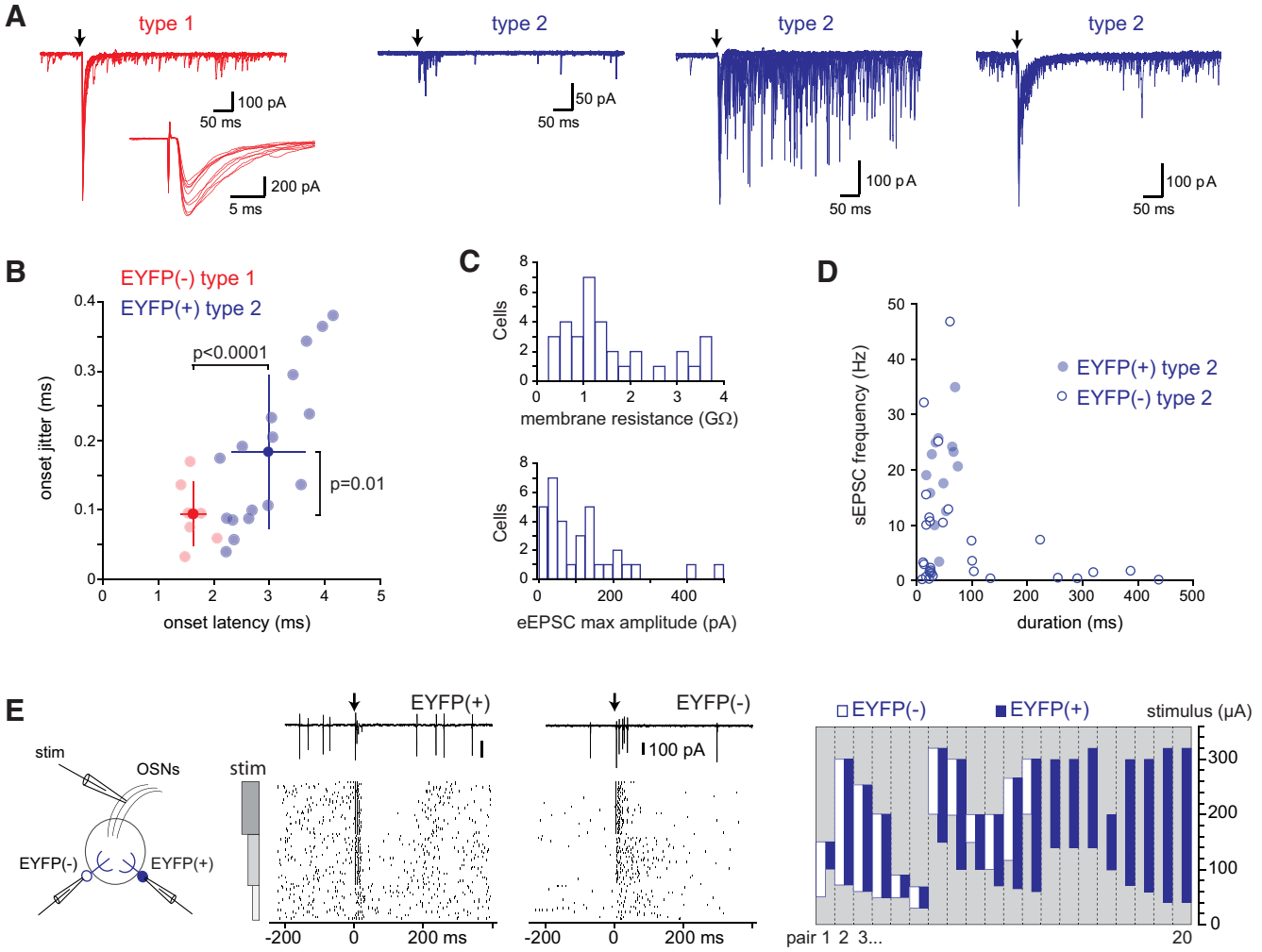

Figure 3. PG cell functional diversity. ***A***, ON stimulation (arrow) evoked different types of responses in EYFP$^-$ PG cells. Type 1 PG cells (red traces) responded with a fast-onset monosynaptic EPSC (the inset is a zoom on the initial part of the response), whereas type 2 PG cells responded with plurisynaptic responses of variable amplitudes and durations (3 examples shown with blue traces). $V_h = -75$ mV. In each case, several traces are superimposed. ***B***, The onset latency versus onset jitter of individual ON-evoked responses is plotted for EYFP$^+$ PG cells (blue circles) and EYFP$^-$ type 1 PG cells (red circles). Dark symbols and bars show the mean ± SD. Strong intensities of stimulation were used here (110 ± 101 μA for EYFP$^+$ PGs and 239 ± 122 μA for EYFP$^-$ PGs). ***C***, Distribution histograms of the membrane resistance (top) and maximal amplitude of ON-evoked responses (eEPSC; bottom) in EYFP$^-$ type 2 PG cells ($n = 33$). ***D***, The duration of the ON-evoked response is plotted against the frequency of spontaneous EPSCs for each individual EYFP$^-$ type 2 PG cells (white circles). Values for EYFP$^+$ PG cells (blue circles) are also plotted for comparison. Durations were estimated from the fit of the latency histogram of each cell. ***E***, Comparison of ON-evoked firing in EYFP$^+$ and EYFP$^-$ PG cells. Action potentials were monitored using paired loose cell-attached recordings (scheme). Middle, Example of a pair that responded to ON stimulation with a similar threshold but different time course. One representative trace (top) and raster plots of 80 consecutive episodes (bottom) are shown. Each point indicates a spike. OSNs were stimulated (arrow) with increasing intensities. Right, Summary graph of the experiment. Each column shows a pair. White and blue vertical bars show the range of stimulus intensities that evoked the firing of the EYFP$^-$ and EYFP$^+$ PG cells, respectively. Columns with no white bars (pairs 13–20) indicate pairs in which the EYFP$^-$ PG cells did not respond to the stimuli tested.

than EYFP$^+$ PG cells in the Kv3.1–EYFP mouse ($p < 0.0001$; Fig. 2*B*). Their average spontaneous EPSC was fast (20–80% rise time, 0.29 ± 0.08 ms; decay, 1.5 ± 0.5 ms) but of smaller amplitude than in EYFP$^+$ PG cells (13.9 ± 6.3 pA, $p < 0.0001$). ON stimulation evoked a barrage of EPSCs that summed up to 33 ± 34 pA ($n = 17$) at maximal intensities of stimulation (320 μA), a much smaller amplitude than responses evoked in EYFP$^+$ PG cells ($p < 0.0001$; Fig. 2*C*). Small inputs could be sufficient to trigger the firing of a neuron with a high membrane resistance. However, most CR–EGFP$^+$ PG cells did not fire any action potentials spontaneously or in response to ON stimulation in the cell-attached (four of six silent cells) or loose cell-attached (six of eight silent cells) configuration. In the remaining four CR–EGFP$^+$ cells, the stimulation evoked only one spike (data not shown). Similarly, in paired recording in the loose cell-attached mode of a CR–EGFP$^+$ and a CR–EGFP-negative (CR–EGFP$^-$) PG cell surrounding the same glomerulus, ON stimulation (50–200 μA) that induced the firing of the nonlabeled PG cell failed to activate the CR–EGFP$^+$ PG cell (in 9 of 11 pairs) or at most elicited a single spike ($n = 2$ of 11 pairs; data not shown). Thus, a large and previously undescribed fraction of CR$^+$ PG cells receives little excitatory inputs from the glomerular network and is not, or only weakly, activated by ON inputs that potently activate other PG cell subtypes.

To further explore PG cell diversity, we next examined ON-evoked whole-cell voltage-clamp excitatory responses of randomly chosen nonfluorescent PG cells in Kv3.1–EYFP mice. We identified 17.5% of type 1 PG cells ($n = 7$ of 40; Fig. 3*A*) that responded with a fast-onset monosynaptic EPSC whose latency (1.64 ± 0.22 ms) and jitter (0.09 ± 0.05 ms) were significantly smaller than those of EYFP$^+$ PG cells (Fig. 3*B*). The other EYFP$^-$ PG cells ($n = 33$) responded with a plurisynaptic barrage of EP-

SCs of variable duration and amplitude. As expected, a large fraction of these type 2 PG cells ($n = 13$) had properties consistent with those of CR–EGFP$^+$ PG cells: a high membrane resistance (>1.5 GΩ), small ON-evoked responses (<100 pA) at maximal stimulation intensities, and a low frequency of spontaneous EPSCs (<2 Hz; Fig. 3*A*,*C*). The remaining EYFP$^-$ type 2 PG cells ($n = 20$) responded either with a long-lasting barrage of EPSCs that could last several hundred milliseconds (11 cells with ON-evoked responses >100 ms) or with a short plurisynaptic response indistinguishable from those of EYFP$^+$ PG cells (Fig. 3*A*). Cells with long-lasting responses usually received a lower frequency of spontaneous EPSCs than cells with short responses (Fig. 3*D*). These different types of responses were neither glomerulus specific nor dependent on the stimulation strength because they were also observed in paired recordings between cells projecting into the same glomerulus ($n = 9$; data not shown). Therefore, they rather reflect specific synaptic connectivity and possibly distinguish functionally distinct subtypes.

In a third set of experiments in Kv3.1–EYFP mice, we made paired recordings in the loose cell-attached mode of an EYFP$^+$ and an EYFP$^-$ PG cell surrounding the same glomerulus and stimulated OSNs with increasing intensities until threshold ($n = 20$ pairs; Fig. 3*E*). Seventy percent of EYFP$^-$ PG cells were not activated by weak stimuli that drive EYFP$^+$ PG cells. Among these, 40% could not be activated at any intensities of stimulation, and 30% had a higher firing threshold than EYFP$^+$ PG cells. Most nonresponding cells were totally silent (five of eight), such as CR–EGFP$^+$ PG cells. The remaining 25% of EYFP$^-$ PG cells (5 of 20) had a threshold that was approximately similar to EYFP$^+$ PG cells. Last, only one EYFP$^-$ PG cell (5%) had a lower threshold than its paired EYFP$^+$ PG cell. Figure 3*E* (middle) illustrates one pair of PG cells with a similar threshold but different firing patterns: the EYFP$^+$ PG cell responded as usual with a brief burst of action potentials, followed by a pause during which the EYFP$^-$ PG cell continued to fire. Thus, although EYFP$^+$ PG cells are not the only PG cell subtype activated by weak ON inputs, they form a large group of neurons with similar synaptic connections that likely plays a dominant role in generating intraglomerular inhibition in response to weak OSN inputs.

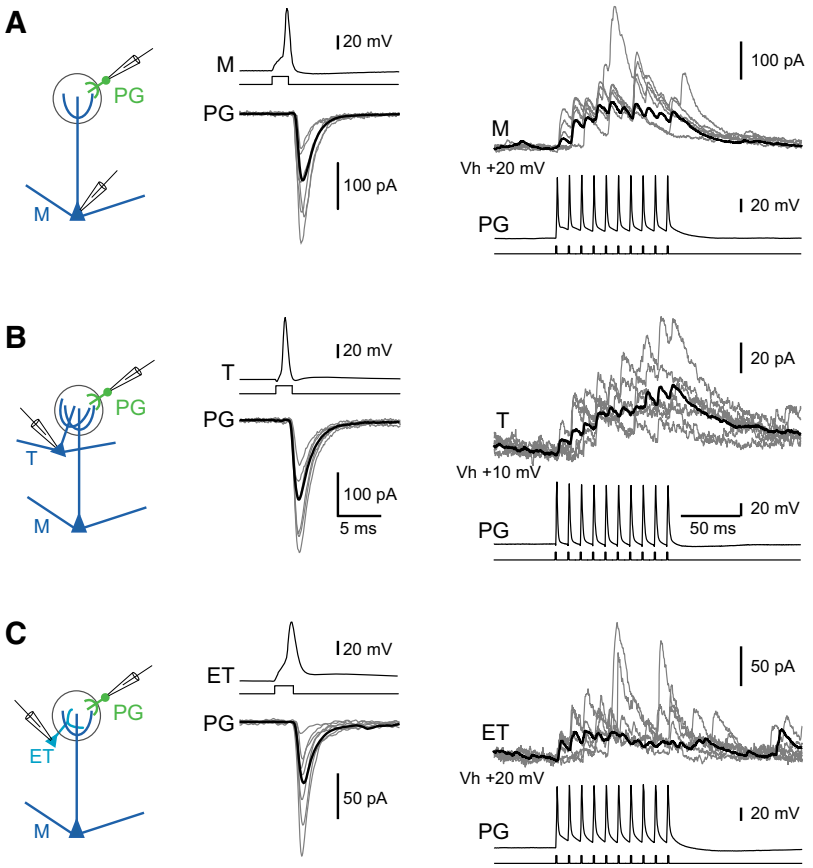

Figure 4. Synaptic connections of EYFP$^+$ PG cells. ***A***, Paired recordings between mitral (M) and EYFP$^+$ PG cells. Left, Single action potentials evoked in the mitral cell produced fast EPSCs in the PG cell recorded at $V_h = -70$ mV. Six representative EPSCs are superimposed in gray, and the average EPSC across all trials is shown in black. Right, In another pair, a train of 10 action potentials evoked in the PG cell produced a barrage of ISPCs in the mitral cell recorded at $V_h = 20$ mV. Six sweeps are superimposed, and the average from all trials appears in black. ***B***, Same for connected pairs of tufted (T) and EYFP$^+$ PG cells. ***C***, Same for connected pairs of ET and EYFP$^+$ PG cells. IPSCs in ***A*** and ***B*** were recorded in the presence of NBQX (10 μM) and D-AP-5 (50 μM); ***C*** in ACSF.

Synaptic circuits formed by EYFP$^+$ PG cells

We used paired recordings to identify the presynaptic partners of EYFP$^+$ PG cells. Three glutamatergic cell types with glomerular projections—mitral, tufted, and ET cells—might provide excitatory inputs onto EYFP$^+$ PG cells. Contrasting with the idea that type 2 PG cells receive their excitatory input principally from ET cells (Shao et al., 2009), we found that action potentials evoked in any of these glutamatergic neurons produced fast EPSCs in EYFP$^+$ PG cells (Fig. 4). EPSC amplitudes varied between pairs and from trials to trials within pairs. On average, the EPSC amplitude was 140 ± 222 pA in ET–PG pairs ($n = 15$), 124 ± 57 pA in mitral–PG pairs ($n = 6$), and 160 ± 122 pA in tufted–PG pairs ($n = 5$) at $V_h = -75$ mV. In different pairs with mitral/tufted cells filled with a Cs^{2+}-based internal solution and voltage clamped around the reversal potential for excitation ($V_h = 0/20$ mV), 100 Hz trains of action potentials in the EYFP$^+$ PG cell produced a barrage of summating IPSCs in mitral ($n = 2$ pairs; Fig. 4*A*), tufted ($n = 4$; Fig. 4*B*), and ET ($n = 3$; Fig. 4*C*) cells. These IPSCs persisted in the presence of NBQX and D-AP-5 ($n = 7$) and were blocked by bath application of GBZ (2 μM, $n = 5$; data not shown). In most pairs (eight of nine), failures of GABAergic transmission were frequent after the first action potential (64 ± 18% of failure). Thus, EYFP$^+$ PG cells are activated by mitral, tufted, and ET cells and in turn release GABA with a low probability onto mitral, tufted, and ET cells.

Intraglomerular lateral inhibition between principal cells projecting into the same glomerulus

We predicted that synaptic circuits made by EYFP$^+$ PG cells may generate lateral inhibition between principal neurons projecting into the same glomerulus (Urban and Sakmann, 2002). Thus, we tested whether principal cells with apical dendrites in the same glomerulus inhibit each other. In pairs of mitral cells, trains of action potentials were evoked in the first cell (Fig. 5, M1), whereas the postsynaptic response of the second cell (M2) was recorded in

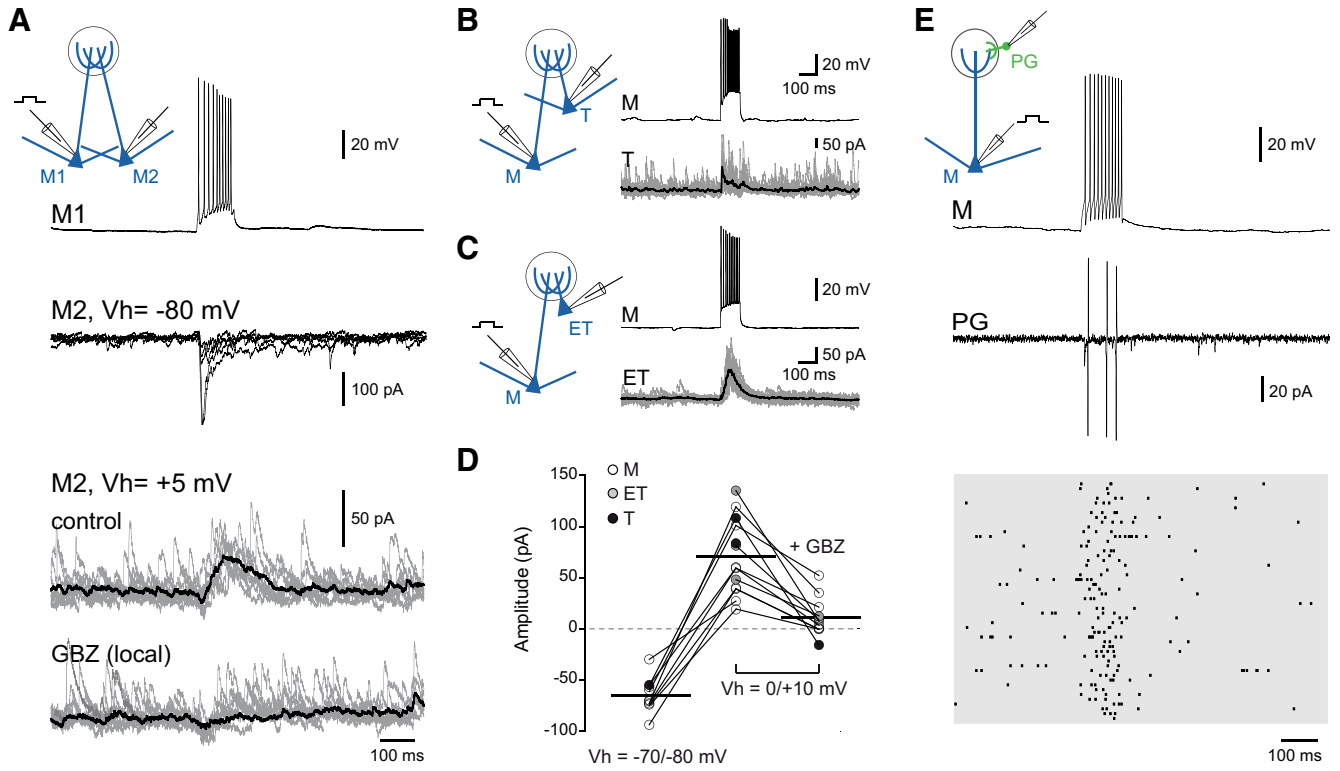

Figure 5. EYFP$^+$ PG cells mediate lateral inhibition between mitral, tufted, and ET cells projecting into the same glomerulus. ***A***, Paired recording between two mitral cells (M1 and M2) projecting into the same glomerulus. A current step (700 pA, 100 ms) was used to evoke a train of action potentials in M1 (top trace) while simultaneously monitoring voltage-clamped responses in M2 (scheme). Inward EPSCs were recorded at $V_h = -80$ mV (top traces, 5 traces superimposed). Outward IPSCs were recorded at $V_h = 5$ mV (bottom gray traces) in control conditions and after a transient puff of GBZ (50 μM, 100 ms) within the glomerulus. This protocol was repeated eight times. Traces before (control) and after (GBZ) the puff are superimposed. Average traces are shown in black. ***B***, Same experiment in a pair of mitral (M) cell–tufted (T) cell. ***C***, Same experiment in a pair of mitral (M) cell–ET cell. Experiments in ***A–C*** in the presence of D-AP-5 (50 μM) and CPCCOEt (100 μM). ***D***, Summary plot showing the amplitudes of the averaged postsynaptic current obtained at negative potentials ($V_h = -70/-80$ mV) and at a potential near 0 mV, under control conditions and in the presence of GBZ. Each plot is a mitral (white), tufted (black), or ET (gray) cell. Horizontal lines show the means. ***E***, Paired recording between a mitral cell (M) recorded in the whole-cell mode and an EYFP$^+$ PG cell recorded in the loose cell-attached mode (PG). Both neurons projected into the same glomerulus. A train of action potentials induced by a current step (400 pA, 100 ms) in the mitral cell (top trace) produced the firing of the PG cell (middle trace). Bottom, Raster plots of spontaneous and evoked action potentials in the PG cell.

voltage-clamp. These experiments were done in the presence of mGlu1 and NMDA receptor antagonists (CPCCOEt and D-AP-5, respectively) (1) to reduce the excitability of the network and spontaneous synaptic activity and (2) to limit the activation of granule cells. Fast synaptic inward currents were evoked when the postsynaptic cell was recorded at $V_h = -70/-80$ mV (Fig. 5*A*,*D*), consistent with the existence of excitatory synaptic interactions and gap junction coupling between principal neurons affiliated with the same glomerulus (Schoppa and Westbrook, 2002; Urban and Sakmann, 2002). When the postsynaptic mitral cell was voltage clamped around the reversal potential for excitation ($V_h = 0/10$ mV), a burst of synaptic outward currents was evoked. The average outward current started 20 ± 17 ms (range of 3–50 ms) after the first spike of the presynaptic mitral cell, had an amplitude of 58 ± 35 pA ($n = 8$; Fig. 5*D*), and was blocked by a transient puff ($n = 3$, 100 ms, 50 μM) or by a local perfusion of GBZ ($n = 2$, 25 μM) inside the glomerulus (Fig. 5*A*,*D*). Importantly, spontaneous IPSCs persisted during intraglomerular application of GBZ, indicating that the spread of GBZ outside the glomerulus was spatially limited (see Fig. 7). Firing of a single mitral cell also evoked a barrage of polysynaptic IPSCs in tufted cells ($n = 2$ pairs; amplitude, 83 and 108 pA; onset, 4.3 and 2.9 ms; Fig. 5*B*) and ET cells (amplitude, 68 ± 49 pA; onset, 20.7 ± 35 ms; range of 2.8–74 ms; $n = 4$ pairs; Fig. 5*C*). The polysynaptic inhibition of ET cells is likely generated by intraglomerular circuits because ET cells, that lack lateral dendrites in the external plexiform layer (EPL), presumably do not interact with granule cells or PV$^+$ interneurons. Thus, our data suggest that glomerular circuits mediate lateral inhibition between principal neurons projecting into the same glomerulus. Do EYFP$^+$ PG cells participate in this form of lateral inhibition? If so, they should be activated by the firing of a single mitral cell. We tested this hypothesis in pairs of mitral and EYFP$^+$ PG cells projecting into the same glomerulus. Trains of action potentials in a mitral cell evoked 1.8 ± 0.9 action potentials in an EYFP$^+$ PG cell recorded simultaneously in the loose cell-attached configuration in control conditions ($n = 4$ pairs; Fig. 5*E*), as well as in the presence of D-AP-5 ($n = 3$; data not shown). Thus, EYFP$^+$ PG cells participate to the circuit mediating intraglomerular lateral inhibition.

Intraglomerular lateral inhibition is highly active *in vivo*

The time course of olfactory processing is constrained by the 2–10 Hz respiratory rhythm. We used two-photon guided targeted patch-clamp recording in freely breathing anesthetized mice to examine the activity of EYFP$^+$ PG cells *in vivo*. Each recorded EYFP$^+$ PG cells exhibited rhythmic bursts of fast EPSCs ($n = 9$), consistent with mitral or tufted cell excitatory inputs. These bursts were correlated with the respiration cycle in eight of nine cells as in the example shown in Figure 6*A*. Moreover, EYFP$^+$ PG recorded in cell-attached mode before breaking the membrane also fired bursts of action potentials at a specific phase of the respiration cycle ($n = 5$ of 5 cells; Fig. 6*A*). These results

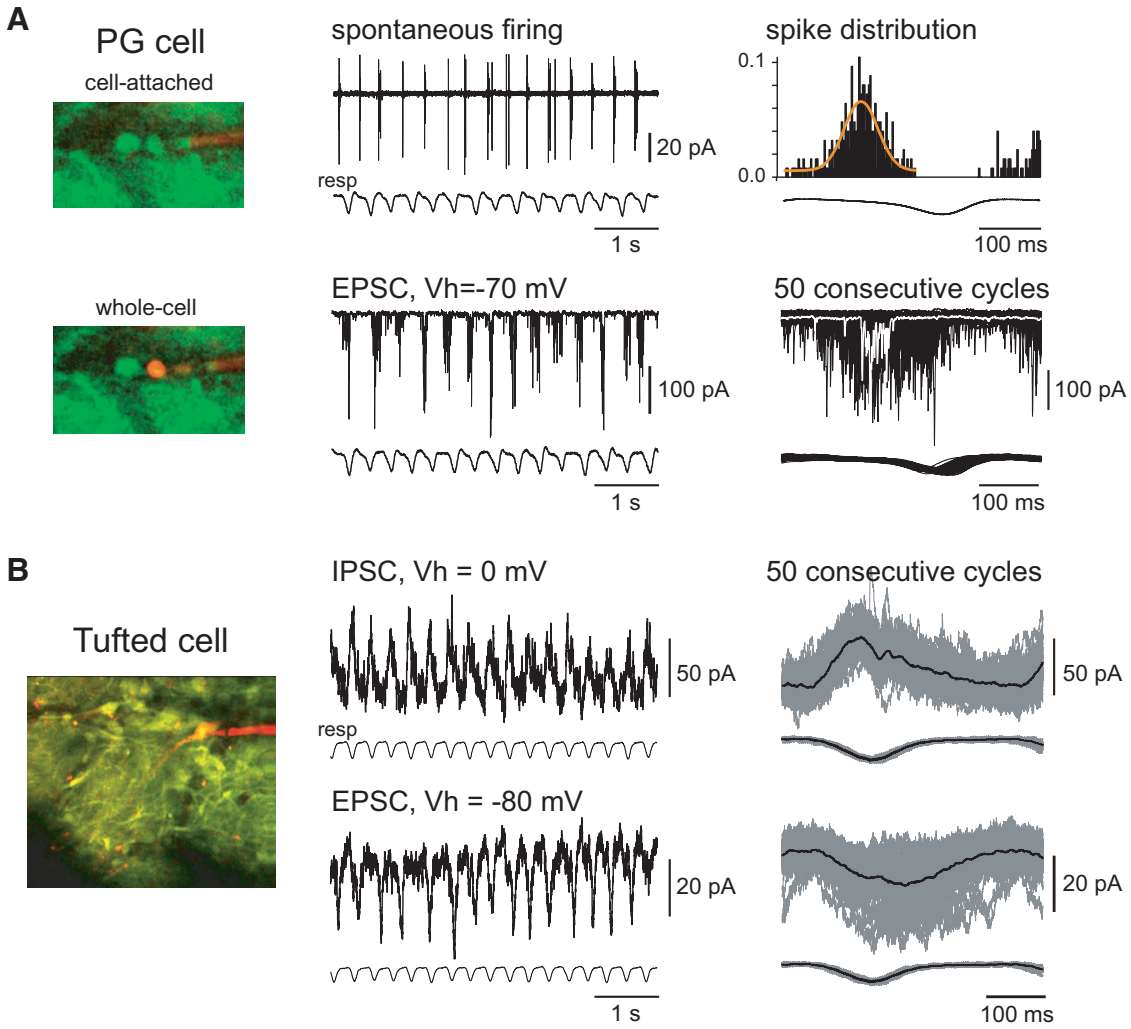

Figure 6. Activity of EYFP $^+$ PG cells in anesthetized mice. ***A***, Picture of an EYFP $^+$ PG cell first recorded in the cell-attached mode (top) and then filled with Alexa Fluor 594 (red) during whole-cell recording (bottom). The spontaneous firing from this cell (top trace) was recorded in the cell-attached configuration before breaking the membrane. The corresponding respiration cycle is shown below the trace (upward deflection corresponds to inhalation). Respiration cycles were aligned, and PSTHs per respiration cycle were constructed (right). Bin width, 2 ms. The orange trace is the best Gaussian fit of the histogram. The average respiration cycle waveform is shown below the PSTH. Bottom, Spontaneous EPSCs recorded in the whole-cell voltage-clamp configuration. Right, Thirty consecutive respiration cycles are superimposed, as are their corresponding whole-cell recordings. The white trace is a typical event. ***B***, Competing EPSCs and IPSCs underlie the spontaneous rhythmic activity of tufted cells *in vivo*. Left, Two-photon image of an EYFP $^+$ tufted cell during whole-cell recording *in vivo*. The patch pipette containing Alexa Fluor 594 (red) comes from the right. Middle traces, Slow outward inhibitory currents locked to the respiration rhythm (resp) dominated the spontaneous activity of this cell at $V_h = 0$ mV (top), whereas slow inward excitatory currents dominated the activity at $V_h = -80$ mV (bottom). Right, Fifty consecutive respiratory cycles with their correlated currents are superimposed. Black traces are the average.

suggest that EYFP $^+$ PG cells faithfully follow the activity of mitral and tufted cells that also fired bursts of action potentials at each respiration cycle (data not shown) as shown previously (Luo and Katz, 2001; Margrie and Schaefer, 2003). Therefore, intraglomerular lateral inhibition should be activated at each sniff and compete with the depolarization that generates the firing of principal neurons (Luo and Katz, 2001; Margrie and Schaefer, 2003). We tested this hypothesis in voltage-clamped tufted rather than mitral cells that are localized deeper in the brain and more difficult to voltage clamp. As expected, rhythmic slow IPSCs (half-width, 88 ± 22 ms; $n = 7$) correlated with the respiration were recorded at the reversal potential for excitation ($V_h = 10/0$ mV). As illustrated in Figure 6*B*, in cells in which EPSCs and IPSCs were recorded successively, IPSCs occurred at the same frequency and at the same phase of the respiration cycle as EPSCs ($n = 5$). Therefore, these data indicate that circuits mediating intraglomerular lateral inhibition operate *in vivo* in the absence of exogenous odorants at each respiration and thus likely provide a rhythmic inhibition that competes with the excitation of mitral and tufted cells.

ON-evoked inhibition is generated within the glomerulus and involves EYFP $^+$ PG cells

In slices, stimulation of OSNs evokes a prominent barrage of summating discrete IPSCs in mitral and tufted cells (Najac et al., 2011). A recent study suggests that intraglomerular circuits mediate the early part of this OSN-evoked inhibition (Shao et al., 2012). Consistent with this study, the early component of the composite ON-evoked IPSC persisted in the presence D-AP-5 and CPCCOEt (onset latency, 7.9 ± 2.1 ms; half-width, 61.6 ± 29.6 ms; $n = 6$ mitral cells; Fig. 7*A*) and was fully blocked when GBZ was applied locally, either continuously (Fig. 7*D*) or transiently (Fig. 7*E*), inside the glomerulus. In both cases, spontaneous IPSCs were not blocked. ON stimulation evoked a similar inhibition in tufted cells (onset latency, 6.7 ± 1.0 ms; half-width, 52.7 ± 29.3 ms; $n = 7$) and ET cells (onset latency, 6.4 ± 1.3 ms;

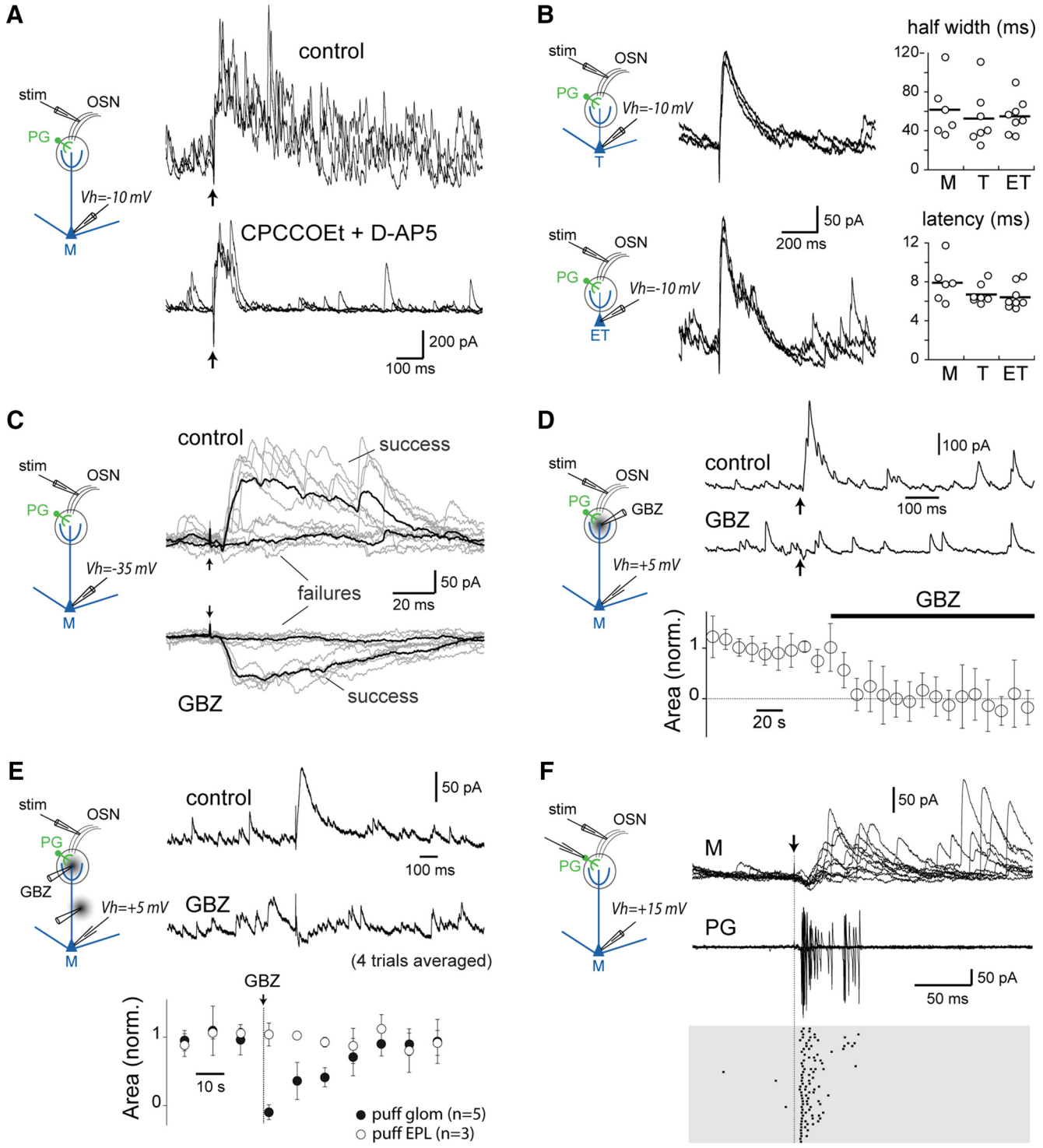

Figure 7. EYFP $^{+}$ PG cells mediate OSN-evoked feedforward inhibition. ***A***, Mitral cell (M) responses evoked by a stimulation of OSNs in control conditions (top) and in the presence of CPCCOEt (100 μM) and D-AP-5 (50 μM; bottom). Individual traces recorded at $V_h = -10$ mV are superimposed. ***B***, ON-evoked feedforward inhibition in a tufted cell (T, top) and in an ET cell (bottom). Individual traces recorded at $V_h = -10$ mV in the presence of CPCCOEt (100 μM) and D-AP-5 (50 μM) are superimposed. Right, Summary plots comparing the half-width and latency of the ISPC in mitral, tufted, and ET cells. Horizontal bars are the average. ***C***, Mitral cell responses evoked by minimal stimulation of OSNs that evoked a response (success) in ~50% of the trials in the presence of CPCCOEt plus D-AP-5 before (top, control) and after (bottom, 4 μM) bath application of GBZ. Individual traces recorded at $V_h = -35$ mV are superimposed in gray. Average responses are shown in black. ***D***, ON-evoked mitral cell responses in the presence of CPCCOEt plus D-AP-5 (top) and during local perfusion of GBZ (25 μM) inside the glomerulus to which the recorded mitral cell projected (middle trace). Single traces recorded at $V_h = 5$ mV. Note that intraglomerular perfusion of GBZ did not block spontaneous IPSCs. Bottom, Normalized area of the evoked IPSCs (measured during the first 100 ms) over time during local perfusion of GBZ within the glomerulus. Average from seven cells (5 mitral and 2 tufted cells). ***E***, Same as in ***D***, but GBZ was applied transiently (50 μM, 150 ms). Bottom, Summary plot for one cell for which GBZ was applied within the glomerulus (filled circles) or in the EPL below the glomerulus (open circles). ***F***, Paired recording of a mitral cell and an EYFP $^{+}$ PG cell projecting into the same glomerulus. The mitral cell was recorded in the whole-cell mode ($V_h = 15$ mV), whereas the PG cell was recorded in loose cell-attached mode. A minimal stimulation (18 μA) was used to stimulate OSNs in the presence of CPCCOEt plus D-AP-5. IPSCs in the mitral cell (top) were correlated with action potentials in the PG cell (middle). Bottom, Raster plot of every successful trial in the PG cell.

half-width, 54.9 ± 17.8 ms; $n = 8$; no statistical difference with values in mitral cells; Fig. 7*B*). Together, D-AP-5 and CPCCOEt shorten the excitation of mitral and tufted cells (De Saint Jan and Westbrook, 2007) and, consequently, the excitatory drive of interneurons. In addition, the NMDA receptor antagonist limits GABA release from granule cells (Isaacson and Strowbridge, 1998; Schoppa et al., 1998). Because IPSCs were evoked even when OSNs were stimulated with minimal intensities (25–50 μA, $n = 10$ mitral cells; Fig. 7*C*), interneurons that mediate this inhibition should be activated by weak ON inputs. Do EYFP$^+$ PG cells participate in ON-evoked inhibition? To investigate this possibility, we recorded IPSCs in a mitral cell while monitoring the activity of an EYFP$^+$ PG cell in the loose cell-attached mode under conditions of minimal stimulation that recruit only a fraction of PG cells but activate inhibition. Under these conditions and in the presence of D-AP-5 and CPCCOEt, EYFP$^+$ PG cells fired 2.4 ± 0.9 action potentials ($n = 4$ pairs) in 95 ± 5% of the trials in which a compound IPSC was evoked in the mitral cell (Fig. 7*F*). Together, these results suggest that glomerular circuits mediate the early phase of ON-evoked inhibition and that EYFP$^+$ PG cells contribute to this inhibition.

Glomerular inhibition promotes spike timing variability in mitral cells

A single stimulation of OSNs evokes polysynaptic EPSCs and IPSCs in mitral and tufted cells (Najac et al., 2011). Whereas the excitation is almost identical from trial to trial, the inhibition is composed of asynchronous discrete IPSCs with variable timing. To assess the influence of intraglomerular inhibition on the spike output of principal cells, we made loose cell-attached recordings in mitral cells and compared their ON-evoked discharge under control conditions and when intraglomerular inhibition was blocked by a local application of GBZ within the glomerulus ($n = 9$; Fig. 8). In some experiments ($n = 3$), we simultaneously monitored evoked IPSCs in a second cell projecting into the same glomerulus to better control the stimulation and the effect of GBZ, as in the example shown in Figure 8, *B* and *C*. Mitral cells responded to the stimulation with a long-lasting barrage of spikes that returned to baseline frequency after a double-exponential decay (25.3 ± 31.4 and 369 ± 184 ms). Intraglomerular application of GBZ increased firing rate (32 ± 26% increase compared with control during the 3 s after the stimulus, $p = 0.006$), especially during the first 200 ms after the stimulus (Fig. 8*B*,*C*). Furthermore, spike rasters of individual neurons suggest that spike time tended to be more reliable in the presence of GBZ (Fig. 8*C*). To quantify the effect of intraglomerular inhibition on spike timing, we ranked the interspike intervals (ISIs) in each trial for each mitral cell. We compared the distribution of their duration across trials in the presence and absence of GBZ in a short time window (200 ms) after ON stimulation (Fig. 8*D*). Most ISIs after the stimulus were significantly different in the two conditions for nearly all neurons (two-sampled Kolmogorov–Smirnov test, $p \leq 6.15 \times 10^{-4}$; Fig. 8*E*). However, these differences in the ISI duration distributions could result from both increased firing rates and increased spike reliability in the presence of GBZ. Therefore, we estimated the coefficient of variation (CV_{ISI}) of each ISI across trials in the two conditions (Fig. 8*F*). We found that the CV of the first two ISIs after the stimulus onset were significantly smaller in the presence of GBZ (first ISI: $CV_{ISI}^{GBZ} = 0.11 \pm 0.06$, $CV_{ISI}^{CNT} = 0.52 \pm 0.35$, $p \leq 0.01$; second ISI: $CV_{ISI}^{GBZ} = 0.18 \pm 0.14$, $CV_{ISI}^{CNT} = 0.44 \pm 0.26$, $p \leq 0.01$). Subsequent ISIs did not show any significant differences in CV across trials. Thus, intraglomerular inhibition not only reduces spike frequency but also promotes trial-to-trial spike timing variability within a short time window after ON stimulation. To understand how intraglomerular lateral inhibition could affect the response of an ensemble of cells that receive a simultaneous ON input, we then simulated an ensemble of nine mitral cells by pooling the data from our individual recordings. For every ensemble response, we calculated the CV of ISIs across the nine mitral cells in the presence and absence of GBZ (Fig. 8*G*). We found that the CV of the first two ISIs after the stimulus onset were significantly larger in the control condition than in the presence of GBZ (first ISI: $CV_{ISI}^{GBZ} = 0.36 \pm 0.08$, $CV_{ISI}^{CNT} = 1.04 \pm 0.20$, $p \leq 0.001$; second ISI: $CV_{ISI}^{GBZ} = 0.24 \pm 0.08$, $CV_{ISI}^{CNT} = 0.61 \pm 0.21$, $p \leq 0.001$). This increase in cell-to-cell spike redundancy in GBZ was restricted to the first few spikes after ON stimulation as for the trial-to-trial reliability described above for each cell.

Thus, intraglomerular inhibition counteracts membrane properties and dendrodendritic electrical and synaptic interactions that constrain mitral cells to fire reliable and precisely timed action potentials in response to a stereotyped excitatory input, thereby reducing the similarity of the discharge of each cell.

Discussion

We characterized a specific population of PG cells that mediates lateral inhibition between olfactory bulb principal neurons projecting into the same glomerulus. This intraglomerular inhibitory pathway is recruited by even the weakest ON input and shapes the spike output of mitral and tufted cells. Moreover, *in vivo* recordings show that intraglomerular lateral inhibition is activated at each respiration cycle.

We took advantage of a transgenic mouse expressing EYFP in a subset of PG cells to characterize the properties of an intraglomerular inhibitory circuit that modulates the spike output of principal neurons. EYFP$^+$ PG cells include, although not exclusively, cells expressing CB but does not overlap with the two other well identified populations of PG cells immunoreactive for CR and TH. Electron microscopy studies of CB$^+$ PG cells have shown that they receive synapses from mitral/tufted cells but rarely from OSNs (Toida et al., 1998; Kosaka and Kosaka, 2007; Panzanelli et al., 2007). Moreover, ultrastructural evidence suggests that CB$^+$ PG cells do not have an axon and release their neurotransmitter from dendrites within their glomerulus (Kosaka and Kosaka, 2010). Our functional and morphological characterization of EYFP$^+$ PG cells is consistent with these data. We have demonstrated that mitral, tufted, and ET cells make excitatory synapses on EYFP$^+$ PG cells. Thus, EYFP$^+$ PG cells responded to a stimulation of OSNs with a short barrage of EPSCs that lasted only few tens of milliseconds. Similar responses were observed in a subgroup of EYFP$^-$ PG cells, suggesting that EYFP$^+$ PG cells, although they constitute 30% of PG cells, might be representative of an even larger group of type 2 PG cells with similar excitatory connections. The transient nature of this response, which contrasts with the long-lasting responses observed in other PG cells, was remarkably consistent despite the diversity of immunohistochemical profiles and membrane properties among EYFP$^+$ PG cells. The onset latency of the response was quite fast (~3 ms) yet longer and more variable than in ET or PG cells connected directly to OSNs, suggesting that EYFP$^+$ PG cells do not receive direct inputs from OSNs. This fast-onset polysynaptic activation likely relies on ET cells that fire as early as 2 ms after the stimulation of OSNs (De Saint Jan et al., 2009) and elicit an EPSC in EYFP$^+$ PG cells in ~1 ms.

Some PG cells are activated by weak ON inputs (Gire and Schoppa, 2009) or the firing of a single principal cell (Murphy et

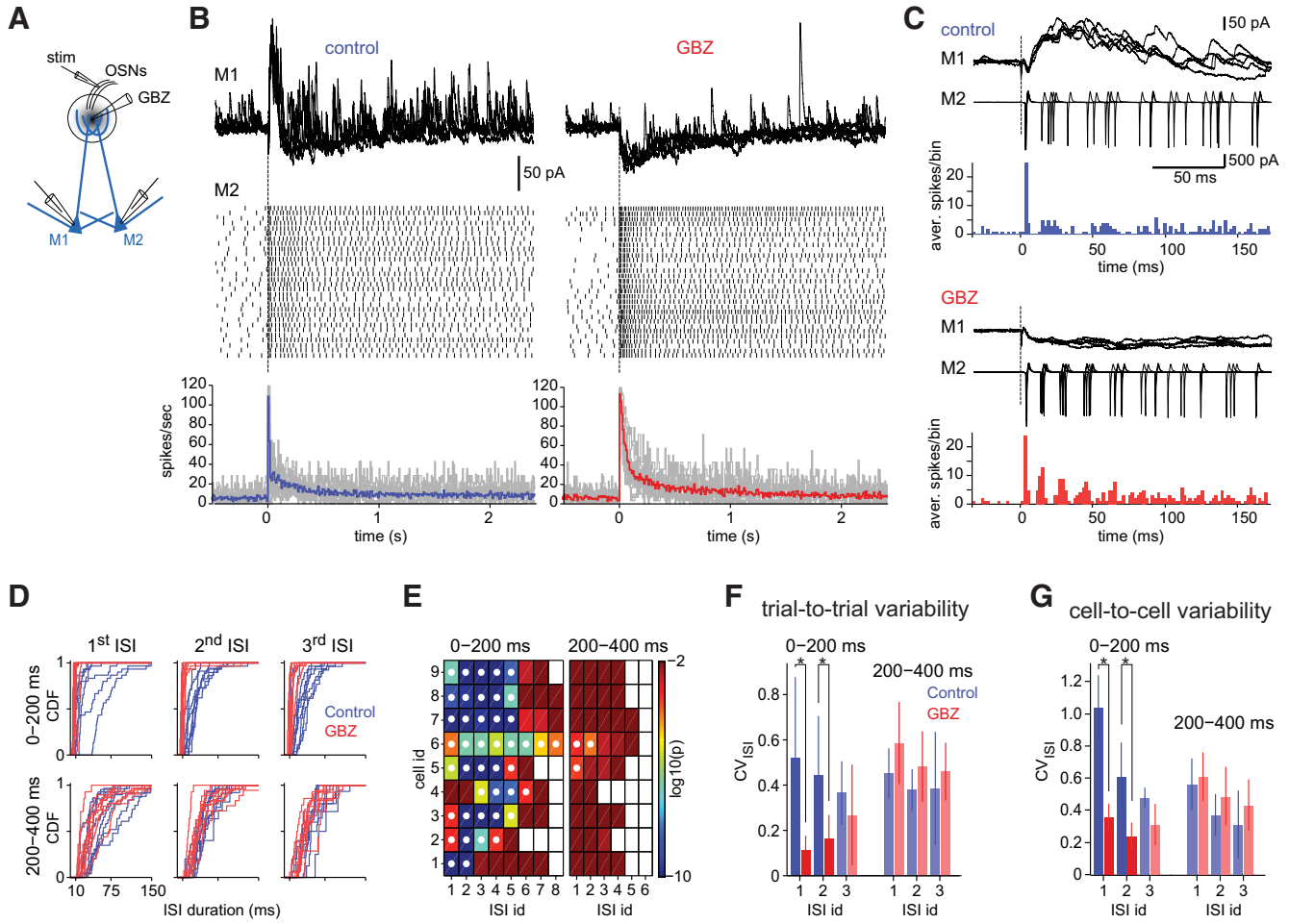

Figure 8. Intraglomerular inhibition reduces output frequency and spike timing redundancy in mitral cells. ***A***, Schematic of the experiment. ***B***, Paired recording of ON-evoked responses in two mitral cells (M1 and M2) projecting into the same glomerulus. M1 (top traces) was recorded in whole-cell mode at $V_h = 5$ mV. Five responses are superimposed under control conditions (left) and during local perfusion of GBZ (25 μM) within the glomerulus (right). Middle, Raster plots of the firing of M2 recorded simultaneously in loose cell-attached mode. The dashed line indicates the stimulation (25 μA) time. Bottom, Mean firing rate across nine mitral cells recorded in cell-attached mode in control conditions (left, blue) and in the presence of GBZ (right, red). Thick traces are grand averages, and gray traces are averages for each cell. Bin width, 10 ms. ***C***, Zoom on the initial phase of the responses shown in ***B***. Bottom, PSTH for the same M2 cell in control conditions (top) and in the presence of GBZ (bottom). Bin width, 2 ms. ***D***, Top, Cumulative density function (CDF) of the first three ISIs (first 4 spikes) in the 0–200 ms time window for nine mitral cells recorded in cell-attached mode. Blue colors correspond to the control data, and red colors indicate GBZ application. The three ISIs are shown in different columns. Bottom, Same as the top for the 200 – 400 ms time window. ***E***, Significance testing of the difference between ISI distribution in control conditions and in the presence of GBZ. Two-sampled Kolmogorov–Smirnov test p values are shown in log scale. Null hypothesis is that the ISI distribution in control conditions and in the presence of GBZ are the same. x-Axis refers to the ISI, and the y-axis refers to the cell number. p values are higher within the 0–200 ms than in the 200 – 400 ms time period. Significantly different ISIs in control and GBZ are marked with a white dot (α values = 0.001, $n = 9$ mitral cells). ***F***, In the presence of GBZ, the first two ISIs after stimulation become highly reliable across trials. CV_{ISI} of the first three ISIs. In ***F*** and ***G***, each bar shows the mean ± SD of CV_{ISI} in control conditions (blue) and in the presence of GBZ (red) for the first three ISIs within the 0–200 and 200 – 400 ms time windows. ***G***, In the presence of GBZ, in each trial, the first two ISIs after stimulation become highly reliable across cells in a simulated ensemble of nine mitral cells ($n = 14$ random trials).

al., 2005). Current models suggest that low-threshold intraglomerular inhibition may serve as a gatekeeper that shunts weak ON inputs (Gire and Schoppa, 2009) and may separate the firing phase of the two output channels (tufted vs mitral cells) along a respiration cycle (Fukunaga et al., 2012). Our results show that EYFP$^+$ PG cells constitute a large fraction of these highly excitable PG cells that also include a minority of EYFP$^-$ PG cells. We have demonstrated that they mediate a form of lateral inhibition, the firing of a single principal neuron producing disynaptic inhibition of other mitral and tufted cells within the same glomerulus. This recurrent pathway is recruited by even the weakest ON input and mediates ON-evoked inhibition of principal neurons. We also found that EYFP$^+$ PG cells indiscriminately release GABA onto mitral, tufted, and ET cells and that ON-evoked intraglomerular inhibition has a similar time course in these three types of neurons. Our experimental results do not support a recent study that stated that, unlike mitral cells, tufted cells are not, or are less, modulated by intraglomerular inhibition (Fukunaga et al., 2012). However, that study relied on a theoretical network model based on experimentally undemonstrated differences in PG cell inputs on mitral and tufted cells. More recently, Burton and Urban (2014) suggested that the different firing phases of mitral and tufted cells may be attributable to a greater intrinsic excitability and a stronger afferent-evoked excitation in tufted cells.

Evaluating the contribution of EYFP$^+$ PG cells in ON-evoked inhibition would require their selective manipulation, for instance, with optogenetics. However, to date, there is no selective marker for this population, which impedes its genetic manipulation. Nevertheless, our data suggest that only a minority of PG cells have a similar activation threshold than EYFP$^+$ PG cells and potentially contribute to ON-evoked inhibition. Moreover, we

show that half of CR$^+$ PG cells are not, or are only weakly, activated by ON inputs and thus unlikely to participate. However, ON-evoked inhibition lasts longer than the firing of EYFP$^+$ PG cells, suggesting that other PG cell subtypes that respond to an ON input with a longer firing may generate late IPSCs. Do granule or PV$^+$ cells also contribute to the early phase of ON-evoked inhibition? Several results argue against this idea. As shown previously (Shao et al., 2012), early IPSCs persisted in the presence of NMDA receptor blockers that limit the activation of granule cells (Isaacson and Strowbridge, 1998; Schoppa et al., 1998). Second, ON-evoked inhibition was abolished by intraglomerular perfusion of GBZ, suggesting that PV$^+$ and granule cells that do not make synapses within the glomerulus do not contribute. Consistent with this conclusion, the time course of ON-evoked inhibition was similar in ET cells that presumably do not interact with granule cells and PV$^+$ interneurons. This indicates that intraglomerular pathways are sufficient to produce a strong inhibition. Finally, granule cells respond to a glomerular stimulation with an ~70 ms delayed firing (Schoppa and Westbrook, 1999; Kapoor and Urban, 2006) that does not match with the early onset of OSN-evoked inhibition (~6 ms).

The short timescale of EYFP$^+$ PG cell-mediated intraglomerular inhibition in slices (~100 ms) is physiologically relevant for odor processing. *In vivo*, spontaneous firing and odor-evoked discharges of mitral and tufted cells are often constrained by the ~2–10 Hz respiratory rhythm. Thus, mitral and tufted cells fire action potentials during a brief (50–150 ms) phase of the respiration cycle (Cang and Isaacson, 2003; Margrie and Schaefer, 2003; Davison and Katz, 2007; Dhawale et al., 2010). As reported previously (Luo and Katz, 2001; Margrie and Schaefer, 2003), rhythmic depolarizations locked to the respiration underlie this activity. We have found that these EPSPs compete with IPSPs in anesthetized mice. Because EYFP$^+$ PG cells fire action potentials at each respiration cycle, they likely mediate at least a fraction of this inhibition. Similar to EYFP$^+$ PG cells, PV$^+$ cells are highly active *in vivo*, even in the absence of exogenously applied odorants (Miyamichi et al., 2013), and thus may contribute to this inhibition. In contrast, granule cells have a low spontaneous firing rate in anesthetized mice (Cang and Isaacson, 2003; Margrie and Schaefer, 2003; Kato et al., 2012). However, their activity is strongly enhanced in the awake animal, suggesting that the influence of each interneuron population may differ in the awake and anesthetized state (Kato et al., 2012).

In classical pathways, feedforward inhibition quickly follows monosynaptic excitation and defines a short temporal window of opportunity for the postsynaptic neuron to fire. Thus, inhibition often promotes spike timing precision (Pouille and Scanziani, 2001). In contrast, we found that ON-evoked intraglomerular inhibition promotes spike timing variability in olfactory bulb mitral cells from trial to trial and also from cell to cell. Intraglomerular lateral inhibition relies on synapses with low release probability, whereas the long-lasting ON-evoked excitation of mitral and tufted cells relies on excitatory synapses with high release probability (Najac et al., 2011). Therefore, IPSC timing and amplitudes vary from trial to trial and from cell to cell, unlike excitation that is highly reproducible. Moreover, membrane properties constrain mitral cells to fire reliable and precisely timed action potentials across trials in response to an identical synaptic-like fluctuating stimulus (Padmanabhan and Urban, 2010) or an EPSP waveform (Balu et al., 2004). This explains why each mitral cell responded to the afferent input with a stereotyped pattern of spikes in the presence of GBZ. In addition, intraglomerular dendrodendritic excitatory interactions and gap-junction coupling drive synchronous firing in principal cells connected to the same glomerulus (Schoppa and Westbrook, 2002; Ma and Lowe, 2010). Thus, intraglomerular inhibition competes with multiple mechanisms that tend to synchronize the output of a glomerulus. Many neurons of the olfactory bulb network fire in synchrony in the presence of an odorant, suggesting that olfactory coding in the olfactory bulb relies, at least in part, on precise spike timing in a population of cells (Bathellier et al., 2010). Although the functional implication of intraglomerular inhibition is at present uncertain, one possible function of this pathway may be to prevent correlated spiking in the absence of exogenous odorants.

References

Abraham NM, Egger V, Shimshek DR, Renden R, Fukunaga I, Sprengel R, Seeburg PH, Klugmann M, Margrie TW, Schaefer AT, Kuner T (2010) Synaptic inhibition in the olfactory bulb accelerates odor discrimination in mice. Neuron 65:399–411. CrossRef Medline

Balu R, Larimer P, Strowbridge BW (2004) Phasic stimuli evoke precisely timed spikes in intermittently discharging mitral cells. J Neurophysiol 92:743–753. CrossRef Medline

Bathellier B, Gschwend O, Carleton A (2010) Temporal coding in olfaction. In: The neurobiology of olfaction (Menini A, ed), pp 329–348. Boca Raton, FL: CRC.

Burton SD, Urban NN (2014) Greater excitability and firing irregularity of tufted cells underlies distinct afferent-evoked activity of olfactory bulb mitral and tufted cells. J Physiol 592:2097–2118. CrossRef Medline

Cang J, Isaacson JS (2003) *In vivo* whole-cell recording of odor-evoked synaptic transmission in the rat olfactory bulb. J Neurosci 23:4108–4116. Medline

Caputi A, Rozov A, Blatow M, Monyer H (2009) Two calretinin-positive GABAergic cell types in layer 2/3 of the mouse neocortex provide different forms of inhibition. Cereb Cortex 19:1345–1359. CrossRef Medline

Charpak S, Mertz J, Beaurepaire E, Moreaux L, Delaney K (2001) Odor-evoked calcium signals in dendrites of rat mitral cells. Proc Natl Acad Sci U S A 98:1230–1234. CrossRef Medline

Christie JM, Schoppa NE, Westbrook GL (2001) Tufted cell dendrodendritic inhibition in the olfactory bulb is dependent on NMDA receptor activity. J Neurophysiol 85:169–173. Medline

Davison IG, Katz LC (2007) Sparse and selective odor coding by mitral/tufted neurons in the main olfactory bulb. J Neurosci 27:2091–2101. CrossRef Medline

De Saint Jan D, Westbrook GL (2007) Disynaptic amplification of metabotropic glutamate receptor 1 responses in the olfactory bulb. J Neurosci 27:132–140. CrossRef Medline

De Saint Jan D, Hirnet D, Westbrook GL, Charpak S (2009) External tufted cells drive the output of olfactory bulb glomeruli. J Neurosci 29:2043–2052. CrossRef Medline

Dhawale AK, Hagiwara A, Bhalla US, Murthy VN, Albeanu DF (2010) Non-redundant odor coding by sister mitral cells revealed by light addressable glomeruli in the mouse. Nat Neurosci 13:1404–1412. CrossRef Medline

Dong HW, Hayar A, Ennis M (2007) Activation of group I metabotropic glutamate receptors on main olfactory bulb granule cells and periglomerular cells enhances synaptic inhibition of mitral cells. J Neurosci 27:5654–5663. CrossRef Medline

Fukunaga I, Berning M, Kollo M, Schmaltz A, Schaefer AT (2012) Two distinct channels of olfactory bulb output. Neuron 75:320–329. CrossRef Medline

Gire DH, Schoppa NE (2009) Control of on/off glomerular signaling by a local GABAergic microcircuit in the olfactory bulb. J Neurosci 29:13454–13464. CrossRef Medline

Hayar A, Karnup S, Ennis M, Shipley MT (2004) External tufted cells: a major excitatory element that coordinates glomerular activity. J Neurosci 24:6676–6685. CrossRef Medline

Isaacson JS, Strowbridge BW (1998) Olfactory reciprocal synapses: dendritic signaling in the CNS. Neuron 20:749–761. CrossRef Medline

Kapoor V, Urban NN (2006) Glomerulus-specific, long-latency activity in the olfactory bulb granule cell network. J Neurosci 26:11709–11719. CrossRef Medline

Kato HK, Chu MW, Isaacson JS, Komiyama T (2012) Dynamic sensory

representations in the olfactory bulb: modulation by wakefulness and experience. Neuron 76:962–975. CrossRef Medline

Kato HK, Gillet SN, Peters AJ, Isaacson JS, Komiyama T (2013) Parvalbumin-expressing interneurons linearly control olfactory bulb output. Neuron 80:1218–1231. CrossRef Medline

Kiyokage E, Pan YZ, Shao Z, Kobayashi K, Szabo G, Yanagawa Y, Obata K, Okano H, Toida K, Puche AC, Shipley MT (2010) Molecular identity of periglomerular and short axon cells. J Neurosci 30:1185–1196. CrossRef Medline

Kosaka K, Kosaka T (2007) Chemical properties of type 1 and type 2 periglomerular cells in the mouse olfactory bulb are different from those in the rat olfactory bulb. Brain Res 1167:42–55. CrossRef Medline

Kosaka T, Kosaka K (2010) Heterogeneity of calbindin-containing neurons in the mouse main olfactory bulb: I. General description. Neurosci Res 67:275–292. CrossRef Medline

Luo M, Katz LC (2001) Response correlation maps of neurons in the mammalian olfactory bulb. Neuron 32:1165–1179. CrossRef Medline

Ma J, Lowe G (2010) Correlated firing in tufted cells of mouse olfactory bulb. Neuroscience 169:1715–1738. CrossRef Medline

Margrie TW, Schaefer AT (2003) Theta oscillation coupled spike latencies yield computational vigour in a mammalian sensory system. J Physiol 546:363–374. CrossRef Medline

Margrie TW, Meyer AH, Caputi A, Monyer H, Hasan MT, Schaefer AT, Denk W, Brecht M (2003) Targeted whole-cell recordings in the mammalian brain in vivo. Neuron 39:911–918. CrossRef Medline

McQuiston AR, Katz LC (2001) Electrophysiology of interneurons in the glomerular layer of the rat olfactory bulb. J Neurophysiol 86:1899–1907. Medline

Metzger F, Repunte-Canonigo V, Matsushita S, Akemann W, Diez-Garcia J, Ho CS, Iwasato T, Grandes P, Itohara S, Joho RH, Knöpfel T (2002) Transgenic mice expressing a pH and Cl^- sensing yellow-fluorescent protein under the control of a potassium channel promoter. Eur J Neurosci 15:40–50. CrossRef Medline

Miyamichi K, Shlomai-Fuchs Y, Shu M, Weissbourd BC, Luo L, Mizrahi A (2013) Dissecting local circuits: parvalbumin interneurons underlie broad feedback control of olfactory bulb output. Neuron 80:1232–1245. CrossRef Medline

Mori K, Nagao H, Yoshihara Y (1999) The olfactory bulb: coding and processing of odor molecule information. Science 286:711–715. CrossRef Medline

Murphy GJ, Darcy DP, Isaacson JS (2005) Intraglomerular inhibition: signaling mechanisms of an olfactory microcircuit. Nat Neurosci 8:354–364. CrossRef Medline

Najac M, De Saint Jan D, Reguero L, Grandes P, Charpak S (2011) Monosynaptic and polysynaptic feed-forward inputs to mitral cells from olfactory sensory neurons. J Neurosci 31:8722–8729. CrossRef Medline

Padmanabhan K, Urban NN (2010) Intrinsic biophysical diversity decorrelates neuronal firing while increasing information content. Nat Neurosci 13:1276–1282. CrossRef Medline

Panzanelli P, Fritschy JM, Yanagawa Y, Obata K, Sassoè-Pognetto M (2007) GABAergic phenotype of periglomerular cells in the rodent olfactory bulb. J Comp Neurol 502:990–1002. CrossRef Medline

Parrish-Aungst S, Shipley MT, Erdelyi F, Szabo G, Puche AC (2007) Quantitative analysis of neuronal diversity in the mouse olfactory bulb. J Comp Neurol 501:825–836. CrossRef Medline

Pinching AJ, Powell TP (1971a) The neuropil of the glomeruli of the olfactory bulb. J Cell Sci 9:347–377. Medline

Pinching AJ, Powell TP (1971b) The neuron types of the glomerular layer of the olfactory bulb. J Cell Sci 9:305–345. Medline

Pouille F, Scanziani M (2001) Enforcement of temporal fidelity in pyramidal cells by somatic feed-forward inhibition. Science 293:1159–1163. CrossRef Medline

Schoppa NE, Westbrook GL (1999) Regulation of synaptic timing in the olfactory bulb by an A-type potassium current. Nat Neurosci 2:1106–1113. CrossRef Medline

Schoppa NE, Westbrook GL (2002) AMPA autoreceptors drive correlated spiking in olfactory bulb glomeruli. Nat Neurosci 5:1194–1202. CrossRef Medline

Schoppa NE, Kinzie JM, Sahara Y, Segerson TP, Westbrook GL (1998) Dendrodendritic inhibition in the olfactory bulb is driven by NMDA receptors. J Neurosci 18:6790–6802. Medline

Shao Z, Puche AC, Kiyokage E, Szabo G, Shipley MT (2009) Two GABAergic intraglomerular circuits differentially regulate tonic and phasic presynaptic inhibition of olfactory nerve terminals. J Neurophysiol 101:1988–2001. CrossRef Medline

Shao Z, Puche AC, Liu S, Shipley MT (2012) Intraglomerular inhibition shapes the strength and temporal structure of glomerular output. J Neurophysiol 108:782–793. CrossRef Medline

Shepherd GM (2004) The synaptic organization of the brain, Ed 5. Oxford, UK: Oxford UP.

Toida K, Kosaka K, Heizmann CW, Kosaka T (1998) Chemically defined neuron groups and their subpopulations in the glomerular layer of the rat main olfactory bulb: III. Structural features of calbindin D28K-immunoreactive neurons. J Comp Neurol 392:179–198. CrossRef Medline

Urban NN, Sakmann B (2002) Reciprocal intraglomerular excitation and intra- and interglomerular lateral inhibition between mouse olfactory bulb mitral cells. J Physiol 542:355–367. CrossRef Medline

Whitman MC, Greer CA (2007) Adult-generated neurons exhibit diverse developmental fates. Dev Neurobiol 67:1079–1093. CrossRef Medline

Yokoi M, Mori K, Nakanishi S (1995) Refinement of odor molecule tuning by dendrodendritic synaptic inhibition in the olfactory bulb. Proc Natl Acad Sci U S A 92:3371–3375. CrossRef Medline

Results II: GABAergic projections from the basal forebrain control multiple inhibitory interneuron subtypes in the olfactory bulb.

Manuscript

GABAergic projections from the basal forebrain control multiple inhibitory interneuron subtypes in the olfactory bulb

Alvaro Sanz Diez[1], Marion Najac[2] and Didier De Saint Jan[1]

[1]Institut des Neurosciences Cellulaires et Intégratives, Centre National de la Recherche Scientifique, Unité Propre de Recherche 3212, Université de Strasbourg, 67084 Strasbourg, France, [2]Department of Neurobiology, Northwestern University, Evanston, Illinois 60208.

Corresponding authors:
desaintjan@inci-cnrs.unistra.fr
Institut des Neurosciences Cellulaires et Intégratives, CNRS UPR 3212, 5 rue Blaise Pascal, 67084 Strasbourg, France

Authors contributions: ASD and DDSJ did the experiments, Marion Najac contributed essential preliminary data, DDSJ wrote the paper. All authors edited the manuscript.

Abstract

Olfactory bulb circuits transform a spatially organized olfactory sensory input into a temporal output code in mitral and tufted cells. This early processing of the olfactory inputs is strongly modulated by diverse subtypes of inhibitory interneurons that, together, vastly outnumber principal neurons. Little is known about the inhibitory circuits that regulate the activity of these interneurons. We examined this question using whole-cell patch-clamp recording and optogenetic in olfactory bulb slices. We demonstrate that long-range centrifugal afferences originating from the horizontal limb of the Diagonal Band of Broca (HDB) provide a major inhibitory input on most subtypes of periglomerular cells, deep short axon cells and granule cells. This GABAergic innervation has variable properties and exerts diverse and complex effects depending on the postsynaptic interneuron subtype. These results suggest that inhibitory fibers from the HDB may have profound and diverse actions on olfactory bulb circuits.

Introduction

Olfactory bulb circuits transform a spatially organized incoming sensory input carried by olfactory sensory neurons (OSNs) into a temporal output code in mitral and tufted cells, the principal neurons that relay the information to cortical areas. In the olfactory bulb, inhibitory interneurons vastly outnumber mitral and tufted cells and multiple inhibitory circuits shape the output of principal neurons. Thousands of newborn inhibitory neurons are also integrated every postnatal day in the pre-existing olfactory bulb network. Inhibition thus plays fundamental roles in early olfactory bulb processing, as demonstrated by multiple evidence *in vivo* (Yokoi et al., 1995; Cang and Isaacson, 2003; Abraham et al., 2010; Fukunaga et al., 2012; Lepousez and Lledo, 2013; Fukunaga et al., 2014; Gschwend et al., 2015; Economo et al., 2016).

Olfactory bulb interneurons are diverse but three large classes dominate: granule cells, periglomerular (PG) cells and short-axon (SA) cells. The most abundant are granule cells that form reciprocal dendrodendritic synapses with the lateral dendrites of mitral and tufted cells in the external plexiform layer. These axonless neurons mediate reciprocal inhibition (Isaacson and Strowbridge, 1998; Schoppa et al., 1998) as well as lateral inhibition between principal cells projecting in different glomeruli (Isaacson and Strowbridge, 1998). PG interneurons surround each spherical neuropil called glomerulus into which OSN axons make synapses onto principal neurons. These small cells that usually project within a single glomerulus and often lack an axon are functionally, morphologically and chemically highly diverse (Kosaka and Kosaka, 2007; Panzanelli et al., 2007; Parrish-Aungst et al., 2007; Whitman and Greer, 2007; Kosaka and Kosaka, 2011). Yet, they can be classified into two broad classes. The majority are so-called type 2 PG cells that receive excitatory inputs exclusively from the dendrites of mitral and tufted cells and in turn generate a potent intra-glomerular inhibition in mitral and tufted cells (Shao et al., 2009; Shao et al., 2012; Shao et al., 2013; Najac et al., 2015; Geramita and Urban, 2017). In contrast, type 1 PG cells receive direct excitatory inputs from OSNs and modulate glutamate release from the incoming sensory afferents (Murphy et al., 2005; Shao et al., 2009). Finally, different subtypes of SA cells with soma located in the glomerular layer (superficial SA cells) or in the granule cell layer (deep SA cells), unlike what their name suggest, rely on long ramifying axons to form broad intrabulbar and interglomerular axonal connections (Aungst et al., 2003; Eyre et al., 2008; Kosaka and Kosaka, 2008; Kiyokage et al., 2010; Burton et al., 2017). Deep SA cell subtypes with diverse morphologies mediate widespread interneuron-specific inhibition (Eyre et al., 2008; Boyd et al., 2012; Burton et al., 2017) whereas superficial SA cells inhibit external tufted cells (Liu et al., 2013; Whitesell et al., 2013).

Each of these interneuron subtypes receives inhibitory inputs. Only few studies, however, have investigated the origin and functional impact of this inhibition. Local interneuron interactions are not unusual in the brain but they are still poorly documented in the bulb. Yet, synaptic or spillover-mediated interactions between PG cells (Smith and Jahr, 2002; Murphy et al., 2005; Parsa et al., 2015) or between neighboring granule cells (Bardy et al., 2010) may provide a local control of interneurons activity. In addition, deep SA cells innervate both granule and PG cells suggesting that they are a widespread intrabulbar regulator of inhibition (Eyre et al., 2008; Burton et al., 2017). Finally, several nuclei in the subcortical basal forebrain, especially the horizontal limb of the Diagonal Band of Broca (HDB), send dense centrifugal GABAergic projections to the olfactory bulb (Zaborszky et al., 1986; Gracia-Llanes et al., 2010; Niedworok et al., 2012). Anatomical evidences indicate that

these centrifugal fibers innervate interneurons in all layers of the bulb but functional connections have only been demonstrated on granule cells (Nunez-Parra et al., 2013). Thus, different sources may inhibit olfactory bulb interneurons and control their activity. We examined this question using patch-clamp recording and optogenetic in olfactory bulb slices, with a specific focus on PG cells. We demonstrate that the different subtypes of type 2 PG cells do not innervate each other. Instead, they all receive robust inhibitory inputs from the HDB, each subtype being diversely modulated by this GABAergic input. HDB fibers also inhibit deep SA cells and granule cells suggesting that this major centrifugal afference has a profound functional impact on the olfactory bulb circuits.

Materials and Methods

Animals. All experimental procedures conformed to the French Ministry and local ethics committee (CREMEAS) guidelines on animal experimentation. Three transgenic mouse lines were used. Kv3.1-EYFP mice express the enhanced yellow fluorescent protein (EYFP) under the control of the Kv3.1 K^+ channel promoter (Metzger et al., 2002). Thy1-ChR2-EYFP mice express the channel rhodopsin 2 (ChR2) fused to EYFP under the control of the thymocyte antigen 1 (Thy1) promoter (B6.Cg-Tg (Thy1-COP4/EYFP) 18 Gfng/J from the Jackson laboratory, USA). Dlx5/6-cre mice express the Cre recombinase under the control of the regulatory sequences of the dlx5 and dlx6 genes (Monory et al., 2006).

Slice preparation. 2 weeks to 3 month-old mice of either sex were killed by decapitation and the olfactory bulbs rapidly removed in ice-cold oxygenated (95% O2-5% CO2) solution containing (in mM): 83 NaCl, 26.2 NaHCO3, 1 NaH2PO4, 2.5 KCl, 3.3 MgSO4, 0.5 CaCl2, 70 sucrose and 22 D-glucose (pH 7.3, osmolarity 300 mOsm/l). Horizontal olfactory bulb slices (300 µm) were cut using a Microm HM650 V vibratome in the same solution; incubated for 30-40 minutes at 34°C; stored at room temperature in a regular artificial cerebrospinal fluid (ACSF) until use. ACSF contained (in mM): 125 NaCl, 25 NaHCO3, 2.5 KCl, 1.25 NaH2PO4, 1 MgCl2, 2 CaCl2 and 25 D-glucose and was continuously bubbled with 95% O2-5% CO2.

Electrophysiological recordings. Experiments were conducted at 32-34°C under an upright microscope with differential interference contrast (DIC) optics. Whole-cell voltage-clamp recordings were made with pipettes (3-6 MΩ) filled with a K-gluconate-based internal solution containing (in mM): 135 K-gluconate, 2 $MgCl_2$, 0.025 $CaCl_2$, 1 EGTA, 4 Na-ATP, 0.5 Na-GTP, 10 Hepes (pH 7.3, 280 mOsm). Atto 594 (10 µM, Sigma) was added to the internal solution in order to visualize the cell morphology. Loose cell-attached recordings (15-100 MΩ seal resistance) were made with pipettes filled with ACSF and used several times on different neurons. OSN axons bundles projecting inside a given glomerulus were stimulated using a theta pipette filled with ACSF as previously described (Najac et al., 2011). The electrical stimulus (100 µs) was delivered using a Digitimer DS3. Optical stimulation was done through a blue Cool LED pE 100 (490 nm) directed through the 40X objective of the microscope. Recordings were acquired with a multiclamp 700B amplifier (Molecular Devices), low-passed filtered at 2-4 kHz and digitized at 10 kHz using AxoGraph X software. In current-clamp recordings a constant hyperpolarizing current was injected in order to maintain the cell at a potential of -60/-70 mV. In voltage-clamp recordings, access resistance (Ra<30 MΩ for PG, granule and deep SA cells) were not compensated. Voltages indicated in the paper were corrected for the junction potential (-15 mV).

Drugs. 6-nitro-7-sulfamoylbenzo[f]quinoxaline-2,3-dione (NBQX), D-2-Amino-5-phosphonopentanoic acid (D-AP5), 2-(3-carboxypropyl)-3-amino-6-(4 methoxyphenyl)pyridazinium bromide (gabazine), tetrodotoxin (TTX) and *N*-Methyl-D-aspartic acid (NMDA) were purchased from Tocris Bioscience (Ellisville, MO, USA).

Cell morphology. To reconstruct the morphology of the recorded cells, biocytin or neurobiotin (Sigma) was added to the intracellular solution (1mg/ml). The patch pipette was slowly withdrawn after the recordings to avoid damaging the cell bodies. Slices were then fixed in 4% paraformaldehyde overnight, washed 3 times and incubated in a permeabilizing solution containing Cy-5 conjugated streptavidin (1 µg/ml; Thermo Fischer) overnight. After 3 wash cycles with PBS, sections were mounted. Labeled cells were imaged with a confocal microscope (Leica TCS SP5).

Brain lesion. 5-6 weeks old Thy1-ChR2-eYFP mice were anesthetized with isoflurane (2-3%), treated with local application of lidocaine (5%) and intraperitoneal injection of Metacam (5%) (100µl/10g). Mice were craneotomized and ~200nl of NMDA (120 mM) was stereotaxically injected with a Pneumatic Picopump PV 820, at 0.2 mm AP, -1.6mm ML and -5.75 DV from bregma. Mice recovered during 2-3 weeks after injection before anatomical or physiological experiments.

Stereotaxic viral injections in the HDB. 3-6 weeks old dlx5/6-cre transgenic mice were anesthetized with intraperitoneal injection of ketamine (20%), acepromazin (6%) and medetomidin (11.8%) mix (100µl/10g) and placed in a stereotaxic apparatus (RWD). Mice were craneotomized and a volume of 200-500 nl of AAV9.EF1a.DIO.hChR2(H134R).eYFP.WPRE.hGH (UPenn, Addgene 20298) was stereotaxically injected with a Pneumatic Picopump PV 820 (WPI), at 0.2 mm AP, -1.6mm ML and -5.75 DV from bregma. After surgery, mice were injected with Metacam (5%) (100µl/10g), Antisedan (2.5%) (100µl/10g) and rehydrated with 1 ml of NaCl 0.9%. Mice recovered during 3-4 weeks after injection before anatomical or physiological experiments.

Analysis. EPSCs, IPSCs or photo-current amplitudes were measured as the peak of an average response computed from multiple sweeps. Rise time values were calculated as the difference between the time at 20% of the peak and at 80% of the EPSC/IPSC peak. The decay of light-evoked IPSCs was most often best fitted with a double exponential with time t=0 at the peak of the current. Time constant values indicated in the text are weighted decay time constant calculated using the following equation: $\tau_w = (\tau_1 A_1 + \tau_2 A_2)/(A_1 + A_2)$ where τ_1 and τ_2 are the fast and slow decay time constants and A_1 and A_2 are the equivalent amplitude weighting factors. To estimate the duration of an OSN-evoked pluri-synaptic excitatory response, individual EPSCs with amplitude >5 pA were first automatically detected by the Axograph X software using a sliding template function. PSTH (peri stimulus time histograms) representing the cumulative number of EPSCs per 20 ms bin across several consecutive sweeps were then constructed. OSN-evoked PSTH peak shortly after the stimulation and then decay to the baseline. The decaying phase was best fitted with a single or with two exponentials to provide the time constant of the response duration.
We used the unpaired t-test to compare two sets of data acquired from different populations. Results are expressed as mean ± SD unless otherwise specified.

Immunohistochemistry. Adult mice (1-3 months) were deeply anesthetized with intraperitoneal injection of xylazine (6.3%) and ketamine (25%) and perfused with 4%

paraformaldehyde (PFA). Brains were removed and kept in 4% PFA overnight. Slices were cut (50 µm thick) with a vibratome (Leica VT 1000S). Blocking steps were performed using a PBS solution containing 2% BSA and 0.3% Triton X-100 during 2h. Sections were incubated 48 hours at 4°C with primary antibodies—Rabbit anti-GFP (1:500) Clontech, Mouse anti-NeuN (1:500) Chemicon, Mouse anti-Calbindin-28Kb (1:500) Sigma, Rabbit anti-GABA (1:100) Sigma or Mouse antiGAD67 (1:500) Chemicon. After three washes in PBS, they were incubated 2 hours at room temperature with secondary antibodies—Alexa fluor 555 and Alexa fluor 488 conjugated anti-mouse or anti-rabbit (1:500) Molecular probes. After three washes, sections were incubated with Hoechst staining (1:1000, 30 min) and finally mounted in Prolong Diamond Antifade Mountant (Molecular probes). Images were taken using a Leica TCS SP5 II confocal microscope or an Axio Imager M2 for mosaic images. Immunostained and EYFP expressing cells in the HDB were manually counted using Cell counter plug-in on Fiji software.

Results

The glomerular network does not provide inhibition on type 2 PG cells

We first used the Kv3.1-EYFP transgenic mouse (Metzger et al., 2002) to investigate whether PG cells innervate each other. In this mouse, a heterogeneous population of type 2 PG cells is selectively labeled and includes, although not exclusively, calbindin-expressing PG cells. A common property of EYFP(+) PG cells is their short polysynaptic response to a single electrical stimulation of the OSNs. This brief barrage of excitatory post-synaptic currents (EPSCs) efficiently drives their firing (Najac et al., 2015). Thus, we reasoned that if EYFP(+) PG cells make synapses between each other, a stimulation of the OSNs should also produce inhibitory post-synaptic currents (IPSCs) in these neurons. However, OSN stimulations that evoked robust excitatory responses in EYFP(+) PG cells voltage-clamped at Vh= -75 mV did not evoke any outward IPSC when cells were clamped around the reversal potential for EPSCs (Vh= 0 mV, n=15, Figure 1A and 1B). One caveat of these experiments is the lack of control that the stimulation induces spiking in other PG cells projecting in the same glomerulus, especially in those that require a stronger stimulation to be activated (Najac et al., 2015). Thus, in a subset of experiments we simultaneously monitored the firing of a control PG cell (either EYFP(+), n=4, or EYFP(-), n=5) projecting into the same glomerulus. Under these conditions, stimulations that produced a discharge in the control PG cell did not evoke any IPSC in the voltage-clamped EYFP(+) PG cell (n=9, supplementary Fig.1). Increasing the stimulation intensity by a factor of 10 also failed to evoke reliable IPSCs (n=6, supplementary Fig.1).

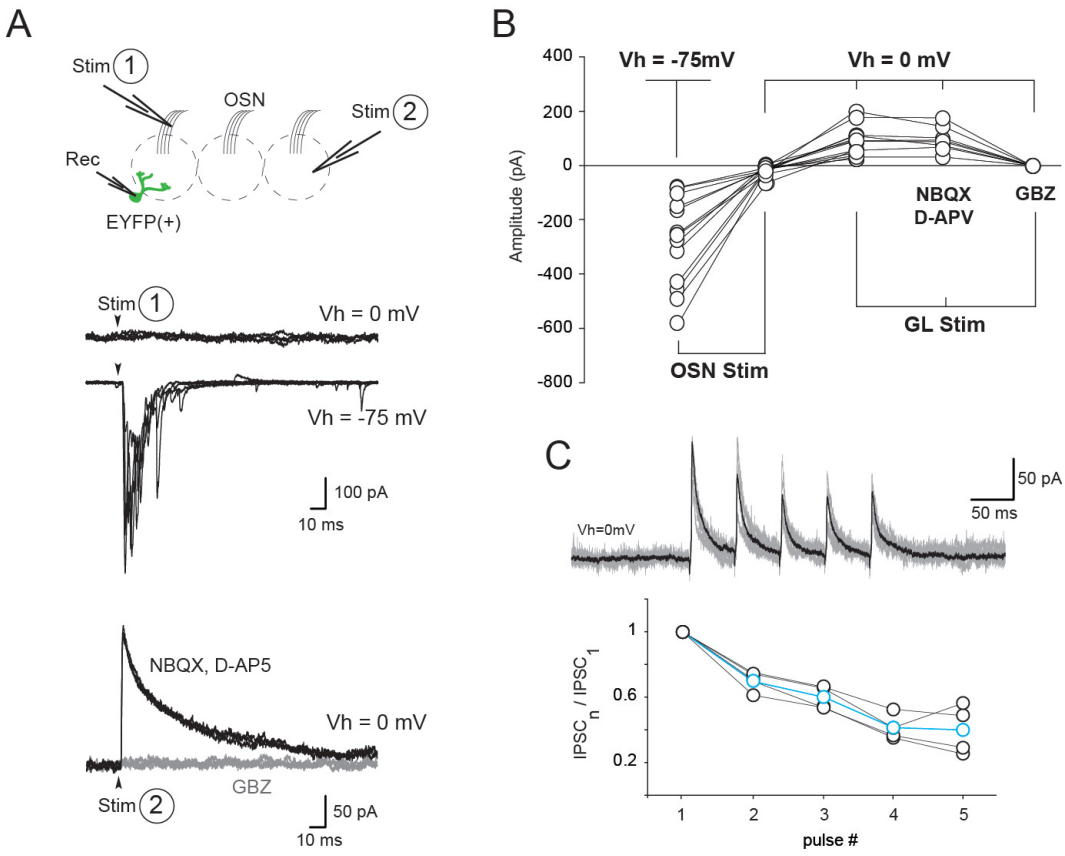

Figure 1 : Inhibitory inputs of Kv3.1-EYFP(+) type 2 PG cells are not mediated by the glomerular network. A, Synaptic responses of labeled type 2 PG cells in the Kv3.1-EYFP transgenic mouse in response to the stimulation of the OSN innervating their glomerulus (1) or in response to a distant stimulation in the glomerular layer (2). EPSCs were recorded at Vh=-75 mV and IPSCs were recorded around the reversal potential for excitation, at Vh=0 mV. OSN stimulation that elicited a robust and fast pluri-synaptic excitatory response did not produce any inhibition (stimulation 1, middle traces). In contrast, stimulation in the glomerular layer >200 µm away from the recorded cell evoked a monosynaptic IPSC in the presence of NBQX (10 µM) and D-AP5 (50 µM). This IPSC was fully blocked by GBZ (5 µM). **B,** Summary plot for all the EYFP(+) PG cells. **C,** Short-term depression of the inhibitory inputs of EYFP(+) PG Cells. Top, IPSCs evoked by a train of 5 electrical stimulations every 50 ms in the glomerular layer in a EYFP(+) PG cells. The average trace (black) is superimposed on single responses (grey). Bottom, amplitude of the n^{th} IPSC relative to the normalized amplitude of the first IPSC is plotted. Blue plots show the average.

The absence of any OSN-evoked inhibitory input does not reflect a lack of inhibitory synapses on EYFP(+) PG cells since spontaneous IPSCs were routinely observed. Moreover, electrical stimulation in the glomerular layer at >200 µm away from the recorded PG cell evoked a reliable IPSC (n=12, averaged amplitude 95 ± 62 pA at Vh= 0 mV) with a fast time course (20-80% rise time, 0.64 ± 0.40 ms; decay time constant: 30.0 ± 10.9 ms) that was blocked by the $GABA_A$ receptor antagonist gabazine (GBZ, Figure 1A and 1B). This electrically-evoked IPSC persisted in the presence of the AMPA and NMDA receptor antagonists NBQX and D-AP5, respectively, demonstrating its monosynaptic nature (Figure 1A and 1B). In many cells the stimulus produced a composite IPSC with multiple peaks at distinct but reliable timing. Decreasing the intensity of stimulation reduced the amplitude of the response in stepwise manner and the occurrence of the multiple peaks suggesting that several convergent inputs can be recruited within the glomerular layer (supplementary Figure 2). To examine the short-term plasticity of this connection, we applied a train of five electrical stimuli delivered at 20 Hz. As illustrated in Figure 1C where the amplitude of the n^{th} IPSC relative to the first is plotted, the GABAergic IPSC strongly depressed (n=4). Finally, a

monosynaptic IPSC with a similar time course was also elicited in the presence of NBQX and D-AP5 when the stimulating pipette was positioned in infra mitral cell layers (n=5, average amplitude 130 ± 152 pA)(supplementary Figure 3). All together, these results suggest that EYFP(+) PG cells receive inhibitory inputs from multiple long-range axonal projections ramifying in different layers of the olfactory bulb.

As EYFP(+) PG cells constitute only ~30% of all PG cells, we next repeated the same experiments in non-labeled PG cells. We have previously shown that a majority of them are diverse classes of type 2 PG cells (Najac et al., 2015). Some of these EYFP(-) type 2 PG cells are indistinguishable from EYFP(+) PG cells, i.e. they have diverse firing patterns but a short-lived (<100 ms) multi-synaptic excitatory response to an OSN stimulation. In addition, two subgroups emerge with clear distinctive features. First, calretinin (CR)-expressing PG cells which are poorly connected to mitral and tufted cells and therefore receive a low rate of spontaneous EPSCs and small OSN-evoked responses (Najac et al., 2015). These cells also fire only once when depolarized (Fogli Iseppe et al., 2016). Second, some PG cells respond to a single stimulation of OSNs with a remarkably long barrage of EPSCs that lasts >100 ms and often several hundreds of milliseconds. These cells with long-lasting OSN-evoked excitation consistently respond to a step depolarization with a regular firing. Similar to EYFP(+) PG cells, OSN stimulation did not evoke any ISPC in these diverse classes of EYFP(-) type 2 PG cells (n=23) whereas stimulation in distant glomeruli elicited a monosynaptic IPSC in the presence of NBQX and D-AP5 (n=12, mean amplitude 64 ± 47 pA)(Figure 2A, 2B)(20-80% rise time: 0.9 ± 0.9 ms; decay time constant: 16.0 ± 18.5 ms, range 6-70 ms). The only PG cells that received IPSCs after OSN stimulations were all type 1 PG cells (seen in 7/17 type 1 PG cells, Figure 2C, 2D). These cells had a fast onset monosynaptic OSN-evoked EPSC at Vh= -75 mV and responded to a membrane supra-threshold depolarization with a train of spikes with accommodating amplitudes and sometime riding on the top of a calcium spike. OSN-evoked IPSCs in type 1 PG cells were blocked in the presence of NBQX and D-AP5 (n=4) consistent with a pluri-synaptic PG cell-mediated input generated within the glomerular network.

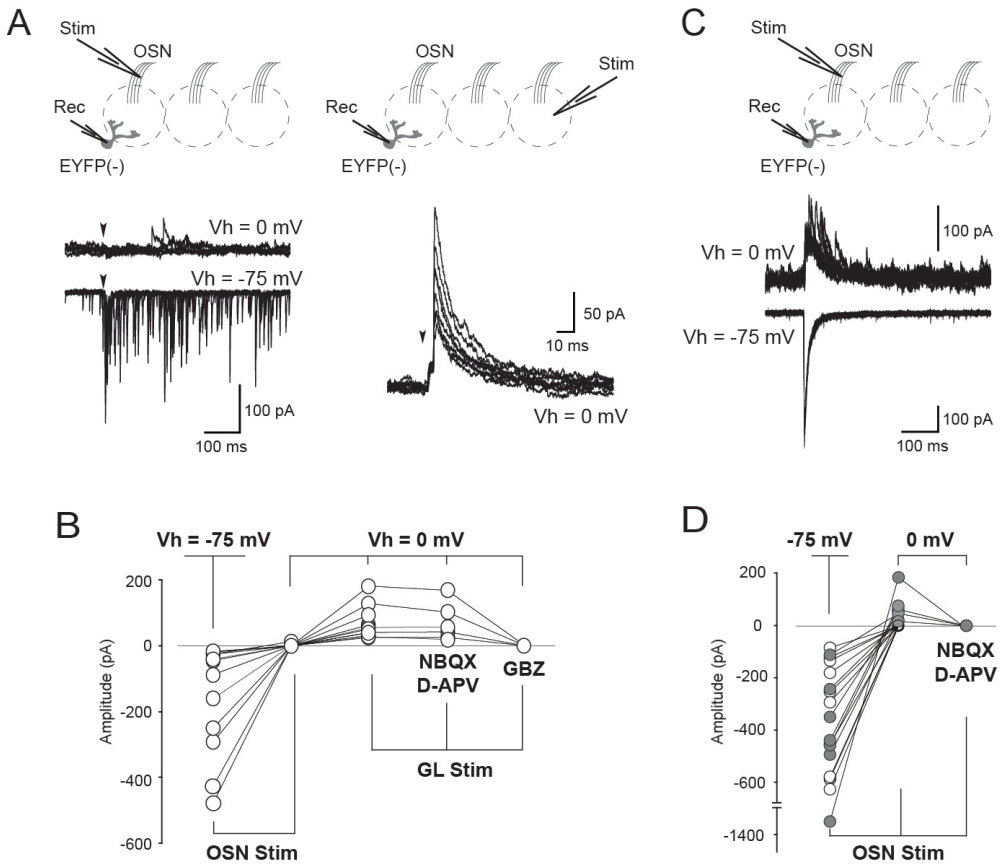

Figure 2 : Type 1 PG cells are the only subtype inhibited by other PG cells. A, Example of a type 2 PG cell, not labeled in the Kv3.1-EYFP mouse, that did not receive any inhibitory input when the glomerulus into which it projected its dendrites was stimulated (left). In contrast, stimulation in distant glomeruli produced a robust ISPC (right). **B,** Summary plot for EYFP (-) type 2 PG cells tested in different stimulation and pharmacological conditions. **C,** Example of a type 1 PG cell responding to the stimulation of OSNs with a monosynaptic EPSC at negative potential and with pluri-synaptic IPSCs at the reversal potential for excitation (Vh=0 mV). **D,** Summary plots for the 17 type 1 PG cells tested. Cells with OSN-evoked IPSCs are shown in grey.

Neurons inhibiting type 2 PG cells express Channelrhodopsin-2 in the Thy1-ChR2-EYFP mouse

To further characterize PG cells inhibitory inputs, we used the Thy1-ChR2-EYFP transgenic mouse expressing the light-gated Channelrhodopsin-2 (ChR2) fused to EYFP in numerous and diverse neuronal subtypes throughout the brain (Arenkiel et al., 2007). Although this mouse model is mostly known to express ChR2 in olfactory bulb mitral cells, we found that a brief (1-10 ms) light stimulation applied on olfactory bulb slices from this transgenic mouse also evokes a mono-synaptic gabazine-sensitive IPSC in about 25% of the cells tested. Light-evoked IPSCs had amplitudes ranging from few pA to several hundreds pA (average 156 ± 168 pA at Vh=0 mV, n=17), variable time courses (decay time constant from 6 to 168 ms, mean 37.9 ± 52 ms, Figure 3E) and were found in PG cells with diverse firing properties and OSN-evoked responses (Figure 3B). Yet, all responsive neurons were type 2 PG cells. None of the n=11 type 1 PG cells tested responded to the photostimulation, consistent with the idea that this particular cell type may have specific inhibitory connections. Light-evoked IPSCs were resistant to NBQX and D-AP5 (n=9) consistent with a mono-synaptic connection, but were abolished by TTX (1 µM) indicating that ChR2 activation must elicit a spike to induce GABA release (n=3). Similar to the electrically-evoked IPSCs, light-evoked IPSCs sometime displayed multiple peaks or bumps during the rising phase

indicating that they were composed of summating IPSCs with unsynchronized timings (see the example in Figure 3B). Moreover, trains of 5 light flashes delivered at 20 Hz elicited an average response that depressed (n=3, not shown). Finally, electrically-evoked IPSCs and light-evoked IPSCs had similar time course in cells in which the two stimuli were tested (n=4, not shown). Thus, properties and targets of ChR2-expressing GABAergic fibers resemble those of the inhibitory fibers activated with an electrical stimulation in the glomerular layer.

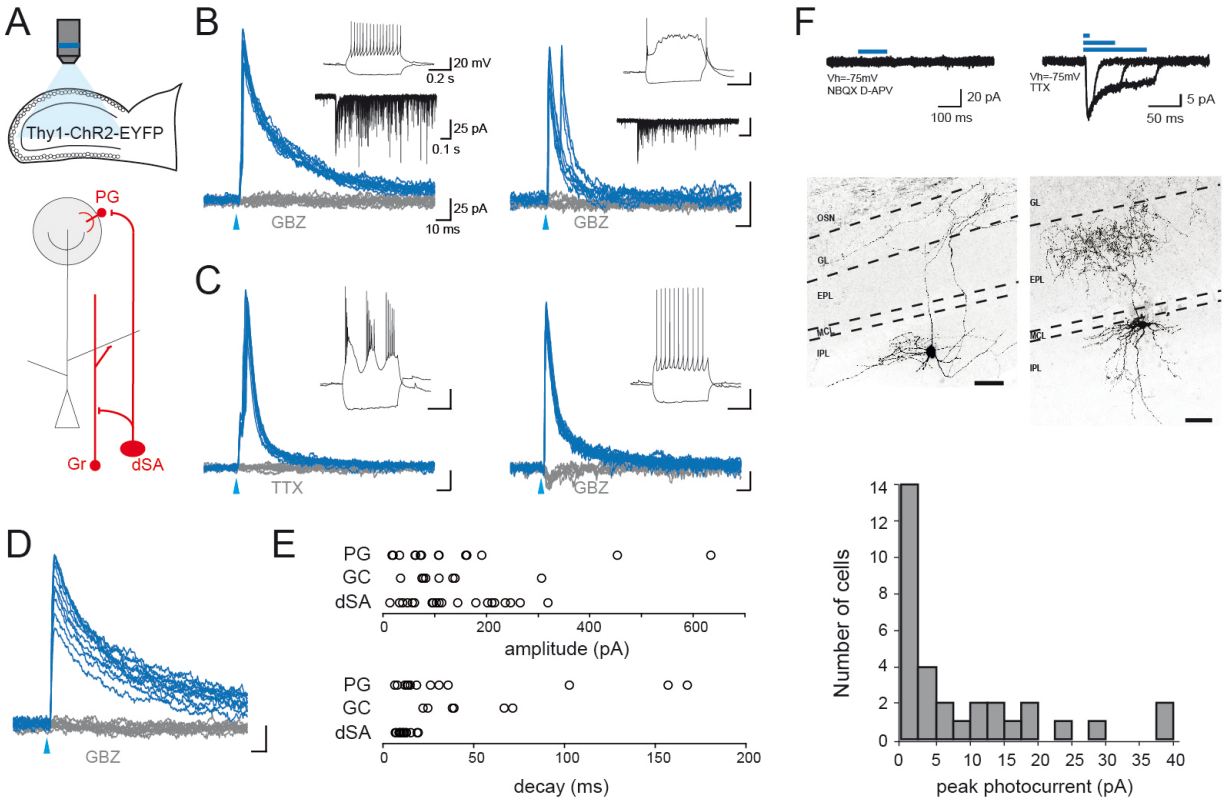

Figure 3 : GABAergic afferences of type 2 PG cells express ChR2 in the Thy1-ChR2-EYFP mouse. **A,** Circuit diagram of the three classes of interneurons tested in olfactory bulb slices from the Thy1-ChR2-EYFP transgenic mouse. **B,** Short blue light flashes (1-10 ms, blue arrowhead) evoked gabazine-sensitive IPSCs (blue traces) in different subtypes of type 2 PG cells. Insets show the intrinsic membrane properties (top) and OSN-evoked responses (bottom, Vh=-75 mV) of the two cells. Note that light sometime evoked pairs of IPSCs (right). **C,** Light-evoked IPSCs recorded at Vh=-75 mV in two deep SA cells with distinct firing patterns. A small inward photo-current persisted in the presence of GBZ in the cell shown on the right. **D,** light-evoked GBZ-sensitive IPSCs in a granule cell. Scale bar values indicated in B apply for all traces in B, C and D. **E,** Light-evoked IPSC amplitudes (top) and decay time constants (bottom) in the three classes of interneurons. PG cells and GC were recorded at Vh=0 mV, dSA at Vh=-75 mV. **F,** Deep SA cells express little or no ChR2 in the Thy1-ChR2-EYFP mouse. Top, Light-evoked responses in two morphologically distinct dSA cells. The cell on the right express small ChR2-mediated photo-currents. Bottom, summary histogram representing the maximal amplitudes of ChR2-mediated photo-currents in all the deep SA cells recorded. Experiments were done in the presence of GBZ, NBQX and D-AP5.

Interestingly, in addition to type 2 PG cells, granule cells and deep SA cells also received robust light-gated monosynaptic IPSCs in slices from the Thy1-ChR2-EYFP mouse (Figure 3C and 3D). In granule cells, gabazine-sensitive light-evoked IPSCs were elicited in 8/19 cells tested. In the presence of NBQX and D-AP5 and at Vh=0 mV, light-evoked IPSCs had an average amplitude of 120 ± 83 pA (range 34-307 pA) and a decay time constant of 41 ± 20.4 ms (range 22-71 ms). In deep SA cells, flashes of light evoked a large ISPC in the majority of the cells tested (n=25/32)(Figure 3C). These IPSCs were sufficiently large to be readily detected at Vh= -75 mV indicating a strong connection (average amplitude 139 ± 89 pA, range 14-319 pA, n= 20; at Vh = 0 mV: amplitude range 80-1564 pA, mean 707 ± 614 pA,

n=5). Light-evoked IPSCs were found in cells with diverse firing pattern (Figure 3C) and various axonal ramifications but were uniformly fast (decay time constant at Vh= -75 mV: 11.2 ± 3.5 ms, range 6.8-19.5 ms, n=20; at Vh=0 mV: 20.7 ± 11.2 ms, n=5). As in PG cells, light-evoked responses were abolished in the presence of TTX in both granule (n=3) and deep SA cells (n=6). All together, these results suggest that a common inhibitory afference expressing ChR2 in the Thy1-ChR2-EYFP mouse innervates type 2 PG cells, granule cells and the diverse subtypes of deep SA cells.

Origin of light-evoked IPSCs in the olfactory bulb of Thy1-ChR2-EYFP mice

The low connection rate of light-evoked responses in PG cells and the expression of ChR2 in glutamatergic principal neurons make it difficult to use the Thy1-ChR2-EYFP model as a tool to examine the functional impact of ChR2-expressing GABAergic inputs. However, this mouse proved to be useful to identify the cellular origin of this innervation. Our data, together with previous reports (Eyre et al., 2008; Boyd et al., 2012; Burton et al., 2017), point to deep SA cells as a likely candidate mediating inhibition of PG, granule and other deep SA cells. To test this hypothesis, we examined light-gated photocurrents in deep SA cells of the Thy1-ChR2-EYFP mouse using whole-cell recordings in the presence of NBQX, D-AP5 and gabazine (Figure 3F). Under these conditions, blue light stimulations did not induce any ChR2-mediated inward current in 13 over 32 deep SA cells whereas small light-gated currents were evoked in the other cells (n=19/32, averaged maximal current: 14.7 ± 11.4 pA). Moreover, none of these cells tested in the cell-attached configuration before breaking the membrane responded to the flashes of light with an action potential current (n=20, not shown). Thus, even though some deep SA cells weakly expressed ChR2, light-evoked depolarizations were likely too small to drive action potentials. The subset of recorded cells filled with biocytin (n=14) did not reveal a preferred expression of ChR2 in a specific deep SA cell subtype. For instance, among the 5 deep SA cells with visible axonal projections in the glomerular layer, only 2 had small light-gated currents (with maximal amplitudes of 10 and 5 pA). Furthermore, we did not observe any inward ChR2 mediated photocurrent across our multiple recordings in diverse types of neurons in the glomerular layer (that likely include PG and superficial SA cells) or in granule cells. Our results thus suggest that ChR2-expressing neurons that innervate PG, granule and deep SA cells in the Thy1-ChR2-EYFP mouse likely reside outside the olfactory bulb.

As the principal source of centrifugal GABAergic afferents to the olfactory bulb is the HDB in the basal forebrain (Zaborszky et al., 1986; Gracia-Llanes et al., 2010; Niedworok et al., 2012), we next verified the expression of ChR2-EYFP in this region in fixed brain tissues from the Thy1-ChR2-EYFP mouse. The basal forebrain of this mouse was indeed strongly fluorescent, especially in the HDB (n=4 mice, Figure 4A). At the cellular level, the EYFP-coupled light-gated channel was expressed in a subset of HDB neurons co-expressing GAD67 (32.4% of GAD67(+) neurons were ChR2-EYFP(+), n=712 GAD67(+) cells counted)(Figure 4B). To further confirm that axonal projections from the HDB are those activated by light in acute bulb slices, we made a lesion of this region in a single hemisphere of Thy1-ChR2-EYFP mice using stereotaxic injection of NMDA (Figure 4C). We then compared the probability of eliciting a mono-synaptic IPSC with a flash of light in ipsilateral bulb slices vs. in contralateral bulb slices from these animals. Consistent with our hypothesis, flashes of light evoked an IPSC in the presence of NBQX and D-AP5 in only 13% (3/23 cells) of the interneurons tested in ipsi lateral slices (0/9 PG cells, 2/6 granule cells and 1/8 deep SA cells from n=6 mice). This

probability was statistically higher (p=0.0003) in contra lateral slices where 62.5% of the cells tested responded to the optical stimulation with an IPSC (5/11 PG cells, 5/8 granule cells and 5/5 deep SA cells)(Figure 4D).

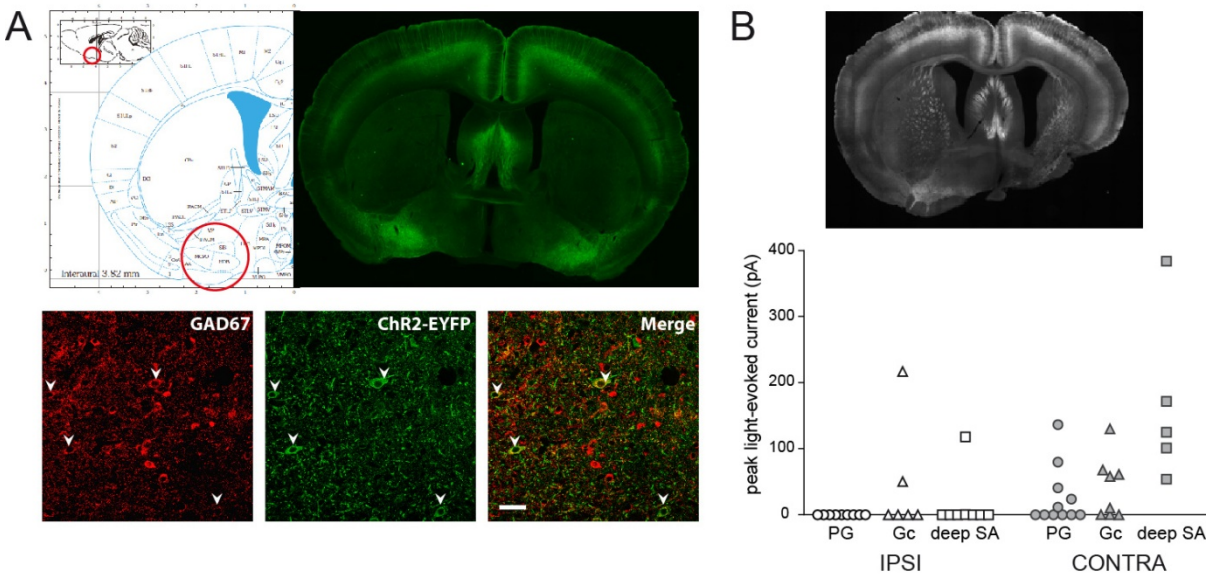

Figure 4 : Basal forebrain GABAergic projections to the olfactory bulb express ChR2-EYFP in the Thy1-ChR2-EYFP mouse. **A,** Coronal section from the brain of a Thy1-ChR2-EYFP mouse (right) superimposed on the corresponding coronal section of the mouse brain (Franklin and Paxinos atlas) at 0.32 mm rostral from bregma. The HDB is located in the red circle. Bottom, Immunofluorescence staining for GAD67 (red) and ChR2-EYFP in the HDB. A fraction of the GABAergic neurons expresses ChR2 (white arrows). Scale bar 50 µm. **B,** Ablation of the basal forebrain reduces light-evoked inhibition in interneurons of the olfactory bulb. Top, coronal section of the brain of a Thy1-ChR2-EYFP mouse that received an injection of NMDA in the left hemisphere basal forebrain. Bottom, amplitudes of light-evoked IPSCs recorded in PG cells (PG), granule cells (Gc) and deep SA cells (deep SA) from ipsi lateral olfactory bulb slices compared with those obtained in contra lateral bulb slices of mice injected with NMDA.

Selective expression of ChR2 in neurons of the HDB

To further verify that GABAergic neurons from the HDB innervate all major olfactory bulb interneurons, we injected an adeno-associated virus (AAV9) encoding a Cre-inducible ChR2-EYFP in the basal forebrain of dlx5/6-Cre mice. These transgenic mice express the Cre recombinase under the control of regulatory sequences of the dlx5/6 genes that encode transcription factors strongly expressed in GABAergic neurons of the forebrain (Monory et al., 2006). Consistent with a previous study (Nunez-Parra et al., 2013), our virus injections produces a strong EYFP labeling of fibers projecting to the olfactory bulb, especially in the granule cell layer and in the glomerular layer (Figure 5A). We then tested the synaptic connections made by these ChR2-expressing HDB fibers using whole-cell voltage-clamp recordings in olfactory bulb slices. Activating ChR2-expressing axons with brief flashes of blue light evoked large outward IPSCs in PG cells (range 13-765 pA, mean 235 ± 214 pA at Vh = 0 mV, n=37), granule cells (range 93-464 pA, mean 181 ± 143 pA at Vh = 0 mV, n=6) and deep SA cells (range 241-681 pA, mean 416 ± 139 pA at Vh between -15 and -35 mV, n=7)(Figure 5D and 5F). The time course of these IPSCs were similar as those observed in the Thy1-ChR2-EYFP mouse, i.e. diverse in PG cells (mean 45.4 ± 58 ms), fast in deep SA cells (mean 12.8 ± 6.2 ms) and intermediate in granule cells (mean 32 ± 5 ms)(Figure 5F). Also consistent with the data obtained in the Thy1-ChR2-EYFP mouse, light-evoked IPSCs were only observed in type 2 PG cells (n=26) but not in type 1 PG cells (n=5). In addition, responses were unaffected by the presence of NBQX and D-AP5 (n=13), abolished by

gabazine (n=12) and depressed at various degrees in PG cells when a train of 5 flashes was applied at 20 Hz (Figure 5E).

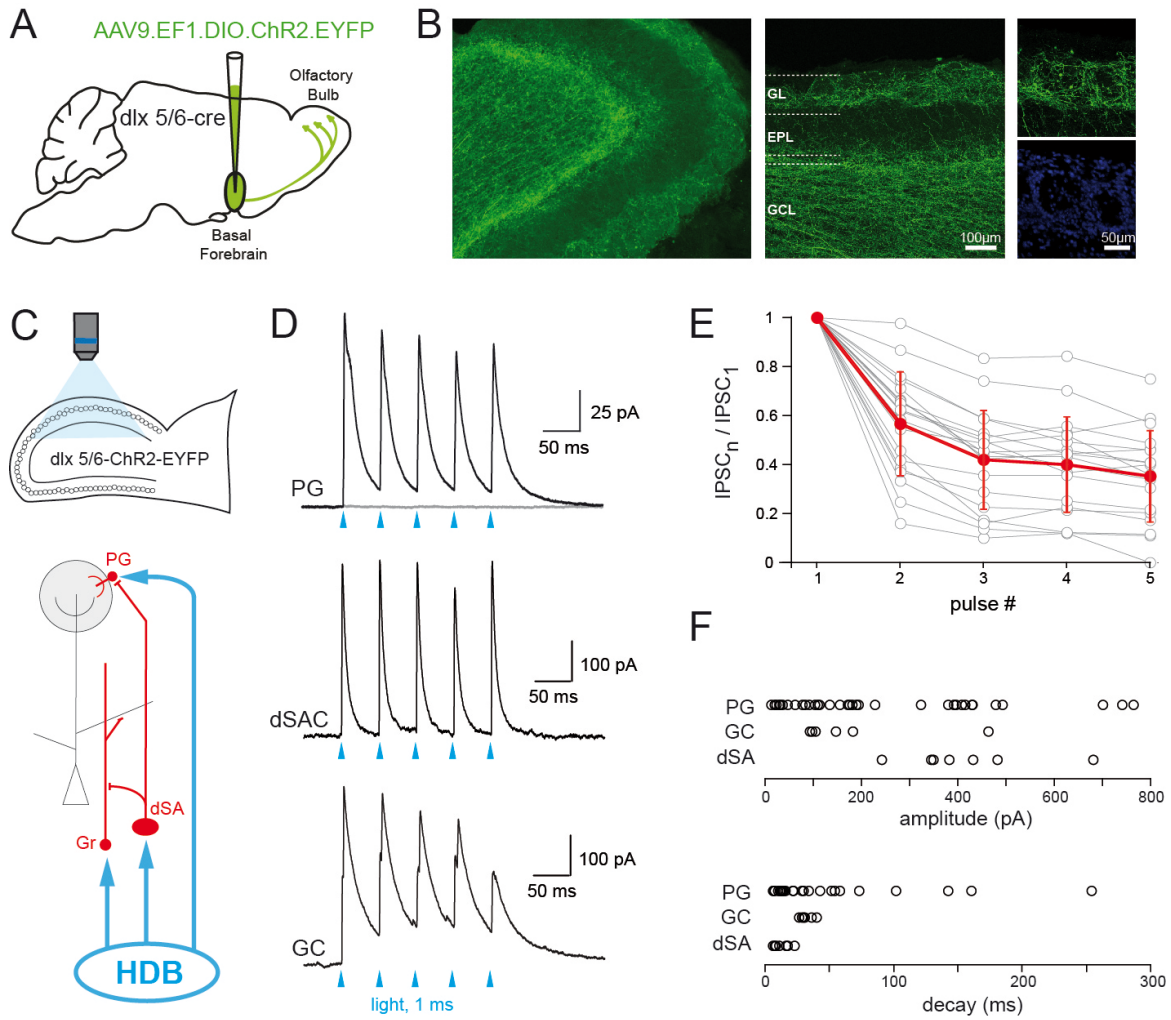

Figure 5 : Conditional expression of ChR2 in GABAergic neurons of the HDB demonstrates their connections with the major inhibitory interneurons of the olfactory bulb. A, Injection of a viral construct in the basal forebrain of dlx5/6-Cre mice was used for conditional expression of ChR2 in GABAergic neurons of the HDB. **B,** 3-5 weeks after injection, fibers expressing ChR2-EYFP colonized all the layers of the olfactory bulb. The two images on the right are a zoom on two glomeruli (top ChR2-EYFP, bottom Hoechst staining). GL: glomerular layer, EPL: external plexiform layer, GCL: granule cell layer. **C,** Circuit diagram illustrating the direct synaptic connections of HDB fibers that were tested in dlx5/6-cre mice expressing ChR2 in the basal forebrain. **D,** Light-evoked IPSCs elicited in a PG cell (Vh=0mV, grey trace is in the presence of GBZ), deep SA cell (dSAC, Vh=-15 mV) and in a granule cell (GC, Vh=0 mV) in response to blue light flashes delivered at 20 Hz. Traces are average responses. **E,** amplitudes of the nth light-evoked IPSC relative to the normalized amplitude of the first IPSC recorded in PG cells. Lines connect plots from the same cells. Red plots show the average. **F,** amplitudes (top) and decay time constants (bottom) of light-evoked IPSCs recorded in PG cells (PG), granule cells (GC) and deep SA cells (dSA). PG and granule cells were recorded at Vh=0mV, deep SA cells at Vh comprised between -35 mV and -15 mV.

Connection rates in the bulb from dlx5/6;ChR2-EYFP mice were much higher than in the Thy1-ChR2-EYFP mouse with >70% of the PG cells tested (n=37/51) responding to the light flash with an IPSC, making it possible to examine this inhibitory input by cell subtype. Regular spiking PG cells with long-lasting OSN-evoked responses (lasting at least 100 ms and up to several seconds) had the longest light-evoked responses (average decay 112.9 ± 81.7 ms, n=5). Two additional regular spiking cells on which the OSN-evoked response was not tested also had slow light-evoked IPSCs (decay > 100 ms). In contrast, cells with membrane

and synaptic properties consistent with those of CR-expressing PG cells (i.e. firing at most one spike, receiving few spontaneous EPSC and small OSN-evoked inputs) all received fast light-evoked IPSCs (average decay 13.1 ± 4.75 ms, n=10). Finally, 5 cells with diverse firing patterns that received a high frequency of spontaneous EPSCs and responded to the stimulation of OSN with a short composite EPSC (average duration 19.9 ± 6.2 ms) similar as Kv3.1-EYFP(+) PG cells had light-evoked responses with a decay time ranging from 6.7 to 51.8 ms (mean 28.9 ± 19.8 ms). Four cells could not be classified according to these criteria. These data thus suggest that the duration of the HDB inhibitory input depends on the postsynaptic PG cell subtype.

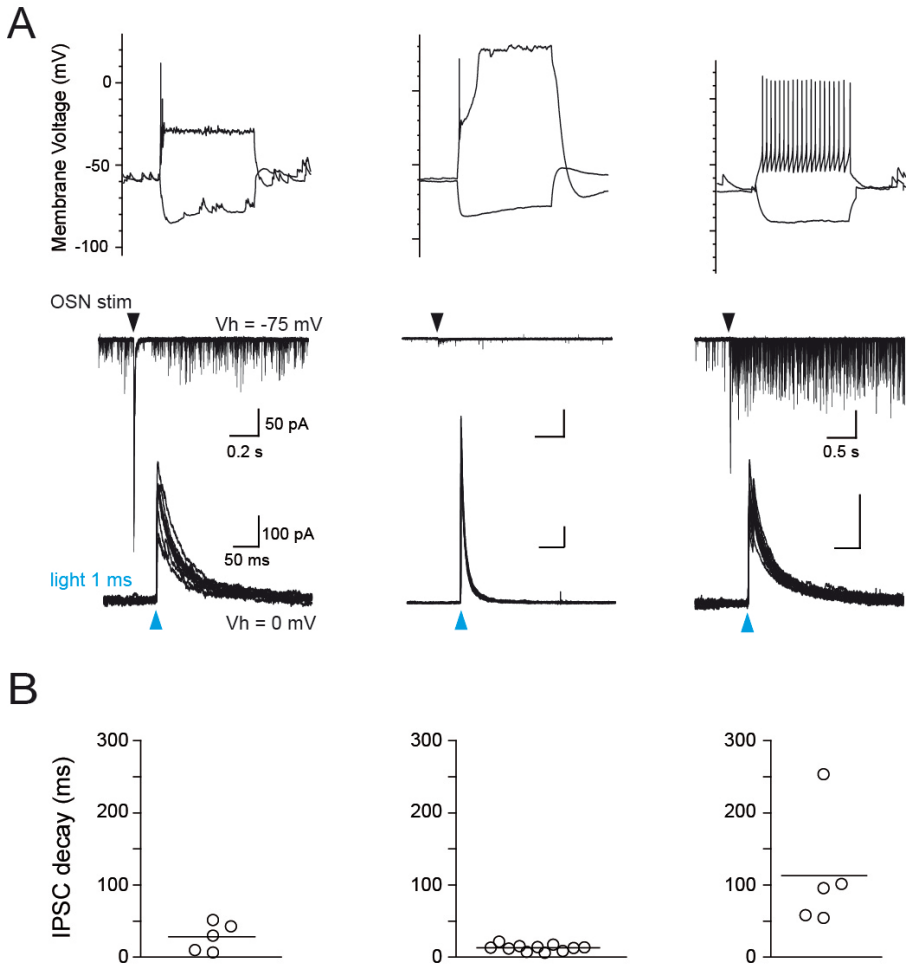

Figure 6 : GABAergic IPSCs from HDB fibers have different time course depending on the postsynaptic PG cell subtype. A, Membrane potential responses to 500 ms depolarizing and hyperpolarizing current injections (top traces), OSN-evoked excitatory responses (middle) and light-evoked IPSCs (bottom) in 3 classes of PG cells recorded in dlx5/6-cre mice expressing ChR2 in HDB neurons. Each column corresponds to one PG cell. Recording and stimulation conditions and scale bar values indicated in the first column apply for all, except where noted. **B,** decay time constants of light-evoked IPSCs recorded in PG cells with the functional profiles shown in the corresponding column in A.

Functional implications of centrifugal inhibition (preliminary results)

Finally, we studied the functional impact of the HDB inhibitory input onto PG cells. The effects of light-evoked IPSCs were examined on the spontaneous firing of PG cells in slices from dlx5/6;ChR2-EYFP mice. We monitored PG cells spiking activity in the cell-attached configuration preceding whole-cell recordings or using less invasive loose cell-attached recordings. A majority of PG cells fired only occasionally or were totally silent (n=26). In some of these cells (n=8), the light-evoked IPSC was detectable as a small fast outward

current (amplitude ranging from few pA up to 50 pA) that did not change the firing activity of the cell (not shown). However, in 8 cells with low spiking activity, light elicited a small inward current that eventually triggered a single spike in 5 cells (Figure 7A). 3 of these cells with light-evoked action potentials were subsequently characterized in the whole-cell configuration and had properties, including fast light-evoked IPSCs, consistent with those of CR-expressing cells (Figure 7B). These results suggest that GABA is depolarizing in a small fraction of PG cells.

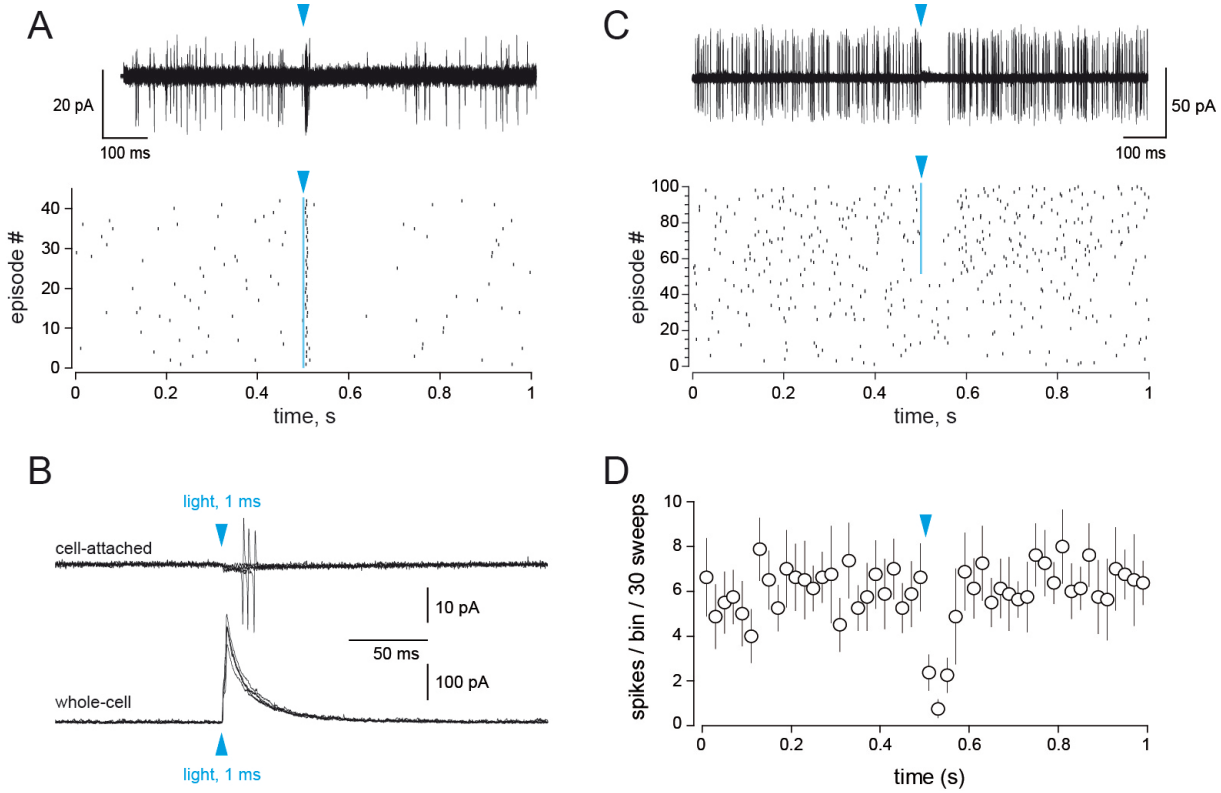

Figure 7 : GABAergic inputs from the HDB are excitatory or inhibitiory depending on the postsynaptic PG cell subtype. A, loose cell-attached recording from a PG cell on which the light evoked-IPSC elicited a spike. 30 superimposed episodes (top) and the corresponding raster plot are (bottom) shown. **B,** another example of cell that fired an action potential in response to the light-evoked GABAergic synaptic current. This cell was recorded first in cell-attached (top) and then in the whole-cell configuration (bottom). 5 consecutive episodes are superimposed in both conditions, a single spike was elicited in 3/5 trials. **C,** loose cell-attached recording from a PG cell on which the light evoked-IPSC transiently blocked the firing. 30 superimposed episodes (top) and the corresponding raster plot are (bottom) shown. **D,** Summary results for cells in which the light-evoked IPSC induced a short pause in the firing (n=8 cells). The average number of spikes per 20 ms bin across 30 consecutives trials per cell is plotted. Bars show SEM.

In another group of PG cells (n=13 cells recorded in loose cell-attached), light-evoked IPSCs blocked the firing for a short period of time (<100 ms)(Figure 7C and 7D). Only one cell showing this transient inhibition of spiking could be characterized in the whole-cell configuration. This cell had a regular firing and a short OSN-evoked excitatory response (not shown).

Finally, a third group of cell was both inhibited and excited by the illumination (Figure 8). Thus, when the light pulse was delivered every 2 s, it resulted in a prolonged (~500 ms) pause of the firing (Figure 8B and 8C). This effect was abolished in the presence of gabazine (Figure 8B). However, delivering the same light pulse on the same cells every 15-20 s revealed that the light-induced pause of firing was followed by a robust and sustained (several seconds) increase in firing rate that persisted in the presence of gabazine (Figure 8D and 8E). Pharmacological experiments are under progress to understand the mechanism of this excitation. This robust double effect was observed in 11 cells recorded in the loose cell-

attached configuration and in 7 cells recorded in cell-attached before their characterization with whole-cell recordings. As illustrated with the cell shown in Figure 8A, all these cells were regularly firing, had long-lasting OSN-evoked excitatory responses (duration range 108 ms-3s) and long light-evoked IPSCs (decay range 54-253 ms)(Figure 8A). Thus, our results indicate that centrifugal fibers originating from the HDB have multiple and complex effects in the olfactory bulb circuits, that largely depend on the postsynaptic cell subtype they connect with.

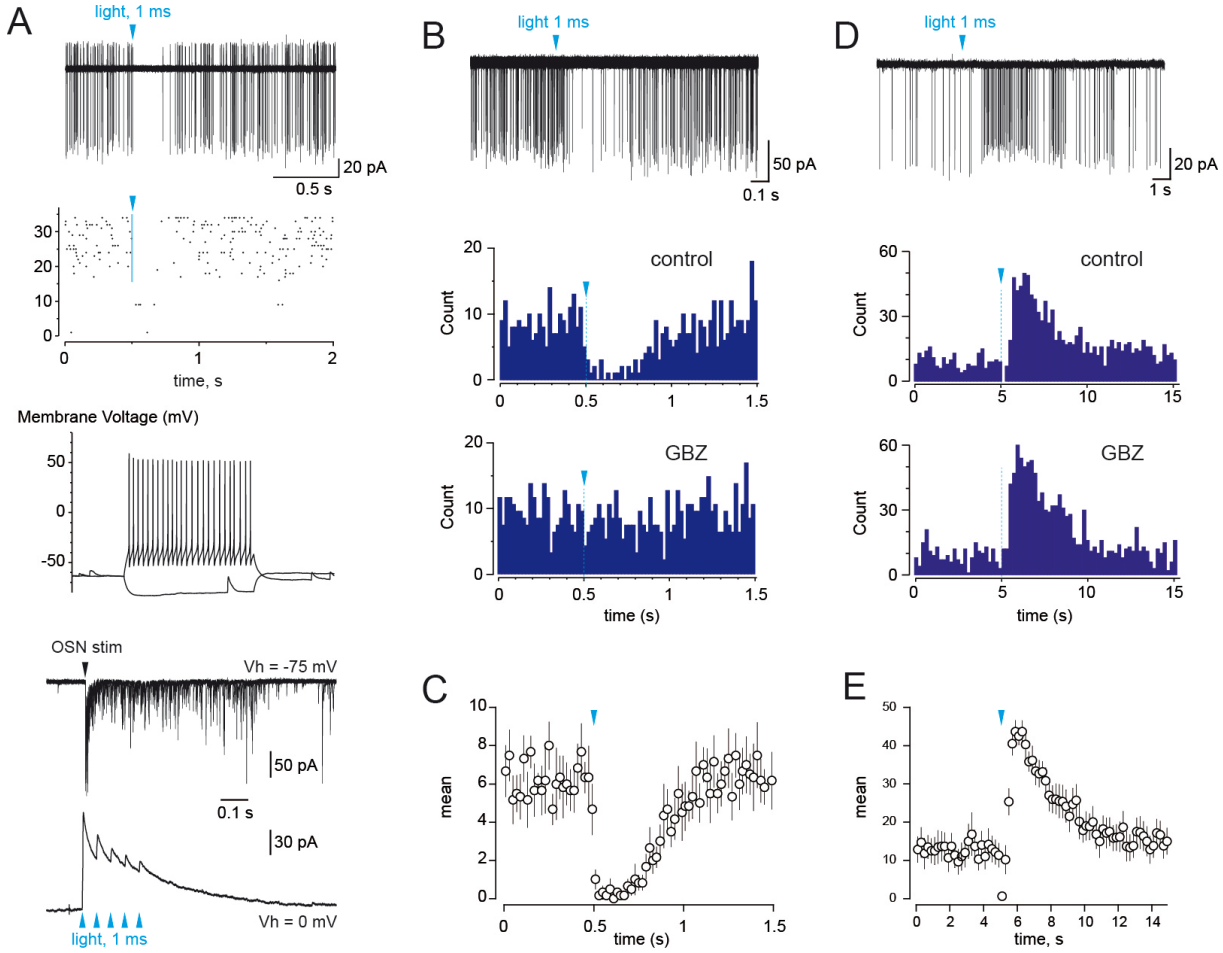

Figure 8 : HDB inputs have a double inhibitory-excitatory effect on a specific PG cell subtype. A, Impact of light-evoked HDB inputs on the spontaneous firing of a PG cell first recorded in the cell-attached configuration and then characterized in the whole-cell configuration. In cell-attached (top traces, 18 trials superimposed) a short light pulse applied every 2 s transiently blocked the firing. However, note on the corresponding raster plot that the cell started to fire at high rate after the first light pulses were delivered (vertical blue bar). Bottom panels show the membrane properties, OSN-evoked excitatory response and light-evoked IPSC (5 pulses at 20 Hz) of this cell. **B-E,** Effect of light-evoked HDB inputs examined at different time scale and with different stimulation frequencies in the same cell (loose cell-attached recordings). **B,** Light stimulation every 2 s reduced the firing for several hundreds of ms. This effect was blocked by gabazine. Cumulative histograms were constructed from 30 (control) and 50 (GBZ) consecutive trials. **C,** Summary data for 6 cells stimulated every 2 s. **D,** Same cell as in C. Light stimulation every 20 s strongly increased the firing rate after a short period of inhibition. This excitatory effect was unaffected by gabazine. Cumulative histograms constructed from 11 (control) and 10 (GBZ) consecutive trials. Plots in C and E represent the average number of spikes ± SEM per 20 ms bin (C) or 200 ms bin (E) across 30-40 (C) or 11-14 consecutive trials (E) per cell (n=6 cells in each graph).

Discussion

Most efforts in understanding the function of olfactory bulb inhibition have focused on the activation mechanisms of the diverse interneuron subtypes and on the impact of their activity in shaping the olfactory bulb output. In comparison, inhibitory circuits that control

the activity of olfactory bulb interneurons have received little attention. We show here that GABAergic neurons from the basal forebrain make strong connections and have diverse effects on multiple interneuron populations in the olfactory bulb. This so far overlooked centrifugal inhibitory pathway is poised to be a major modulator of olfactory bulb circuits.

The HDB provides major centrifugal inputs to the olfactory bulb

The HDB is a cholinergic/GABAergic structure located in the basal forebrain that innervates many cortical areas with both GABAergic and cholinergic fibers. The olfactory bub receives massive cholinergic fibers from the HDB, essentially in the glomerular layer and, moderately, in infraglomerular layers (Macrides et al., 1981; Zaborszky et al., 1986; Salcedo et al., 2011). GABAergic projections to the bulb are also known but their functional contributions have received less attention. These two centrifugal systems are not clearly segregated in the HDB although the majority of cholinergic neurons are located in the medial half of the HDB, whereas most of the GABA neurons are located in the caudal part of the HDB, especially in its lateral part also called the magnocellular preoptic nucleus (Zaborszky et al., 1986). Moreover, recent data indicate that some HDB neurons co-express neurochemical markers of GABAergic and cholinergic neurons and co-release GABA and acetylcholine (Saunders et al., 2015). Our viral injections of a flexed ChR2-EYFP construct in the HDB of dlx5/6-Cre mice labeled fibers that projected in all the layers of the olfactory bulb. This result is consistent with previous mapping studies of HDB projections using anterograde tracer injections (Macrides et al., 1981; Gracia-Llanes et al., 2010) or a similar Cre-dependent viral approach in the GAD65-Cre mouse (Nunez-Parra et al., 2013). Functional connections of HDB fibers on granule cells have been demonstrated with electrical stimulation in the HDB (Kunze et al., 1992) or optogenetic activation of HDB fibers (Nunez-Parra et al., 2013). In contrast, connections on deep SA cells have never been reported and although some projections in the glomerular layer have been described anatomically (Gracia-Llanes et al., 2010), their cellular targets have remained uncertain.

GABergic fibers from the HDB are a major inhibitory input of type 2 PG cells, deep SA cells and granule cells

We found that HDB fibers make synapses with the different subtypes of type 2 PG cells, but not with type 1 PG cells. Moreover, we show that type 2 PG cells unlikely interact with other PG cells whereas type 1 PG cells do. Inhibitory connections are therefore an additional criterion that helps classifying the diverse PG cell subtypes. Our findings contradict previous results demonstrating GABAergic interactions in pairs of neighboring PG cells (Murphy et al., 2005). However, this GABAergic signaling requires the activation of an L-type mediated calcium spike in the presynaptic PG cell, a strong activation that induces a slow composite postsynaptic IPSC. In contrast, fast sodium action potentials in the presynaptic cell fail to evoke any postsynaptic IPSC suggesting that PG-PG cells interactions may rely on GABA spillover. In our experiments, we used OSN stimulation to activate the glomerular network, including PG cells. Our previous recordings indicate that this protocol induces spiking in most PG neurons (Najac et al., 2015). Under these conditions, however, IPSCs were only evoked in type 1 PG cells. We have also used high intensity OSN stimulations to induce a strong synaptic activation of PG cells but even in these conditions we did not observe any evoked IPSC in type 2 PG cells. One possibility that can reconcile our results with those of Murphy et al. is that GABAergic signaling exclusively occurs between type 1 PG cells.

Deep SA cells are another inhibitory input of type 2 PG cells. Ultrastructural examination of deep SA cell terminals demonstrated that CB-expressing PG cell are postsynaptic targets (Eyre et al., 2008). Consistent with this, Burton et al. recently reported that optical activation of deep SA cells elicits a monosynaptic IPSC on type 2 PG cells (Burton et al., 2017). Our data do not contradict these previous data but show that other circuits inhibit PG cells as well. Moreover, in our experiments we rarely (n=5 cells over several hundreds of recorded cells) recorded PG cells receiving regular spontaneous inhibitory inputs that match the highly regular spiking frequency of GL-deep SA cells in bulb slices (Eyre et al., 2008; Burton et al., 2017). Although this can be explained by the fact that axons are often cut during slice preparation, it may also suggest that deep SA cells are not the most prevalent inhibitory input of type 2 PG cells.

Our results also suggest that HDB inputs have different time course and short term plasticity depending on the PG cell subtype they make synapse on. GABAergic HDB neurons are chemically and functionally diverse, each subtype making specific connections in multiple regions of the brain (Do et al., 2016). It would thus be interesting to test if chemically defined HDB neurons preferentially connect specific postsynaptic interneurons in the bulb. We concentrated our study on PG cells to illustrate the diversity of HDB targets in the olfactory bulb and to show that the functional implications of this innervation are multiple, complex and dependent on the postsynaptic target. We have also shown that HDB fibers connect strongly with deep SA cells and granule cells. These connections were less diverse than in PG cells, although our data need to be confirmed with more experiments. We have not systematically tested if principal neurons, superficial SA cells or interneurons located in the EPL are also directly contacted by HDB fibers. These results nonetheless underlie the diversity of HDB targets in the olfactory bulb suggesting that the functional impact of this centrifugal input may be profound.

Role of HDB centrifugal afferences in olfactory bulb odor processing

Electrical lesion of the HDB (Paolini and Mc Kenzie, 1993, 1996) or pharmacological inactivation of HDB GABAergic neurons using a DREADD/CNO paradigm (Nunez-Parra et al., 2013) impair olfactory sensitivity and odor discrimination indicating that the inhibitory control of olfactory bulb interneurons modulates olfactory bulb processing. Yet, the diversity of olfactory bulb interneurons under the control of HDB fibers makes it challenging to predict the functional implications of this GABAergic innervation on olfactory bulb circuits. In the simplest way, inhibition of olfactory bulb interneurons should induce a desinhibition of mitral and tufted cells, the output neurons of the bulb, thus facilitating their firing. In addition, as olfactory bulb processing is fundamentally rhythmic and tightly coupled to the respiration, a synchronized inhibition of olfactory bulb interneurons may reset the activity of the olfactory bulb circuits before a new respiration cycle. Finally, the activity of the HDB is thought to be correlated with animal behaving states, such as attention. Centrifugal inputs from the HDB could therefore contextually modulate olfactory bulb circuits as a function of the internal state.

Our experiments characterizing the targets of HDB GABAergic fibers in the olfactory bulb complement the previous study of Nunez-Parra et al. (Nunez-Parra et al., 2013) and are a starting point to investigate how inhibition of inhibitory circuits guides sensory processing in the olfactory bulb. The functional impact of HDB centrifugal inputs will likely depend on their temporal dynamics along a respiration cycle as well as on their spatial distribution

within the olfactory bulb during an odor presentation. Moreover, their timing relative to the timing of olfactory cortex excitatory feedback as well as the spatial overlap of these two pathways may be important to examine towards understanding their functions. Both pathways indeed target the same populations of interneuron in the bulb. Thus, axonal feedback from the piriform cortex or from the anterior olfactory nucleus directly excites olfactory bulb interneurons and facilitates mitral cell inhibition (Boyd et al., 2012; Markopoulos et al., 2012), i.e. the exact opposite of what HDB fibers might do. However, cortical feedback exerts spatially diffuse, temporally complex and non uniform actions on olfactory bulb interneurons in response to odors (Boyd et al., 2015; Otazu et al., 2015). Because functional (Paolini and McKenzie, 1997) and anatomical (Do et al., 2016) evidence suggest that HDB neurons are activated by pyramidal cells from the olfactory cortex, it will be important to determine if cortical feedback and HDB fibers inputs balance each others on the same postsynaptic bulbar interneurons or instead have opposite actions on different ensemble of interneurons.

References

Abraham NM, Egger V, Shimshek DR, Renden R, Fukunaga I, Sprengel R, Seeburg PH, Klugmann M, Margrie TW, Schaefer AT, Kuner T (2010) Synaptic inhibition in the olfactory bulb accelerates odor discrimination in mice. Neuron 65:399-411.

Arenkiel BR, Peca J, Davison IG, Feliciano C, Deisseroth K, Augustine GJ, Ehlers MD, Feng G (2007) In vivo light-induced activation of neural circuitry in transgenic mice expressing channelrhodopsin-2. Neuron 54:205-218.

Aungst JL, Heyward PM, Puche AC, Karnup SV, Hayar A, Szabo G, Shipley MT (2003) Centre-surround inhibition among olfactory bulb glomeruli. Nature 426:623-629.

Bardy C, Alonso M, Bouthour W, Lledo PM (2010) How, when, and where new inhibitory neurons release neurotransmitters in the adult olfactory bulb. J Neurosci 30:17023-17034.

Boyd AM, Sturgill JF, Poo C, Isaacson JS (2012) Cortical feedback control of olfactory bulb circuits. Neuron 76:1161-1174.

Boyd AM, Kato HK, Komiyama T, Isaacson JS (2015) Broadcasting of cortical activity to the olfactory bulb. Cell Rep 10:1032-1039.

Burton SD, LaRocca G, Liu A, Cheetham CE, Urban NN (2017) Olfactory Bulb Deep Short-Axon Cells Mediate Widespread Inhibition of Tufted Cell Apical Dendrites. J Neurosci 37:1117-1138.

Cang J, Isaacson JS (2003) In vivo whole-cell recording of odor-evoked synaptic transmission in the rat olfactory bulb. J Neurosci 23:4108-4116.

Do JP, Xu M, Lee SH, Chang WC, Zhang S, Chung S, Yung TJ, Fan JL, Miyamichi K, Luo L, Dan Y (2016) Cell type-specific long-range connections of basal forebrain circuit. Elife 5.

Economo MN, Hansen KR, Wachowiak M (2016) Control of Mitral/Tufted Cell Output by Selective Inhibition among Olfactory Bulb Glomeruli. Neuron 91:397-411.

Eyre MD, Antal M, Nusser Z (2008) Distinct deep short-axon cell subtypes of the main olfactory bulb provide novel intrabulbar and extrabulbar GABAergic connections. J Neurosci 28:8217-8229.

Fogli Iseppe A, Pignatelli A, Belluzzi O (2016) Calretinin-Periglomerular Interneurons in Mice Olfactory Bulb: Cells of Few Words. Front Cell Neurosci 10:231.

Fukunaga I, Berning M, Kollo M, Schmaltz A, Schaefer AT (2012) Two distinct channels of olfactory bulb output. Neuron 75:320-329.

Fukunaga I, Herb JT, Kollo M, Boyden ES, Schaefer AT (2014) Independent control of gamma and theta activity by distinct interneuron networks in the olfactory bulb. Nat Neurosci 17:1208-1216.

Geramita M, Urban NN (2017) Differences in Glomerular-Layer-Mediated Feedforward Inhibition onto Mitral and Tufted Cells Lead to Distinct Modes of Intensity Coding. J Neurosci 37:1428-1438.

Gracia-Llanes FJ, Crespo C, Blasco-Ibanez JM, Nacher J, Varea E, Rovira-Esteban L, Martinez-Guijarro FJ (2010) GABAergic basal forebrain afferents innervate selectively GABAergic targets in the main olfactory bulb. Neuroscience 170:913-922.

Gschwend O, Abraham NM, Lagier S, Begnaud F, Rodriguez I, Carleton A (2015) Neuronal pattern separation in the olfactory bulb improves odor discrimination learning. Nat Neurosci 18:1474-1482.

Isaacson JS, Strowbridge BW (1998) Olfactory reciprocal synapses: dendritic signaling in the CNS. Neuron 20:749-761.

Kiyokage E, Pan YZ, Shao Z, Kobayashi K, Szabo G, Yanagawa Y, Obata K, Okano H, Toida K, Puche AC, Shipley MT (2010) Molecular identity of periglomerular and short axon cells. J Neurosci 30:1185-1196.

Kosaka K, Kosaka T (2007) Chemical properties of type 1 and type 2 periglomerular cells in the mouse olfactory bulb are different from those in the rat olfactory bulb. Brain Res 1167:42-55.

Kosaka T, Kosaka K (2008) Tyrosine hydroxylase-positive GABAergic juxtaglomerular neurons are the main source of the interglomerular connections in the mouse main olfactory bulb. Neurosci Res 60:349-354.

Kosaka T, Kosaka K (2011) "Interneurons" in the olfactory bulb revisited. Neurosci Res 69:93-99.

Kunze WA, Shafton AD, Kem RE, McKenzie JS (1992) Intracellular responses of olfactory bulb granule cells to stimulating the horizontal diagonal band nucleus. Neuroscience 48:363-369.

Lepousez G, Lledo PM (2013) Odor discrimination requires proper olfactory fast oscillations in awake mice. Neuron 80:1010-1024.

Liu S, Plachez C, Shao Z, Puche A, Shipley MT (2013) Olfactory bulb short axon cell release of GABA and dopamine produces a temporally biphasic inhibition-excitation response in external tufted cells. J Neurosci 33:2916-2926.

Macrides F, Davis BJ, Youngs WM, Nadi NS, Margolis FL (1981) Cholinergic and catecholaminergic afferents to the olfactory bulb in the hamster: a neuroanatomical, biochemical, and histochemical investigation. J Comp Neurol 203:495-514.

Markopoulos F, Rokni D, Gire DH, Murthy VN (2012) Functional properties of cortical feedback projections to the olfactory bulb. Neuron 76:1175-1188.

Metzger F, Repunte-Canonigo V, Matsushita S, Akemann W, Diez-Garcia J, Ho CS, Iwasato T, Grandes P, Itohara S, Joho RH, Knopfel T (2002) Transgenic mice expressing a pH and Cl- sensing yellow-fluorescent protein under the control of a potassium channel promoter. Eur J Neurosci 15:40-50.

Monory K et al. (2006) The endocannabinoid system controls key epileptogenic circuits in the hippocampus. Neuron 51:455-466.

Murphy GJ, Darcy DP, Isaacson JS (2005) Intraglomerular inhibition: signaling mechanisms of an olfactory microcircuit. Nat Neurosci 8:354-364.

Najac M, De Saint Jan D, Reguero L, Grandes P, Charpak S (2011) Monosynaptic and polysynaptic feed-forward inputs to mitral cells from olfactory sensory neurons. J Neurosci 31:8722-8729.

Najac M, Sanz Diez A, Kumar A, Benito N, Charpak S, De Saint Jan D (2015) Intraglomerular lateral inhibition promotes spike timing variability in principal neurons of the olfactory bulb. J Neurosci 35:4319-4331.

Niedworok CJ, Schwarz I, Ledderose J, Giese G, Conzelmann KK, Schwarz MK (2012) Charting monosynaptic connectivity maps by two-color light-sheet fluorescence microscopy. Cell Rep 2:1375-1386.

Nunez-Parra A, Maurer RK, Krahe K, Smith RS, Araneda RC (2013) Disruption of centrifugal inhibition to olfactory bulb granule cells impairs olfactory discrimination. Proc Natl Acad Sci U S A 110:14777-14782.

Otazu GH, Chae H, Davis MB, Albeanu DF (2015) Cortical Feedback Decorrelates Olfactory Bulb Output in Awake Mice. Neuron 86:1461-1477.

Panzanelli P, Fritschy JM, Yanagawa Y, Obata K, Sassoe-Pognetto M (2007) GABAergic phenotype of periglomerular cells in the rodent olfactory bulb. J Comp Neurol 502:990-1002.

Paolini AG, McKenzie JS (1997) Intracellular recording of magnocellular preoptic neuron responses to olfactory brain. Neuroscience 78:229-242.

Parrish-Aungst S, Shipley MT, Erdelyi F, Szabo G, Puche AC (2007) Quantitative analysis of neuronal diversity in the mouse olfactory bulb. J Comp Neurol 501:825-836.

Parsa PV, D'Souza RD, Vijayaraghavan S (2015) Signaling between periglomerular cells reveals a bimodal role for GABA in modulating glomerular microcircuitry in the olfactory bulb. Proc Natl Acad Sci U S A 112:9478-9483.

Salcedo E, Tran T, Ly X, Lopez R, Barbica C, Restrepo D, Vijayaraghavan S (2011) Activity-Dependent Changes in Cholinergic Innervation of the Mouse Olfactory Bulb. Plos One 6.

Saunders A, Granger AJ, Sabatini BL (2015) Corelease of acetylcholine and GABA from cholinergic forebrain neurons. Elife 4.

Schoppa NE, Kinzie JM, Sahara Y, Segerson TP, Westbrook GL (1998) Dendrodendritic inhibition in the olfactory bulb is driven by NMDA receptors. J Neurosci 18:6790-6802.

Shao Z, Puche AC, Shipley MT (2013) Intraglomerular inhibition maintains mitral cell response contrast across input frequencies. J Neurophysiol.

Shao Z, Puche AC, Liu S, Shipley MT (2012) Intraglomerular inhibition shapes the strength and temporal structure of glomerular output. J Neurophysiol 108:782-793.

Shao Z, Puche AC, Kiyokage E, Szabo G, Shipley MT (2009) Two GABAergic intraglomerular circuits differentially regulate tonic and phasic presynaptic inhibition of olfactory nerve terminals. J Neurophysiol 101:1988-2001.

Smith TC, Jahr CE (2002) Self-inhibition of olfactory bulb neurons. Nat Neurosci 5:760-766.

Whitesell JD, Sorensen KA, Jarvie BC, Hentges ST, Schoppa NE (2013) Interglomerular lateral inhibition targeted on external tufted cells in the olfactory bulb. J Neurosci 33:1552-1563.

Whitman MC, Greer CA (2007) Adult-generated neurons exhibit diverse developmental fates. Dev Neurobiol 67:1079-1093.

Yokoi M, Mori K, Nakanishi S (1995) Refinement of odor molecule tuning by dendrodendritic synaptic inhibition in the olfactory bulb. Proc Natl Acad Sci U S A 92:3371-3375.
Zaborszky L, Carlsen J, Brashear HR, Heimer L (1986) Cholinergic and GABAergic afferents to the olfactory bulb in the rat with special emphasis on the projection neurons in the nucleus of the horizontal limb of the diagonal band. J Comp Neurol 243:488-509.

Supplementary Figures

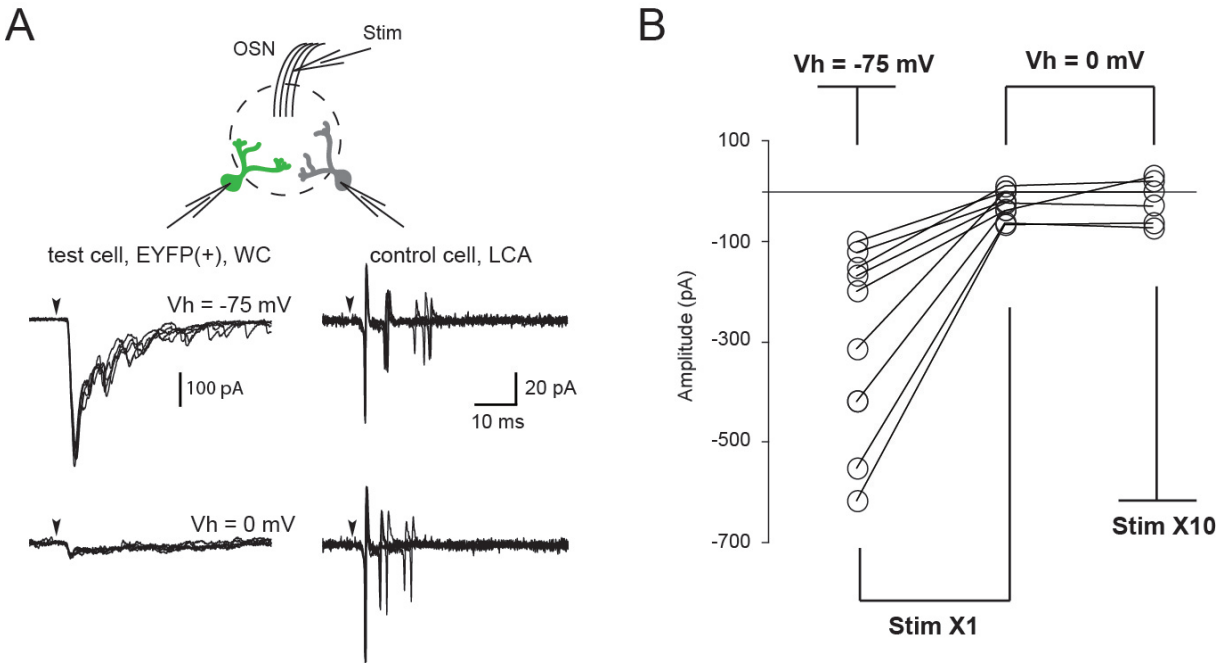

Supplementary Figure 1 : OSN-evoked firing of PG cells does not produce IPSCs in EYFP(+) PG cells. **A,** Paired recording of two PG cells projecting in the same glomerulus. The "test" EYFP(+) PG cell was recorded in the whole-cell configuration at Vh= -75 mV to monitor EPSCs (top) and at Vh= 0 mV to monitor IPSCs (bottom). The second "control" PG cell was recorded in the loose cell-attached configuration to monitor its firing. OSNs were stimulated at an intensity inducing the firing of the control PG cell (stim X1). **B,** The summary graph shows that OSN stimulations did not evoke any outward IPSC in the test cell even when the stimulation was increased by a factor of 10. Control cells were either EYFP(+) (n=4) or EYFP(-) (n=5).

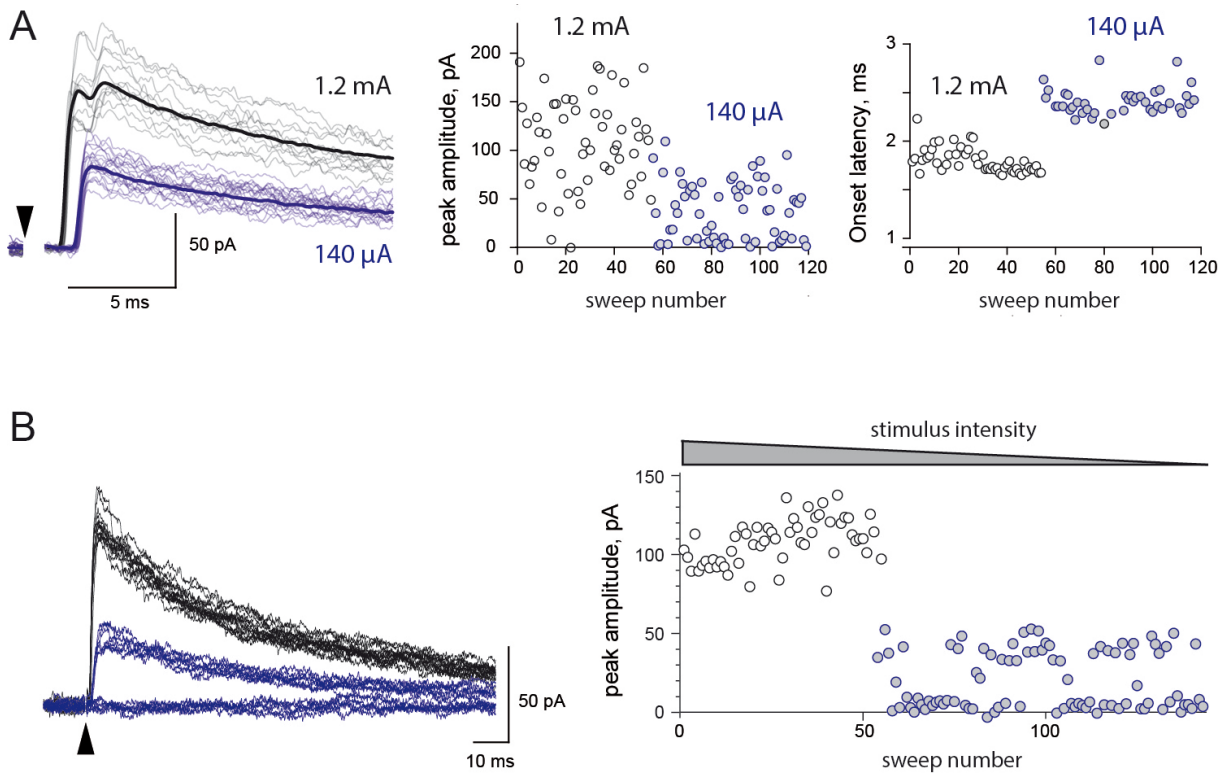

Supplementary Figure 2 : Multiple convergent inhibitory inputs of EYFP(+) PG cells can be recruited in the glomerular layer. A, Example of a EYFP(+) PG cells in which electrical stimulations in the glomerular layer at an intensity of 1.2 mA induced a short latency IPSC with two peaks (grey traces, average in black). Decreasing the intensity of stimulation to 140 µA evoked responses lacking the first peak and with longer latencies. Plots show the peak amplitudes (middle) and onset latencies (right) of consecutive episodes at the two intensities of stimulation. **B,** Example of another EYFP(+) PG cells in which progressive decrease of the stimulus strength suddenly reduced the amplitude of the response in a step-wise manner. Low intensity stimulations evoked an all-or-none minimal IPSC (blue traces).

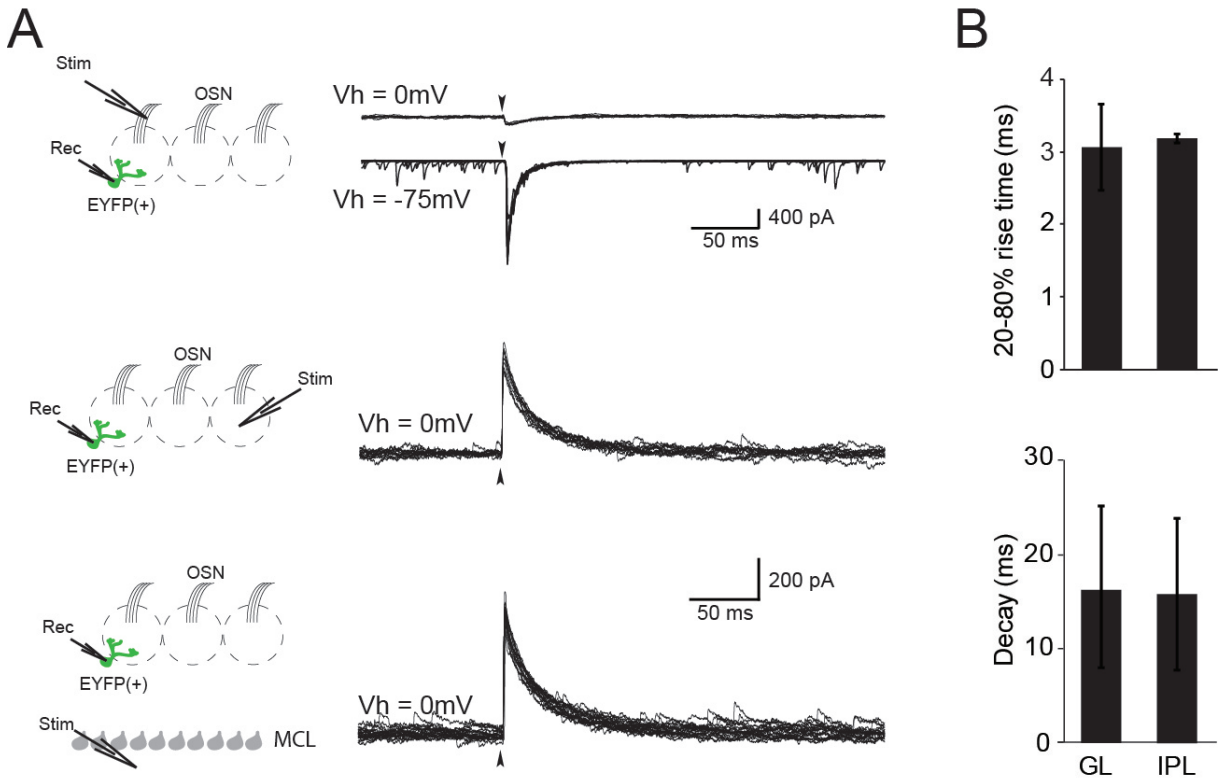

Supplementary Figure 3 : Electrical stimulations in the glomerular layer or in the internal plexiform layer produce similar monosynaptic IPSCs. **A,** EYFP(+) PG cell responses to focal stimulations at different locations. Electrical stimulations in the internal plexiform layer (bottom) evoked IPSCs with similar time course as those evoked by stimulation the glomerular layer (middle). Several traces are superimposed in each case. **B,** Summary graphs for n=5 cells in which IPSCs were evoked with stimulation in the glomerular layer (GL) and in the internal plexiform layer (IPL). The rise time (top) and decay time (bottom) of these responses are similar. 4/5 cells were recorded in the presence of NBQX and D-AP5.

Discussion

In this study I functionally demonstrated that centrifugal GABAergic projections originating in the HDB in the basal forebrain constitute a major source of inhibition for a wide range of bulbar GABAergic interneurons. In addition, my data indicate that HDB inputs have different time course and effects on firing depending on the postsynaptic PG cell subtype. Thus, HDB-mediated IPSCs are fast in CR-expressing type 2 PG cells, intermediate in type 2 PG cells with fast OSN-evoked responses and much slower in regular firing type 2 PG cells with long-lasting OSN-evoked responses. Moreover, a dual inhibitory-excitatory effect on firing, most likely caused by co-release of GABA and Ach, was demonstrated in the latter population. Inducing ChR2 expression in the HDB of transgenic models with genetically-identified subtypes of PG cells such as the Kv3.1-EYFP and CR-EGFP mice would help to further confirm these observations. We also demonstrate that type 1 PG cells do not receive inputs from the HDB but, unlike type 2 PG cells, are inhibited by other PG cells, thus reinforcing the idea that this particular subtype of PG cell has specific synaptic connections. Together, these results indicate that inhibitory inputs are another criterion to identify four distinct PG cell subtypes.

This work thus provides a new PG cell classification that is much richer and complex than previously thought. Along my thesis, I systematically recorded the firing profile as well as the excitatory and inhibitory synaptic inputs of PG cells eventually identified based on the expression of a specific molecular marker. Adding to the previously described membrane properties of CR-EGFP(+) PG cells and Kv3.1-EYFP(+) PG cells (Najac et al., 2015), I described a PG cell subclass that responds to the nerve stimulation with a long lasting barrage of EPSCs, consistently fires regularly in response to a step depolarization and that receives prolonged IPSC from the HDB. My data also indicate that type 1 PG cells do not receive inhibitory inputs from the HDB and respond to a membrane supra-threshold depolarization with a train of spikes with accommodating amplitudes and sometime riding on the top of a calcium spike. Table 1 summarizes this new classification.

	Periglomerular cells			
OSN synaptic connectivity	Type 1	Type 2		
Molecular markers	?	CB + others	CR	?
Excitatory input	OSN	Mitral / Tufted **short OSN-evoked response**	Mitral / Tufted **small OSN-evoked response**	Mitral / Tufted **long OSN-evoked response**
Inhibitory input	**Glomerular**	dSAC? **HDB**	**HDB** **fast IPSC**	**HDB** **slow IPSC**
Membrane properties	**Irregular firing**	**Diverse**	**Single spike**	**Regular firing**

Table 1. Periglomerular cell classification. *This table summarizes the diversity of PG cells considering different molecular, synaptic and biophysical properties. On the white cases, in bold, is shown how this thesis contributes to PG cell classification.*

Such physiological characterization and classification is necessary to understand the functional implication of each PG cell subtype in early odor processing. However, this characterization is far from being complete and our results should now be complemented and refine using other transgenic mouse lines allowing the identification of subtypes of PG cells that at present can not be identified. These models will improve the molecular, morphological, biophysical and synaptic characterization of PG cells. Eventually, they could make possible the selective

manipulation of specific subclasses of PG cells using optogenetics and Cre lines. The functional implications of multiple inhibitory patways within the glomerular network may emerge from this type of study.

We found that GABAergic IPSCs are excitatory in only a small group of cells and evoke at most a single action potential. These PG cells could be recently generated immature neurons with a high intracellular chloride concentration, an idea that needs to be further confirmed. Our results contrast with those of Parsa and colleagues who recently reported that GABA is depolarizing in all PG cells (Parsa et al, 2015). However, as often in the literature, the authors of this study neglected PG cell diversity and did not characterize the PG cell subtypes that were depolarized by exogenous application of GABA. Thus, they generalized their conclusions to the whole population of PG cells as if they formed a homogenous population. Moreover, most of the experiments of this calcium imaging study were done on OB slices from young animals (12d-18d old mice) where immature PG cells may be over-represented.

We did stereotaxic injections of viral constructs encoding the Cre-inducible ChR2-EYFP in the Dlx5/6-Cre mouse to selectively target GABAergic neurons from the HDB. As illustrated in the manuscript, our injections successfully labeled basal forebrain centrifugal GABAergic neurons in the olfactory bulb. However, the Cre system has been reported to show some degree of unspecific labeling. Moreover, we observed non GABAergic effects on PG cell spiking. The possibility that our viral injections also infected cholinergic HDB neurons has therefore to be considered. Acetylcholine release likely explains the delayed and sustained excitation of a specific PG cell subtype observed in our cell-attached recordings. The time course of this response is consistent with the activation of cholinergic metabotropic receptors, an hypothesis since confirmed by pharmacological experiments. Immunohistochemical stainings in the other hand suggest that most ChAt-expressing cholinergic neurons were not infected by the viral construct. However, the results of these experiments may be difficult to interpret since some HDB neurons co-release ACh and GABA and coexpress immunohistochemical markers of GABAergic neurons (VGAT, GAD-65) and cholinergic neurons (ChAT)(Saunders et al, 2015). Our conclusions would therefore be strengthened if we reproduce the results using

another mouse line that also selectively express the Cre-recombinase in GABAergic neurons (Gad-Cre mice for instance).

We found that GABAergic neurons from the basal forebrain express ChR2-EYFP in the Thy1-ChR2-EYFP transgenic mouse. This conclusion principally relies on unilateral lesions of the HDB using stereotaxic injections of NMDA at a high concentration. NMDA causes massive Ca^{2+} entry in neurons and subsequent cell death. Using the contralateral hemisphere as a control, our results show a clear decrease in the probability of eliciting a light-evoked inhibition in OB interneurons from the injured hemisphere. However, light evoked IPSCs were still present in some cells, and spontaneous IPSCs were not abolished suggesting partial ablation of the HDB. Alternatively, this could be interpreted as an evidence that PG cells receive additional GABAergic inputs.

The results that I presented here open the door to many questions about the HDB-OB circuits. It would be interesting for instance to study what mechanisms underlie the target dependent action of HDB inputs and whether they are pre- or postsynaptic. One possibility is that the same fibers from the HDB contact different cell subtypes in the OB and adapt their release properties depending on the target. In contrast, specific HDB populations with unique release properties and expressing specific molecular markers may connect with specific populations of OB interneuron.

Second, although this study demonstrates that the majority of bulbar interneurons receive GABAergic inputs from the HDB, it remains to be determined if other cell types like superficial SACs and the interneurons from the EPL also receive GABAergic inputs from the HDB. Perhaps more important, the impact of the HDB on the output neurons of the OB needs to be elucidated. The influence of the HDB on mitral and tufted cells may be complex and difficult to predict especially if several bulbar inhibitory pathways, all differently modulated by the HDB, are challenged at the same time. Co-release of ACh and GABA may further complicate the read-out of the experiments. Does the activation of the HDB produce the expected disinhibition of mitral and tufted cells? Whatever the results of these experiments, one can wonder whether the broad and simultaneous optogenetic activation of the HDB has any physiological relevance. This question also points the limit of our approach which does not allow to manipulate a specific HDB-OB pathway. However, the broad

optogenetic activation of the HDB can be combined with lesion experiments in the OB to circumvent this limitation. For instance, recordings of mitral and/or tufted cells with a cut apical dendrite (this often happens in OB slices) might be useful to understand how the modulation of granule cells and dSA cells by HDB interneurons influences the activity of principal cells.

It will also be interesting to test *in vivo* if HDB projections somehow modulate or coordinate rhythms in OB circuits. Moreover, understanding what drives the activity of HDB GABAergic neurons will be critical to evaluate the physiological implication of the HDB-OB GABAergic pathways. Some evidence suggests that the activation of the HDB comes from the olfactory cortex (Paolini et al., 1997) thus suggesting the existence of a loop between the OB, the olfactory cortex and the HDB.

This work contributes to the study of long-range GABAergic projections in the brain. This type of connections is still poorly studied and little is known about their functions. The most studied long-range GABAergic projections are those found between different hippocampal regions and the cortigofugal or corticopetal projections (Kohler et al., 1984; Fisher et al., 1988; Toth et al., 1992; Freund et al., 1991). Interestingly, these long-range GABAergic connections seem to exclusively target GABAergic interneurons (Jinno et al., 2007) suggesting that they mediate principal cell disinhibition. It has also been recently proposed that these projections connect distant areas of the brain in order to synchronize their activity (Caputi et al., 2013). This hypothesis could be tested with the manipulation of HDB GABAergic neurons that are known to contact GABAergic interneurons in multiple sensory cortices.

.

References

References

Abraham NM, Spors H, Carleton A, Margrie TW, Kuner T, Schaefer AT (2004) Maintaining accuracy at the expense of speed: Stimulus similarity defines odor discrimination time in mice. Neuron 44:865-876.

Abraham NM, Egger V, Shimshek DR, Renden R, Fukunaga I, Sprengel R, Seeburg PH, Klugmann M, Margrie TW, Schaefer AT, Kuner T (2010) Synaptic Inhibition in the Olfactory Bulb Accelerates Odor Discrimination in Mice. Neuron 65:399-411.

Alonso A, Kohler C (1982) Evidence for separate projections of hippocampal pyramidal and non-pyramidal neurons to different parts of the septum in the rat brain. Neuroscience Letters 31:209-214.

Alvarez-Buylla A, Garcia-Verdugo JM (2002) Neurogenesis in adult subventricular zone. Journal of Neuroscience 22:629-634.

Antal M, Eyre M, Finklea B, Nusser Z (2006) External tufted cells in the main olfactory bulb form two distinct subpopulations. European Journal of Neuroscience 24:1124-1136.

Apicella A, Yuan Q, Scanziani M, Isaacson JS (2010) Pyramidal Cells in Piriform Cortex Receive Convergent Input from Distinct Olfactory Bulb Glomeruli. Journal of Neuroscience 30:14255-14260.

Arenkiel BR, Peca J, Davison IG, Feliciano C, Deisseroth K, Augustine GJ, Ehlers MD, Feng G (2007) In vivo light-induced activation of neural circuitry in transgenic mice expressing channelrhodopsin-2. Neuron 54:205-218.

Arevian AC, Kapoor V, Urban NN (2008) Activity-dependent gating of lateral inhibition in the mouse olfactory bulb. Nature Neuroscience 11:80-87.

Aungst JL, Heyward PM, Puche AC, Karnup SV, Hayar A, Szabo G, Shipley MT (2003) Centre-surround inhibition among olfactory bulb glomeruli. Nature 426:623-629.

Balu R, Pressler RT, Strowbridge BW (2007) Multiple modes of synaptic excitation of olfactory bulb granule cells. Journal of Neuroscience 27:5621-5632.

Banerjee A, Marbach F, Anselmi F, Koh MS, Davis MB, da Silva PG, Delevich K, Oyibo HK, Gupta P, Li B, Albeanu DF (2015) An Interglomerular Circuit Gates Glomerular Output and Implements Gain Control in the Mouse Olfactory Bulb. Neuron 87:193-207.

Bardy C, Alonso M, Bouthour W, Lledo PM (2010) How, When, and Where New Inhibitory Neurons Release Neurotransmitters in the Adult Olfactory Bulb. Journal of Neuroscience 30:17023-17034.

Batista-Brito R, Close J, Machold R, Fishell G (2008) The distinct temporal origins of olfactory bulb interneuron subtypes. Journal of Neuroscience 28:3966-3975.

Belluzzi O, Benedusi M, Ackman J, LoTurco JJ (2003) Electrophysiological differentiation of new neurons in the olfactory bulb. J Neurosci 23:10411-10418.

Bischofberger J, Jonas P (1997) Action potential propagation into the presynaptic dendrites of rat mitral cells. Journal of Physiology-London 504:359-365.

Bourne JN, Schoppa NE (2017) Three-Dimensional Synaptic Analyses of Mitral Cell and External Tufted Cell Dendrites in Rat Olfactory Bulb Glomeruli. Journal of Comparative Neurology 525:592-609.

Boyd AM, Sturgill JF, Poo C, Isaacson JS (2012) Cortical Feedback Control of Olfactory Bulb Circuits. Neuron 76:1161-1174.

Boyd AM, Kato HK, Komiyama T, Isaacson JS (2015) Broadcasting of cortical activity to the olfactory bulb. Cell Rep 10:1032-1039.

Bozza T, McGann JP, Mombaerts P, Wachowiak M (2004) In vivo imaging of neuronal activity - Neurotechnique by targeted expression of a genetically encoded probe in the mouse. Neuron 42:9-21.

Brinon JG, Alonso JR, Arevalo R, Garciaojeda E, Lara J, Aijon J (1992) Calbindin 28K positive neurons in the rat olfactory bulb. An immunohistochemical study. Cell and Tissue Research 269:289-297.

Brunert D, Tsuno Y, Rothermel M, Shipley MT, Wachowiak M (2016) Cell-Type-Specific Modulation of Sensory Responses in Olfactory Bulb Circuits by Serotonergic Projections from the Raphe Nuclei. Journal of Neuroscience 36:6820-6835.

Buck L, Axel R (1991) A novel multigene family may encode odorant receptors. A molecular basis for odor recognition. Cell 65:175-187.

Buonviso N, Chaput MA, Scott JW (1991) Mitral cell to glomerulus connectivity. An HRP study of the orientation of mitral cell apical dendrites. Journal of Comparative Neurology 307:57-64.

Buonviso N, Amat C, Litaudon P, Roux S, Royet JP, Farget V, Sicard G (2003) Rhythm sequence through the olfactory bulb layers during the time window of a respiratory cycle. European Journal of Neuroscience 17:1811-1819.

Burton SD, Urban NN (2014) Greater excitability and firing irregularity of tufted cells underlies distinct afferent-evoked activity of olfactory bulb mitral and tufted cells. Journal of Physiology-London 592:2097-2118.

Burton SD, LaRocca G, Liu A, Cheetham CEJ, Urban NN (2017) Olfactory Bulb Deep Short-Axon Cells Mediate Widespread Inhibition of Tufted Cell Apical Dendrites. Journal of Neuroscience 37:1117-1138.

Buzsaki G, Chrobak JJ (1995) Temporal structure in spatially organized neuronal ensembles. A role for interneuronal networks. Current Opinion in Neurobiology 5:504-510.

Caggiano M, Kauer JS, Hunter DD (1994) Globose basal cells are neuronal progenitors in the olfactort epithelium. A lineage analysis using a replication-incompetent retrovirus. Neuron 13:339-352.

Cang J, Isaacson JS (2003) In vivo whole-cell recording of odor-evoked synaptic transmission in the rat olfactory bulb. J Neurosci 23:4108-4116.

Carey RM, Wachowiak M (2011) Effect of Sniffing on the Temporal Structure of Mitral/Tufted Cell Output from the Olfactory Bulb. Journal of Neuroscience 31:10615-10626.

Carleton A, Petreanu LT, Lansford R, Alvarez-Buylla A, Lledo PM (2003) Becoming a new neuron in the adult olfactory bulb. Nat Neurosci 6:507-518.

Carlson GC, Shipley MT, Keller A (2000) Long-lasting depolarizations in mitral cells of the rat olfactory bulb. Journal of Neuroscience 20:2011-2021.

Chand AN, Galliano E, Chesters RA, Grubb MS (2015) A Distinct Subtype of Dopaminergic Interneuron Displays Inverted Structural Plasticity at the Axon Initial Segment. Journal of Neuroscience 35:1573-1590.

Chao TI, Kasa P, Wolff JR (1997) Distribution of astroglia in glomeruli of the rat main olfactory bulb: Exclusion from the sensory subcompartment of neuropil. Journal of Comparative Neurology 388:191-210.

Chen WR, Midtgaard J, Shepherd GM (1997) Forward and backward propagation of dendritic impulses and their synaptic control in mitral cells. Science 278:463-467.

Chen WR, Xiong WH, Shepherd GM (2000) Analysis of relations between NMDA receptors and GABA release at olfactory bulb reciprocal synapses. Neuron 25:625-633.

Chen WR, Shen GY, Shepherd GM, Hines ML, Midtgaard J (2002) Multiple modes of action potential initiation and propagation in mitral cell primary dendrite. Journal of Neurophysiology 88:2755-2764.

Costanzo RM (1991) Regeneration of olfactory receptor cells. Ciba Foundation Symposia 160:233-248.

Crespo C, Blasco-Ibanez JM, Marques-Mari AI, Alonso JR, Brinon JG, Martinez-Guijarro FJ (2002) Vasoactive intestinal polypeptide-containing elements in the olfactory bulb of the hedgehog (Erinaceus europaeus). Journal of Chemical Neuroanatomy 24:49-63.

Crespo C, Gracia-Llanes FJ, Blasco-Ibanez JM, Gutierrez-Mecinas M, Marques-Mari AI, Martinez-Guijarro FJ (2003) Nitric oxide synthase containing periglomerular cells are GABAergic in the rat olfactory bulb. Neuroscience Letters 349:151-154.

Davis BJ, Macrides F (1983) Tyrosine-hydroxylase immunoreactive neurons and fibers in the olfactory system of the hamster. Journal of Comparative Neurology 214:427-440.

Davison IG, Katz LC (2007) Sparse and selective odor coding by mitral/tufted neurons in the main olfactory bulb. Journal of Neuroscience 27:2091-2101.

De Marchis S, Bovetti S, Carletti B, Hsieh YC, Garzotto D, Peretto P, Fasolo A, Puche AC, Rossi F (2007) Generation of distinct types of periglomerular olfactory bulb interneurons during development and in adult mice: Implication for intrinsic properties of the subventricular zone progenitor population. Journal of Neuroscience 27:657-664.

De Saint Jan D, Westbrook GL (2007) Disynaptic amplification of metabotropic glutamate receptor 1 responses in the olfactory bulb. Journal of Neuroscience 27:132-140.

De Saint Jan D, Hirnet D, Westbrook GL, Charpak S (2009) External Tufted Cells Drive the Output of Olfactory Bulb Glomeruli. Journal of Neuroscience 29:2043-2052.

Debarbieux F, Audinat E, Charpak S (2003) Action potential propagation in Dendrites of rat mitral cells in vivo. Journal of Neuroscience 23:5553-5560.

Demeulemeester H, Arckens L, Vandesande F, Orban GA, Heizmann CW, Pochet R (1991) Calcium-binding proteins and neuropeptides as molecular markers of GABAergic interneurons in the cat visual cortex. Experimental Brain Research 84:538-544.

Deolmos J, Hardy H, Heimer L (1978) Afferent connections of main and accessory olfactory bulb formations in rat. experimental HRP study. Journal of Comparative Neurology 181:213-244.

Dietz SB, Murthy VN (2005) Contrasting short-term plasticity at two sides of the mitral-granule reciprocal synapse in the mammalian olfactory bulb. Journal of Physiology-London 569:475-488.

Do JP, Xu M, Lee SH, Chang WC, Zhang S, Chung S, Yung TJ, Fan JL, Miyamichi K, Luo L, Dan Y (2016) Cell type-specific long-range connections of basal forebrain circuit. Elife 5.

Dong HW, Hayar A, Ennis M (2007) Activation of group I metabotropic glutamate receptors on main olfactory bulb granule cells and periglomerular cells enhances synaptic inhibition of mitral cells. Journal of Neuroscience 27:5654-5663.

Economo MN, Hansen KR, Wachowiak M (2016) Control of Mitral/Tufted Cell Output by Selective Inhibition among Olfactory Bulb Glomeruli. Neuron 91:397-411.

Escanilla O, Arrellanos A, Karnow A, Ennis M, Linster C (2010) Noradrenergic modulation of behavioral odor detection and discrimination thresholds in the olfactory bulb. European Journal of Neuroscience 32:458-468.

Eyre MD, Antal M, Nusser Z (2008) Distinct deep short-axon cell subtypes of the main olfactory bulb provide novel intrabulbar and extrabulbar GABAergic connections. J Neurosci 28:8217-8229.

Eyre MD, Kerti K, Nusser Z (2009) Molecular diversity of deep short-axon cells of the rat main olfactory bulb. European Journal of Neuroscience 29:1397-1407.

Fernandez ME, Croce S, Boutin C, Cremer H, Raineteau O (2011) Targeted electroporation of defined lateral ventricular walls: a novel and rapid method to study fate specification during postnatal forebrain neurogenesis. Neural Development 6:12.

Figueres-Onate M, Lopez-Mascaraque L (2016) Adult Olfactory Bulb Interneuron Phenotypes Identified by Targeting Embryonic and Postnatal Neural Progenitors. Frontiers in Neuroscience 10.

Firestein S (2001) How the olfactory system makes sense of scents. Nature 413:211-218.

Fleischmann A, Shykind BM, Sosulski DL, Franks KM, Glinka ME, Mei DF, Sun YH, Kirkland J, Mendelsohn M, Albers MW, Axel R (2008) Mice with a "Monoclonal Nose": Perturbations in an Olfactory Map Impair Odor Discrimination. Neuron 60:1068-1081.

Fletcher ML, Masurkar AV, Xing JL, Imamura F, Xiong WH, Nagayama S, Mutoh H, Greer CA, Knopfel T, Chen WR (2009) Optical Imaging of Postsynaptic Odor Representation in the Glomerular Layer of the Mouse Olfactory Bulb. Journal of Neurophysiology 102:817-830.

Fogli Iseppe A, Pignatelli A, Belluzzi O (2016) Calretinin-Periglomerular Interneurons in Mice Olfactory Bulb: Cells of Few Words. Front Cell Neurosci 10:231.

Friedrich RW, Korsching SI (1997) Combinatorial and chemotopic odorant coding in the zebrafish olfactory bulb visualized by optical imaging. Neuron 18:737-752.

Fukunaga I, Berning M, Kollo M, Schmaltz A, Schaefer AT (2012) Two Distinct Channels of Olfactory Bulb Output. Neuron 75:320-329.

Fukunaga I, Herb JT, Kollo M, Boyden ES, Schaefer AT (2014) Independent control of gamma and theta activity by distinct interneuron networks in the olfactory bulb. Nat Neurosci 17:1208-1216.

Geramita M, Urban NN (2017) Differences in Glomerular-Layer-Mediated Feedforward Inhibition onto Mitral and Tufted Cells Lead to Distinct Modes of Intensity Coding. Journal of Neuroscience 37:1428-1438.

Geramita MA, Burton SD, Urban NN (2016) Distinct lateral inhibitory circuits drive parallel processing of sensory information in the mammalian olfactory bulb. Elife 5.

Ghosh S, Larson SD, Hefzi H, Marnoy Z, Cutforth T, Dokka K, Baldwin KK (2011) Sensory maps in the olfactory cortex defined by long-range viral tracing of single neurons. Nature 472:217-220.

Gire DH, Schoppa NE (2009) Control of on/off glomerular signaling by a local GABAergic microcircuit in the olfactory bulb. J Neurosci 29:13454-13464.

Gire DH, Franks KM, Zak JD, Tanaka KF, Whitesell JD, Mulligan AA, Hen R, Schoppa NE (2012) Mitral Cells in the Olfactory Bulb Are Mainly Excited through a Multistep Signaling Path. Journal of Neuroscience 32:2964-2975.

Gracia-Llanes FJ, Crespo C, Blasco-Ibanez JM, Nacher J, Varea E, Rovira-Esteban L, Martinez-Guijarro FJ (2010) GABAergic basal forebrain afferents innervate selectively GABAergic targets in the main olfactory bulb. Neuroscience 170:913-922.

Gschwend O, Abraham NM, Lagier S, Begnaud F, Rodriguez I, Carleton A (2015) Neuronal pattern separation in the olfactory bulb improves odor discrimination learning. Nat Neurosci 18:1474-1482.

Hack MA, Saghatelyan A, de Chevigny A, Pfeifer A, Ashery-Padan R, Lledo PM, Gotz M (2005) Neuronal fate determinants of adult olfactory bulb neurogenesis. Nature Neuroscience 8:865-872.

Halabisky B, Strowbridge BW (2003) gamma-frequency excitatory input to granule cells facilitates dendrodendritic inhibition in the rat olfactory bulb. Journal of Neurophysiology 90:644-654.

Halabisky B, Friedman D, Radojicic M, Strowbridge BW (2000) Calcium influx through NMDA receptors directly evokes GABA release in olfactory bulb granule cells. Journal of Neuroscience 20:5124-5134.

Hardy A, Palouzier-Paulignan B, Duchamp A, Royet JP, Duchamp-Viret P (2005) 5-hydroxytryptamine action in the rat olfactory bulb: In vitro electrophysiological patch-clamp recordings of juxtaglomerular and mitral cells. Neuroscience 131:717-731.

Hayar A, Karnup S, Shipley MT, Ennis M (2004a) Olfactory bulb glomeruli: External tufted cells intrinsically burst at theta frequency and are entrained by patterned olfactory input. Journal of Neuroscience 24:1190-1199.

Hayar A, Karnup S, Ennis M, Shipley MT (2004b) External tufted cells: A major excitatory element that coordinates glomerular activity. Journal of Neuroscience 24:6676-6685.

Hayar A, Heyward PM, Heinbockel T, Shipley MT, Ennis M (2001) Direct excitation of mitral cells via activation of alpha 1-noradrenergic receptors in rat olfactory bulb slices. Journal of Neurophysiology 86:2173-2182.

Holderith NB, Shigemoto R, Nusser Z (2003) Cell type-dependent expression of HCN1 in the main olfactory bulb. European Journal of Neuroscience 18:344-354.

Huang LW, Garcia I, Jen HI, Arenkiel BR (2013) Reciprocal connectivity between mitral cells and external plexiform layer interneurons in the mouse olfactory bulb. Frontiers in Neural Circuits 7.

Huang ZB, Thiebaud N, Fadool DA (2016) Differential serotonergic modulation across the main and accessory olfactory bulb. Chemical Senses 41:E195-E195.

Igarashi KM, Ieki N, An M, Yamaguchi Y, Nagayama S, Kobayakawa K, Kobayakawa R, Tanifuji M, Sakano H, Chen WR, Mori K (2012) Parallel Mitral and Tufted Cell Pathways Route Distinct Odor Information to Different Targets in the Olfactory Cortex. Journal of Neuroscience 32:7970-7985.

Imai T, Sakano H (2007) Roles of odorant receptors in projecting axons in the mouse olfactory system. Current Opinion in Neurobiology 17:507-515.

Imamura F, Nagao H, Naritsuka H, Murata Y, Taniguchi H, Mori K (2006) A leucine-rich repeat membrane protein, 5T4, is expressed by a subtype of granule cells with dendritic arbors in specific strata of the mouse olfactory bulb. Journal of Comparative Neurology 495:754-768.

Isaacson JS (2001) Mechanisms governing dendritic gamma-aminobutyric acid (GABA) release in the rat olfactory bulb. Proceedings of the National Academy of Sciences of the United States of America 98:337-342.

Isaacson JS, Strowbridge BW (1998) Olfactory reciprocal synapses: dendritic signaling in the CNS. Neuron 20:749-761.

Jahr CE, Nicoll RA (1982) An intracellular analysis of dendrodendritic inhibition in the turtle in vitro olfactory bulb. Journal of Physiology-London 326:213-234.

Jinno S, Kosaka T (2004) Parvalbumin is expressed in glutamatergic and GABAergic corticostriatal pathway in mice. Journal of Comparative Neurology 477:188-201.

Jinno S, Klausberger T, Marton LF, Dalezios Y, Roberts JDB, Fuentealba P, Bushong EA, Henze D, Buzsaki G, Somogyi P (2007) Neuronal diversity in GABAergic long-range projections from the hippocampus. Journal of Neuroscience 27:8790-8804.

Johnson BA, Leon M (2007) Chemotopic odorant coding in a mammalian olfactory system. Journal of Comparative Neurology 503:1-34.

Kapoor V, Provost AC, Agarwal P, Murthy VN (2016) Activation of raphe nuclei triggers rapid and distinct effects on parallel olfactory bulb output channels. Nature Neuroscience 19:271-+.

Kasowski HJ, Kim H, Greer CA (1999) Compartmental organization of the olfactory bulb glomerulus. Journal of Comparative Neurology 407:261-274.

Kato HK, Chu MW, Isaacson JS, Komiyama T (2012) Dynamic Sensory Representations in the Olfactory Bulb: Modulation by Wakefulness and Experience. Neuron 76:962-975.

Kato HK, Gillet SN, Peters AJ, Isaacson JS, Komiyama T (2013) Parvalbumin-Expressing Interneurons Linearly Control Olfactory Bulb Output. Neuron 80:1218-1231.

Kawaguchi Y, Kondo S (2002) Parvalbumin, somatostatin and cholecystokinin as chemical markers for specific GABAergic interneuron types in the rat frontal cortex. Journal of Neurocytology 31:277-287.

Ke MT, Fujimoto S, Imai T (2013) SeeDB: a simple and morphology-preserving optical clearing agent for neuronal circuit reconstruction. Nature Neuroscience 16:1154-U1246.

Kelsch W, Lin CW, Lois C (2008) Sequential development of synapses in dendritic domains during adult neurogenesis. Proceedings of the National Academy of Sciences of the United States of America 105:16803-16808.

Kikuta S, Fletcher ML, Homma R, Yamasoba T, Nagayama S (2013) Odorant Response Properties of Individual Neurons in an Olfactory Glomerular Module. Neuron 77:1122-1135.

Kirmse K, Witte OW, Holthoff K (2010) GABA Depolarizes Immature Neocortical Neurons in the Presence of the Ketone Body beta-Hydroxybutyrate. Journal of Neuroscience 30:16002-16007.

Kishi K, Mori K, Ojima H (1984) Distribution of local axon collaterals of mitral, displaced mitral and tufted cells in the rabbit olfactory bulb. Journal of Comparative Neurology 225:511-526.

Kiyokage E, Kobayashi K, Toida K (2017) Spatial distribution of synapses on tyrosine hydroxylase-expressing juxtaglomerular cells in the mouse olfactory glomerulus. Journal of Comparative Neurology 525:1059-1074.

Kiyokage E, Pan YZ, Shao Z, Kobayashi K, Szabo G, Yanagawa Y, Obata K, Okano H, Toida K, Puche AC, Shipley MT (2010) Molecular identity of periglomerular and short axon cells. J Neurosci 30:1185-1196.

Kohwi M, Petryniak MA, Long JE, Ekker M, Obata K, Yanagawa Y, Rubenstein JLR, Alvarez-Buylla A (2007) A subpopulation of olfactory bulb GABAergic interneurons is derived from Emx1- and Dlx5/6-expressing progenitors. Journal of Neuroscience 27:6878-6891.

Kosaka K, Kosaka T (2007) Chemical properties of type 1 and type 2 periglomerular cells in the mouse olfactory bulb are different from those in the rat olfactory bulb. Brain Res 1167:42-55.

Kosaka K, Kosaka T (2013) Secretagogin-containing neurons in the mouse main olfactory bulb. Neuroscience Research 77:16-32.

Kosaka K, Heizmann CW, Kosaka T (1994) Calcium-binding protein Parvalbumin immunoreactive neurons in the rat olfactory bulb. 1. Distribution and structural features in adult rat. Experimental Brain Research 99:191-204.

Kosaka K, Toida K, Margolis FL, Kosaka T (1997) Chemically defined neuron groups and their subpopulations in the glomerular layer of the rat main olfactory bulb .2. Prominent differences in the intraglomerular dendritic arborization and their relationship to olfactory nerve terminals. Neuroscience 76:775-786.

Kosaka K, Toida K, Aika Y, Kosaka T (1998) How simple is the organization of the olfactory glomerulus? the heterogeneity of so-called periglomerular cells. Neuroscience Research 30:101-110.

Kosaka T, Kosaka K (2005) Structural organization of the glomerulus in the main olfactory bulb. Chemical Senses 30:I107-i108.

Kosaka T, Kosaka K (2007) Heterogeneity of nitric oxide synthase-containing neurons in the mouse main olfactory bulb. Neuroscience Research 57:165-178.

Kosaka T, Kosaka K (2008) Tyrosine hydroxylase-positive GABAergic juxtaglomerular neurons are the main source of the interglomerular connections in the mouse main olfactory bulb. Neurosci Res 60:349-354.

Kosaka T, Kosaka K (2009) Two types of tyrosine hydroxylase positive GABAergic juxtaglomerular neurons in the mouse main olfactory bulb are different in their time of origin. Neuroscience Research 64:436-441.

Kosaka T, Kosaka K (2010) Heterogeneity of calbindin-containing neurons in the mouse main olfactory bulb: I. General description. Neuroscience Research 67:275-292.

Kosaka T, Kosaka K (2011) "Interneurons" in the olfactory bulb revisited. Neuroscience Research 69:93-99.

Kunze WA, Shafton AD, Kem RE, McKenzie JS (1992) Intracellular responses of olfactory bulb granule cells to stimulating the horizontal diagonal band nucleus. Neuroscience 48:363-369.

Kunze WAA, Shafton AD, Kemm RE, McKenzie JS (1991) Effect of stimulating the nucleus of the horizontal limb of the diagonal band on single unit activity in the olfactory bulb. Neuroscience 40:21-27.

Lagier S, Carleton A, Lledo PM (2004) Interplay between local GABAergic Interneurons and relay neurons generates gamma oscillations in the rat olfactory bulb. Journal of Neuroscience 24:4382-4392.

Lagier S, Panzanelli P, Russo RE, Nissant A, Bathellier B, Sassoe-Pognetto M, Fritschy JM, Lledo PM (2007) GABAergic inhibition at dendrodendritic synapses tunes gamma oscillations in the olfactory bulb. Proceedings of the National Academy of Sciences of the United States of America 104:7259-7264.

Lecoq J, Tiret P, Charpak S (2009) Peripheral Adaptation Codes for High Odor Concentration in Glomeruli. Journal of Neuroscience 29:3067-3072.

Lemasson M, Saghatelyan A, Olivo-Marin JC, Lledo PM (2005) Neonatal and adult neurogenesis provide two distinct populations of newborn neurons to the mouse olfactory bulb. Journal of Neuroscience 25:6816-6825.

Lepousez G, Lledo PM (2013) Odor discrimination requires proper olfactory fast oscillations in awake mice. Neuron 80:1010-1024.

Lepousez G, Mouret A, Loudes C, Epelbaum J, Viollet C (2010a) Somatostatin Contributes to In Vivo Gamma Oscillation Modulation and Odor Discrimination in the Olfactory Bulb. Journal of Neuroscience 30:870-875.

Lepousez G, Csaba Z, Bernard V, Loudes C, Videau C, Lacombe J, Epelbaum J, Viollet C (2010b) Somatostatin Interneurons Delineate the Inner Part of the External Plexiform Layer in the Mouse Main Olfactory Bulb. Journal of Comparative Neurology 518:1976-1994.

Leranth C, Frotscher M (1987) GABAergic input of cholecystokynin-immunoreactive neurons in the hilar region of the rat hippocampus. An electron microscopic double staining study. Histochemistry 86:287-290.

Liu S, Plachez C, Shao Z, Puche A, Shipley MT (2013) Olfactory bulb short axon cell release of GABA and dopamine produces a temporally biphasic inhibition-excitation response in external tufted cells. J Neurosci 33:2916-2926.

Liu SL, Shipley MT (2008) Multiple conductances cooperatively regulate spontaneous bursting in mouse olfactory bulb external tufted cells. Journal of Neuroscience 28:1625-1639.

Liu SL, Puche AC, Shipley MT (2016) The Interglomerular Circuit Potently Inhibits Olfactory Bulb Output Neurons by Both Direct and Indirect Pathways. Journal of Neuroscience 36:9604-9617.

Liu SL, Shao ZY, Puche A, Wachowiak M, Rothermel M, Shipley MT (2015) Muscarinic Receptors Modulate Dendrodendritic Inhibitory Synapses to Sculpt Glomerular Output. Journal of Neuroscience 35:5680-5692.

Livneh Y, Adam Y, Mizrahi A (2014) Odor Processing by Adult-Born Neurons. Neuron 81:1097-1110.

Lois C, Alvarezbuylla A (1994) Long-distance neuronal migration in the adult mammalian brain. Science 264:1145-1148.

Lopezmascaraque L, Villalba RM, Decarlos JA (1989) Vasoactive intestinal polypeptide-immunoractive neurons in the main olfactory bulb of the hedgehog (Erinaceus europaeus). Neuroscience Letters 98:19-24.

Lopezmascaraque L, Decarlos JA, Valverde F (1990) Structure if the olfactory bulb of the hedgehog (Erinaceus europaeus). A Golgi study of the intrinsic organization of the superficial layers. Journal of Comparative Neurology 301:243-261.

Luo M, Katz LC (2001) Response correlation maps of neurons in the mammalian olfactory bulb. Neuron 32:1165-1179.

Luskin MB (1993) Restricted proliferation and migration of postnatally generated neurons derived from the forebrain subventricular zone. Neuron 11:173-189.

Luskin MB, Price JL (1983) The topographic organization of associational fibers to the olfactory system un the rat, including centrifugal fibers to the olfactory bulb. Journal of Comparative Neurology 216:264-291.

Macrides F, Schneider SP (1982) Laminar organization of mitral and tufted cells in the main olfactory bulb of the adult hamster. Journal of Comparative Neurology 208:419-430.

Macrides F, Davis BJ, Youngs WM, Nadi NS, Margolis FL (1981) Cholinergic and catecholaminergic afferents to the olfactory bulb in the hamster: a neuroanatomical, biochemical, and histochemical investigation. J Comp Neurol 203:495-514.

Magavi SSP, Mitchell BD, Szentirmai O, Carter BS, Macklis JD (2005) Adult-born and preexisting olfactory granule neurons undergo distinct experience-dependent modifications of their olfactory responses in vivo. Journal of Neuroscience 25:10729-10739.

Maher BJ, Westbrook GL (2008) Co-transmission of dopamine and GABA in periglomerular cells. Journal of Neurophysiology 99:1559-1564.

Mandairon N, Sacquet J, Jourdan F, Didier A (2006) Long-term fate and distribution of newborn cells in the adult mouse olfactory bulb: Influences of olfactory deprivation. Neuroscience 141:443-451.
Margrie TW, Schaefer AT (2003) Theta oscillation coupled spike latencies yield computational vigour in a mammalian sensory system. Journal of Physiology-London 546:363-374.
Markopoulos F, Rokni D, Gire DH, Murthy VN (2012) Functional properties of cortical feedback projections to the olfactory bulb. Neuron 76:1175-1188.
McGann JP, Pirez N, Gainey MA, Muratore C, Elias AS, Wachowiak M (2005) Odorant representations are modulated by intra- but not interglomerular presynaptic inhibition of olfactory sensory neurons. Neuron 48:1039-1053.
McLean JH, Shipley MT (1987) Serotoninergic afferents to the rat olfactory bulb. 1. Origins and laminar specificity of serotoninergic inputs in the adult rat. Journal of Neuroscience 7:3016-3028.
McLean JH, Shipley MT, Nickell WT, Astonjones G, Reyher CKH (1989) Chemoanatomical organization of the noradrenergic input from Locus coeruleus to the olfactory bulb of the adult rat. Journal of Comparative Neurology 285:339-349.
McQuiston AR, Katz LC (2001) Electrophysiology of interneurons in the glomerular layer of the rat olfactory bulb. Journal of Neurophysiology 86:1899-1907.
Meisami E, Safari L (1981) A quantitative study of the effects of early unilateral olfactory deprivation on the number and distribution of mitral and tufted cells and of glomeruli in the rat olfactory bulb. Brain Research 221:81-107.
Merkle FT, Mirzadeh Z, Alvarez-Buylla A (2007) Mosaic organization of neural stem cells in the adult brain. Science 317:381-384.
Merkle FT, Fuentealba LC, Sanders TA, Magno L, Kessaris N, Alvarez-Buylla A (2014) Adult neural stem cells in distinct microdomains generate previously unknown interneuron types. Nature Neuroscience 17:207-214.
Metzger F, Repunte-Canonigo V, Matsushita S, Akemann W, Diez-Garcia J, Ho CS, Iwasato T, Grandes P, Itohara S, Joho RH, Knopfel T (2002) Transgenic mice expressing a pH and Cl- sensing yellow-fluorescent protein under the control of a potassium channel promoter. Eur J Neurosci 15:40-50.
Miyamichi K, Shlomai-Fuchs Y, Shu M, Weissbourd BC, Luo LQ, Mizrahi A (2013) Dissecting Local Circuits: Parvalbumin Interneurons Underlie Broad Feedback Control of Olfactory Bulb Output. Neuron 80:1232-1245.
Miyamichi K, Amat F, Moussavi F, Wang C, Wickersham I, Wall NR, Taniguchi H, Tasic B, Huang ZJ, He ZG, Callaway EM, Horowitz MA, Luo LQ (2011) Cortical representations of olfactory input by trans-synaptic tracing. Nature 472:191-196.
Mombaerts P (1999) Seven-transmembrane proteins as odorant and chemosensory receptors. Science 286:707-711.
Mombaerts P (2006) Olfaction targeted. Journal of Neurogenetics 20:181-181.
Mombaerts P, Wang F, Dulac C, Chao SK, Nemes A, Mendelsohn M, Edmondson J, Axel R (1996) Visualizing an olfactory sensory map. Cell 87:675-686.
Monory K et al. (2006) The endocannabinoid system controls key epileptogenic circuits in the hippocampus. Neuron 51:455-466.
Mori K, Kishi K, Ojima H (1983) Distribution of dendrites of mitral, displaced mitral, tufted, and granule cells in the rabbit olfactory bulb. Journal of Comparative Neurology 219:339-355.

Mori K, Nagao H, Yoshihara Y (1999) The olfactory bulb: Coding and processing of odor molecule information. Science 286:711-715.
Murphy GJ, Darcy DP, Isaacson JS (2005) Intraglomerular inhibition: signaling mechanisms of an olfactory microcircuit. Nature Neuroscience 8:354-364.
Nai Q, Dong HW, Linster C, Ennis M (2010) Activation of alpha 1 and alpha 2 noradrenergic receptors exert opposing effects on excitability of main olfactory bulb granule cells. Neuroscience 169:882-892.
Nai Q, Dong HW, Hayar A, Linster C, Ennis M (2009) Noradrenergic Regulation of GABAergic Inhibition of Main Olfactory Bulb Mitral Cells Varies as a Function of Concentration and Receptor Subtype. Journal of Neurophysiology 101:2472-2484.
Najac M, De Saint Jan D, Reguero L, Grandes P, Charpak S (2011) Monosynaptic and Polysynaptic Feed-Forward Inputs to Mitral Cells from Olfactory Sensory Neurons. Journal of Neuroscience 31:8722-8729.
Najac M, Diez AS, Kumar A, Benito N, Charpak S, De Saint Jan D (2015) Intraglomerular Lateral Inhibition Promotes Spike Timing Variability in Principal Neurons of the Olfactory Bulb. The Journal of Neuroscience 35:4319-4331.
Neville KR, Haberly LB (2003) Beta and gamma oscillations in the olfactory system of the urethane-anesthetized rat. Journal of Neurophysiology 90:3921-3930.
Niedworok CJ, Schwarz I, Ledderose J, Giese G, Conzelmann KK, Schwarz MK (2012) Charting monosynaptic connectivity maps by two-color light-sheet fluorescence microscopy. Cell Rep 2:1375-1386.
Nunez-Parra A, Maurer RK, Krahe K, Smith RS, Araneda RC (2013) Disruption of centrifugal inhibition to olfactory bulb granule cells impairs olfactory discrimination. Proc Natl Acad Sci U S A 110:14777-14782.
Orona E, Scott JW, Rainer EC (1983) Diferent granule cell populations innervate superficial and deep regions of the external plexiform layer in the rat olfactory bulb. Journal of Comparative Neurology 217:227-237.
Orona E, Rainer EC, Scott JW (1984) Dendritic and axonal organization of mitral and tufted cells in the rat olfactory bulb. Journal of Comparative Neurology 226:346-356.
Otazu GH, Chae H, Davis MB, Albeanu DF (2015) Cortical Feedback Decorrelates Olfactory Bulb Output in Awake Mice. Neuron 86:1461-1477.
Overstreet LS, Hentges ST, Bumaschny VF, de Souza FS, Smart JL, Santangelo AM, Low MJ, Westbrook GL, Rubinstein M (2004) A transgenic marker for newly born granule cells in dentate gyrus. J Neurosci 24:3251-3259.
Overstreet-Wadiche LS, Westbrook GL (2006) Functional maturation of adult-generated granule cells. Hippocampus 16:208-215.
Panzanelli P, Fritschy JM, Yanagawa Y, Obata K, Sassoe-Pognetto M (2007) GABAergic phenotype of periglomerular cells in the rodent olfactory bulb. Journal of Comparative Neurology 502:990-1002.
Paolini AG, McKenzie JS (1993) Effects of lessons in the horizontal diagonal band nucleus on olfactory habituation in the rat. Neuroscience 57:717-724.
Paolini AG, McKenzie JS (1996) Lesions in the magnocellular preoptic nucleus decrease olfactory investigation in rats. Behavioural Brain Research 81:223-231.
Paolini AG, McKenzie JS (1997) Intracellular recording of magnocellular preoptic neuron responses to olfactory brain. Neuroscience 78:229-242.
Parmentier M, Libert F, Schurmans S, Schiffmann S, Lefort A, Eggerickx D, Ledent C, Mollereau C, Gerard C, Perret J, Grootegoed A, Vassart G (1992) Expression of

members of the putative olfactory receptor gene family in mammalian germ cells. Nature 355:453-455.
Parrish-Aungst S, Shipley MT, Erdelyi F, Szabo G, Puche AC (2007) Quantitative analysis of neuronal diversity in the mouse olfactory bulb. J Comp Neurol 501:825-836.
Parsa PV, D'Souza RD, Vijayaraghavan S (2015) Signaling between periglomerular cells reveals a bimodal role for GABA in modulating glomerular microcircuitry in the olfactory bulb. Proc Natl Acad Sci U S A 112:9478-9483.
Petreanu L, Alvarez-Buylla A (2002) Maturation and death of adult-born olfactory bulb granule neurons: Role of olfaction. Journal of Neuroscience 22:6106-6113.
Petzold GC, Hagiwara A, Murthy VN (2009) Serotonergic modulation of odor input to the mammalian olfactory bulb. Nature Neuroscience 12:784-U142.
Pignatelli A, Kobayashi K, Okano H, Belluzzi O (2005) Functional properties of dopaminergic neurones in the mouse olfactory bulb. Journal of Physiology-London 564:501-514.
Pinching AJ, Powell TP (1971) The neuron types of the glomerular layer of the olfactory bulb. Cell Sci. 9(2):305-45
Pinching AJ, Powell TP (1971) The neuropil of the glomeruli of the olfactory bulb. Cell Sci 9, 347-377
Pirez N, Wachowiak M (2008) In vivo modulation of sensory input to the olfactory bulb by tonic and activity-dependent presynaptic inhibition of receptor neurons. Journal of Neuroscience 28:6360-6371.
Price JL, Powell TPS (1970) The Mitral and Short Axon Cells of the Olfactory Bulb. Journal of Cell Science 7: 631-651
Poo C, Isaacson JS (2009) Odor Representations in Olfactory Cortex: "Sparse" Coding, Global Inhibition, and Oscillations. Neuron 62:850-861.
Potter SM, Zheng C, Koos DS, Feinstein P, Fraser SE, Mombaerts P (2001) Structure and emergence of specific olfactory glomeruli in the mouse. Journal of Neuroscience 21:9713-9723.
Pressler RT, Strowbridge BW (2006) Blanes cells mediate persistent feedforward inhibition onto granule cells in the olfactory bulb. Neuron 49:889-904.
Puopolo M, Belluzzi O (1998a) Inhibitory synapses among interneurons in the glomerular layer of rat and frog olfactory bulbs. Journal of Neurophysiology 80:344-349.
Puopolo M, Belluzzi O (1998b) Functional heterogeneity of periglomerular cells in the rat olfactory bulb. European Journal of Neuroscience 10:1073-1083.
Ressler KJ, Sullivan SL, Buck LB (1993) A zonal organization of odorant receptor gene expression in the olfactory epithelium. Cell 73:597-609.
Rheims S, Holmgren CD, Chazal G, Mulder J, Harkany T, Zilberter T, Zilberter Y (2009) GABA action in immature neocortical neurons directly depends on the availability of ketone bodies. Journal of Neurochemistry 110:1330-1338.
Ribak CE, Seress L, Peterson GM, Seroogy KB, Fallon JH, Schmued LC (1986) A GABAergic inhibitory component within the hipocampal commisural pathway. Journal of Neuroscience 6:3492-3498.
Richard MB, Taylor SR, Greer CA (2010) Age-induced disruption of selective olfactory bulb synaptic circuits. Proceedings of the National Academy of Sciences of the United States of America 107:15613-15618.
Rojas-Libano D, Frederick DE, Egana JI, Kay LM (2014) The olfactory bulb theta rhythm follows all frequencies of diaphragmatic respiration in the freely behaving rat. Frontiers in Behavioral Neuroscience 8.

Rubin BD, Katz LC (1999) Optical imaging of odorant representations in the mammalian olfactory bulb. Neuron 23:499-511.

Rudy B, Fishell G, Lee S, Hjerling-Leffler J (2011) Three Groups of Interneurons Account for Nearly 100% of Neocortical GABAergic Neurons. Developmental Neurobiology 71:45-61.

Salcedo E, Tran T, Ly X, Lopez R, Barbica C, Restrepo D, Vijayaraghavan S (2011) Activity-Dependent Changes in Cholinergic Innervation of the Mouse Olfactory Bulb. Plos One 6.

Saunders A, Granger AJ, Sabatini BL (2015) Corelease of acetylcholine and GABA from cholinergic forebrain neurons. Elife 4.

Schneider SP, Macrides F (1978) Laminar distributions of interneurons in main olfactory bulb of adult hamsters. Brain Research Bulletin 3:73-82.

Schoppa NE (2006) Synchronization of olfactory bulb mitral cells by precisely timed inhibitory inputs. Neuron 49:271-283.

Schoppa NE, Westbrook GL (2001) Glomerulus-specific synchronization of mitral cells in the olfactory bulb. Neuron 31:639-651.

Schoppa NE, Westbrook GL (2002) AMPA autoreceptors drive correlated spiking in olfactory bulb glomeruli. Nature Neuroscience 5:1194-1202.

Schoppa NE, Kinzie JM, Sahara Y, Segerson TP, Westbrook GL (1998) Dendrodendritic inhibition in the olfactory bulb is driven by NMDA receptors. J Neurosci 18:6790-6802.

Scott JW (1981) Electrophysiological identification of mitral and tufted cells and distribution of their axons in olfactory system of the rat. Journal of Neurophysiology 46:918-931.

Shao Z, Puche AC, Shipley MT (2013) Intraglomerular inhibition maintains mitral cell response contrast across input frequencies. J Neurophysiol.

Shao Z, Puche AC, Liu S, Shipley MT (2012) Intraglomerular inhibition shapes the strength and temporal structure of glomerular output. J Neurophysiol 108:782-793.

Shao Z, Puche AC, Kiyokage E, Szabo G, Shipley MT (2009) Two GABAergic Intraglomerular Circuits Differentially Regulate Tonic and Phasic Presynaptic Inhibition of Olfactory Nerve Terminals. Journal of Neurophysiology 101:1988-2001.

Shepherd GM, Chen WR, Greer CA (2004) The synaptic organization of the brain (5^{th} ed.) Oxford university press 165-216.

Shepherd GM, Chen WR, Willhite D, Migliore M, Greer CA (2007) The olfactory granule cell: From classical enigma to central role in olfactory processing. Brain Research Reviews 55:373-382.

Shipley MT, Adamek GD (1984) The connections of the mouse olfactory bulb. A study using orthograde and retrograde transport of wheat germ agglutinin cojugated to horseradish peroxidase. Brain Research Bulletin 12:669-688.

Shipley MT, Halloran FJ, Delatorre J (1985) Surprisingly rich projection from Locus coeruleus to the olfactory bulb in the rat. Brain Research 329:294-299.

Smith RS, Hu RL, DeSouza A, Eberly CL, Krahe K, Chan W, Araneda RC (2015) Differential Muscarinic Modulation in the Olfactory Bulb. Journal of Neuroscience 35:10773-10785.

Smith TC, Jahr CE (2002) Self-inhibition of olfactory bulb neurons. Nat Neurosci 5:760-766.

Sosulski DL, Bloom ML, Cutforth T, Axel R, Datta SR (2011) Distinct representations of olfactory information in different cortical centres. Nature 472:213-216.

Soucy ER, Albeanu DF, Fantana AL, Murthy VN, Meister M (2009) Precision and diversity in an odor map on the olfactory bulb. Nature Neuroscience 12:210-220.

Spors H, Grinvald A (2002) Spatio-temporal dynamics of odor representations in the mammalian olfactory bulb. Neuron 34:301-315.

Spors H, Wachowiak M, Cohen LB, Friedrich RW (2006) Temporal dynamics and latency patterns of receptor neuron input to the olfactory bulb. Journal of Neuroscience 26:1247-1259.

Stettler DD, Axel R (2009) Representations of Odor in the Piriform Cortex. Neuron 63:854-864.

Tan J, Savigner A, Ma MH, Luo MM (2010) Odor Information Processing by the Olfactory Bulb Analyzed in Gene-Targeted Mice. Neuron 65:912-926.

Toida K, Kosaka K, Heizmann CW, Kosaka T (1994) Synaptic contacts between mitral/tufted cells and GABAergic neurons containing calcium binding protein Parvalbumin in the rat olfactory bulb, with special reference to reciprocal synapses between them. Brain Research 650:347-352.

Toida K, Kosaka K, Heizmann CW, Kosaka T (1998) Chemically defined neuron groups and their subpopulations in the glomerular layer of the rat main olfactory bulb: III. Structural features of calbindin D28K-immunoreactive neurons. Journal of Comparative Neurology 392:179-198.

Toida K, Kosaka K, Aika Y, Kosaka T (2000) Chemically defined neuron groups and their subpopulations in the glomerular layer of the rat main olfactory bulb - IV. Intraglomerular synapses of tyrosine hydroxylase-immunoreactive neurons. Neuroscience 101:11-17.

Tomioka R, Okamoto K, Furuta T, Fujiyama F, Iwasato T, Yanagawa Y, Obata K, Kaneko T, Tamamaki N (2005) Demonstration of long-range GABAergic connections distributed throughout the mouse neocortex. European Journal of Neuroscience 21:1587-1600.

Tucker ES, Polleux F, LaMantia AS (2006) Position and time specify the migration of a pioneering population of olfactory bulb interneurons. Developmental Biology 297:387-401.

Uchida N, Mainen ZF (2003) Speed and accuracy of olfactory discrimination in the rat. Nature Neuroscience 6:1224-1229.

Urban NN (2002) Lateral inhibition in the olfactory bulb and in olfaction. Physiology & Behavior 77:607-612.

Urban NN, Sakmann B (2002) Reciprocal intraglomerular excitation and intra- and interglomerular lateral inhibition between mouse olfactory bulb mitral cells. Journal of Physiology-London 542:355-367.

Vaaga CE, Westbrook GL (2016) Parallel processing of afferent olfactory sensory information. Journal of Physiology-London 594:6715-6732.

Vaaga CE, Yorgason JT, Williams JT, Westbrook GL (2017) Presynaptic gain control by endogenous cotransmission of dopamine and GABA in the olfactory bulb. Journal of Neurophysiology 117:1163-1170.

Valeeva G, Tressard T, Mukhtarov M, Baude A, Khazipov R (2016) An Optogenetic Approach for Investigation of Excitatory and Inhibitory Network GABA Actions in Mice Expressing Channelrhodopsin-2 in GABAergic Neurons. Journal of Neuroscience 36:5961-5973.

Vandenpol AN (1995) Presynaptic metabotropic glutamate receptors in adult and developing neurons. Autoexcitation in the olfactory bulb. Journal of Comparative Neurology 359:253-271.

Vassar R, Ngai J, Axel R (1993) Spatial segregation of odorant receptor expression in the mammalian olfactory epithelium. Cell 74:309-318.

Vincis R, Lagier S, Van De Ville D, Rodriguez I, Carleton A (2015) Sensory-Evoked Intrinsic Imaging Signals in the Olfactory Bulb Are Independent of Neurovascular Coupling. Cell Reports 12:313-325.

Wachowiak M, Cohen LB (2001) Representation of odorants by receptor neuron input to the mouse olfactory bulb. Neuron 32:723-735.

Wahl-Schott C, Biel M (2009) HCN channels: Structure, cellular regulation and physiological function. Cellular and Molecular Life Sciences 66:470-494.

Wellis DP, Scott JW (1990) Intracellular responses of identified rat olfactory bulb interneurons to electrical and odor stimulation. Journal of Neurophysiology 64:932-947.

Whitesell JD, Sorensen KA, Jarvie BC, Hentges ST, Schoppa NE (2013) Interglomerular lateral inhibition targeted on external tufted cells in the olfactory bulb. J Neurosci 33:1552-1563.

Whitman MC, Greer CA (2007) Adult-generated neurons exhibit diverse developmental fates. Developmental Neurobiology 67:1079-1093.

Whitman MC, Greer CA (2009) Adult neurogenesis and the olfactory system. Progress in Neurobiology 89:162-175.

Winner B, Cooper-Kuhn CM, Aigner R, Winkler J, Kuhn HG (2002) Long-term survival and cell death of newly generated neurons in the adult rat olfactory bulb. European Journal of Neuroscience 16:1681-1689.

Yamamoto K, Takei H, Koyanagi Y, Koshikawa N, Kobayashi M (2015) Presynaptic cell type-dependent regulation of GABAergic synaptic transmission by nitric oxide in rat insular cortex. Neuroscience 284:65-77.

Yokoi M, Mori K, Nakanishi S (1995) Refinement of odor molecule tuning by dendrodendritic synaptic inhibition in the olfactory bulb. Proc Natl Acad Sci U S A 92:3371-3375.

Yoshihara S, Takahashi H, Nishimura N, Naritsuka H, Shirao T, Hirai H, Yoshihara Y, Mori K, Stern PL, Tsuboi A (2012) 5T4 Glycoprotein Regulates the Sensory Input-Dependent Development of a Specific Subtype of Newborn Interneurons in the Mouse Olfactory Bulb. Journal of Neuroscience 32:2217-2226.

Zaborszky L, Carlsen J, Brashear HR, Heimer L (1986) Cholinergic and GABAergic afferents to the olfactory bulb in the rat with special emphasis on the projection neurons in the nucleus of the horizontal limb of the diagonal band. J Comp Neurol 243:488-509.

Zaborszky L, Pang K, Somogyi J, Nadasdy Z, Kallo I (1999) The basal forebrain corticopetal system revisited. Advancing from the Ventral Striatum to the Extended Amygdala: Implications for Neuropsychiatry and Drug Abuse: in Honor of Lennart Heimer 877:339-367.

Zimnik NC, Treadway T, Smith RS, Araneda RC (2013) alpha(1A)-Adrenergic regulation of inhibition in the olfactory bulb. Journal of Physiology-London 591:1631-1643.

References

References

Abraham NM, Spors H, Carleton A, Margrie TW, Kuner T, Schaefer AT (2004) Maintaining accuracy at the expense of speed: Stimulus similarity defines odor discrimination time in mice. Neuron 44:865-876.

Abraham NM, Egger V, Shimshek DR, Renden R, Fukunaga I, Sprengel R, Seeburg PH, Klugmann M, Margrie TW, Schaefer AT, Kuner T (2010) Synaptic Inhibition in the Olfactory Bulb Accelerates Odor Discrimination in Mice. Neuron 65:399-411.

Alonso A, Kohler C (1982) Evidence for separate projections of hippocampal pyramidal and non-pyramidal neurons to different parts of the septum in the rat brain. Neuroscience Letters 31:209-214.

Alvarez-Buylla A, Garcia-Verdugo JM (2002) Neurogenesis in adult subventricular zone. Journal of Neuroscience 22:629-634.

Antal M, Eyre M, Finklea B, Nusser Z (2006) External tufted cells in the main olfactory bulb form two distinct subpopulations. European Journal of Neuroscience 24:1124-1136.

Apicella A, Yuan Q, Scanziani M, Isaacson JS (2010) Pyramidal Cells in Piriform Cortex Receive Convergent Input from Distinct Olfactory Bulb Glomeruli. Journal of Neuroscience 30:14255-14260.

Arenkiel BR, Peca J, Davison IG, Feliciano C, Deisseroth K, Augustine GJ, Ehlers MD, Feng G (2007) In vivo light-induced activation of neural circuitry in transgenic mice expressing channelrhodopsin-2. Neuron 54:205-218.

Arevian AC, Kapoor V, Urban NN (2008) Activity-dependent gating of lateral inhibition in the mouse olfactory bulb. Nature Neuroscience 11:80-87.

Aungst JL, Heyward PM, Puche AC, Karnup SV, Hayar A, Szabo G, Shipley MT (2003) Centre-surround inhibition among olfactory bulb glomeruli. Nature 426:623-629.

Balu R, Pressler RT, Strowbridge BW (2007) Multiple modes of synaptic excitation of olfactory bulb granule cells. Journal of Neuroscience 27:5621-5632.

Banerjee A, Marbach F, Anselmi F, Koh MS, Davis MB, da Silva PG, Delevich K, Oyibo HK, Gupta P, Li B, Albeanu DF (2015) An Interglomerular Circuit Gates Glomerular Output and Implements Gain Control in the Mouse Olfactory Bulb. Neuron 87:193-207.

Bardy C, Alonso M, Bouthour W, Lledo PM (2010) How, When, and Where New Inhibitory Neurons Release Neurotransmitters in the Adult Olfactory Bulb. Journal of Neuroscience 30:17023-17034.

Batista-Brito R, Close J, Machold R, Fishell G (2008) The distinct temporal origins of olfactory bulb interneuron subtypes. Journal of Neuroscience 28:3966-3975.

Belluzzi O, Benedusi M, Ackman J, LoTurco JJ (2003) Electrophysiological differentiation of new neurons in the olfactory bulb. J Neurosci 23:10411-10418.

Bischofberger J, Jonas P (1997) Action potential propagation into the presynaptic dendrites of rat mitral cells. Journal of Physiology-London 504:359-365.

Bourne JN, Schoppa NE (2017) Three-Dimensional Synaptic Analyses of Mitral Cell and External Tufted Cell Dendrites in Rat Olfactory Bulb Glomeruli. Journal of Comparative Neurology 525:592-609.

Boyd AM, Sturgill JF, Poo C, Isaacson JS (2012) Cortical Feedback Control of Olfactory Bulb Circuits. Neuron 76:1161-1174.

Boyd AM, Kato HK, Komiyama T, Isaacson JS (2015) Broadcasting of cortical activity to the olfactory bulb. Cell Rep 10:1032-1039.

Bozza T, McGann JP, Mombaerts P, Wachowiak M (2004) In vivo imaging of neuronal activity - Neurotechnique by targeted expression of a genetically encoded probe in the mouse. Neuron 42:9-21.

Brinon JG, Alonso JR, Arevalo R, Garciaojeda E, Lara J, Aijon J (1992) Calbindin 28K positive neurons in the rat olfactory bulb. An immunohistochemical study. Cell and Tissue Research 269:289-297.

Brunert D, Tsuno Y, Rothermel M, Shipley MT, Wachowiak M (2016) Cell-Type-Specific Modulation of Sensory Responses in Olfactory Bulb Circuits by Serotonergic Projections from the Raphe Nuclei. Journal of Neuroscience 36:6820-6835.

Buck L, Axel R (1991) A novel multigene family may encode odorant receptors. A molecular basis for odor recognition. Cell 65:175-187.

Buonviso N, Chaput MA, Scott JW (1991) Mitral cell to glomerulus connectivity. An HRP study of the orientation of mitral cell apical dendrites. Journal of Comparative Neurology 307:57-64.

Buonviso N, Amat C, Litaudon P, Roux S, Royet JP, Farget V, Sicard G (2003) Rhythm sequence through the olfactory bulb layers during the time window of a respiratory cycle. European Journal of Neuroscience 17:1811-1819.

Burton SD, Urban NN (2014) Greater excitability and firing irregularity of tufted cells underlies distinct afferent-evoked activity of olfactory bulb mitral and tufted cells. Journal of Physiology-London 592:2097-2118.

Burton SD, LaRocca G, Liu A, Cheetham CEJ, Urban NN (2017) Olfactory Bulb Deep Short-Axon Cells Mediate Widespread Inhibition of Tufted Cell Apical Dendrites. Journal of Neuroscience 37:1117-1138.

Buzsaki G, Chrobak JJ (1995) Temporal structure in spatially organized neuronal ensembles. A role for interneuronal networks. Current Opinion in Neurobiology 5:504-510.

Caggiano M, Kauer JS, Hunter DD (1994) Globose basal cells are neuronal progenitors in the olfactort epithelium. A lineage analysis using a replication-incompetent retrovirus. Neuron 13:339-352.

Cang J, Isaacson JS (2003) In vivo whole-cell recording of odor-evoked synaptic transmission in the rat olfactory bulb. J Neurosci 23:4108-4116.

Carey RM, Wachowiak M (2011) Effect of Sniffing on the Temporal Structure of Mitral/Tufted Cell Output from the Olfactory Bulb. Journal of Neuroscience 31:10615-10626.

Carleton A, Petreanu LT, Lansford R, Alvarez-Buylla A, Lledo PM (2003) Becoming a new neuron in the adult olfactory bulb. Nat Neurosci 6:507-518.

Carlson GC, Shipley MT, Keller A (2000) Long-lasting depolarizations in mitral cells of the rat olfactory bulb. Journal of Neuroscience 20:2011-2021.

Chand AN, Galliano E, Chesters RA, Grubb MS (2015) A Distinct Subtype of Dopaminergic Interneuron Displays Inverted Structural Plasticity at the Axon Initial Segment. Journal of Neuroscience 35:1573-1590.

Chao TI, Kasa P, Wolff JR (1997) Distribution of astroglia in glomeruli of the rat main olfactory bulb: Exclusion from the sensory subcompartment of neuropil. Journal of Comparative Neurology 388:191-210.

Chen WR, Midtgaard J, Shepherd GM (1997) Forward and backward propagation of dendritic impulses and their synaptic control in mitral cells. Science 278:463-467.

Chen WR, Xiong WH, Shepherd GM (2000) Analysis of relations between NMDA receptors and GABA release at olfactory bulb reciprocal synapses. Neuron 25:625-633.

Chen WR, Shen GY, Shepherd GM, Hines ML, Midtgaard J (2002) Multiple modes of action potential initiation and propagation in mitral cell primary dendrite. Journal of Neurophysiology 88:2755-2764.

Costanzo RM (1991) Regeneration of olfactory receptor cells. Ciba Foundation Symposia 160:233-248.

Crespo C, Blasco-Ibanez JM, Marques-Mari AI, Alonso JR, Brinon JG, Martinez-Guijarro FJ (2002) Vasoactive intestinal polypeptide-containing elements in the olfactory bulb of the hedgehog (Erinaceus europaeus). Journal of Chemical Neuroanatomy 24:49-63.

Crespo C, Gracia-Llanes FJ, Blasco-Ibanez JM, Gutierrez-Mecinas M, Marques-Mari AI, Martinez-Guijarro FJ (2003) Nitric oxide synthase containing periglomerular cells are GABAergic in the rat olfactory bulb. Neuroscience Letters 349:151-154.

Davis BJ, Macrides F (1983) Tyrosine-hydroxylase immunoreactive neurons and fibers in the olfactory system of the hamster. Journal of Comparative Neurology 214:427-440.

Davison IG, Katz LC (2007) Sparse and selective odor coding by mitral/tufted neurons in the main olfactory bulb. Journal of Neuroscience 27:2091-2101.

De Marchis S, Bovetti S, Carletti B, Hsieh YC, Garzotto D, Peretto P, Fasolo A, Puche AC, Rossi F (2007) Generation of distinct types of periglomerular olfactory bulb interneurons during development and in adult mice: Implication for intrinsic properties of the subventricular zone progenitor population. Journal of Neuroscience 27:657-664.

De Saint Jan D, Westbrook GL (2007) Disynaptic amplification of metabotropic glutamate receptor 1 responses in the olfactory bulb. Journal of Neuroscience 27:132-140.

De Saint Jan D, Hirnet D, Westbrook GL, Charpak S (2009) External Tufted Cells Drive the Output of Olfactory Bulb Glomeruli. Journal of Neuroscience 29:2043-2052.

Debarbieux F, Audinat E, Charpak S (2003) Action potential propagation in Dendrites of rat mitral cells in vivo. Journal of Neuroscience 23:5553-5560.

Demeulemeester H, Arckens L, Vandesande F, Orban GA, Heizmann CW, Pochet R (1991) Calcium-binding proteins and neuropeptides as molecular markers of GABAergic interneurons in the cat visual cortex. Experimental Brain Research 84:538-544.

Deolmos J, Hardy H, Heimer L (1978) Afferent connections of main and accessory olfactory bulb formations in rat. experimental HRP study. Journal of Comparative Neurology 181:213-244.

Dietz SB, Murthy VN (2005) Contrasting short-term plasticity at two sides of the mitral-granule reciprocal synapse in the mammalian olfactory bulb. Journal of Physiology-London 569:475-488.

Do JP, Xu M, Lee SH, Chang WC, Zhang S, Chung S, Yung TJ, Fan JL, Miyamichi K, Luo L, Dan Y (2016) Cell type-specific long-range connections of basal forebrain circuit. Elife 5.

Dong HW, Hayar A, Ennis M (2007) Activation of group I metabotropic glutamate receptors on main olfactory bulb granule cells and periglomerular cells enhances synaptic inhibition of mitral cells. Journal of Neuroscience 27:5654-5663.

Economo MN, Hansen KR, Wachowiak M (2016) Control of Mitral/Tufted Cell Output by Selective Inhibition among Olfactory Bulb Glomeruli. Neuron 91:397-411.

Escanilla O, Arrellanos A, Karnow A, Ennis M, Linster C (2010) Noradrenergic modulation of behavioral odor detection and discrimination thresholds in the olfactory bulb. European Journal of Neuroscience 32:458-468.

Eyre MD, Antal M, Nusser Z (2008) Distinct deep short-axon cell subtypes of the main olfactory bulb provide novel intrabulbar and extrabulbar GABAergic connections. J Neurosci 28:8217-8229.

Eyre MD, Kerti K, Nusser Z (2009) Molecular diversity of deep short-axon cells of the rat main olfactory bulb. European Journal of Neuroscience 29:1397-1407.

Fernandez ME, Croce S, Boutin C, Cremer H, Raineteau O (2011) Targeted electroporation of defined lateral ventricular walls: a novel and rapid method to study fate specification during postnatal forebrain neurogenesis. Neural Development 6:12.

Figueres-Onate M, Lopez-Mascaraque L (2016) Adult Olfactory Bulb Interneuron Phenotypes Identified by Targeting Embryonic and Postnatal Neural Progenitors. Frontiers in Neuroscience 10.

Firestein S (2001) How the olfactory system makes sense of scents. Nature 413:211-218.

Fleischmann A, Shykind BM, Sosulski DL, Franks KM, Glinka ME, Mei DF, Sun YH, Kirkland J, Mendelsohn M, Albers MW, Axel R (2008) Mice with a "Monoclonal Nose": Perturbations in an Olfactory Map Impair Odor Discrimination. Neuron 60:1068-1081.

Fletcher ML, Masurkar AV, Xing JL, Imamura F, Xiong WH, Nagayama S, Mutoh H, Greer CA, Knopfel T, Chen WR (2009) Optical Imaging of Postsynaptic Odor Representation in the Glomerular Layer of the Mouse Olfactory Bulb. Journal of Neurophysiology 102:817-830.

Fogli Iseppe A, Pignatelli A, Belluzzi O (2016) Calretinin-Periglomerular Interneurons in Mice Olfactory Bulb: Cells of Few Words. Front Cell Neurosci 10:231.

Friedrich RW, Korsching SI (1997) Combinatorial and chemotopic odorant coding in the zebrafish olfactory bulb visualized by optical imaging. Neuron 18:737-752.

Fukunaga I, Berning M, Kollo M, Schmaltz A, Schaefer AT (2012) Two Distinct Channels of Olfactory Bulb Output. Neuron 75:320-329.

Fukunaga I, Herb JT, Kollo M, Boyden ES, Schaefer AT (2014) Independent control of gamma and theta activity by distinct interneuron networks in the olfactory bulb. Nat Neurosci 17:1208-1216.

Geramita M, Urban NN (2017) Differences in Glomerular-Layer-Mediated Feedforward Inhibition onto Mitral and Tufted Cells Lead to Distinct Modes of Intensity Coding. Journal of Neuroscience 37:1428-1438.

Geramita MA, Burton SD, Urban NN (2016) Distinct lateral inhibitory circuits drive parallel processing of sensory information in the mammalian olfactory bulb. Elife 5.

Ghosh S, Larson SD, Hefzi H, Marnoy Z, Cutforth T, Dokka K, Baldwin KK (2011) Sensory maps in the olfactory cortex defined by long-range viral tracing of single neurons. Nature 472:217-220.

Gire DH, Schoppa NE (2009) Control of on/off glomerular signaling by a local GABAergic microcircuit in the olfactory bulb. J Neurosci 29:13454-13464.

Gire DH, Franks KM, Zak JD, Tanaka KF, Whitesell JD, Mulligan AA, Hen R, Schoppa NE (2012) Mitral Cells in the Olfactory Bulb Are Mainly Excited through a Multistep Signaling Path. Journal of Neuroscience 32:2964-2975.

Gracia-Llanes FJ, Crespo C, Blasco-Ibanez JM, Nacher J, Varea E, Rovira-Esteban L, Martinez-Guijarro FJ (2010) GABAergic basal forebrain afferents innervate selectively GABAergic targets in the main olfactory bulb. Neuroscience 170:913-922.

Gschwend O, Abraham NM, Lagier S, Begnaud F, Rodriguez I, Carleton A (2015) Neuronal pattern separation in the olfactory bulb improves odor discrimination learning. Nat Neurosci 18:1474-1482.

Hack MA, Saghatelyan A, de Chevigny A, Pfeifer A, Ashery-Padan R, Lledo PM, Gotz M (2005) Neuronal fate determinants of adult olfactory bulb neurogenesis. Nature Neuroscience 8:865-872.

Halabisky B, Strowbridge BW (2003) gamma-frequency excitatory input to granule cells facilitates dendrodendritic inhibition in the rat olfactory bulb. Journal of Neurophysiology 90:644-654.

Halabisky B, Friedman D, Radojicic M, Strowbridge BW (2000) Calcium influx through NMDA receptors directly evokes GABA release in olfactory bulb granule cells. Journal of Neuroscience 20:5124-5134.

Hardy A, Palouzier-Paulignan B, Duchamp A, Royet JP, Duchamp-Viret P (2005) 5-hydroxytryptamine action in the rat olfactory bulb: In vitro electrophysiological patch-clamp recordings of juxtaglomerular and mitral cells. Neuroscience 131:717-731.

Hayar A, Karnup S, Shipley MT, Ennis M (2004a) Olfactory bulb glomeruli: External tufted cells intrinsically burst at theta frequency and are entrained by patterned olfactory input. Journal of Neuroscience 24:1190-1199.

Hayar A, Karnup S, Ennis M, Shipley MT (2004b) External tufted cells: A major excitatory element that coordinates glomerular activity. Journal of Neuroscience 24:6676-6685.

Hayar A, Heyward PM, Heinbockel T, Shipley MT, Ennis M (2001) Direct excitation of mitral cells via activation of alpha 1-noradrenergic receptors in rat olfactory bulb slices. Journal of Neurophysiology 86:2173-2182.

Holderith NB, Shigemoto R, Nusser Z (2003) Cell type-dependent expression of HCN1 in the main olfactory bulb. European Journal of Neuroscience 18:344-354.

Huang LW, Garcia I, Jen HI, Arenkiel BR (2013) Reciprocal connectivity between mitral cells and external plexiform layer interneurons in the mouse olfactory bulb. Frontiers in Neural Circuits 7.

Huang ZB, Thiebaud N, Fadool DA (2016) Differential serotonergic modulation across the main and accessory olfactory bulb. Chemical Senses 41:E195-E195.

Igarashi KM, Ieki N, An M, Yamaguchi Y, Nagayama S, Kobayakawa K, Kobayakawa R, Tanifuji M, Sakano H, Chen WR, Mori K (2012) Parallel Mitral and Tufted Cell Pathways Route Distinct Odor Information to Different Targets in the Olfactory Cortex. Journal of Neuroscience 32:7970-7985.

Imai T, Sakano H (2007) Roles of odorant receptors in projecting axons in the mouse olfactory system. Current Opinion in Neurobiology 17:507-515.

Imamura F, Nagao H, Naritsuka H, Murata Y, Taniguchi H, Mori K (2006) A leucine-rich repeat membrane protein, 5T4, is expressed by a subtype of granule cells with dendritic arbors in specific strata of the mouse olfactory bulb. Journal of Comparative Neurology 495:754-768.

Isaacson JS (2001) Mechanisms governing dendritic gamma-aminobutyric acid (GABA) release in the rat olfactory bulb. Proceedings of the National Academy of Sciences of the United States of America 98:337-342.

Isaacson JS, Strowbridge BW (1998) Olfactory reciprocal synapses: dendritic signaling in the CNS. Neuron 20:749-761.

Jahr CE, Nicoll RA (1982) An intracellular analysis of dendrodendritic inhibition in the turtle in vitro olfactory bulb. Journal of Physiology-London 326:213-234.

Jinno S, Kosaka T (2004) Parvalbumin is expressed in glutamatergic and GABAergic corticostriatal pathway in mice. Journal of Comparative Neurology 477:188-201.

Jinno S, Klausberger T, Marton LF, Dalezios Y, Roberts JDB, Fuentealba P, Bushong EA, Henze D, Buzsaki G, Somogyi P (2007) Neuronal diversity in GABAergic long-range projections from the hippocampus. Journal of Neuroscience 27:8790-8804.

Johnson BA, Leon M (2007) Chemotopic odorant coding in a mammalian olfactory system. Journal of Comparative Neurology 503:1-34.

Kapoor V, Provost AC, Agarwal P, Murthy VN (2016) Activation of raphe nuclei triggers rapid and distinct effects on parallel olfactory bulb output channels. Nature Neuroscience 19:271-+.

Kasowski HJ, Kim H, Greer CA (1999) Compartmental organization of the olfactory bulb glomerulus. Journal of Comparative Neurology 407:261-274.

Kato HK, Chu MW, Isaacson JS, Komiyama T (2012) Dynamic Sensory Representations in the Olfactory Bulb: Modulation by Wakefulness and Experience. Neuron 76:962-975.

Kato HK, Gillet SN, Peters AJ, Isaacson JS, Komiyama T (2013) Parvalbumin-Expressing Interneurons Linearly Control Olfactory Bulb Output. Neuron 80:1218-1231.

Kawaguchi Y, Kondo S (2002) Parvalbumin, somatostatin and cholecystokinin as chemical markers for specific GABAergic interneuron types in the rat frontal cortex. Journal of Neurocytology 31:277-287.

Ke MT, Fujimoto S, Imai T (2013) SeeDB: a simple and morphology-preserving optical clearing agent for neuronal circuit reconstruction. Nature Neuroscience 16:1154-U1246.

Kelsch W, Lin CW, Lois C (2008) Sequential development of synapses in dendritic domains during adult neurogenesis. Proceedings of the National Academy of Sciences of the United States of America 105:16803-16808.

Kikuta S, Fletcher ML, Homma R, Yamasoba T, Nagayama S (2013) Odorant Response Properties of Individual Neurons in an Olfactory Glomerular Module. Neuron 77:1122-1135.

Kirmse K, Witte OW, Holthoff K (2010) GABA Depolarizes Immature Neocortical Neurons in the Presence of the Ketone Body beta-Hydroxybutyrate. Journal of Neuroscience 30:16002-16007.

Kishi K, Mori K, Ojima H (1984) Distribution of local axon collaterals of mitral, displaced mitral and tufted cells in the rabbit olfactory bulb. Journal of Comparative Neurology 225:511-526.

Kiyokage E, Kobayashi K, Toida K (2017) Spatial distribution of synapses on tyrosine hydroxylase-expressing juxtaglomerular cells in the mouse olfactory glomerulus. Journal of Comparative Neurology 525:1059-1074.

Kiyokage E, Pan YZ, Shao Z, Kobayashi K, Szabo G, Yanagawa Y, Obata K, Okano H, Toida K, Puche AC, Shipley MT (2010) Molecular identity of periglomerular and short axon cells. J Neurosci 30:1185-1196.

Kohwi M, Petryniak MA, Long JE, Ekker M, Obata K, Yanagawa Y, Rubenstein JLR, Alvarez-Buylla A (2007) A subpopulation of olfactory bulb GABAergic interneurons is derived from Emx1- and Dlx5/6-expressing progenitors. Journal of Neuroscience 27:6878-6891.

Kosaka K, Kosaka T (2007) Chemical properties of type 1 and type 2 periglomerular cells in the mouse olfactory bulb are different from those in the rat olfactory bulb. Brain Res 1167:42-55.

Kosaka K, Kosaka T (2013) Secretagogin-containing neurons in the mouse main olfactory bulb. Neuroscience Research 77:16-32.

Kosaka K, Heizmann CW, Kosaka T (1994) Calcium-binding protein Parvalbumin immunoreactive neurons in the rat olfactory bulb. 1. Distribution and structural features in adult rat. Experimental Brain Research 99:191-204.

Kosaka K, Toida K, Margolis FL, Kosaka T (1997) Chemically defined neuron groups and their subpopulations in the glomerular layer of the rat main olfactory bulb .2. Prominent differences in the intraglomerular dendritic arborization and their relationship to olfactory nerve terminals. Neuroscience 76:775-786.

Kosaka K, Toida K, Aika Y, Kosaka T (1998) How simple is the organization of the olfactory glomerulus? the heterogeneity of so-called periglomerular cells. Neuroscience Research 30:101-110.

Kosaka T, Kosaka K (2005) Structural organization of the glomerulus in the main olfactory bulb. Chemical Senses 30:I107-i108.

Kosaka T, Kosaka K (2007) Heterogeneity of nitric oxide synthase-containing neurons in the mouse main olfactory bulb. Neuroscience Research 57:165-178.

Kosaka T, Kosaka K (2008) Tyrosine hydroxylase-positive GABAergic juxtaglomerular neurons are the main source of the interglomerular connections in the mouse main olfactory bulb. Neurosci Res 60:349-354.

Kosaka T, Kosaka K (2009) Two types of tyrosine hydroxylase positive GABAergic juxtaglomerular neurons in the mouse main olfactory bulb are different in their time of origin. Neuroscience Research 64:436-441.

Kosaka T, Kosaka K (2010) Heterogeneity of calbindin-containing neurons in the mouse main olfactory bulb: I. General description. Neuroscience Research 67:275-292.

Kosaka T, Kosaka K (2011) "Interneurons" in the olfactory bulb revisited. Neuroscience Research 69:93-99.

Kunze WA, Shafton AD, Kem RE, McKenzie JS (1992) Intracellular responses of olfactory bulb granule cells to stimulating the horizontal diagonal band nucleus. Neuroscience 48:363-369.

Kunze WAA, Shafton AD, Kemm RE, McKenzie JS (1991) Effect of stimulating the nucleus of the horizontal limb of the diagonal band on single unit activity in the olfactory bulb. Neuroscience 40:21-27.

Lagier S, Carleton A, Lledo PM (2004) Interplay between local GABAergic Interneurons and relay neurons generates gamma oscillations in the rat olfactory bulb. Journal of Neuroscience 24:4382-4392.

Lagier S, Panzanelli P, Russo RE, Nissant A, Bathellier B, Sassoe-Pognetto M, Fritschy JM, Lledo PM (2007) GABAergic inhibition at dendrodendritic synapses tunes gamma oscillations in the olfactory bulb. Proceedings of the National Academy of Sciences of the United States of America 104:7259-7264.

Lecoq J, Tiret P, Charpak S (2009) Peripheral Adaptation Codes for High Odor Concentration in Glomeruli. Journal of Neuroscience 29:3067-3072.

Lemasson M, Saghatelyan A, Olivo-Marin JC, Lledo PM (2005) Neonatal and adult neurogenesis provide two distinct populations of newborn neurons to the mouse olfactory bulb. Journal of Neuroscience 25:6816-6825.

Lepousez G, Lledo PM (2013) Odor discrimination requires proper olfactory fast oscillations in awake mice. Neuron 80:1010-1024.

Lepousez G, Mouret A, Loudes C, Epelbaum J, Viollet C (2010a) Somatostatin Contributes to In Vivo Gamma Oscillation Modulation and Odor Discrimination in the Olfactory Bulb. Journal of Neuroscience 30:870-875.

Lepousez G, Csaba Z, Bernard V, Loudes C, Videau C, Lacombe J, Epelbaum J, Viollet C (2010b) Somatostatin Interneurons Delineate the Inner Part of the External Plexiform Layer in the Mouse Main Olfactory Bulb. Journal of Comparative Neurology 518:1976-1994.

Leranth C, Frotscher M (1987) GABAergic input of cholecystokynin-immunoreactive neurons in the hilar region of the rat hippocampus. An electron microscopic double staining study. Histochemistry 86:287-290.

Liu S, Plachez C, Shao Z, Puche A, Shipley MT (2013) Olfactory bulb short axon cell release of GABA and dopamine produces a temporally biphasic inhibition-excitation response in external tufted cells. J Neurosci 33:2916-2926.

Liu SL, Shipley MT (2008) Multiple conductances cooperatively regulate spontaneous bursting in mouse olfactory bulb external tufted cells. Journal of Neuroscience 28:1625-1639.

Liu SL, Puche AC, Shipley MT (2016) The Interglomerular Circuit Potently Inhibits Olfactory Bulb Output Neurons by Both Direct and Indirect Pathways. Journal of Neuroscience 36:9604-9617.

Liu SL, Shao ZY, Puche A, Wachowiak M, Rothermel M, Shipley MT (2015) Muscarinic Receptors Modulate Dendrodendritic Inhibitory Synapses to Sculpt Glomerular Output. Journal of Neuroscience 35:5680-5692.

Livneh Y, Adam Y, Mizrahi A (2014) Odor Processing by Adult-Born Neurons. Neuron 81:1097-1110.

Lois C, Alvarezbuylla A (1994) Long-distance neuronal migration in the adult mammalian brain. Science 264:1145-1148.

Lopezmascaraque L, Villalba RM, Decarlos JA (1989) Vasoactive intestinal polypeptide-immunoractive neurons in the main olfactory bulb of the hedgehog (Erinaceus europaeus). Neuroscience Letters 98:19-24.

Lopezmascaraque L, Decarlos JA, Valverde F (1990) Structure if the olfactory bulb of the hedgehog (Erinaceus europaeus). A Golgi study of the intrinsic organization of the superficial layers. Journal of Comparative Neurology 301:243-261.

Luo M, Katz LC (2001) Response correlation maps of neurons in the mammalian olfactory bulb. Neuron 32:1165-1179.

Luskin MB (1993) Restricted proliferation and migration of postnatally generated neurons derived from the forebrain subventricular zone. Neuron 11:173-189.

Luskin MB, Price JL (1983) The topographic organization of associational fibers to the olfactory system un the rat, including centrifugal fibers to the olfactory bulb. Journal of Comparative Neurology 216:264-291.

Macrides F, Schneider SP (1982) Laminar organization of mitral and tufted cells in the main olfactory bulb of the adult hamster. Journal of Comparative Neurology 208:419-430.

Macrides F, Davis BJ, Youngs WM, Nadi NS, Margolis FL (1981) Cholinergic and catecholaminergic afferents to the olfactory bulb in the hamster: a neuroanatomical, biochemical, and histochemical investigation. J Comp Neurol 203:495-514.

Magavi SSP, Mitchell BD, Szentirmai O, Carter BS, Macklis JD (2005) Adult-born and preexisting olfactory granule neurons undergo distinct experience-dependent modifications of their olfactory responses in vivo. Journal of Neuroscience 25:10729-10739.

Maher BJ, Westbrook GL (2008) Co-transmission of dopamine and GABA in periglomerular cells. Journal of Neurophysiology 99:1559-1564.

Mandairon N, Sacquet J, Jourdan F, Didier A (2006) Long-term fate and distribution of newborn cells in the adult mouse olfactory bulb: Influences of olfactory deprivation. Neuroscience 141:443-451.
Margrie TW, Schaefer AT (2003) Theta oscillation coupled spike latencies yield computational vigour in a mammalian sensory system. Journal of Physiology-London 546:363-374.
Markopoulos F, Rokni D, Gire DH, Murthy VN (2012) Functional properties of cortical feedback projections to the olfactory bulb. Neuron 76:1175-1188.
McGann JP, Pirez N, Gainey MA, Muratore C, Elias AS, Wachowiak M (2005) Odorant representations are modulated by intra- but not interglomerular presynaptic inhibition of olfactory sensory neurons. Neuron 48:1039-1053.
McLean JH, Shipley MT (1987) Serotoninergic afferents to the rat olfactory bulb. 1. Origins and laminar specificity of serotoninergic inputs in the adult rat. Journal of Neuroscience 7:3016-3028.
McLean JH, Shipley MT, Nickell WT, Astonjones G, Reyher CKH (1989) Chemoanatomical organization of the noradrenergic input from Locus coeruleus to the olfactory bulb of the adult rat. Journal of Comparative Neurology 285:339-349.
McQuiston AR, Katz LC (2001) Electrophysiology of interneurons in the glomerular layer of the rat olfactory bulb. Journal of Neurophysiology 86:1899-1907.
Meisami E, Safari L (1981) A quantitative study of the effects of early unilateral olfactory deprivation on the number and distribution of mitral and tufted cells and of glomeruli in the rat olfactory bulb. Brain Research 221:81-107.
Merkle FT, Mirzadeh Z, Alvarez-Buylla A (2007) Mosaic organization of neural stem cells in the adult brain. Science 317:381-384.
Merkle FT, Fuentealba LC, Sanders TA, Magno L, Kessaris N, Alvarez-Buylla A (2014) Adult neural stem cells in distinct microdomains generate previously unknown interneuron types. Nature Neuroscience 17:207-214.
Metzger F, Repunte-Canonigo V, Matsushita S, Akemann W, Diez-Garcia J, Ho CS, Iwasato T, Grandes P, Itohara S, Joho RH, Knopfel T (2002) Transgenic mice expressing a pH and Cl- sensing yellow-fluorescent protein under the control of a potassium channel promoter. Eur J Neurosci 15:40-50.
Miyamichi K, Shlomai-Fuchs Y, Shu M, Weissbourd BC, Luo LQ, Mizrahi A (2013) Dissecting Local Circuits: Parvalbumin Interneurons Underlie Broad Feedback Control of Olfactory Bulb Output. Neuron 80:1232-1245.
Miyamichi K, Amat F, Moussavi F, Wang C, Wickersham I, Wall NR, Taniguchi H, Tasic B, Huang ZJ, He ZG, Callaway EM, Horowitz MA, Luo LQ (2011) Cortical representations of olfactory input by trans-synaptic tracing. Nature 472:191-196.
Mombaerts P (1999) Seven-transmembrane proteins as odorant and chemosensory receptors. Science 286:707-711.
Mombaerts P (2006) Olfaction targeted. Journal of Neurogenetics 20:181-181.
Mombaerts P, Wang F, Dulac C, Chao SK, Nemes A, Mendelsohn M, Edmondson J, Axel R (1996) Visualizing an olfactory sensory map. Cell 87:675-686.
Monory K et al. (2006) The endocannabinoid system controls key epileptogenic circuits in the hippocampus. Neuron 51:455-466.
Mori K, Kishi K, Ojima H (1983) Distribution of dendrites of mitral, displaced mitral, tufted, and granule cells in the rabbit olfactory bulb. Journal of Comparative Neurology 219:339-355.

Mori K, Nagao H, Yoshihara Y (1999) The olfactory bulb: Coding and processing of odor molecule information. Science 286:711-715.
Murphy GJ, Darcy DP, Isaacson JS (2005) Intraglomerular inhibition: signaling mechanisms of an olfactory microcircuit. Nature Neuroscience 8:354-364.
Nai Q, Dong HW, Linster C, Ennis M (2010) Activation of alpha 1 and alpha 2 noradrenergic receptors exert opposing effects on excitability of main olfactory bulb granule cells. Neuroscience 169:882-892.
Nai Q, Dong HW, Hayar A, Linster C, Ennis M (2009) Noradrenergic Regulation of GABAergic Inhibition of Main Olfactory Bulb Mitral Cells Varies as a Function of Concentration and Receptor Subtype. Journal of Neurophysiology 101:2472-2484.
Najac M, De Saint Jan D, Reguero L, Grandes P, Charpak S (2011) Monosynaptic and Polysynaptic Feed-Forward Inputs to Mitral Cells from Olfactory Sensory Neurons. Journal of Neuroscience 31:8722-8729.
Najac M, Diez AS, Kumar A, Benito N, Charpak S, De Saint Jan D (2015) Intraglomerular Lateral Inhibition Promotes Spike Timing Variability in Principal Neurons of the Olfactory Bulb. The Journal of Neuroscience 35:4319-4331.
Neville KR, Haberly LB (2003) Beta and gamma oscillations in the olfactory system of the urethane-anesthetized rat. Journal of Neurophysiology 90:3921-3930.
Niedworok CJ, Schwarz I, Ledderose J, Giese G, Conzelmann KK, Schwarz MK (2012) Charting monosynaptic connectivity maps by two-color light-sheet fluorescence microscopy. Cell Rep 2:1375-1386.
Nunez-Parra A, Maurer RK, Krahe K, Smith RS, Araneda RC (2013) Disruption of centrifugal inhibition to olfactory bulb granule cells impairs olfactory discrimination. Proc Natl Acad Sci U S A 110:14777-14782.
Orona E, Scott JW, Rainer EC (1983) Diferent granule cell populations innervate superficial and deep regions of the external plexiform layer in the rat olfactory bulb. Journal of Comparative Neurology 217:227-237.
Orona E, Rainer EC, Scott JW (1984) Dendritic and axonal organization of mitral and tufted cells in the rat olfactory bulb. Journal of Comparative Neurology 226:346-356.
Otazu GH, Chae H, Davis MB, Albeanu DF (2015) Cortical Feedback Decorrelates Olfactory Bulb Output in Awake Mice. Neuron 86:1461-1477.
Overstreet LS, Hentges ST, Bumaschny VF, de Souza FS, Smart JL, Santangelo AM, Low MJ, Westbrook GL, Rubinstein M (2004) A transgenic marker for newly born granule cells in dentate gyrus. J Neurosci 24:3251-3259.
Overstreet-Wadiche LS, Westbrook GL (2006) Functional maturation of adult-generated granule cells. Hippocampus 16:208-215.
Panzanelli P, Fritschy JM, Yanagawa Y, Obata K, Sassoe-Pognetto M (2007) GABAergic phenotype of periglomerular cells in the rodent olfactory bulb. Journal of Comparative Neurology 502:990-1002.
Paolini AG, McKenzie JS (1993) Effects of lessons in the horizontal diagonal band nucleus on olfactory habituation in the rat. Neuroscience 57:717-724.
Paolini AG, McKenzie JS (1996) Lesions in the magnocellular preoptic nucleus decrease olfactory investigation in rats. Behavioural Brain Research 81:223-231.
Paolini AG, McKenzie JS (1997) Intracellular recording of magnocellular preoptic neuron responses to olfactory brain. Neuroscience 78:229-242.
Parmentier M, Libert F, Schurmans S, Schiffmann S, Lefort A, Eggerickx D, Ledent C, Mollereau C, Gerard C, Perret J, Grootegoed A, Vassart G (1992) Expression of

members of the putative olfactory receptor gene family in mammalian germ cells. Nature 355:453-455.
Parrish-Aungst S, Shipley MT, Erdelyi F, Szabo G, Puche AC (2007) Quantitative analysis of neuronal diversity in the mouse olfactory bulb. J Comp Neurol 501:825-836.
Parsa PV, D'Souza RD, Vijayaraghavan S (2015) Signaling between periglomerular cells reveals a bimodal role for GABA in modulating glomerular microcircuitry in the olfactory bulb. Proc Natl Acad Sci U S A 112:9478-9483.
Petreanu L, Alvarez-Buylla A (2002) Maturation and death of adult-born olfactory bulb granule neurons: Role of olfaction. Journal of Neuroscience 22:6106-6113.
Petzold GC, Hagiwara A, Murthy VN (2009) Serotonergic modulation of odor input to the mammalian olfactory bulb. Nature Neuroscience 12:784-U142.
Pignatelli A, Kobayashi K, Okano H, Belluzzi O (2005) Functional properties of dopaminergic neurones in the mouse olfactory bulb. Journal of Physiology-London 564:501-514.
Pinching AJ, Powell TP (1971) The neuron types of the glomerular layer of the olfactory bulb. Cell Sci. 9(2):305-45
Pinching AJ, Powell TP (1971) The neuropil of the glomeruli of the olfactory bulb. Cell Sci 9, 347-377
Pirez N, Wachowiak M (2008) In vivo modulation of sensory input to the olfactory bulb by tonic and activity-dependent presynaptic inhibition of receptor neurons. Journal of Neuroscience 28:6360-6371.
Price JL, Powell TPS (1970) The Mitral and Short Axon Cells of the Olfactory Bulb. Journal of Cell Science 7: 631-651
Poo C, Isaacson JS (2009) Odor Representations in Olfactory Cortex: "Sparse" Coding, Global Inhibition, and Oscillations. Neuron 62:850-861.
Potter SM, Zheng C, Koos DS, Feinstein P, Fraser SE, Mombaerts P (2001) Structure and emergence of specific olfactory glomeruli in the mouse. Journal of Neuroscience 21:9713-9723.
Pressler RT, Strowbridge BW (2006) Blanes cells mediate persistent feedforward inhibition onto granule cells in the olfactory bulb. Neuron 49:889-904.
Puopolo M, Belluzzi O (1998a) Inhibitory synapses among interneurons in the glomerular layer of rat and frog olfactory bulbs. Journal of Neurophysiology 80:344-349.
Puopolo M, Belluzzi O (1998b) Functional heterogeneity of periglomerular cells in the rat olfactory bulb. European Journal of Neuroscience 10:1073-1083.
Ressler KJ, Sullivan SL, Buck LB (1993) A zonal organization of odorant receptor gene expression in the olfactory epithelium. Cell 73:597-609.
Rheims S, Holmgren CD, Chazal G, Mulder J, Harkany T, Zilberter T, Zilberter Y (2009) GABA action in immature neocortical neurons directly depends on the availability of ketone bodies. Journal of Neurochemistry 110:1330-1338.
Ribak CE, Seress L, Peterson GM, Seroogy KB, Fallon JH, Schmued LC (1986) A GABAergic inhibitory component within the hipocampal commisural pathway. Journal of Neuroscience 6:3492-3498.
Richard MB, Taylor SR, Greer CA (2010) Age-induced disruption of selective olfactory bulb synaptic circuits. Proceedings of the National Academy of Sciences of the United States of America 107:15613-15618.
Rojas-Libano D, Frederick DE, Egana JI, Kay LM (2014) The olfactory bulb theta rhythm follows all frequencies of diaphragmatic respiration in the freely behaving rat. Frontiers in Behavioral Neuroscience 8.

Rubin BD, Katz LC (1999) Optical imaging of odorant representations in the mammalian olfactory bulb. Neuron 23:499-511.

Rudy B, Fishell G, Lee S, Hjerling-Leffler J (2011) Three Groups of Interneurons Account for Nearly 100% of Neocortical GABAergic Neurons. Developmental Neurobiology 71:45-61.

Salcedo E, Tran T, Ly X, Lopez R, Barbica C, Restrepo D, Vijayaraghavan S (2011) Activity-Dependent Changes in Cholinergic Innervation of the Mouse Olfactory Bulb. Plos One 6.

Saunders A, Granger AJ, Sabatini BL (2015) Corelease of acetylcholine and GABA from cholinergic forebrain neurons. Elife 4.

Schneider SP, Macrides F (1978) Laminar distributions of interneurons in main olfactory bulb of adult hamsters. Brain Research Bulletin 3:73-82.

Schoppa NE (2006) Synchronization of olfactory bulb mitral cells by precisely timed inhibitory inputs. Neuron 49:271-283.

Schoppa NE, Westbrook GL (2001) Glomerulus-specific synchronization of mitral cells in the olfactory bulb. Neuron 31:639-651.

Schoppa NE, Westbrook GL (2002) AMPA autoreceptors drive correlated spiking in olfactory bulb glomeruli. Nature Neuroscience 5:1194-1202.

Schoppa NE, Kinzie JM, Sahara Y, Segerson TP, Westbrook GL (1998) Dendrodendritic inhibition in the olfactory bulb is driven by NMDA receptors. J Neurosci 18:6790-6802.

Scott JW (1981) Electrophysiological identification of mitral and tufted cells and distribution of their axons in olfactory system of the rat. Journal of Neurophysiology 46:918-931.

Shao Z, Puche AC, Shipley MT (2013) Intraglomerular inhibition maintains mitral cell response contrast across input frequencies. J Neurophysiol.

Shao Z, Puche AC, Liu S, Shipley MT (2012) Intraglomerular inhibition shapes the strength and temporal structure of glomerular output. J Neurophysiol 108:782-793.

Shao Z, Puche AC, Kiyokage E, Szabo G, Shipley MT (2009) Two GABAergic Intraglomerular Circuits Differentially Regulate Tonic and Phasic Presynaptic Inhibition of Olfactory Nerve Terminals. Journal of Neurophysiology 101:1988-2001.

Shepherd GM, Chen WR, Greer CA (2004) The synaptic organization of the brain (5^{th} ed.) Oxford university press 165-216.

Shepherd GM, Chen WR, Willhite D, Migliore M, Greer CA (2007) The olfactory granule cell: From classical enigma to central role in olfactory processing. Brain Research Reviews 55:373-382.

Shipley MT, Adamek GD (1984) The connections of the mouse olfactory bulb. A study using orthograde and retrograde transport of wheat germ agglutinin cojugated to horseradish peroxidase. Brain Research Bulletin 12:669-688.

Shipley MT, Halloran FJ, Delatorre J (1985) Surprisingly rich projection from Locus coeruleus to the olfactory bulb in the rat. Brain Research 329:294-299.

Smith RS, Hu RL, DeSouza A, Eberly CL, Krahe K, Chan W, Araneda RC (2015) Differential Muscarinic Modulation in the Olfactory Bulb. Journal of Neuroscience 35:10773-10785.

Smith TC, Jahr CE (2002) Self-inhibition of olfactory bulb neurons. Nat Neurosci 5:760-766.

Sosulski DL, Bloom ML, Cutforth T, Axel R, Datta SR (2011) Distinct representations of olfactory information in different cortical centres. Nature 472:213-216.

Soucy ER, Albeanu DF, Fantana AL, Murthy VN, Meister M (2009) Precision and diversity in an odor map on the olfactory bulb. Nature Neuroscience 12:210-220.

Spors H, Grinvald A (2002) Spatio-temporal dynamics of odor representations in the mammalian olfactory bulb. Neuron 34:301-315.

Spors H, Wachowiak M, Cohen LB, Friedrich RW (2006) Temporal dynamics and latency patterns of receptor neuron input to the olfactory bulb. Journal of Neuroscience 26:1247-1259.

Stettler DD, Axel R (2009) Representations of Odor in the Piriform Cortex. Neuron 63:854-864.

Tan J, Savigner A, Ma MH, Luo MM (2010) Odor Information Processing by the Olfactory Bulb Analyzed in Gene-Targeted Mice. Neuron 65:912-926.

Toida K, Kosaka K, Heizmann CW, Kosaka T (1994) Synaptic contacts between mitral/tufted cells and GABAergic neurons containing calcium binding protein Parvalbumin in the rat olfactory bulb, with special reference to reciprocal synapses between them. Brain Research 650:347-352.

Toida K, Kosaka K, Heizmann CW, Kosaka T (1998) Chemically defined neuron groups and their subpopulations in the glomerular layer of the rat main olfactory bulb: III. Structural features of calbindin D28K-immunoreactive neurons. Journal of Comparative Neurology 392:179-198.

Toida K, Kosaka K, Aika Y, Kosaka T (2000) Chemically defined neuron groups and their subpopulations in the glomerular layer of the rat main olfactory bulb - IV. Intraglomerular synapses of tyrosine hydroxylase-immunoreactive neurons. Neuroscience 101:11-17.

Tomioka R, Okamoto K, Furuta T, Fujiyama F, Iwasato T, Yanagawa Y, Obata K, Kaneko T, Tamamaki N (2005) Demonstration of long-range GABAergic connections distributed throughout the mouse neocortex. European Journal of Neuroscience 21:1587-1600.

Tucker ES, Polleux F, LaMantia AS (2006) Position and time specify the migration of a pioneering population of olfactory bulb interneurons. Developmental Biology 297:387-401.

Uchida N, Mainen ZF (2003) Speed and accuracy of olfactory discrimination in the rat. Nature Neuroscience 6:1224-1229.

Urban NN (2002) Lateral inhibition in the olfactory bulb and in olfaction. Physiology & Behavior 77:607-612.

Urban NN, Sakmann B (2002) Reciprocal intraglomerular excitation and intra- and interglomerular lateral inhibition between mouse olfactory bulb mitral cells. Journal of Physiology-London 542:355-367.

Vaaga CE, Westbrook GL (2016) Parallel processing of afferent olfactory sensory information. Journal of Physiology-London 594:6715-6732.

Vaaga CE, Yorgason JT, Williams JT, Westbrook GL (2017) Presynaptic gain control by endogenous cotransmission of dopamine and GABA in the olfactory bulb. Journal of Neurophysiology 117:1163-1170.

Valeeva G, Tressard T, Mukhtarov M, Baude A, Khazipov R (2016) An Optogenetic Approach for Investigation of Excitatory and Inhibitory Network GABA Actions in Mice Expressing Channelrhodopsin-2 in GABAergic Neurons. Journal of Neuroscience 36:5961-5973.

Vandenpol AN (1995) Presynaptic metabotropic glutamate receptors in adult and developing neurons. Autoexcitation in the olfactory bulb. Journal of Comparative Neurology 359:253-271.

Vassar R, Ngai J, Axel R (1993) Spatial segregation of odorant receptor expression in the mammalian olfactory epithelium. Cell 74:309-318.

Vincis R, Lagier S, Van De Ville D, Rodriguez I, Carleton A (2015) Sensory-Evoked Intrinsic Imaging Signals in the Olfactory Bulb Are Independent of Neurovascular Coupling. Cell Reports 12:313-325.

Wachowiak M, Cohen LB (2001) Representation of odorants by receptor neuron input to the mouse olfactory bulb. Neuron 32:723-735.

Wahl-Schott C, Biel M (2009) HCN channels: Structure, cellular regulation and physiological function. Cellular and Molecular Life Sciences 66:470-494.

Wellis DP, Scott JW (1990) Intracellular responses of identified rat olfactory bulb interneurons to electrical and odor stimulation. Journal of Neurophysiology 64:932-947.

Whitesell JD, Sorensen KA, Jarvie BC, Hentges ST, Schoppa NE (2013) Interglomerular lateral inhibition targeted on external tufted cells in the olfactory bulb. J Neurosci 33:1552-1563.

Whitman MC, Greer CA (2007) Adult-generated neurons exhibit diverse developmental fates. Developmental Neurobiology 67:1079-1093.

Whitman MC, Greer CA (2009) Adult neurogenesis and the olfactory system. Progress in Neurobiology 89:162-175.

Winner B, Cooper-Kuhn CM, Aigner R, Winkler J, Kuhn HG (2002) Long-term survival and cell death of newly generated neurons in the adult rat olfactory bulb. European Journal of Neuroscience 16:1681-1689.

Yamamoto K, Takei H, Koyanagi Y, Koshikawa N, Kobayashi M (2015) Presynaptic cell type-dependent regulation of GABAergic synaptic transmission by nitric oxide in rat insular cortex. Neuroscience 284:65-77.

Yokoi M, Mori K, Nakanishi S (1995) Refinement of odor molecule tuning by dendrodendritic synaptic inhibition in the olfactory bulb. Proc Natl Acad Sci U S A 92:3371-3375.

Yoshihara S, Takahashi H, Nishimura N, Naritsuka H, Shirao T, Hirai H, Yoshihara Y, Mori K, Stern PL, Tsuboi A (2012) 5T4 Glycoprotein Regulates the Sensory Input-Dependent Development of a Specific Subtype of Newborn Interneurons in the Mouse Olfactory Bulb. Journal of Neuroscience 32:2217-2226.

Zaborszky L, Carlsen J, Brashear HR, Heimer L (1986) Cholinergic and GABAergic afferents to the olfactory bulb in the rat with special emphasis on the projection neurons in the nucleus of the horizontal limb of the diagonal band. J Comp Neurol 243:488-509.

Zaborszky L, Pang K, Somogyi J, Nadasdy Z, Kallo I (1999) The basal forebrain corticopetal system revisited. Advancing from the Ventral Striatum to the Extended Amygdala: Implications for Neuropsychiatry and Drug Abuse: in Honor of Lennart Heimer 877:339-367.

Zimnik NC, Treadway T, Smith RS, Araneda RC (2013) alpha(1A)-Adrenergic regulation of inhibition in the olfactory bulb. Journal of Physiology-London 591:1631-1643.

Álvaro SANZ DÍEZ

Functional study of mouse olfactory bulb inhibitory circuits

In the olfactory bulb, periglomerular cells form a heterogeneous population of interneurons with diverse molecular, synaptic, morphological and intrinsic membrane properties, suggesting that different subtypes may have different functions in odor processing. I have contributed to characterize genetically-identified periglomerular cell subtypes. In the first part of this thesis, I show that these results provide a new and more elaborated periglomerular cell classification that underlies their diversity. In the second part, I used a combination of patch-clamp recordings and optogenetics to demonstrate for the first time that centrifugal GABAergic projections from the basal forebrain provide robust and cell-specific synaptic inputs on most periglomerular cell subtypes but also on granule cells and deep short axon cells, two other large classes of interneurons. These results suggest that GABAergic fibers from the basal forebrain may have profound and diverse actions on olfactory bulb circuits.

Key words: Olfactory bulb, periglomerular cells, inhibition.

Les cellules périglomerulaires du bulbe olfactif constituent une population hétérogène avec des propriétés moléculaires, synaptiques, morphologiques et intrinsèques diverses. Cette diversité suggère que différents types de cellules périglomerulaires pourraient avoir des rôles différents dans le traitement de l'information olfactive. Dans la première partie de ma thèse, j'ai contribué à la caractérisation de populations de cellules périglomérulaires spécifiques. Mes travaux conduisent à une nouvelle classification fonctionnelle plus élaborée des diverses cellules périglomérulaires. Dans la deuxième partie, j'ai combiné des techniques d'électrophysiologie et d'optogénétique pour démontrer pour la première fois que des projections centrifuges GABAergiques en provenance du télencéphale basal contactent de manière spécifique la plupart des cellules périglomerulaires ainsi que d'autres classes d'interneurones bulbaires. Ces résultats suggèrent que cette région du télencéphale pourrait exercer un contrôle majeur et complexe des circuits du bulbe olfactif.

Mots clés : Bulbe olfactif, cellules periglomerulaires, inhibition